R-09-30

# Statistical analysis of results from the quantitative mapping of fracture minerals in Forsmark

## Site descriptive modelling – complementary studies

Martin Löfgren
Niressa AB

Magnus Sidborn
Kemakta Konsult AB

December 2010

**Svensk Kärnbränslehantering AB**
Swedish Nuclear Fuel
and Waste Management Co

Box 250, SE-101 24 Stockholm
Phone +46 8 459 84 00

ISSN 1402-3091
SKB R-09-30

# Statistical analysis of results from the quantitative mapping of fracture minerals in Forsmark

## Site descriptive modelling – complementary studies

Martin Löfgren
Niressa AB

Magnus Sidborn
Kemakta Konsult AB

December 2010

*Keywords:* Fracture, Minerals, Quantitative mapping, Coating, Infill, Forsmark.

# Abstract

Within the Forsmark site investigation campaign, quantitative mapping of different fracture minerals has been performed. This has been done by studying fracture surfaces of drill core sections from many different boreholes at the Forsmark site /Eklund and Mattsson 2009/. The drill core mapping was focused on the rock in the vicinity of flow anomalies detected by the Posiva Flow Log (PFL). The quantitative mapping was performed only on open fractures. The fracture minerals that were mapped are calcite, chlorite, clay minerals (as a group), hematite, and pyrite. In this present report, data from the quantitative mineral mapping campaign are refined, sorted into different data subsets, and analysed by parametric and non-parametric statistical methods.

The data subsets are associated with 21 different rock volumes, representing different elevations, rock domains, fracture domains, and groups of deformation zones. In total 2,071 fractures were mapped at the site, and the most frequent mineral was calcite. Its amount could be quantitatively estimated in 32% of the mapped fractures. Of the other minerals, chlorite was quantitatively estimated in 24%, clay minerals in 11%, pyrite in 10%, and hematite in 0.4% of the mapped fractures. For fractures where the averaged fracture mineral thickness, $d_{mean}$ [mm], and visible coverage, $C_{vis}$ [%], could be quantitatively estimated, the following arithmetic means were found: calcite = 0.11 mm and 18%, chlorite = 0.22 mm and 38%, clay minerals = 0.14 mm and 40%, pyrite = 2.3 µm and 0.5%, hematite = 19 µm and 14%. These quantities are based on visual inspection of fracture surfaces and do not include the contribution from non-consolidated fracture fillings.

It is shown that there is significant spatial variability of $d_{mean}$ and $C_{vis}$ within the examined rock volumes. Furthermore, the non-parametric analyses indicate that there are differences in $d_{mean}$ and $C_{vis}$ between the different rock volumes. Even so, the differences are generally shown to be small and if comparing the cumulative distribution functions for the data subsets of the 21 rock volumes, more similarities than dissimilarities are found. No general trends can be observed in data with respect to elevation and location of the rock volumes. These conclusions are made from the perspective of radionuclide retention and groundwater composition modelling. Such modelling is not so sensitive to local deviations in fracture mineral abundances, as flow path averaging is of major importance. In other scientific fields, these deviations may be attributed greater importance.

It is shown from parametric analyses that the normal distribution fairly well describes the logarithm of $d_{mean}$ data. Concerning the visible coverage, $\log_{10}(C_{vis})$ data are fairly well described by truncated normal distributions. The distributions fitted to data from the entire site fairly well represent the individual rock volumes.

In fractures where the mineral amounts could be quantified, the following means and standard deviations for the normal distribution of $\log_{10}(d_{mean}$ [mm]) are suggested: calcite $\mu = -1.47$ and $\sigma = 0.70$, chlorite $\mu = -0.93$ and $\sigma = 0.46$, clay minerals $\mu = -1.09$ and $\sigma = 0.44$, pyrite $\mu = -4.01$ and $\sigma = 1.26$.

In fractures where the mineral visible coverage could be estimated, the following parameters for a truncated normal distribution of $\log_{10}(C_{vis})$ are suggested: calcite $\alpha = 0.85$ and $\beta = 0.65$, chlorite $\alpha = 1.38$ and $\beta = 0.51$, clay minerals $\alpha = 1.47$ and $\beta = 0.40$, pyrite $\alpha = -1.52$ and $\beta = 1.18$.

For hematite, the data are so scarce that no well founded conclusion can be drawn.

The potential correlation between the abundance of fracture minerals and the local transmissivity (which is related to the groundwater flow rate) has been evaluated, but no apparent correlation has been found. However, this evaluation is of preliminary character.

# Contents

# 1 Introduction

## 1.1 Background

When setting up a safety assessment for a repository for spent nuclear fuel, two important scientific fields are hydrogeochemistry and radionuclide transport. The former describes the present and evolving groundwater chemistry of the natural and engineered barriers of the repository system, and the latter describes radionuclide migration from the engineered part of the repository to ground surface.

Groundwater flowing through the natural barrier will interact with the rock surrounding the flow paths by way of mineral dissolution, precipitation, and various reactions. This may alter the groundwater composition, which is primarily of concern for the function of the engineered barrier. In case radionuclides escape from the engineered barrier, they may be transported with flowing water towards the surface. These radionuclides will interact with the rock surrounding the flow paths, resulting in retardation.

The rock surrounding the flow paths is comprised of undisturbed rock matrix, altered rock matrix adjacent to fractures, fracture coatings, and fracture fillings. The mineralogy of the rock matrix has been carefully characterised and its mineral content is quantitatively described. However, until recently there has been a lack of data concerning quantities and coverages of fracture coatings, although they have previously been characterised qualitatively (e.g. /Sandström et al. 2008/).

In recent investigations at the Forsmark site, the occurrence of a number of fracture minerals associated with more than 2,000 fractures have been quantitatively mapped /Eklund and Mattsson 2009/. The drill core mapping was focused on the rock in the vicinity of flow anomalies detected by the Posiva Flow Low (PFL). The mapping has been performed on drill cores from many boreholes and from different depths as shown in Table 2-1. The drill sites concerned are shown in Figure 1-1. For detailed maps of each drill site showing the location and projection of the boreholes, see Figure D-2 in Appendix D. In these studies, fracture coatings have been mapped but not loose non-consolidated fracture fillings, as they to a large extent are flushed away in the drilling of the borehole.

Before using the observed data in hydrogeochemical and radionuclide transport modelling, analysis and data reduction is required. This is attempted in this present report.

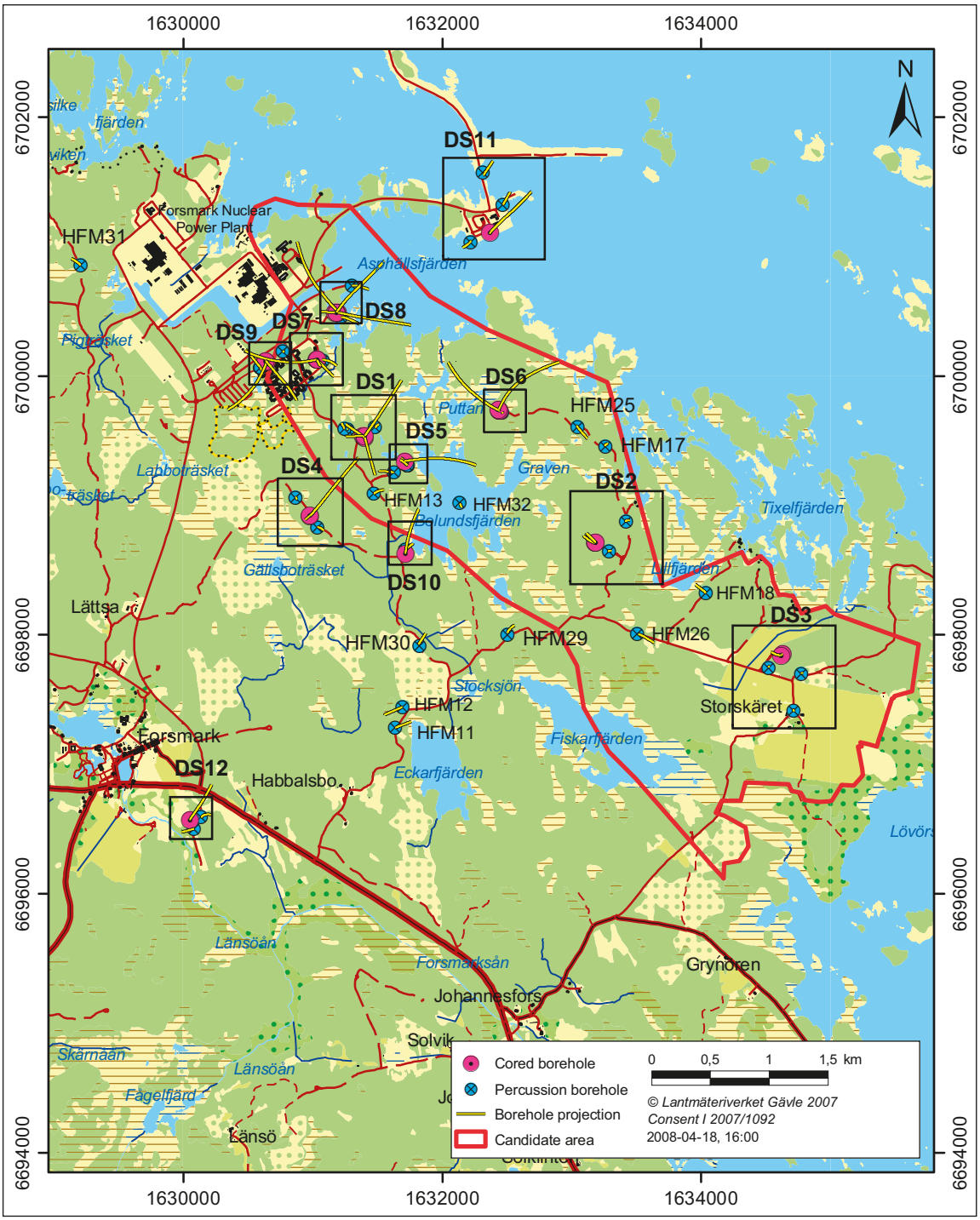


***Figure 1-1.*** *Location of the drill sites included in the quantitative mineral mapping campaign. Figure adopted from /SKB 2008/.*

## 1.2 Scope and objectives

The objective of this report is to analyse the quantitative data reported within the Forsmark site investigation report /Eklund and Mattsson 2009/ and related files from the Sicada database. The analyses aim to result in a set of distribution parameters suggested for subsequent modelling, for example in the SR-Site safety assessment. Parametric and non-parametric statistical methods are used in the analysis with the aim to present mean values, histograms, and probability distributions of fracture mineral quantities and coverages. The quantity will be expressed as a thickness of each fracture mineral coating, as averaged over the entire fracture area. The coverage will be expressed as the fraction of the fracture surface that is covered by the particular fracture mineral.

The fracture minerals that were quantitatively mapped in the quantitative mineral mapping campaign are calcite, chlorite, clay minerals (as a group), hematite (may also include other iron oxides/hydroxides), and pyrite[1]. It was also noted if the fracture mineral is pigmented (impregnated) by hematite. In addition, open fractures with fresh fracture surfaces of uncoated and unaltered rock matrix were mapped.

The results presented in this report concern the entire set of data obtained at the Forsmark site, but also a number of data subsets representing different rock volumes. This facilitates comparisons between different rock volumes that may be of use in subsequent analysis. It is recognised that as one aim has been to deliver distribution parameters, as suggested for subsequent modelling, we have tended to look at similarities between rock volumes rather than dissimilarities. However, a wealth of data and illustrations are delivered to the reader, so that he/she can form an own opinion.

We acknowledge that conclusions are made from the perspective of radionuclide retention and groundwater composition modelling. Such modelling is not so sensitive to minor deviations in fracture mineral abundances. If considering the data in the perspective of other scientific fields, what we judge as minor deviations in this report may be of considerable importance.

This report only aims at presenting analyses of the data obtained in the site investigation, and does not intend to interpret data in the light of, for example, geology, mineralogy, hydrogeochemistry, or radionuclide transport.

Parallel to performing the analyses in this report, efforts were made to identify which geological features mapped as fractures or crush zones that correspond to flow anomalies identified with the Posiva Flow Log method (e.g. /Teurneau et al. 2008/). It has not been within the scope for this report to include the results from these efforts.

## 1.3 Outline

This report consists of seven chapters. In Chapter 1, an introduction is given presenting the background, aim, and scope of this work. In Chapter 2, the methodology of this work is given. This includes both summarising the methodology of the data collection and presenting the methodology of the data refinement. Furthermore, the methods of non-parametric and parametric statistical analysis utilised are described. In Chapter 3, the averaged fracture mineral thickness, $d_{mean}$, is presented for a number of selected data subsets, representing the entire Forsmark site, different elevation ranges, rock domains, fracture domains, and groups of deformation zones. In Chapter 4, the visible coverage, $C_{vis}$, is presented for the same data subsets. In Chapter 5, distribution parameters are given as suggested for subsequent use in, for example, the SR-Site safety assessment. In Chapter 6 conclusions are given and Chapter 7 is the reference list.

Furthermore, for the different rock volumes and fracture minerals, figures showing histograms and fitted probability distributions are appended in Appendix A for $d_{mean}$ and Appendix B for $C_{vis}$. Appendix C of this report has been structured to contain all sections requested by the data supplier in the SKB internal instruction for data qualification associated with the SR-Site Data report /SKB 2010/. This will simplify the integration of these data in the SR-Site safety assessment, if one chooses to do so. Appendix D was written prior to the initiation of the quantitative mineral mapping campaign, and gives the rational for choosing the drill core sections to be mapped.

[1] The justifications for the selection of the minerals mapped are given in the internal document “Forsmark kompletterande undersökningar. Statistik och kvantitativ kartering av sprickmineral”.

# 2 Methodology

## 2.1 Methodology of data collection

The methodology of quantitative fracture mineral mapping is described in detail in the site investigation report /Eklund and Mattsson 2008/ and in the method description (MD 143.009). In this section, the methodology is summarised to facilitate a better understanding of the results presented in this present report.

### 2.1.1 Selection of drill core sections to map

The work done before the quantitative mineral mapping campaign, defining which drill core sections to map, is described in Appendix D. It was decided to focus the campaign upon open fractures (which apertures had previously been mapped to be > 0) that potentially constitute groundwater flow paths. Hydraulic data resulting from the Posiva flow log, a tool frequently used within the site investigations, were used. This tool is able to detect the locations where groundwater flows in or out of the borehole, through open fractures, with a resolution of 1 dm along the borehole. Such a detected in- or outflow is called a PFL-anomaly, where PFL is the abbreviation for Posiva flow log.

Prior to the quantitative mineral mapping campaign, there had been no coupling made between PFL-anomalies and discrete fractures detected in the drill core mapping. Therefore, it was decided to map all open fractures of a section of the drill core within a distance of one meter from a PFL-anomaly. Such a section is called a PFL-section.

At the time of the planning of the campaign, 769 PFL-anomalies had been detected within the Forsmark site investigation area. 401 anomalies out of these were chosen for the campaign, including all anomalies below the elevation –400 masl (metres above sea level). Figure 2-1 shows the approximate elevation of all 769 PFL-anomalies detected in different boreholes at the site, while Figure 2-2 shows the approximate elevation of the selected PFL-sections. The locations of these anomalies in terms of borehole name and elevation are also given in Table 2-1. See Figures D-1 and D-2 in Appendix D for the location of the different boreholes.

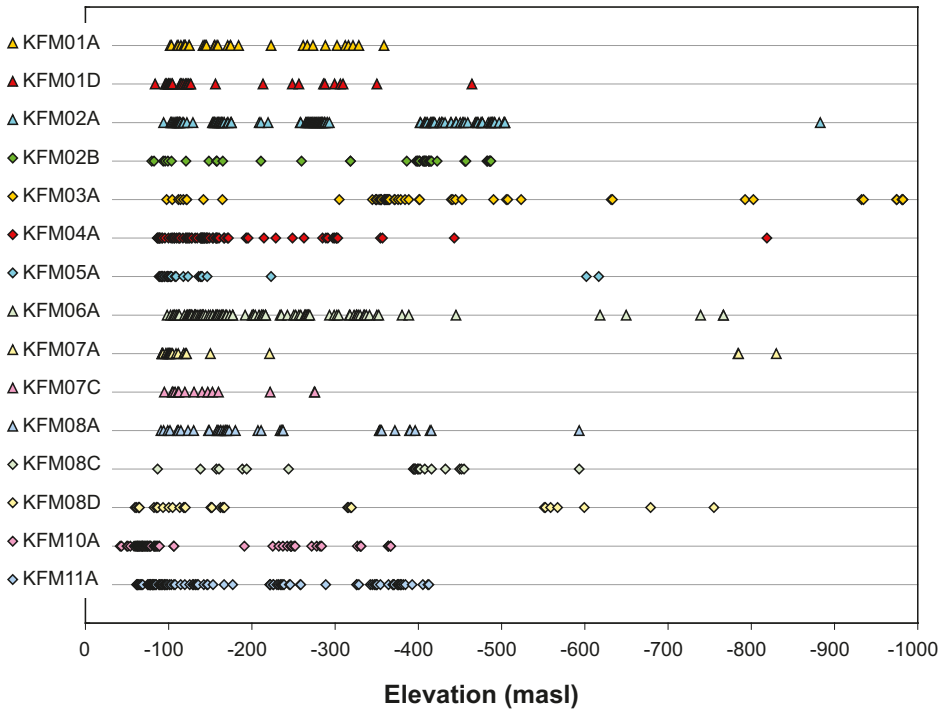


***Figure 2-1.*** *Approximate elevation of all 769 PFL-anomalies detected at Forsmark.*

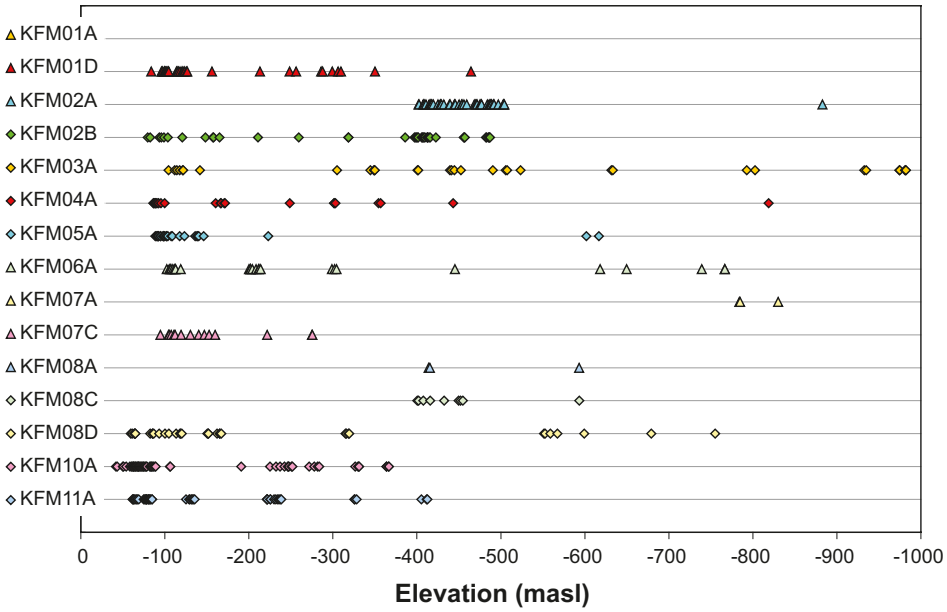


***Figure 2-2.*** *Approximate elevation of all 401 PFL-anomalies selected for the campaign.*

**Table 2-1. Number of mapped PFL-sections in different elevation (*E*) and transmissivity (*T*) ranges. See also Appendix D.**

| Borehole | *E* > –100 masl | –100 ≥ *E* ≥ –400 masl | –400 > *E* ≥ –600 masl | *E* < –600 masl | *T* < $10^{-8}$ m²/s | $10^{-8}$ ≤ *T* ≤ $10^{-6}$ m²/s | *T* > $10^{-6}$ m²/s |
|---|---|---|---|---|---|---|---|
| KFM01A | – | – | – | – | – | – | – |
| KFM01D | 7 | 26 | 1 | – | 13 | 19 | 2 |
| KFM02A | – | – | 49 | 1 | 23 | 26 | 1 |
| KFM02B | 5 | 14 | 22 | – | 2 | 25 | 14 |
| KFM03A | – | 12 | 10 | 11 | 11 | 19 | 3 |
| KFM04A | 10 | 11 | 1 | 1 | 7 | 10 | 6 |
| KFM05A | 12 | 13 | – | 2 | 10 | 13 | 4 |
| KFM06A | – | 21 | 1 | 5 | 16 | 10 | 1 |
| KFM07A[1] | – | – | – | 3 | – | – | – |
| KFM07C | 1 | 14 | – | – | 6 | 7 | 2 |
| KFM08A | – | – | 3 | – | 1 | 1 | 1 |
| KFM08C | – | – | 9 | – | 7 | 2 | – |
| KFM08D[2] | 11 | 17 | 5 | 2 | 15 | 17 | 2 |
| KFM10A | 32 | 24 | – | – | 14 | 27 | 15 |
| KFM11A | 21 | 21 | 3 | – | 16 | 24 | 5 |
| **Total** | **99** | **173** | **104** | **25** | **141** | **200** | **56** |

[1] No transmissivity obtained for the three selected anomalies.
[2] No transmissivity obtained for one selected anomalies.

In addition to the selected PFL-sections, it was decided to map in total 104 m of drill core from above –60 masl, where no PFL-logging has been performed. Furthermore, in total 60 m of drill core at least 5 m distant from any PFL-anomaly was mapped, to facilitate comparisons between conducting and non-conducting rock volumes.

### 2.1.2 Methodology of fracture mineral mapping

Once the drill core sections included in the campaign had been selected, the previously performed drill core mapping was consulted and all discrete fractures previously mapped as open were revisited. In addition, crush zones were revisited. A crush zone is a section of the drill core with enhanced (open) fracture frequency, commonly with loose rock and fracture coating material of grain sizes ranging from clay to gravel.All other fractures or features were disregarded. The coverages and thickness of different fracture mineral layers were quantitatively mapped with respect to the following minerals:

- Calcite.
- Chlorite.
- Clay minerals (as a group).
- Hematite (may include other iron oxides/hydroxides).
- Pyrite.

It should be noted that chlorite found in fractures in Forsmark commonly consists of chlorite interlayered with the clay mineral corrensite (see e.g. /Sandström et al. 2008/). In addition, spot minerals were quantitatively mapped in the case of pyrite. Furthermore, a note was made in case:

- The fracture mineral is pigmented by hematite.
- Both the upper and lower fracture surface are fresh (no detectable fracture mineral and unaltered matrix rock).

Studies at Laxemar /Eklund and Mattsson 2008/ showed that the fraction of pure hematite in minerals mapped as hematite was below unity, and in minerals mapped as pigmented by hematite was low. Concerning the fracture mineral layers, the following parameters (in bold typeface) were estimated:

**Mineral thickness:** The mineral thickness is the integrated average of the thickness of a specific fracture mineral layer, where it covers the fracture surface, as estimated by the operator. This is done with a resolution of 0.1 mm. If the mineral layer is visible but significantly thinner than 0.1 mm, the mineral layer is noted for a qualitative purpose, but no quantitative thickness is assigned. Figure 2-3 and the discussion below aim at facilitating an understanding of how the mineral thickness is quantitatively estimated.

The rock sample in Figure 2-3 is covered by three fracture mineral layers. For the sake of simplicity, let us assume that the rock sample is a slab and not a cylinder, but keep in mind that the cylindrical shape of the drill core complicates the estimates made by the operator. Let us further assume that the layers do not vary along the z-axis in Figure 2-3. The mineral thickness is the average of the layer's thickness where it covers the underlying rock matrix. This means that the part of the fracture surface that is not covered by the specific layer should be disregarded. In Figure 2-3, fracture mineral layer A is represented by a triangle covering half the fracture surface, with the maximum thickness of 1 mm. In the mapping the correct estimate of the layer thickness should be 0.5 mm.

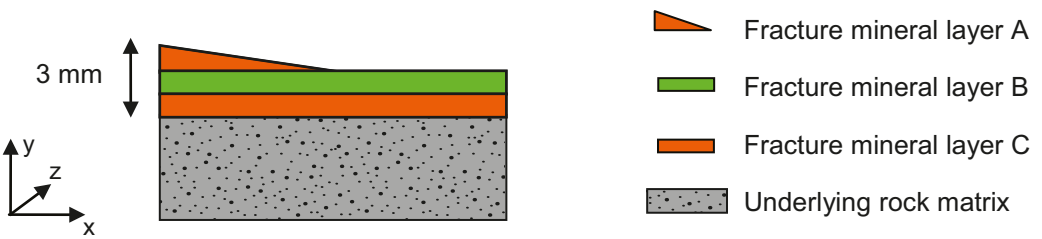


***Figure 2-3.*** *Illustration of a rock sample covered by three layers of fracture minerals.*

**Visible coverage of layer:** The visible coverage of a specific layer is the fraction of the fracture surface that is covered by the layer, as estimated from visual inspection of the fracture surface from above. If inspecting the fracture surface in Figure 2-3 from above, mineral layer A would cover 50% of it, as would mineral layer B. Layer C would not be visible from above, resulting in 0% visible coverage. In /Eklund and Mattsson 2008/ the visible coverage is also denoted as the surface coverage.

**Total coverage:** The total coverage is the actual fraction of the fracture surface that is covered by the mineral layer. In Figure 2-3, the total coverage would be 50% for mineral layer A, 100% for mineral layer B, and 100% for mineral layer C.

Some minerals commonly exist as spot minerals. In this campaign pyrite has been mapped as both spot mineral and layer mineral. Spot minerals are reported as *frequency* or number of crystals per $cm^2$, where the lower detection limit in the campaign is one crystal per ten $cm^2$. All mineral crystals on a fracture surface are assumed to be identical, with an average crystal size defined by the average squared base and an average thickness. The *length of the base* and the *thickness* are estimated with a resolution of 0.1 mm. The total as well as visible coverage of a spot mineral is the square of the length of the base times the frequency. It should be noted that only the uppermost crystal surface, parallel to the fracture surface, is included in the visible coverage, and not the surfaces of the sides of the pyrite grain.

For each of the upper and lower fracture surface of a fracture, up to four layers of fracture minerals are recorded, plus spot minerals if such exist. For crush zones, the same parameters are delivered as for discrete fractures, for three mineral layers and spot minerals. However, it is assumed that all fracture surfaces in a crush zone are identical. The delivered parameters are therefore estimated averages of the above parameters, based on the inspection of all fractures surfaces in the crush zone. In addition the number of fractures constituting the crush zone has been estimated.

In some fractures, the fracture minerals are pigmented (impregnated) with hematite. An investigation of such fracture minerals has indicated that their fraction of hematite is small, on the order of a couple of percents or less /Eklund and Mattsson 2008/. Furthermore, it has been concluded that by means of visual inspection only, the fraction of hematite cannot be determined. Therefore, the hematite associated with pigmented fracture minerals is not quantitatively mapped. It is only noted whether a fracture mineral is pigmented or not. This is done for calcite, chlorite, and clay minerals.

A special note is made concerning fractures where both the upper and lower fracture surfaces are fresh, as such fractures have recently become a focus of attention. In this campaign such fractures have been noted for a qualitative purpose, but only if previously assigned as open.

## 2.2 Methodology of data refinement

In the work presented in this report, data reported in the site investigation report /Eklund and Mattsson 2009/ and associated Sicada files have been refined and analysed. This is done by, as a first step, performing elementary arithmetic operations including the parameters underlined in Section 2.1. As a second step, the data are sorted into subsets associated with different rock volumes. These two steps are described in this section. In a third step, described in Sections 2.3 and 2.4, the data subsets are statistically analysed by non-parametric and parametric methods.

### 2.2.1 Defining output parameters

The parameters written in bold typeface in Section 2.1 are used to describe each layer, fracture, or crush zone. This present report aims at delivering output parameters representative for entire rock volumes. The data delivered as outputs in this report are:

- **Visible coverage, $C_{vis}$ (%):**
  The visible coverage for each fracture is calculated in two steps. Firstly, the visible coverages for the different mineral layers of the same mineral are summed. This includes layers on both the upper and lower fracture surfaces. Secondly, the sum is divided by two, in order to compensate for the fact that layers on both fractures surfaces are summed.

- **Average fracture mineral thickness $d_{mean}$ (mm):**
  In the fracture mineral mapping, the output data concern different layers of fracture minerals in a fracture. From the product of the mineral thickness and total coverage for a specific layer, the *layer mean thickness* (mm) is obtained. If returning to the example of Figure 2-3, the layer mean thickness of mineral layer A is 0.25 mm, as its mineral thickness is 0.5 mm and only half the surface is covered. The layer mean thickness of mineral layer B and C is 1 mm.

  In some cases, different layers within a fracture (including both the upper and lower fracture surfaces) are of the same fracture mineral. If summarising the layer mean thicknesses of a specific fracture mineral in a fracture, the averaged fracture mineral thickness, $d_{mean}$, is obtained. If once more returning to the example of Figure 2-3; if mineral layers A and C are of the same fracture mineral and the upper fracture surface is uncoated by the mineral, $d_{mean}$ is 1.25 mm.

  In case of spot minerals, the layer mean thickness is calculated by total coverage times the crystal thickness. For pyrite, which exists both as layer mineral and spot mineral, the averaged fracture mineral thickness is the sum of the layer mean thicknesses for both types of occurrences of the mineral.
- **Fraction of fractures where the averaged fracture mineral thickness could be quantitatively estimated $f_{quant}$ (%):**
  In the fracture mineral mapping it has become apparent that not all of the investigated open fractures are coated by the fracture minerals studied. The fraction of fractures where the amount of a certain fracture mineral is sufficiently large to be quantitatively estimated is in this report called $f_{quant}$.
- **Fraction of fractures where the visible coverage could be quantitatively estimated $f_{quant}^{c}$ (%):**
  The fraction of fractures where the visible coverage of a certain fracture mineral is sufficiently large to be quantitatively estimated is in this report called $f_{quant}^{c}$.
- **Fraction of fractures qualitatively populated by a certain mineral $f_{qual}$ (%):**
  The parameter $f_{qual}$ is similar to $f_{quant}$, except for the fact that it also includes the fraction of fractures where a specific mineral is observed, but only in such small amounts that it cannot be quantitatively estimated with the current methodology. In other words, $f_{qual}$ is the fraction of fractures where a specific mineral has been observed at any amounts.

### 2.2.2 Associating data subsets with different rock volumes

It is not known exactly how the information delivered by his report will be used, and what the demands are on coupling the results to different rock volumes. Therefore, it was decided to associate the data with a multitude of rock volumes. Different data subsets are assigned to different ranges of elevation, rock domains, fracture domains, and deformation zones as groups based on their orientation. Concerning elevation, six data subsets representing different elevation ranges are assigned as in the following:

- GS – 1,000: Ground surface to 1,000 mbsl (metres below sea level).
- GS – 100: Ground surface to 100 mbsl.
- 100 to 300 mbsl.
- 300 to 500 mbsl.
- 500 to 700 mbsl.
- 700 to 1,000 mbsl.

It should be noted that the first data subset, ground surface to 1,000 mbsl, includes the data set from the entire Forsmark site, as no drill core from below 1,000 mbsl was mapped. Concerning rock domains, the data subsets are based on the six rock domains defined in /Stephens et al. 2007, 2008/, as following:

- RFM012.
- RFM018.
- RFM021.
- RFM029.
- RFM044.
- RFM045.

Concerning fracture domains, the data subsets are based on the six fracture domains defined in /Stephens et al. 2007, 2008/:

- All FD: All fracture domains.
- FFM01.
- FFM02.
- FFM03.
- FFM04.
- FFM05.
- FFM06.

The first data subset includes all data in fracture domains, which excludes deformation zone data. Sometimes, part of a fracture domain may be affected by deformation zones /Stephens et al. 2007, 2008/. Data from such rock is associated with the fracture domain. For borehole KFM11A, which is outside the Forsmark target area, no fracture domain is modelled. Concerning deformation zones, five data subsets are assigned:

- All DZ: All deformation zones.
- GDZ: All gently dipping deformation zones.
- WNW-NW: All steeply dipping deformation zones with orientation WNW to NW.
- NNW: All steeply dipping deformation zones with orientation NNW.
- ENE-NNE: All steeply dipping deformation zones with orientation ENE to NNE.

For more information on the deformation zone orientation, see /SKB 2008, Section 5.5.4/. The data set All DZ only includes data associated with deformation zones of a high confidence, and does not include data associated with possible deformation zones. For KFM01C, a number of fractures are located in a borehole section that is intersected by both the gently dipping deformation zone ZFMA2 and the steeply dipping deformation zone ZFMENE1192. Although these fractures are included in the data subsets All DZ, they are neither included in the data subsets GDZ nor ENE-NNE.

For borehole KFM02B, KFM08D, and KFM11A, only predictions of rock domains and deformation zones are made, which has later been compared with information from single hole interpretations /Stephens et al. 2008/. In Appendix E, the rock volumes assumed in this work are displayed.

As it turns out, and as described in Section 3.8, crush zones are scarce within the investigated drill core sections. Furthermore, upon analysing the data from crush zones it is shown that they do not considerably differ in amount and coverage values from those of discrete fractures. Therefore, it was decided to include only discrete open fractures in the assigned data subsets, and to use data from crush zones for a comparative purpose only. However, it should be noted that non-consolidated fracture fillings, which often is the most common fracture filling material in crush zones, has not been quantified in the mineral mapping campaign. Clay minerals often occur as non-consolidated fracture fillings. Therefore, the results for the crush zones are only giving a minimum value of the amount of clay minerals in the fractures.

### 2.2.3 Sorting of data into different subsets

In the Sicada files presenting the data from the quantitative mineral mapping campaign, all discrete fractures and crush zones are assigned coordinates. Furthermore, all rock volumes presented in Section 2.2.2 are bounded by coordinates. As a result, sorting the data into different subsets representing the rock volumes presented no obstacle. A standard sorting routine was programmed in GNU Octave, automating the sorting process. To check the sorting routine, a test case was made for one data subset, making the same sorting manually (with aid from MS Excel) and comparing the results.

## 2.3 Non-parametric statistical analysis of data subsets

The data subsets were analysed by non-parametric statistical methods, as described below.

### 2.3.1 Kruskal-Wallis test

The first analysis made for the different data subsets is the Kruskal-Wallis test. This test aims to investigate whether different data sets are samples of the same population, which is the null hypothesis. In the test, two or more data sets are compared. This is done by sorting the data based on their values and assigning each data point a rank. For each data set, the ranks of its data points are summed. By comparing the sum of the ranks for the different data sets, the likeliness that they are samples of the same population can be evaluated. The test returns a confidence, or $p$-value. If the $p$-value is high, this indicates that the null hypothesis may be true, and that the data sets may be samples of the same population. If the $p$-value is small, this indicates that the null hypothesis should be rejected. For further explanation of the test, /NIST 2009/ is recommended.

### 2.3.2 Arithmetic mean and standard deviation of data subset

For each data subset, the arithmetic mean $\overline{x}$ and standard deviation *STD* are computed by standard methods. The arithmetic mean $\overline{x}$ of the data subset should not be mistaken for the mean value $\mu$ of the population which is sampled. Likewise, the standard deviation *STD* of the data subset should not be mistaken for the standard deviation $\sigma$ of the sampled population.

### 2.3.3 Two-sided confidence limits for the mean

If sampling a number of data sets from the same population, it is unlikely that their arithmetic means $\overline{x}$ all coincide with the mean $\mu$ of the population. If one has access to a single data set, one may assign confidence limits around the arithmetic mean $\overline{x}$ of the sample. Within these limits, it is likely that the population mean $\mu$ is found. Confidence limits are expressed in terms of a confidence coefficient, and in this work the confidence coefficient used is 0.95. For further explanation of the confidence limits of the mean, /NIST 2009/ is recommended.

### 2.3.4 Histograms and cumulative distribution functions

In this work, data have been visualised by histograms and cumulative distribution functions. Histograms are useful when visualising how data of one data subset are distributed, and also when making comparisons with fitted probability distributions. In Figure 2-4 this is done for $\log_{10}(d_{mean})$ data for calcite. The comparison is made with the normal distribution.

When comparing different data sets, this is better visualised by the cumulative distribution function, CDF. In Figure 2-5, this is exemplified for $\log_{10}(d_{mean})$ for calcite data from different elevation ranges. The blue curve represents the same data as the histogram does in Figure 2-4.

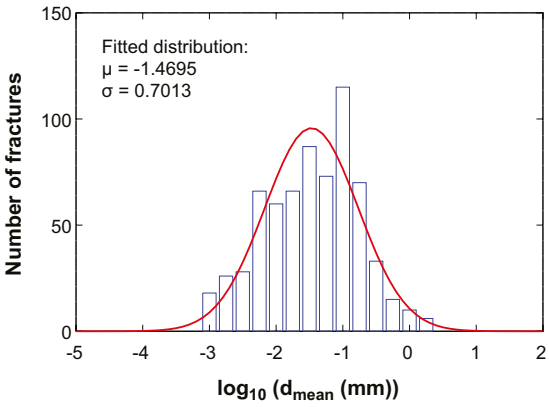


***Figure 2-4.*** *Example of how data can be visualised by a histogram, facilitating visual comparisons with a fitted probability distribution.*

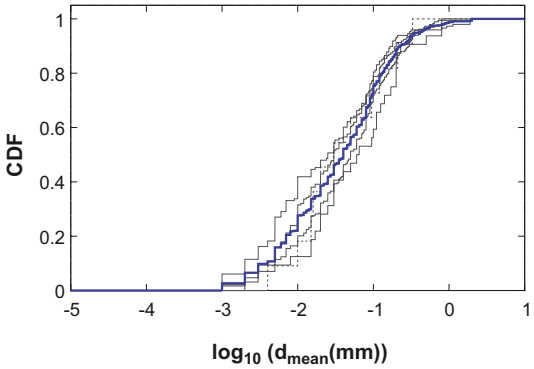


***Figure 2-5.*** *Example of how several data subsets can be visualised by cumulative distribution functions.*

One can extract much information from Figure 2-5, for example that the median of $\log_{10}(d_{mean})$ for the different data subsets (CDF = 0.5) varies between about –1.2 and –1.6.

## 2.4 Parametric statistical analysis of data subsets

The distribution of a data set can be described by different probability distributions (also called probability density functions), such as the normal distribution, the chi square distribution, the beta distribution, etc. Due to bias issues discussed in Section 2.4.4, we have judged that there is no ground for making elaborate analyses with the aim at estimating possible skewness and kurtosis of the distribution. Based on how the sampled data are distributed, we have made the approximation that the populations are normally or truncated normally distributed in this report.

### 2.4.1 The normal distribution and truncated normal distribution

Equation 2-1 shows the equation for the normal distribution where $\varphi$ is the probability that $x$ will have a certain value, and $x$ is the studied parameter that could be replaced for $d_{mean}$, $C_{vis}$, etc. One can also replace $x$ for some expression including $d_{mean}$ or $C_{vis}$, such as $\log_{10}(d_{mean})$. $\mu$ and $\sigma$ are the mean and standard deviation of the distribution, respectively.

$$\varphi(x) = \frac{1}{\sigma\sqrt{2\pi}} \exp\left(-\frac{(x-\mu)^2}{2\sigma^2}\right) \qquad \text{Equation 2-1}$$

The logarithm of $d_{mean}$ can in theory take any value while $d_{mean}$ can only be $\geq 0$. As the normal distribution permits both positive and negative values, it is strictly speaking not suitable for $d_{mean}$. For the visible coverage, the normal distribution is unsuitable for both $\log_{10}(C_{vis})$ and $C_{vis}$, as $C_{vis}$ range from 0 to 100% and $\log_{10}(C_{vis})$ is $\leq 2$. So solve this problem, the singly or doubly truncated normal distribution can be used /Cohen 1950, Barr and Sherrill 1999/. Equation 2-2 shows the singly truncated normal distribution that is used for $\log_{10}(C_{vis})$.

$$C_{vis} \leq 100\% \text{ ; } \log_{10}(C_{vis}\,[\%]) \leq 2 : \quad \varphi\left(\log_{10}(C_{vis})\right) = \frac{\frac{1}{\beta\sqrt{2\pi}} \exp\left(-\frac{\left(\log_{10}(C_{vis})-\alpha\right)^2}{2\beta^2}\right)}{\int_{-\infty}^{2} \frac{1}{\beta\sqrt{2\pi}} \exp\left(-\frac{\left(\log_{10}(C_{vis})-\alpha\right)^2}{2\beta^2}\right)}$$

$$C_{vis} > 100\% \text{ ; } \log_{10}(C_{vis}\,[\%]) > 2 : \quad \varphi\left(\log_{10}(C_{vis})\right) = 0 \qquad \text{Equation 2-2 a,b}$$

In the truncated normal distribution, we have chosen to denote the parameter corresponding to $\mu$ in the normal distribution by $\alpha$. Furthermore, we have chosen to denote the parameter corresponding to $\sigma$ in the normal distribution by $\beta$. This is done to minimise the risk that the parameter values for the truncated normal distribution are, by mistake, used for the normal distribution in subsequent modelling.

### 2.4.2 Shapiro-Wilk *W* test

The normality of a data set can be tested by the Shapiro-Wilk *W* test, also called the Shapiro-Wilk normality test. The theory behind the test can be read elsewhere (e.g. /Shapiro and Wilk 1965/) but it is based on linear regression of ordered observations. The test returns a *W*-value between zero and one. If one is returned, the data are normally distributed. The lower the *W*-value returned is, the less degree of normality the data set has. To exemplify, if taking the $\log_{10}(d_{mean})$ data for calcite of Figure 2-4, the *W*-value returned from the Shapiro-Wilk *W* test is 0.99. If instead using the $d_{mean}$ data directly, as illustrated by the histogram in Figure 2-6, the *W*-value returned is 0.43. Clearly the $d_{mean}$ values are not normally distributed.

If sampling a perfectly normally distributed population, the more data points one takes, the more likely it is that the data set agrees with the normal distribution. This would result in a returned *W*-value very close to one. In a development of the Shapiro-Wilk *W* test, the number of data points is taken into account, and a confidence (*p*-value) is given, which indicates whether or not the data set is a sample of a perfectly normally distributed population. The data set of Figure 2-4 contains hundreds of data points and still deviates from the normal distribution, for example at $\log_{10}(d_{mean}) \sim -1$. Even if one would sample more data points, it is unlikely that the situation would change. The *p*-value of the $\log_{10}(d_{mean})$ data displayed in Figure 2-4 is less than 0.0001, indicating that it is very unlikely that the data set is a sample of a perfectly normally distributed population.

It should be noted that a truncated distribution by definition deviates from normality. If the truncation is considerable, the Shapiro-Wilk *W* test is unsuitable. However, if the truncation is small, the errors introduced in the Shapiro-Wilk *W* test are small. Therefore, we have in some cases used the Shapiro-Wilk test to indicate which of $d_{mean}$ or $\log_{10}(d_{mean})$ data to a larger degree are normally distributed, and whether $C_{vis}$ or $\log_{10}(C_{vis})$ data to a larger degree are normally distributed.

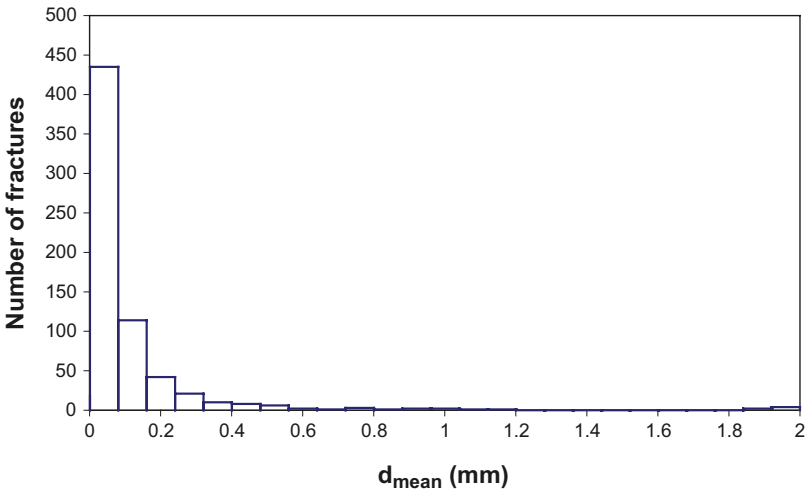


***Figure 2-6.*** *Histogram of $d_{mean}$ data for calcite (compare with Figure 2-4).*

### 2.4.3 Normal score plot

If a data set is fairly well normally distributed, one way of estimating the mean $\mu$ and standard deviation $\sigma$ of the population is by the normal score plot (also called Q-Q plot). In a normal score plot, the data points are organised in ascending order depending on their value, and given a corresponding index. Based on the index and on the total number of data points in the data set, each data point is given a rank. Thereafter, each data point is assigned an x.y-coordinate. The y-coordinate is the actual value of the data point, for example $\log_{10}(d_{mean}) = -1.59$, while the x-coordinate depends on the rank. For further reading /Johnson 1994/ is recommended. In Figure 2-7, the normal score plot based on the same calcite $\log_{10}(d_{mean})$ data as displayed in Figure 2-4 are shown.

If the data would have been perfectly normally distributed, all the data points should have been in line with the linear fitting (red line). As this is not the case, this shows that there are some deviations from normality. For example, such a deviation can be seen at $\log_{10}(d_{mean}) \sim -1$ in both Figure 2-4 and Figure 2-7. As the $r^2$-value of the linear fitting is 0.99, one can say that the data are reasonably well normally distributed. From the slope and intercept of the linear fitting, the standard deviation $\sigma$ and $\mu$ of the normal distribution can be obtained.

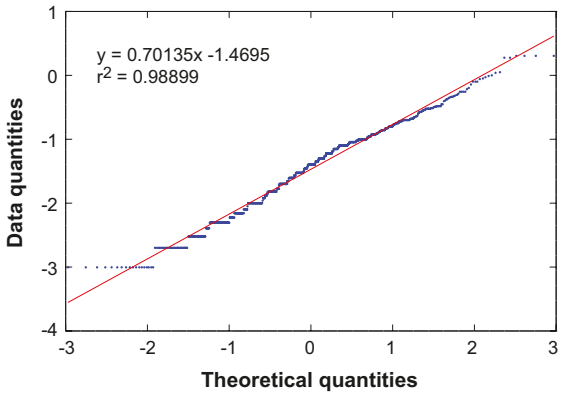


***Figure 2-7.*** *Normal score plot of $\log_{10}(d_{mean})$ data for calcite.*

### 2.4.4 Underlying reasons to deviations from normality

As seen in Figure 2-7, the data in a normal score plot may deviate from the linear fitting. An obvious underlying reason is that the parameter studied is not normally distributed. This possible reason should be remembered throughout the reading of this report.

An additional reason may be that rounding issues in the estimations of the parameter give rise to bias. This is well illustrated by $\log_{10}(d_{mean})$ data for chlorite, a fracture mineral that often covers the entire fracture surface. Below, a few examples of common situations are given. In all examples, the total coverage of the chlorite mineral layer(s) is 100%. Firstly, consider a fracture where both fracture surfaces are covered by chlorite, and where the mineral thickness of both layers is rounded to 0.1 mm (which is the minimum quantitative layer thickness that can be assigned with this methodology). This gives rise to a $\log_{10}(d_{mean}[\text{mm}])$ value of –0.7. Secondly consider a fracture where only one fracture surface is totally covered by chlorite, and the other fracture surface is uncovered by chlorite (this is not uncommon). If rounding the mineral thickness to 0.1 mm, $\log_{10}(d_{mean})$ becomes –1. Thirdly, consider the same situation but where the mineral thickness is rounded to 0.2 mm, giving rise to a $\log_{10}(d_{mean})$ value of –0.7.

There are a few combinations of common total coverages and mineral thicknesses giving rise to favoured $d_{mean}$ values. As there is an element of rounding involved in the estimations, this gives rise to bias. This bias is shown in both the corresponding histogram and normal score plot in Figure 2-8.

In the histogram, one can see that the two bins around –1 and –0.75 feature surprisingly many data points, compared to the best fit normal distribution (red curve). In the normal score plot one can see two distinct plateaus at –1 and –0.7, which are highlighted by dashed arrows. These plateaus indicate that there are more data with the exact values –1 and –0.7 than expected.

Another example that illustrates bias is that of $\log_{10}(d_{mean})$ data for pyrite, a fracture mineral that is mapped as both spot mineral and layer mineral. Figure 2-9 shows the histogram and normal score plot for pyrite data from the entire site.

For pyrite as a layer mineral, it is common that there is a small speck of pyrite that is estimated to roundly cover 1% of the surface, with a 0.1 mm mineral thickness. This results in $\log_{10}(d_{mean}) = -3$. A few combinations of common total coverages and mineral thicknesses result in the plateaus at about –3 in the normal score plot in Figure 2-9. For pyrite as spot mineral, if one only finds one or two small pyrite cubes in a fracture, the frequency may be rounded to 1 crystal per 10 cm$^2$. Furthermore it is common that the length of the base and mineral thickness are rounded to 0.1 mm. This give rise to a $\log_{10}(d_{mean}) = -6$, which is seen as a distinct plateau in the normal score plot.

Due to the fact that rounding (and resolution) issues affect the shape of the histograms and normal score plots, it is judged that there is no ground for making elaborate analyses determining the potential skewness and kurtosis of the distributions.

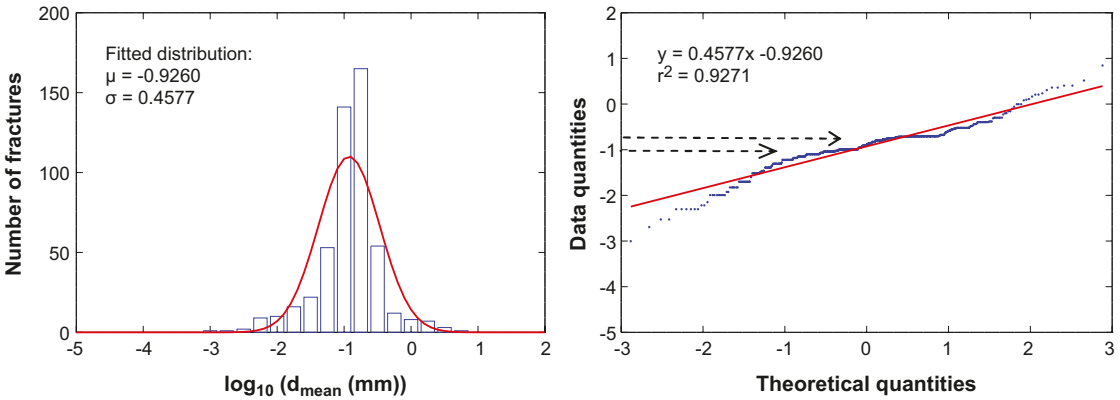


***Figure 2-8.*** *Histogram and normal score plot of chlorite $\log_{10}(d_{mean})$ data.*

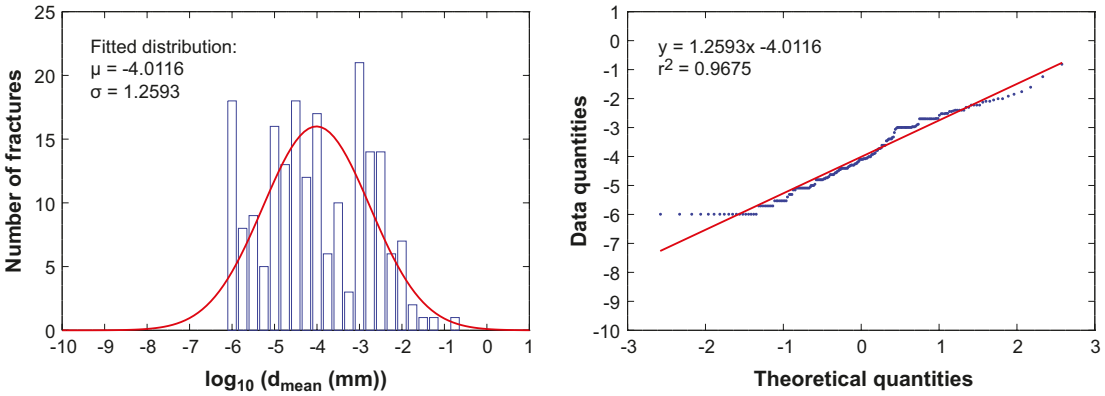


***Figure 2-9.*** *Histogram and normal score plot of pyrite $\log_{10}(d_{mean})$ data.*

### 2.4.5 Normal score plot for truncated normal distribution

In this work we have used the normal score plot to obtain the $\alpha$ and $\beta$ parameters for the truncated normal distribution (see Equation 2-2). The $\alpha$-value is obtained from the intercept of the linear fitting while the $\beta$ value is obtained from the slope. In making the linear fit, we have censored all $C_{vis}$ values $\geq$ 100%.

Figure 2-10 shows $\log_{10}(C_{vis})$ data for clay minerals from the entire site. The left image shows the histogram together with the truncated normal distribution. The right image shows the normal score plot.

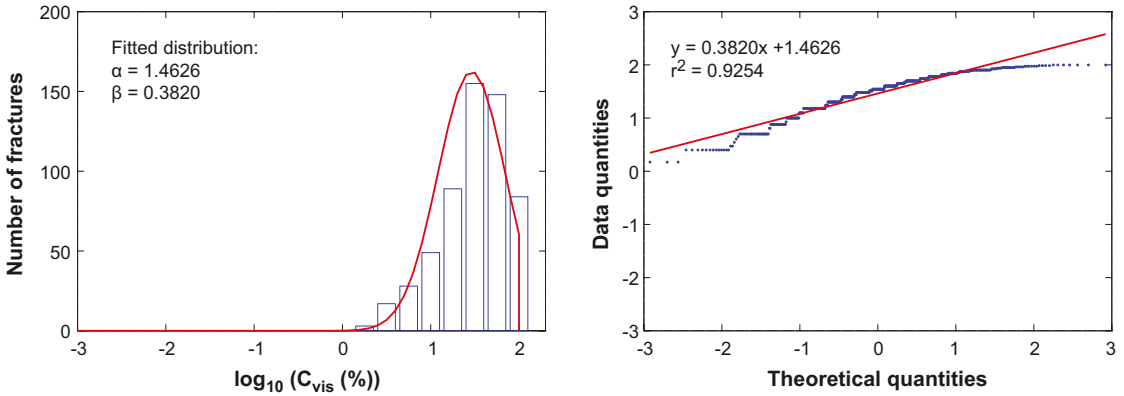


***Figure 2-10.*** *Truncated distribution, histogram, and censored normal score plot for clay minerals $\log_{10}(C_{vis})$ data at the Forsmark site.*

# 3 Fracture mineral thickness, $d_{mean}$

The open fractures chosen for this campaign are predominantly located close to PFL anomalies. However, some fractures that are distant from any PFL anomaly are also included in the campaign, to facilitate comparisons between conducting and non-conducting zones. As shown later in this chapter (Section 3.7), the location of the fracture with respect to PFL anomalies has little impact on the results. Neither does the occurrence of fracture minerals seem to be correlated with the measured transmissivities associated with the PFL anomalies. Therefore, the results presented for the different fracture minerals (Sections 3.1 to 3.6) are based upon all mapped open fractures.

In addition to open fractures, a few crush zones are mapped in this campaign. As seen in Section 2.1.2, the methodology of mapping crush zones differs from that of mapping discrete fractures. Even so, data from these crush zones are similar to data obtained from open fractures. It was decided to exclude these data from the general analysis in Sections 3.1 to 3.6 and instead include them in a separate study (see Section 3.8).

As described in Section 2.2.2, different data subsets of $d_{mean}$ are assigned for different rock volumes. These rock volumes represent different ranges of elevation, rock domains, fracture domains, and deformation zones as groups based on orientation. In this chapter, these data subsets are analysed and results for $d_{mean}$ are presented. For each fracture mineral, we will start with presenting the data subsets. Thereafter a non-parametric statistical analysis is presented. Finally a parametric statistical analysis is presented.

## 3.1 Calcite

### 3.1.1 The data subsets

In Table 3-1, information concerning calcite data subsets is summarised. For an introduction to the different rock volumes represented by the data subsets, Section 2.2.2 is recommended. In Table 3-1, firstly the total number of fractures mapped in the concerned rock volume is presented. Secondly, the number of data points in the subset is presented. This corresponds to the number of studied fractures in the rock volume holding a sufficient amount of calcite for quantitative mapping. Thirdly $f_{quant}$ is presented, which is the fraction of all fractures holding quantitative amounts of calcite. Fourthly, $f_{qual}$ is presented, which is the fraction of all fractures holding qualitative amounts of calcite.

The data are illustrated in Figure 3-1, showing the fractions of the fractures where calcite is found in quantitative amounts, qualitative amounts only, or not at all. With qualitative only, we mean the fractures holding so small fracture mineral amounts that although their occurrence can be qualitatively established, their amounts can not be quantitative estimated with the current methodology.

As can be seen from Table 3-1 and Figure 3-1, on average 32% of all fractures contain enough calcite to be quantitatively mapped, while 43% of all fractures contain no calcite at all. Furthermore, one can see that the occurrence of calcite in general is similar in the different rock volumes. The bars in Figure 3-1 that clearly deviate represent rock volumes where only few fractures were mapped, and it can be questioned how representative they are.

**Table 3-1. Amounts of data in different data subsets, calcite.**

| Calcite | | Total number of fractures | Number of data points | $f_{qual}$ (%) | $f_{quant}$ (%) |
|---|---|---|---|---|---|
| Elevation (mbsl) | GS–1,000[1] | 2,071 | 673 | 57 | 32 |
| | GS–100 | 835 | 298 | 59 | 36 |
| | 100–300 | 531 | 184 | 60 | 35 |
| | 300–500 | 543 | 148 | 53 | 27 |
| | 500–700 | 114 | 32 | 54 | 28 |
| | 700–1,000 | 48 | 11 | 46 | 23 |
| Rock domain | RFM012 | 79 | 20 | 42 | 25 |
| | RFM018 | 30 | 10 | 57 | 33 |
| | RFM021 | 226 | 80 | 65 | 35 |
| | RFM029 | 1,596 | 528 | 56 | 33 |
| | RFM044 | 8 | 1 | 50 | 13 |
| | RFM045 | 132 | 34 | 65 | 26 |
| Fracture domain | All FD | 602 | 199 | 59 | 33 |
| | FFM01 | 152 | 41 | 55 | 27 |
| | FFM02 | 321 | 134 | 69 | 42 |
| | FFM03 | 107 | 21 | 38 | 20 |
| | FFM04 | 8 | 1 | 63 | 13 |
| | FFM05 | 3 | 0 | 0 | 0 |
| | FFM06 | 11 | 2 | 55 | 18 |
| Deformation zone | All DZ | 1,333 | 422 | 55 | 32 |
| | GDZ | 640 | 181 | 47 | 28 |
| | WNW-NW | 371 | 137 | 60 | 37 |
| | NNW | 22 | 5 | 50 | 23 |
| | ENE-NNE | 280 | 88 | 64 | 31 |

[1] Data set represents the entire site.

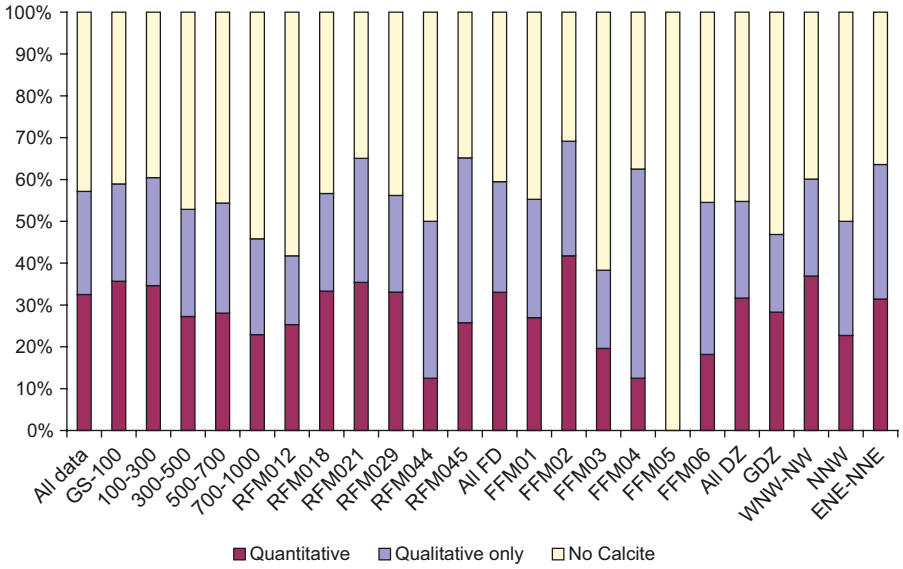


***Figure 3-1.*** *Fractions of fractures populated or unpopulated by calcite.*

### 3.1.2 Non-parametric analysis

To determine whether or not the different calcite data subsets are samples of the same population, they were analysed by the Kruskal-Wallis test (see Section 2.3.1). With great confidence it can be determined that the data subsets are not samples of the same population. For example, if comparing the five separate elevation data subsets for calcite, the *p*-value (confidence) returned from the Kruskal-Wallis test is 0.0006. Simply put, this means that there is a 0.06% chance that the different data subsets are all samples of the same population. If comparing all separate data subsets, the *p*-value returned is <0.0001. If comparing only two data subsets, the *p*-value returned may be larger. For example, if comparing the data subsets for rock domains RFM029 and RFM045, the returned *p*-value is 0.081 (which still is low). It should be noted that although the Kruskal-Wallis test gives information on whether the data subsets differ, it does not say whether the differences are large or small.

For all data subsets (including quantitative data only) the arithmetic mean $\bar{x}$ and the standard deviation *STD* of $d_{mean}$ and $\log_{10}(d_{mean})$ were calculated. These data are shown in Table 3-2.

The arithmetic mean of $\log_{10}(d_{mean})$ of each data subset is marked by a black ring in Figure 3-2 (left images). When sampling a number of data points from a population, the arithmetic mean $\bar{x}$ of the data subset may not coincide with the mean $\mu$ of the population. This gives rise to an uncertainty in how well the data subset's arithmetic mean represents the mean of the population. This uncertainty has been analysed resulting in a two-sided confidence limit for the mean (see Section 2.3.3) with the underlying assumption that the uncertainty is symmetrically distributed. For each data subset, the uncertainty range of $\mu$ is shown by the black line. In addition, in Figure 3-2 (left images), the standard deviation of $\log_{10}(d_{mean})$ for each data subset is illustrated by the green line. Here one standard deviation on each side of $\bar{x}$ is displayed. To avoid including too much information in Figure 3-2, we have refrained from including uncertainty ranges for how well the standard deviation *STD* of the sample represents the standard deviation $\sigma$ of the population.

**Table 3-2. Non-parametric data for calcite.**

| Calcite | | Number of data points | $\bar{x}$ of $d_{mean}$ [mm] | *STD* of $d_{mean}$ [mm] | $\bar{x}$ of $\log_{10}(d_{mean}$ [mm]) | *STD* of $\log_{10}(d_{mean}$ [mm]) |
|---|---|---|---|---|---|---|
| Elevation (mbsl) | GS–1,000[1] | 673 | 0.11 | 0.23 | –1.47 | 0.70 |
| | GS–100 | 298 | 0.12 | 0.22 | –1.37 | 0.66 |
| | 100–300 | 184 | 0.087 | 0.19 | –1.54 | 0.68 |
| | 300–500 | 148 | 0.11 | 0.30 | –1.64 | 0.77 |
| | 500–700 | 32 | 0.14 | 0.20 | –1.26 | 0.67 |
| | 700–1,000 | 11 | 0.082 | 0.10 | –1.42 | 0.59 |
| Rock domain | RFM012 | 20 | 0.32 | 0.61 | –1.16 | 0.88 |
| | RFM018 | 10 | 0.040 | 0.039 | –1.70 | 0.62 |
| | RFM021 | 80 | 0.12 | 0.29 | –1.62 | 0.76 |
| | RFM029 | 528 | 0.10 | 0.20 | –1.47 | 0.69 |
| | RFM044 | 1 | 0.030 | – | –1.52 | – |
| | RFM045 | 34 | 0.079 | 0.052 | –1.28 | 0.51 |
| Fracture domain | All FD | 199 | 0.079 | 0.18 | –1.56 | 0.65 |
| | FFM01 | 41 | 0.095 | 0.31 | –1.68 | 0.68 |
| | FFM02 | 134 | 0.074 | 0.13 | –1.56 | 0.65 |
| | FFM03 | 21 | 0.073 | 0.083 | –1.43 | 0.56 |
| | FFM04 | 1 | 0.025 | – | –1.60 | – |
| | FFM05 | 0 | – | – | – | – |
| | FFM06 | 2 | 0.19 | 0.021 | –0.73 | 0.050 |
| Deformation zone | All DZ | 422 | 0.11 | 0.23 | –1.42 | 0.70 |
| | GDZ | 181 | 0.088 | 0.18 | –1.60 | 0.76 |
| | WNW-NW | 137 | 0.13 | 0.24 | –1.29 | 0.64 |
| | NNW | 5 | 0.036 | 0.021 | –1.50 | 0.25 |
| | ENE-NNE | 88 | 0.15 | 0.32 | –1.25 | 0.63 |

[1] Data set represents the entire site.

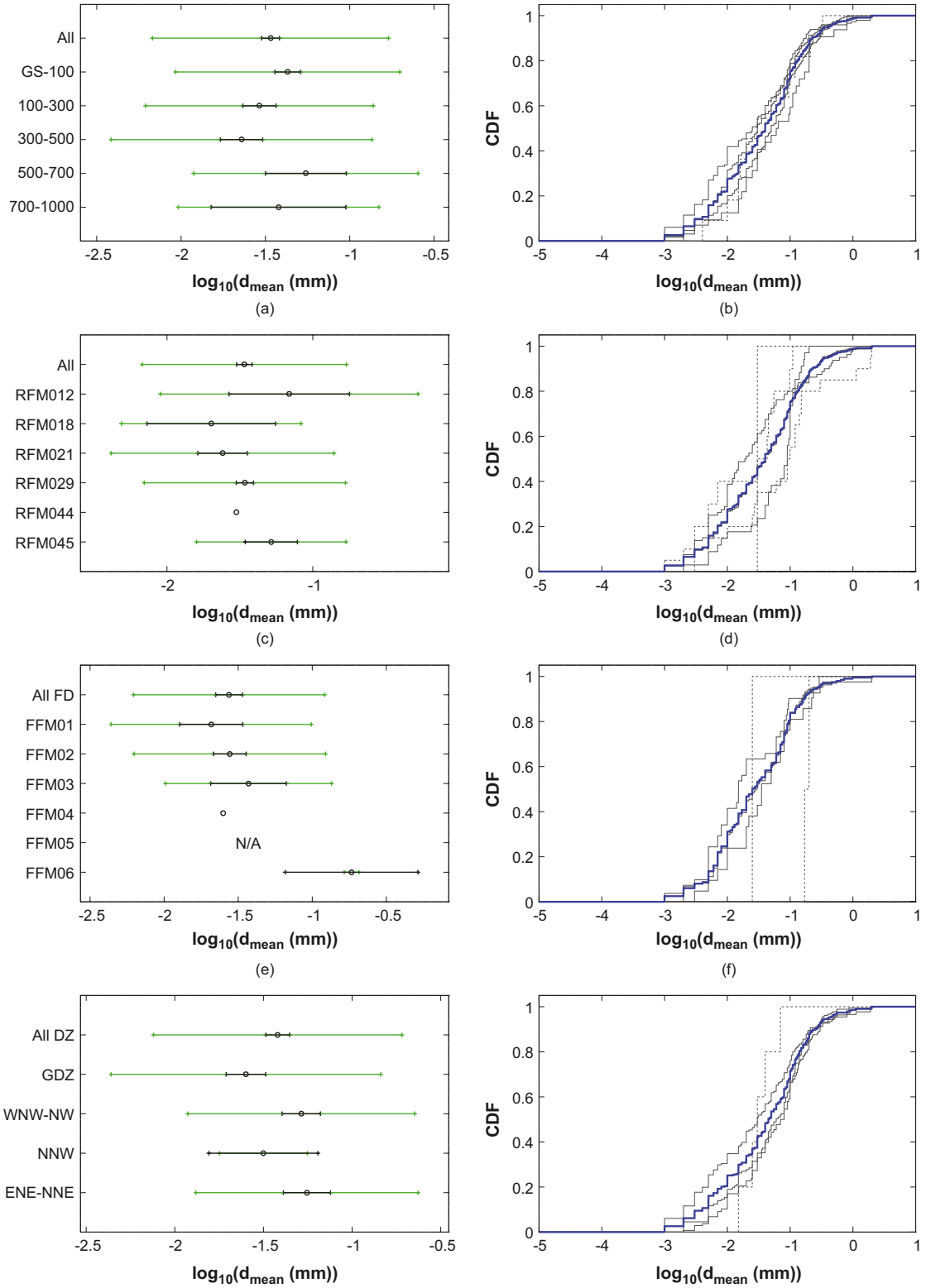


***Figure 3-2.*** *Calcite: a, c, e, g) Arithmetic mean (black dot) and standard deviation (green range) of data subsets, and uncertainty range (black range) of population mean value. b, d, f, h) Cumulative distribution functions of the separate data subsets (black curves) and of the combined data set (blue curves). CDFs for data subsets with only up to 20 data points are dotted.*

In Figure 3-2 a) and c), the combined data sets "All" for all elevations and all rock domains are identical. Note that the x-axes of the left hand figures differ in scales.

It is seen in Figure 3-2 (left images) that although there are significant differences in the arithmetic mean $\bar{x}$ for the data subsets, the uncertainty ranges of the population means $\mu$ generally overlap (or almost overlap). In Figure 3-2 (right images) one can see that there are similarities in the cumulative distribution functions of the different data subsets. The results shown in Figure 3-1 and Figure 3-2 suggest that both the occurrence and amount of calcite are similar in different rock volumes at the Forsmark site.

### 3.1.3 Parametric analysis

For the calcite data subsets from the entire site, it has been examined how well $d_{mean}$ and $\log_{10}(d_{mean})$ data fit the normal distribution. This can be done by the Shapiro-Wilk $W$ test for normality (see Section 2.4.2). In this test, the higher the $W$-value returned is, the higher degree of normality the data set has. If $W = 1$ is returned, this signify that the data are normally distributed. The Shapiro-Wilk W test can be performed for all data subsets but here, we only account for the tests on calcite data from the entire site. In this case, $W = 0.99$ is returned for $\log_{10}(d_{mean})$ data while $W = 0.43$ is returned for $d_{mean}$ data. This clearly indicates a higher degree of normality for $\log_{10}(d_{mean})$ data. This is also supported in Figure 3-3, showing a histogram of $\log_{10}(d_{mean})$ for calcite data from the entire site. Furthermore, the best fit normal distribution (red curve in left figure) and the corresponding normal score plot (right figure) are shown. For an introduction to these concepts turn to Section 2.4.

It is seen in Figure 3-3 that the normal distribution reasonably well describes the $\log_{10}(d_{mean})$ data, with $r^2 = 0.99$ in the normal score plot. Similar figures are shown for all calcite data subsets in Appendix A.

With the Shapiro-Wilk $W$ test one can also investigate whether or not the data set is a sample of a perfectly normally distributed population. However, for the data studied in this campaign, it is shown with great confidence that this is not the case. This can be exemplified with calcite data from the entire site, where the returned confidence is as low as $p < 0.0001$. This is not surprising, as one in Figure 3-3 clearly can see that the histogram deviates from the normal distribution, especially at $\log_{10}(d_{mean}) = -1$.

By making a normal score plot for each calcite data subset, taking $\mu$ from the intercept and $\sigma$ from the slope, the data in Table 3-3 are obtained.

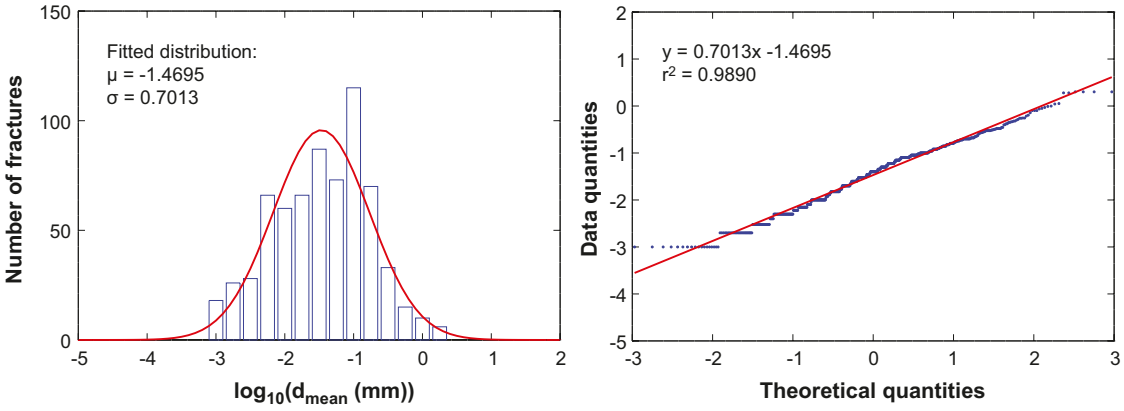


***Figure 3-3.*** *Left: Histogram of $\log_{10}(d_{mean})$ data together with best fit normal distribution. Right: normal score plot of $\log_{10}(d_{mean})$ data. Data subset used: Calcite from the entire site.*

**Table 3-3. Distribution parameters of populated fractures, calcite.**

| Calcite | | Number of data points | $\log_{10}(d_{mean})$ $\mu$ | $\sigma$ |
|---|---|---|---|---|
| Elevation (mbsl) | GS–1,000[1] | 673 | –1.47 | 0.70 |
| | GS–100 | 298 | –1.37 | 0.67 |
| | 100–300 | 184 | –1.54 | 0.69 |
| | 300–500 | 148 | –1.64 | 0.78 |
| | 500–700 | 32 | –1.26 | 0.71 |
| | 700–1,000 | 11 | –1.42 | 0.70 |
| Rock domain | RFM012 | 20 | –1.16 | 0.97 |
| | RFM018 | 10 | –1.70 | 0.71 |
| | RFM021 | 80 | –1.62 | 0.79 |
| | RFM029 | 528 | –1.47 | 0.69 |
| | RFM044 | 1 | –1.52 | – |
| | RFM045 | 34 | –1.28 | 0.51 |
| Fracture domain | All FD | 199 | –1.56 | 0.66 |
| | FFM01 | 41 | –1.68 | 0.70 |
| | FFM02 | 134 | –1.56 | 0.66 |
| | FFM03 | 21 | –1.43 | 0.62 |
| | FFM04 | 1 | –1.60 | – |
| | FFM05 | 0 | – | – |
| | FFM06 | 2 | –0.73 | 0.082 |
| Deformation zone | All DZ | 422 | –1.42 | 0.70 |
| | GDZ | 181 | –1.60 | 0.77 |
| | WNW-NW | 137 | –1.29 | 0.65 |
| | NNW | 5 | –1.50 | 0.33 |
| | ENE-NNE | 88 | –1.25 | 0.64 |

[1] Data set represents the entire site.

Figure 3-4 illustrates the distributions of Table 3-3, where the distribution representing the entire site is shown by the red line. Distributions of data subsets with more than 20 data points are shown by the solid lines, while distributions of data subsets with fewer data points are shown by the shaded lines.

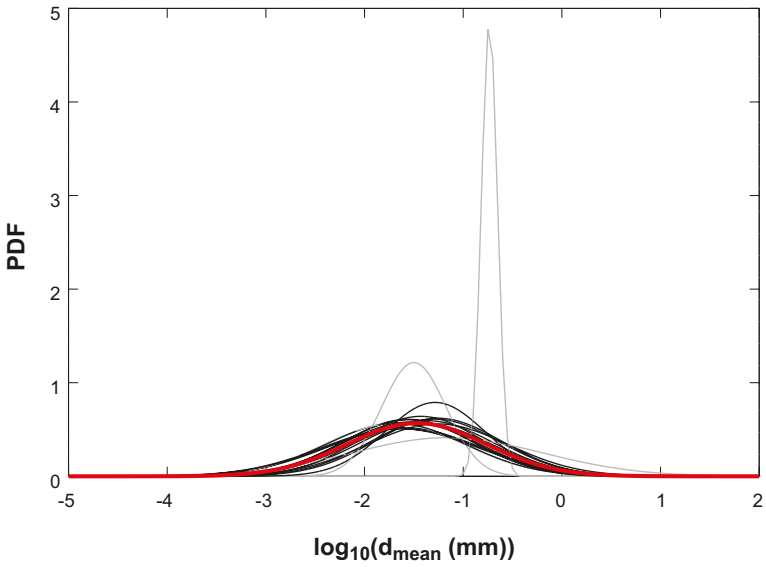


***Figure 3-4.*** *Illustration of normal distributions of Table 3-3. Distributions of data subsets with only up to 20 data points are shaded.*

Upon examination of Figure 3-4 one could suggest that the best fit distribution for data from the entire site reasonably well represents the different rock volumes of the site. The distributions for deformation zones WNW-NW and ENE-NNE are slightly shifted towards higher calcite thickness. The distribution that deviates the most represents the data set from FFM06, consisting of only two data points. Also the data set from NNW deformation zones, consisting of only five data points, significantly deviates.

## 3.2 Chlorite

In this section, equivalent tables and figures are presented for chlorite as for calcite in Section 3.1. In Section 3.1 information on how to interpret the tables, figures, and notations is found. An introduction to the rock volumes represented by the data subsets is found in Section 2.2.2.

### 3.2.1 The data subsets

In Table 3-4, information on the number of data points, $f_{quant}$, and $f_{qual}$ is summarised for the different chlorite data subsets.

The data are illustrated in Figure 3-5, showing the fractions of the fractures where chlorite is found in quantitative amounts, qualitative amounts only, or not at all.

**Table 3-4. Amounts of data in different data subsets, chlorite.**

| Chlorite | | Total number of fractures | Number of data points | $f_{qual}$ (%) | $f_{quant}$ (%) |
|---|---|---|---|---|---|
| Elevation (mbsl) | GS–1,000[1] | 2,071 | 505 | 52 | 24 |
| | GS–100 | 835 | 173 | 42 | 21 |
| | 100–300 | 531 | 115 | 58 | 22 |
| | 300–500 | 543 | 142 | 54 | 26 |
| | 500–700 | 114 | 43 | 81 | 38 |
| | 700–1,000 | 48 | 32 | 75 | 67 |
| Rock domain | RFM012 | 79 | 21 | 57 | 27 |
| | RFM018 | 30 | 17 | 90 | 57 |
| | RFM021 | 226 | 40 | 54 | 18 |
| | RFM029 | 1,596 | 383 | 49 | 24 |
| | RFM044 | 8 | 4 | 63 | 50 |
| | RFM045 | 132 | 40 | 75 | 30 |
| Fracture domain | All FD | 602 | 139 | 55 | 23 |
| | FFM01 | 152 | 31 | 58 | 20 |
| | FFM02 | 321 | 71 | 56 | 22 |
| | FFM03 | 107 | 28 | 44 | 26 |
| | FFM04 | 8 | 3 | 88 | 38 |
| | FFM05 | 3 | 2 | 67 | 67 |
| | FFM06 | 11 | 4 | 82 | 36 |
| Deformation zone | All DZ | 1,333 | 338 | 51 | 25 |
| | GDZ | 640 | 164 | 46 | 26 |
| | WNW-NW | 371 | 79 | 44 | 21 |
| | NNW | 22 | 9 | 86 | 41 |
| | ENE-NNE | 280 | 76 | 66 | 27 |

[1] Data set represents the entire site.

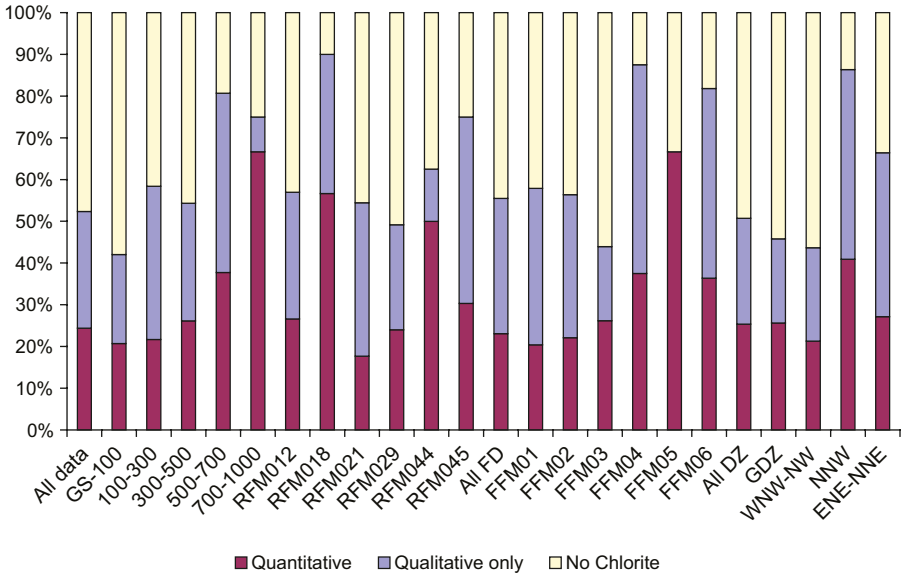


***Figure 3-5.*** *Fractions of fractures populated or unpopulated by chlorite.*

As can be seen from Table 3-4 and Figure 3-5, on average 24% of all fractures contain enough chlorite to be quantitatively mapped, while 48% of all fractures contain no chlorite at all. The bars in Figure 3-5 that clearly deviates represent rock volumes where only few fractures were mapped, and it can be questioned how representative they are. Perhaps one can suggest that chlorite is somewhat more abundantly present below repository depth than above.

### 3.2.2 Non-parametric analysis

As for calcite, an analysis was made by the Kruskal-Wallis test, indicating with great confidence that the different chlorite data subsets are not all samples of the exact same population. If comparing all separate data subsets, the *p*-value returned is 0.0006.

For all data subsets (including quantitative data only) the arithmetic mean $\bar{x}$ and the standard deviation *STD* of $d_{mean}$ and $\log_{10}(d_{mean})$ were calculated. These data are shown in Table 3-5**.**

The arithmetic mean $\bar{x}$ of $\log_{10}(d_{mean})$ of each data subset is marked by a black ring in Figure 3-6 (left). The uncertainty range of $\mu$ is shown by the black line. In addition, in Figure 3-6 (left), the standard deviation of $\log_{10}(d_{mean})$ for each data subset is illustrated by the green line. Here one standard deviation on each side of $\bar{x}$ is displayed.

It is seen in Figure 3-6 (left) that although there are significant differences in the arithmetic mean $\bar{x}$ for the data subsets, the uncertainty ranges of the population means $\mu$ generally overlap, or almost overlap. In Figure 3-6 (right images) one can see that there are similarities in the cumulative distribution functions of the different data subsets. The results shown in Figure 3-5 and Figure 3-6 suggest that both the occurrence and amount of chlorite are similar in different rock volumes at the Forsmark site.

**Table 3-5. Non-parametric data for chlorite.**

| Chlorite | | Number of data points | $\overline{x}$ of $d_{mean}$ [mm] | *STD* of $d_{mean}$ [mm] | $\overline{x}$ of $\log_{10}(d_{mean}$ [mm]) | *STD* of $\log_{10}(d_{mean}$ [mm]) |
|---|---|---|---|---|---|---|
| Elevation (mbsl) | GS–1,000[1] | 505 | 0.22 | 0.44 | –0.93 | 0.47 |
| | GS–100 | 173 | 0.16 | 0.18 | –0.98 | 0.45 |
| | 100–300 | 115 | 0.26 | 0.48 | –0.89 | 0.53 |
| | 300–500 | 142 | 0.20 | 0.31 | –0.93 | 0.44 |
| | 500–700 | 43 | 0.19 | 0.16 | –0.88 | 0.42 |
| | 700–1,000 | 32 | 0.48 | 1.28 | –0.80 | 0.57 |
| Rock domain | RFM012 | 21 | 0.34 | 0.55 | –0.89 | 0.67 |
| | RFM018 | 17 | 0.29 | 0.37 | –0.66 | 0.28 |
| | RFM021 | 40 | 0.15 | 0.17 | –1.13 | 0.63 |
| | RFM029 | 383 | 0.22 | 0.48 | –0.93 | 0.45 |
| | RFM044 | 4 | 0.14 | 0.050 | –0.88 | 0.16 |
| | RFM045 | 40 | 0.17 | 0.10 | –0.84 | 0.34 |
| Fracture domain | All FD | 139 | 0.25 | 0.46 | –0.90 | 0.50 |
| | FFM01 | 31 | 0.21 | 0.20 | –0.85 | 0.45 |
| | FFM02 | 71 | 0.17 | 0.32 | –1.03 | 0.49 |
| | FFM03 | 28 | 0.50 | 0.81 | –0.68 | 0.55 |
| | FFM04 | 3 | 0.28 | 0.19 | –0.62 | 0.29 |
| | FFM05 | 2 | 0.15 | 0.064 | –0.86 | 0.20 |
| | FFM06 | 4 | 0.17 | 0.024 | –0.77 | 0.063 |
| Deformation zone | All DZ | 338 | 0.21 | 0.46 | –0.91 | 0.43 |
| | GDZ | 164 | 0.24 | 0.63 | –0.94 | 0.47 |
| | WNW-NW | 79 | 0.19 | 0.22 | –0.89 | 0.37 |
| | NNW | 9 | 0.23 | 0.11 | –0.68 | 0.22 |
| | ENE-NNE | 76 | 0.18 | 0.12 | –0.89 | 0.43 |

[1] Data set represents the entire site.

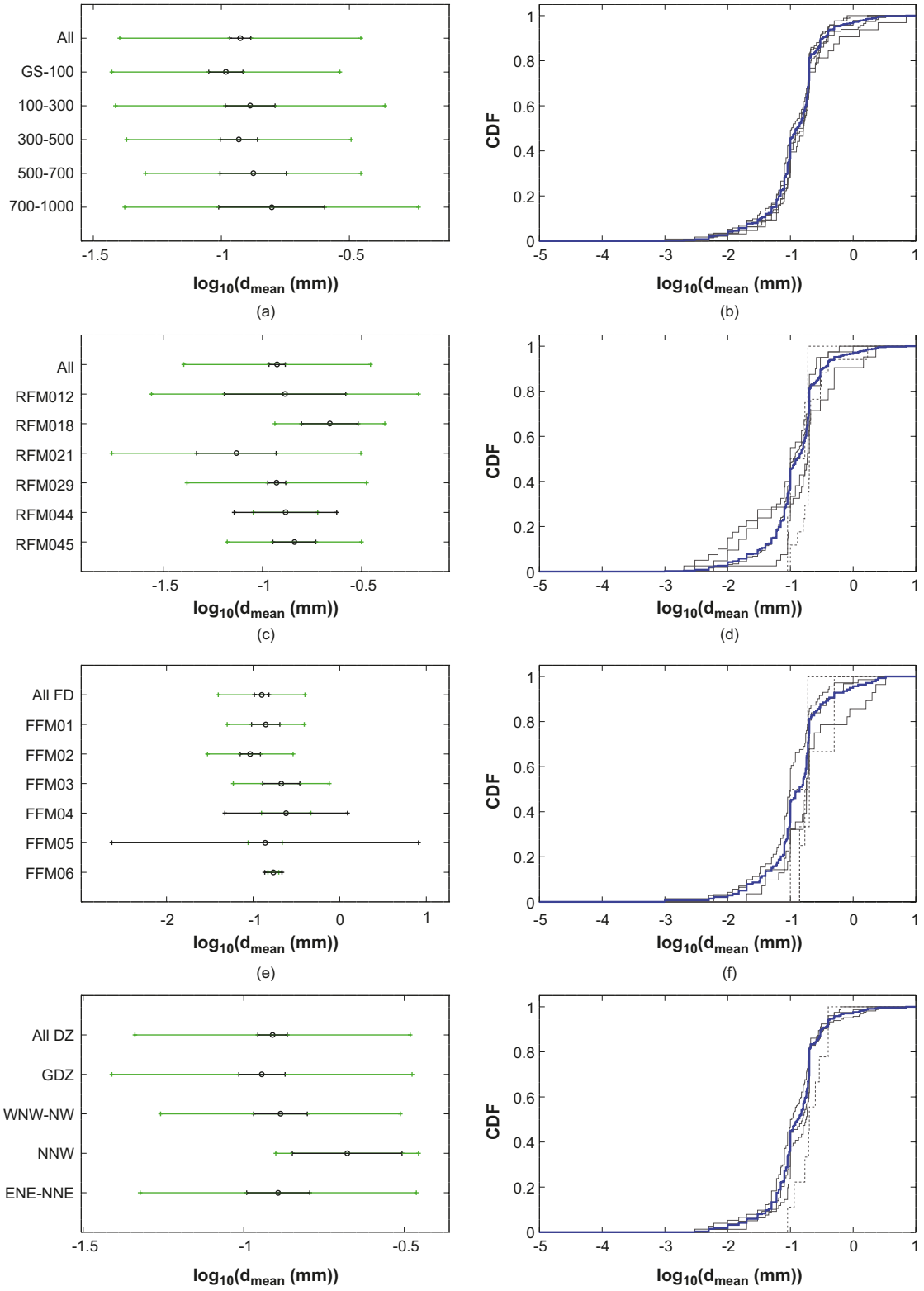


***Figure 3-6.*** *Chlorite: a, c, e, g) Arithmetic mean (black dot) and standard deviation (green range) of data subsets, and uncertainty range (black range) of population mean value. b, d, f, h) Cumulative distribution functions of the separate data subsets (black curves) and of the combined data set (blue curves). CDFs for data subsets with only up to 20 data points are dotted.*

### 3.2.3 Parametric analysis

As for calcite, the normality of the chlorite data subset from the entire site was investigated by means of the Shapiro-Wilk $W$ test. It was shown that the normal distribution is much better fitted to $\log_{10}(d_{mean})$ data than to $d_{mean}$ data. The $W$-value retuned for $d_{mean}$ data is 0.32 and for $\log_{10}(d_{mean})$ data the returned $W$-value is 0.93. Concerning $\log_{10}(d_{mean})$ data, this is a lower $W$-value than for calcite, and one can expect a larger deviation from the normal distribution. Figure 3-7 (left) shows a histogram of $\log_{10}(d_{mean})$ for chlorite data from the entire site, together with the normal distribution that is best fitted to the data. In the right image the associated normal score plot is shown.

It is seen in Figure 3-7 that the normal distribution only fairly well describes the $\log_{10}(d_{mean})$ data, with $r^2 = 0.93$ in the normal score plot. The plateaus at $\log_{10}(d_{mean}) = -1$ and $-0.7$ (also seen in Figure 3-6) stems from a bias effect that is discussed in Section 2.4.4. Similar figures are shown for all chlorite data subsets in Appendix A.

By making a normal score plot for each chlorite data subset, taking $\mu$ from the intercept and $\sigma$ from the slope, the data in Table 3-6 are obtained.

Figure 3-8 illustrates the distributions of Table 3-6, where the distribution representing the entire site is shown by the red line. Distributions of data subsets with more than 20 data points are shown by the solid lines, while distributions of data subsets with up to 20 data points are shown by the shaded lines.

Upon examination of Figure 3-8, one could suggest that the best fit distribution for data from the entire site reasonably well represents the different rock volumes of the site. The distributions that deviate the most represent data subsets of few data points, such as FFM06.

**Table 3-6. Distribution parameters of populated fractures, chlorite.**

| Chlorite | | Number of data points | $\log_{10}(d_{mean})$ $\mu$ | $\sigma$ |
|---|---|---|---|---|
| Elevation (mbsl) | GS–1,000[1] | 505 | –0.93 | 0.46 |
| | GS–100 | 173 | –0.98 | 0.44 |
| | 100–300 | 115 | –0.89 | 0.51 |
| | 300–500 | 142 | –0.93 | 0.43 |
| | 500–700 | 43 | –0.88 | 0.43 |
| | 700–1,000 | 32 | –0.80 | 0.59 |
| Rock domain | RFM012 | 21 | –0.89 | 0.74 |
| | RFM018 | 17 | –0.66 | 0.27 |
| | RFM021 | 40 | –1.13 | 0.64 |
| | RFM029 | 383 | –0.93 | 0.44 |
| | RFM044 | 4 | –0.88 | 0.21 |
| | RFM045 | 40 | –0.84 | 0.29 |
| Fracture domain | All FD | 139 | –0.90 | 0.49 |
| | FFM01 | 31 | –0.85 | 0.45 |
| | FFM02 | 71 | –1.03 | 0.49 |
| | FFM03 | 28 | –0.68 | 0.58 |
| | FFM04 | 3 | –0.62 | 0.41 |
| | FFM05 | 2 | –0.86 | 0.32 |
| | FFM06 | 4 | –0.77 | 0.080 |
| Deformation zone | All DZ | 338 | –0.91 | 0.42 |
| | GDZ | 164 | –0.94 | 0.47 |
| | WNW-NW | 79 | –0.89 | 0.37 |
| | NNW | 9 | –0.68 | 0.27 |
| | ENE-NNE | 76 | –0.89 | 0.40 |

[1] Data set represents the entire site.

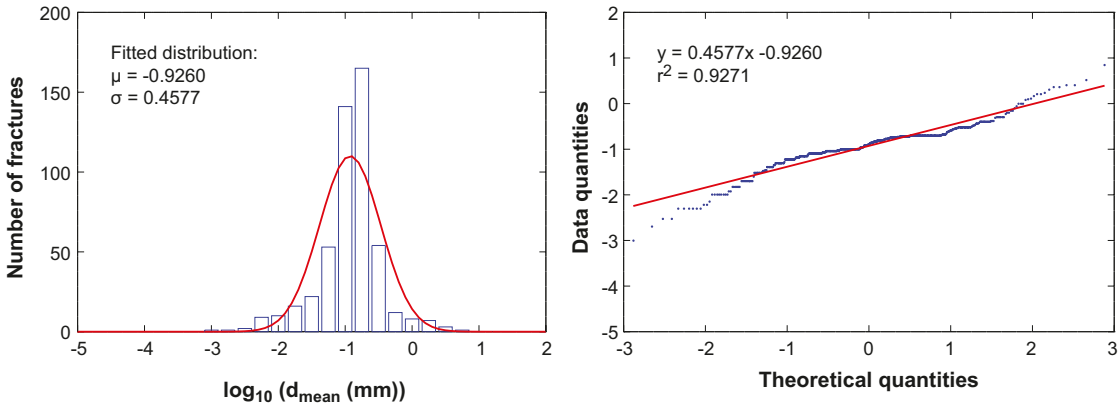


***Figure 3-7.*** *Left: Histogram of $log_{10}(d_{mean})$ data together with best fit normal distribution. Right: Normal score plot of $log_{10}(d_{mean})$ data. Data subset used: Chlorite from the entire site.*

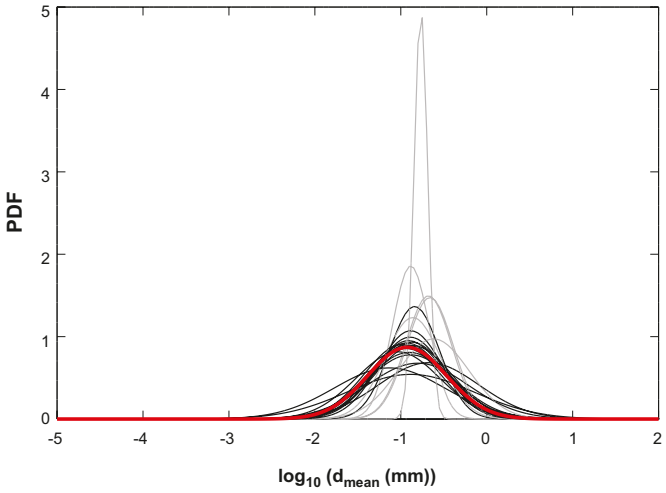


***Figure 3-8.*** *Illustration of normal distributions of Table 3-6. Distributions of data sets with only up to 20 data points are shaded.*

## 3.3 Clay minerals, as a group

In this section results from what is mapped as "clay minerals as a group" are shown. In the following text we sometimes use the shorter notation "clay minerals". In this section, equivalent tables and figures are presented for clay minerals, as for calcite in Section 3.1. In Section 3.1 information on how to interpret the tables, figures, and notations is found. An introduction to the rock volumes represented by the data subsets is found in Section 2.2.2.

### 3.3.1 The data subsets

In Table 3-7, information on the number of data points, $f_{quant}$, and $f_{qual}$ is summarised for the different clay minerals data subsets.

The data are illustrated in Figure 3-9, showing the fractions of the fractures where clay minerals are found in quantitative amounts, qualitative amounts only, or not at all.

As can be seen from Table 3-7 and Figure 3-9, on average 11% of all fractures contain enough clay minerals to be quantitatively mapped, while 72% of all fractures contain no clay mineral at all. For the data sets containing much data, fairly similar values are shown. For example, if only examining the data sets representing rock volumes where more than 100 fractures were mapped, 4 to 18% of the fractures were quantitatively mapped whereas 65 to 84% of the fractures contained no clay mineral.

**Table 3-7. Amounts of data in different data subsets, clay minerals as a group.**

| Clay minerals as a group | | Total number of fractures | Number of data points | $f_{qual}$ (%) | $f_{quant}$ (%) |
|---|---|---|---|---|---|
| Elevation (mbsl) | GS–1,000[1] | 2,071 | 231 | 28 | 11 |
| | GS–100 | 835 | 118 | 34 | 14 |
| | 100–300 | 531 | 41 | 19 | 8 |
| | 300–500 | 543 | 50 | 28 | 9 |
| | 500–700 | 114 | 8 | 20 | 7 |
| | 700–1,000 | 48 | 14 | 40 | 29 |
| Rock domain | RFM012 | 79 | 14 | 27 | 18 |
| | RFM018 | 30 | 6 | 30 | 20 |
| | RFM021 | 226 | 6 | 20 | 3 |
| | RFM029 | 1,596 | 189 | 28 | 12 |
| | RFM044 | 8 | 2 | 38 | 25 |
| | RFM045 | 132 | 14 | 33 | 11 |
| Fracture domain | All FD | 602 | 50 | 26 | 8 |
| | FFM01 | 152 | 6 | 26 | 4 |
| | FFM02 | 321 | 39 | 29 | 12 |
| | FFM03 | 107 | 4 | 16 | 4 |
| | FFM04 | 8 | 0 | 0 | 0 |
| | FFM05 | 3 | 1 | 67 | 33 |
| | FFM06 | 11 | 0 | 18 | 0 |
| Deformation zone | All DZ | 1,333 | 180 | 30 | 14 |
| | GDZ | 640 | 115 | 35 | 18 |
| | WNW-NW | 371 | 28 | 22 | 8 |
| | NNW | 22 | 6 | 55 | 27 |
| | ENE-NNE | 280 | 30 | 26 | 11 |

[1] Data set represents the entire site.

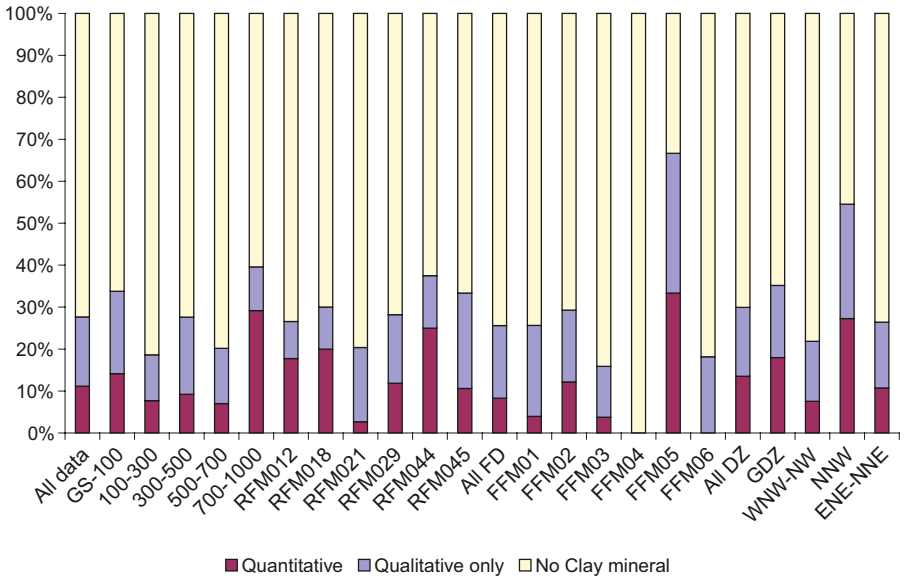


***Figure 3-9.*** *Fractions of fractures populated or unpopulated by clay minerals, as a group.*

### 3.3.2 Non-parametric analysis

As for calcite, an analysis was made by the Kruskal-Wallis test, indicating that it is likely that the different data subsets are not all samples of the exact same population ($p = 0.29$ if comparing all separate data sets).

For all data subsets (including quantitative data only) the arithmetic mean $\overline{x}$ and the standard deviation *STD* of $d_{mean}$ and $\log_{10}(d_{mean})$ were calculated. These data are shown in Table 3-8.

The arithmetic mean $\overline{x}$ of $\log_{10}(d_{mean})$ of each data subset is marked by a black ring in Figure 3-10 (left). The uncertainty range of $\mu$ is shown by the black line. In addition, the standard deviation of $\log_{10}(d_{mean})$ for each data subset is illustrated by the green line. Here one standard deviation on each side of $\overline{x}$ is displayed.

As can be seen in Table 3-7, the data subsets for clay minerals do not include as many data points as for calcite and chlorite. Therefore, there is in many cases a larger uncertainty in $\mu$. However, generally the uncertainty ranges overlap (note the different scales of the x-axes in the left hand figures). In Figure 3-10 (right) one can see that there are similarities in the cumulative distribution functions of the different data subsets. This is especially true for the data sets of more than 20 data points. The results shown in Figure 3-9 and Figure 3-10 suggest that both the occurrence and amount of clay minerals are similar in different rock volumes at the Forsmark site.

**Table 3-8. Non-parametric data for clay minerals as a group.**

| Clay minerals as a group | | Number of data points | $\overline{x}$ of $d_{mean}$ [mm] | *STD* of $d_{mean}$ [mm] | $\overline{x}$ of $\log_{10}(d_{mean}$ [mm]) | *STD* of $\log_{10}(d_{mean}$ [mm]) |
|---|---|---|---|---|---|---|
| | GS–1,000[1] | 231 | 0.14 | 0.27 | –1.09 | 0.44 |
| Elevation (mbsl) | GS–100 | 118 | 0.15 | 0.27 | –1.03 | 0.41 |
| | 100–300 | 41 | 0.11 | 0.13 | –1.21 | 0.52 |
| | 300–500 | 50 | 0.15 | 0.40 | –1.14 | 0.42 |
| | 500–700 | 8 | 0.07 | 0.055 | –1.39 | 0.52 |
| | 700–1,000 | 14 | 0.16 | 0.094 | –0.90 | 0.34 |
| Rock domain | RFM012 | 14 | 0.10 | 0.065 | –1.12 | 0.36 |
| | RFM018 | 6 | 0.13 | 0.13 | –1.09 | 0.54 |
| | RFM021 | 6 | 0.086 | 0.060 | –1.24 | 0.55 |
| | RFM029 | 189 | 0.15 | 0.30 | –1.09 | 0.45 |
| | RFM044 | 2 | 0.13 | 0.042 | –0.92 | 0.15 |
| | RFM045 | 14 | 0.14 | 0.093 | –0.99 | 0.37 |
| Fracture domain | All FD | 50 | 0.21 | 0.54 | –1.09 | 0.52 |
| | FFM01 | 6 | 0.060 | 0.055 | –1.43 | 0.54 |
| | FFM02 | 39 | 0.18 | 0.43 | –1.07 | 0.47 |
| | FFM03 | 4 | 0.76 | 1.39 | –0.85 | 0.93 |
| | FFM04 | 0 | – | – | – | – |
| | FFM05 | 1 | 0.095 | – | –1.02 | – |
| | FFM06 | 0 | – | – | – | – |
| Deformation zone | All DZ | 180 | 0.12 | 0.12 | –1.09 | 0.42 |
| | GDZ | 115 | 0.12 | 0.13 | –1.06 | 0.39 |
| | WNW-NW | 28 | 0.10 | 0.093 | –1.22 | 0.49 |
| | NNW | 6 | 0.20 | 0.18 | –0.94 | 0.60 |
| | ENE-NNE | 30 | 0.11 | 0.08 | –1.09 | 0.40 |

[1] Data set represents the entire site.

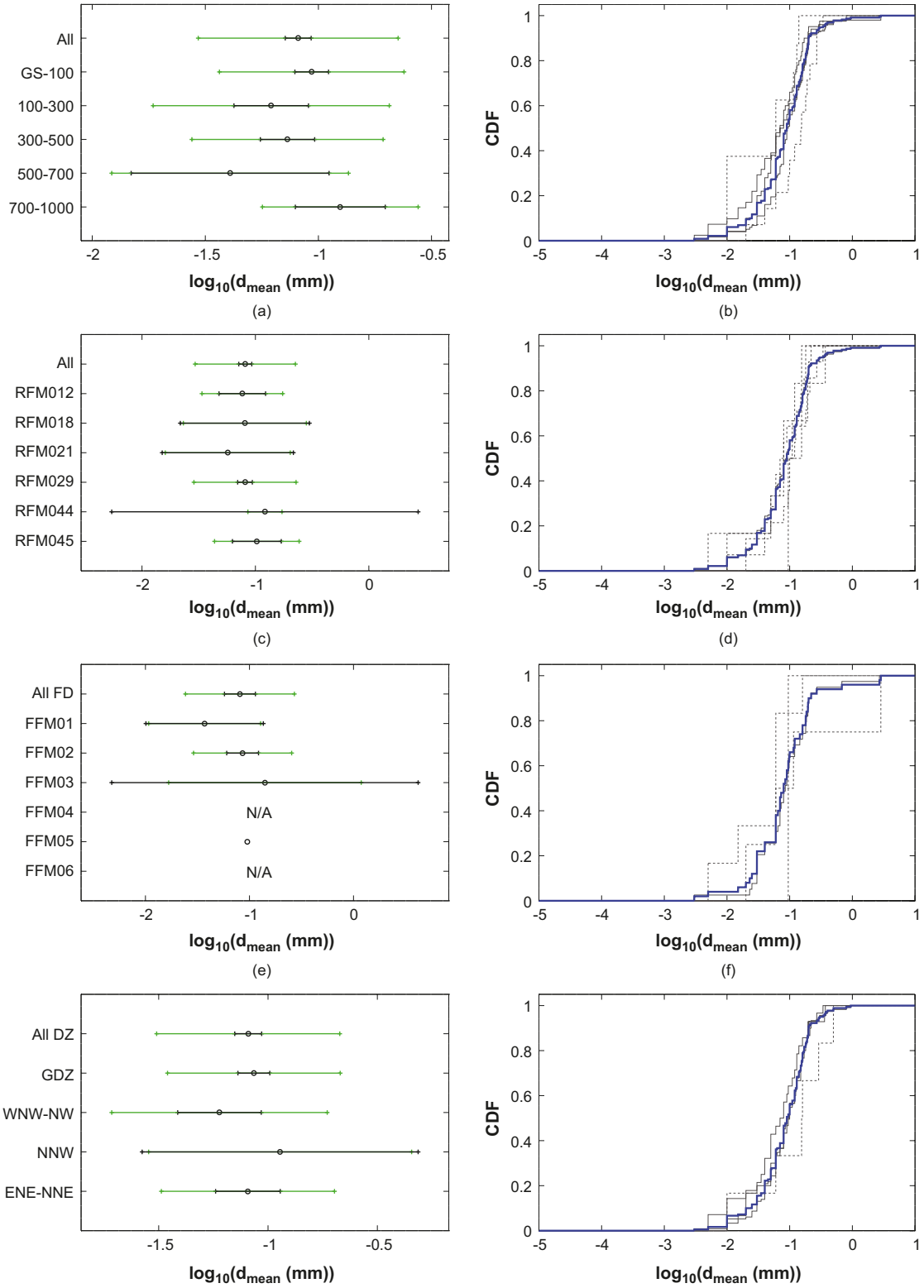


***Figure 3-10.*** *Clay minerals: a, c, e, g) Arithmetic mean (black dot) and standard deviation (green range) of data subsets, and uncertainty range (black range) of population mean value. b, d, f, h) Cumulative distribution functions of the separate data subsets (black curves) and of the combined data set (blue curves). CDFs for data subsets with only up to 20 data points are dotted.*

### 3.3.3 Parametric analysis

The normality of the clay minerals data set from the entire site was investigated by means of the Shapiro-Wilk $W$ test. It was shown that the normal distribution is much better fitted to $\log_{10}(d_{mean})$ data than to $d_{mean}$ data. The $W$-value retuned for $d_{mean}$ data is 0.32 and for $\log_{10}(d_{mean})$ data the returned $W$-value is 0.96. Figure 3-11 (left) shows a histogram of $\log_{10}(d_{mean})$ for clay minerals data from the entire site, together with the normal distribution that is best fitted to the data (red curve in left figure). In the right image the associated normal score plot is shown.

It is seen in Figure 3-11 that the normal distribution reasonably well describes the $\log_{10}(d_{mean})$ data, with $r^2$=0.95 in the normal score plot. Similar figures are shown for all clay minerals data subsets in Appendix A.

By making a normal score plot for each clay minerals data subset, taking $\mu$ from the intercept and $\sigma$ from the slope, the data in Table 3-9 are obtained.

Figure 3-12 illustrates the distributions of Table 3-9, where the distribution representing the entire site is shown by the red line. Distributions of data subsets with more than 20 data points are shown by the solid lines, while distributions of data subsets with up to 20 data points are shown by the shaded lines.

Upon examination of Figure 3-12, one can suggest that the best fit distribution for data from the entire site reasonably well represents the different rock volumes of the site. The distributions that deviate the most represent data subsets of few data points, such as RFM044 and FFM03.

**Table 3-9. Distribution parameters of populated fractures, clay minerals as a group.**

| Clay minerals as a group | | Number of data points | $\log_{10}(d_{mean})$ | |
|---|---|---|---|---|
| | | | $\mu$ | $\sigma$ |
| Elevation (mbsl) | GS–1,000[1] | 231 | –1.09 | 0.44 |
| | GS–100 | 118 | –1.03 | 0.41 |
| | 100–300 | 41 | –1.21 | 0.54 |
| | 300–500 | 50 | –1.14 | 0.43 |
| | 500–700 | 8 | –1.39 | 0.59 |
| | 700–1,000 | 14 | –0.90 | 0.38 |
| Rock domain | RFM012 | 14 | –1.12 | 0.39 |
| | RFM018 | 6 | –1.09 | 0.68 |
| | RFM021 | 6 | –1.24 | 0.63 |
| | RFM029 | 189 | –1.09 | 0.45 |
| | RFM044 | 2 | –0.92 | 0.25 |
| | RFM045 | 14 | –0.99 | 0.41 |
| Fracture domain | All FD | 50 | –1.09 | 0.53 |
| | FFM01 | 6 | –1.43 | 0.65 |
| | FFM02 | 39 | –1.07 | 0.48 |
| | FFM03 | 4 | –0.85 | 1.22 |
| | FFM04 | 0 | – | – |
| | FFM05 | 1 | –1.02 | – |
| | FFM06 | 0 | – | – |
| Deformation zone | All DZ | 180 | –1.09 | 0.42 |
| | GDZ | 115 | –1.06 | 0.40 |
| | WNW-NW | 28 | –1.22 | 0.52 |
| | NNW | 6 | –0.94 | 0.74 |
| | ENE-NNE | 30 | –1.09 | 0.42 |

[1] Data set represents the entire site.

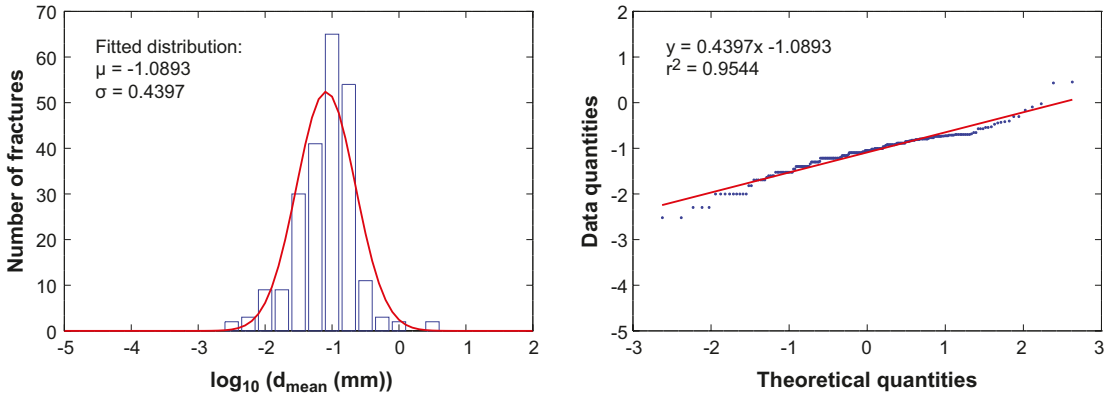


***Figure 3-11.*** *Left: Histogram of $log_{10}(d_{mean})$ data together with best fit normal distribution. Right: normal score plot of $log_{10}(d_{mean})$ data. Data subset used: Clay minerals from the entire site.*

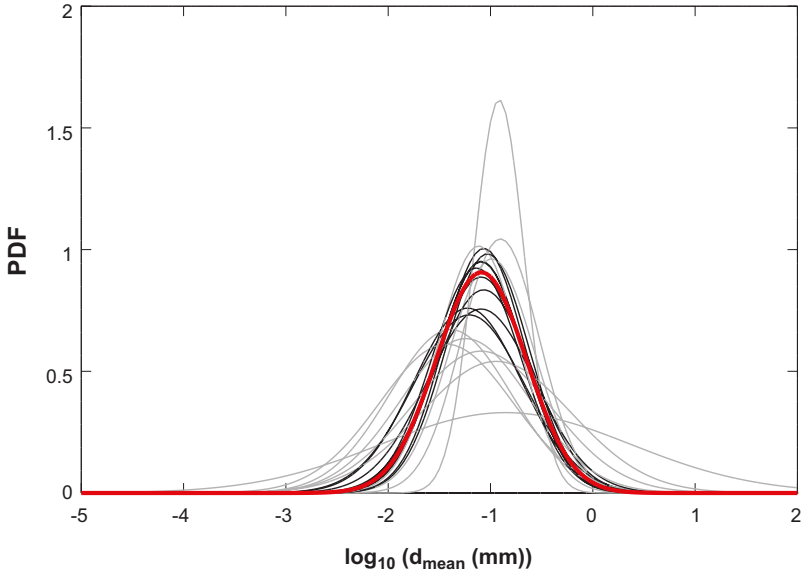


***Figure 3-12.*** *Illustration of normal distributions of Table 3-9. Distributions of data subsets with only up to 20 data points are shaded.*

## 3.4 Hematite and hematite pigmented minerals

This section presents results for hematite and hematite pigmented minerals. For the latter, only qualitative results are presented. The reason for this is that there is little quantitative knowledge on the fraction of hematite that different hematite pigmented minerals hold, except for that the fraction is very small /Eklund and Mattsson 2009/.

In this section, equivalent tables and figures are presented for hematite as for calcite in Section 3.1. In Section 3.1 information on how to interpret the tables, figures, and notations is found. In addition some qualitative information concerning the hematite pigmented minerals are added to the tables and figures. An introduction to the rock volumes represented by the data subsets is found in Section 2.2.2.

### 3.4.1 The data subsets

In Table 3-10, information on the number of data points, $f_{quant}$, and $f_{qual}$ is summarised for the different hematite data subsets. In addition, the number of fractures containing any amount of hematite pigmented minerals is shown, together with $f_{qual}$ for hematite pigmented minerals.

The data for hematite is illustrated in Figure 3-13, showing the fractions of the fractures where hematite is found in quantitative amounts, qualitative amounts only, or not at all.

As can be seen from Table 3-10 and Figure 3-13, on average less than 1% of all fractures contain enough amount of hematite to be quantitatively mapped, while 98% of all fractures contain no hematite at all.

In Figure 3-14, the fractions of fractures containing hematite pigmented (impregnated) mineral are show. As seen, on average 14% of the fractures contain hematite pigmented mineral.

**Table 3-10. Amounts of data in different data subsets, hematite and hematite pigmented minerals.**

| Hematite and hematite pigmented minerals | | Total number of fractures | Hematite: Number of data points | Hematite: $f_{qual}$ (%) | Hematite: $f_{quant}$ (%) | Hem. pig.[2] Number of data points | Hem. pig.[2] $f_{qual}$ (%) |
|---|---|---|---|---|---|---|---|
| Elevation (mbsl) | GS–1,000[1] | 2,071 | 8 | 2 | 0.4 | 292 | 14 |
| | GS–100 | 835 | 5 | 2 | 1 | 176 | 21 |
| | 100–300 | 531 | 2 | 2 | 0.4 | 53 | 10 |
| | 300–500 | 543 | 1 | 0 | 0.2 | 37 | 7 |
| | 500–700 | 114 | 0 | 2 | 0 | 17 | 15 |
| | 700–1,000 | 48 | 0 | 2 | 0 | 9 | 19 |
| Rock domain | RFM012 | 79 | 2 | 5 | 3 | 29 | 37 |
| | RFM018 | 30 | 0 | 0 | 0 | 6 | 20 |
| | RFM021 | 226 | 0 | 4 | 0 | 42 | 19 |
| | RFM029 | 1,596 | 6 | 1 | 0.4 | 198 | 12 |
| | RFM044 | 8 | 0 | 0 | 0 | 0 | 0 |
| | RFM045 | 132 | 0 | 1 | 0 | 17 | 13 |
| Fracture domain | All FD | 602 | 4 | 2 | 1 | 39 | 6 |
| | FFM01 | 152 | 0 | 1 | 0 | 5 | 3 |
| | FFM02 | 321 | 4 | 3 | 1 | 29 | 9 |
| | FFM03 | 107 | 0 | 0 | 0 | 1 | 1 |
| | FFM04 | 8 | 0 | 0 | 0 | 3 | 38 |
| | FFM05 | 3 | 0 | 0 | 0 | 0 | 0 |
| | FFM06 | 11 | 0 | 0 | 0 | 1 | 9 |
| Deformation zone | All DZ | 1,333 | 4 | 1 | 0.3 | 213 | 16 |
| | GDZ | 640 | 3 | 1 | 0.5 | 121 | 19 |
| | WNW-NW | 371 | 1 | 1 | 0.3 | 56 | 15 |
| | NNW | 22 | 0 | 0 | 0 | 5 | 23 |
| | ENE-NNE | 280 | 0 | 1 | 0 | 30 | 11 |

[1] Data set represents the entire site.
[2] Hem. pig. = hematite pigmented minerals.

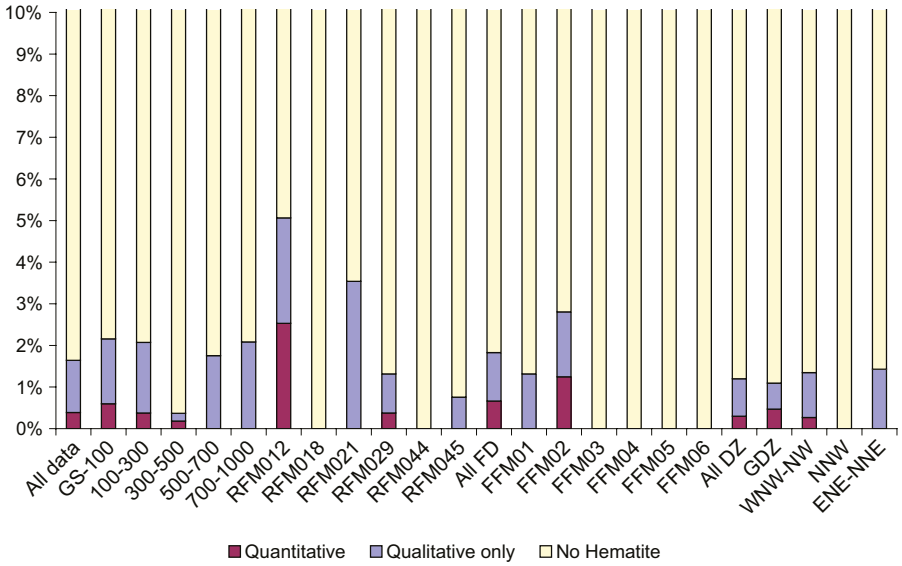


***Figure 3-13.*** *Fractions of fractures populated or unpopulated by hematite (excluding hematite pigmented minerals).*

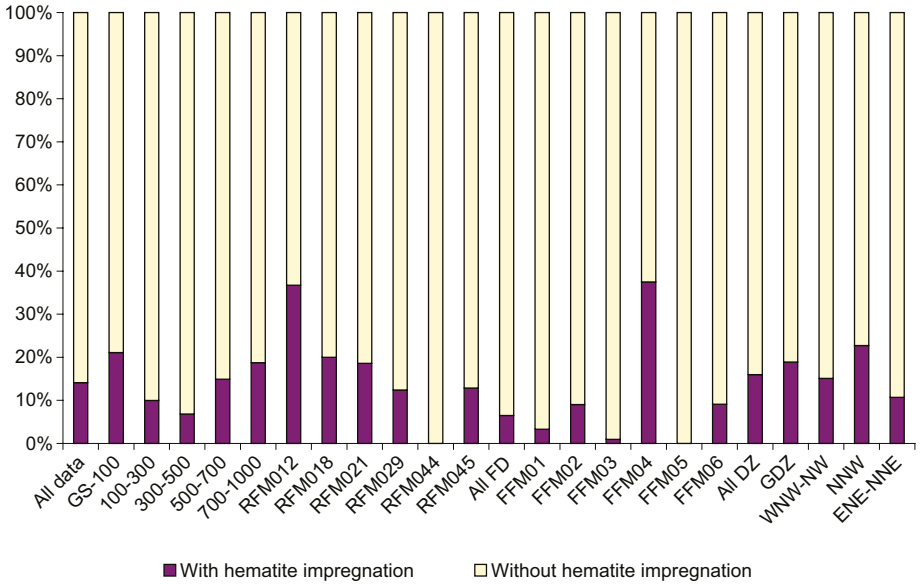


***Figure 3-14.*** *Fractions of fractures populated or unpopulated by hematite pigmented minerals.*

### 3.4.2 Non-parametric analysis – hematite

In the quantitative mineral mapping campaign, only eight fractures out of the 2,071 mapped were found to hold quantitative amounts of hematite. Due to the few data, a limited non-parametric analysis was made. No Kruskal-Wallis test was performed. For all data subsets (including quantitative data only) the arithmetic mean $\bar{x}$ and the standard deviation *STD* of $d_{mean}$ and $\log_{10}(d_{mean})$ were calculated. These data are shown in Table 3-11.

**Table 3-11. Non-parametric data for hematite.**

| Hematite | | Number of data points | $\overline{x}$ of $d_{mean}$ [mm] | *STD* of $d_{mean}$ [mm] | $\overline{x}$ of $\log_{10}(d_{mean}$ [mm]) | *STD* of $\log_{10}(d_{mean}$ [mm]) |
|---|---|---|---|---|---|---|
| Elevation (mbsl) | GS–1,000[1] | 8 | 0.019 | 0.022 | –2.01 | 0.54 |
| | GS–100 | 5 | $4.8 \cdot 10^{-3}$ | $2.3 \cdot 10^{-3}$ | –2.37 | 0.24 |
| | 100–300 | 2 | 0.053 | $3.5 \cdot 10^{-3}$ | –1.28 | 0.03 |
| | 300–500 | 1 | 0.020 | – | –1.70 | – |
| | 500–700 | 0 | – | – | – | – |
| | 700–1,000 | 0 | – | – | – | – |
| Rock domain | RFM012 | 2 | 0.053 | $3.5 \cdot 10^{-3}$ | –1.28 | 0.029 |
| | RFM018 | 0 | – | – | – | – |
| | RFM021 | 0 | – | – | – | – |
| | RFM029 | 6 | $7.3 \cdot 10^{-3}$ | $6.5 \cdot 10^{-3}$ | –2.26 | 0.35 |
| | RFM044 | 0 | – | – | – | – |
| | RFM045 | 0 | – | – | – | – |
| Fracture domain | All FD | 4 | $5.5 \cdot 10^{-3}$ | $1.9 \cdot 10^{-3}$ | –2.28 | 0.17 |
| | FFM01 | 0 | – | – | – | – |
| | FFM02 | 4 | $5.5 \cdot 10^{-3}$ | $1.9 \cdot 10^{-3}$ | –2.28 | 0.17 |
| | FFM03 | 0 | – | – | – | – |
| | FFM04 | 0 | – | – | – | – |
| | FFM05 | 0 | – | – | – | – |
| | FFM06 | 0 | – | – | – | – |
| Deformation zone | All DZ | 4 | 0.032 | 0.025 | –1.74 | 0.67 |
| | GDZ | 3 | 0.042 | 0.019 | –1.42 | 0.24 |
| | WNW-NW | 1 | $2.0 \cdot 10^{-3}$ | – | –2.70 | – |
| | NNW | 0 | – | – | – | – |
| | ENE-NNE | 0 | – | – | – | – |

[1] Data set represents the entire site.

For the elevation subsets, the arithmetic mean $\overline{x}$ of $\log_{10}(d_{mean})$ is marked by a ring in Figure 3-15. The uncertainty range of $\mu$ is shown by the black line. In addition, the standard deviation of $\log_{10}(d_{mean})$ for each data subsets is illustrated by the green line. Here one standard deviation on each side of $\overline{x}$ is displayed. Due to the scarcity of data only the elevation data subsets are displayed.

As only so few quantitative data exist, we refrain from drawing any conclusions from comparing the data subsets.

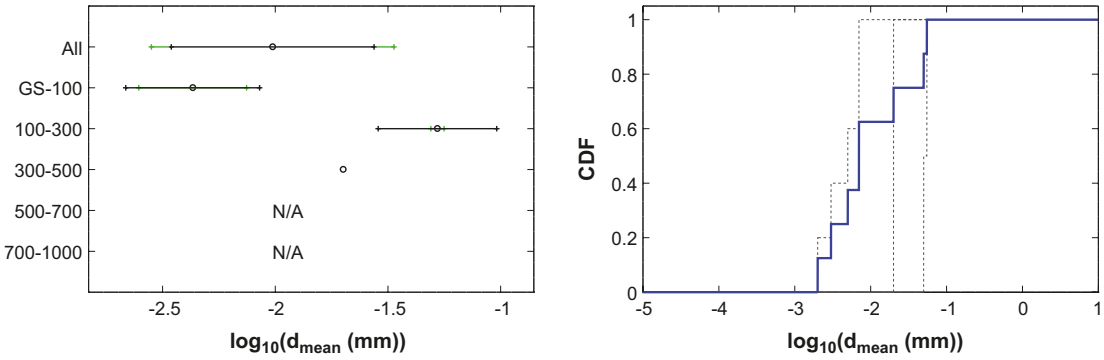


***Figure 3-15.*** *Hematite: Left, arithmetic mean and standard deviation of data subsets, and uncertainty range of population mean value. Right, cumulative distribution functions of the separate data subsets (black curves) and of the combined data set (blue curves). CDFs for data subsets with only up to 20 data points are dotted.*

### 3.4.3 Parametric analysis – hematite

The normality of the few hematite data existing was investigated by means of the Shapiro-Wilk $W$ test. It was shown that the normal distribution is better fitted to $\log_{10}(d_{mean})$ data than to $d_{mean}$ data. The $W$-values returned are 0.92 and 0.75, respectively. Figure 3-16 (left) shows a histogram of $\log_{10}(d_{mean})$ for hematite data from the entire site, together with the normal distribution that is best fitted to the data. In the right image the associated normal score plot is shown.

Due to the scarcity of data we have refrained from fitting distributions to data subsets other than the elevation data subsets. The parameters are shown in Table 3-12.

The main conclusion from this study of hematite is that it is found as fracture mineral in only very few fractures.

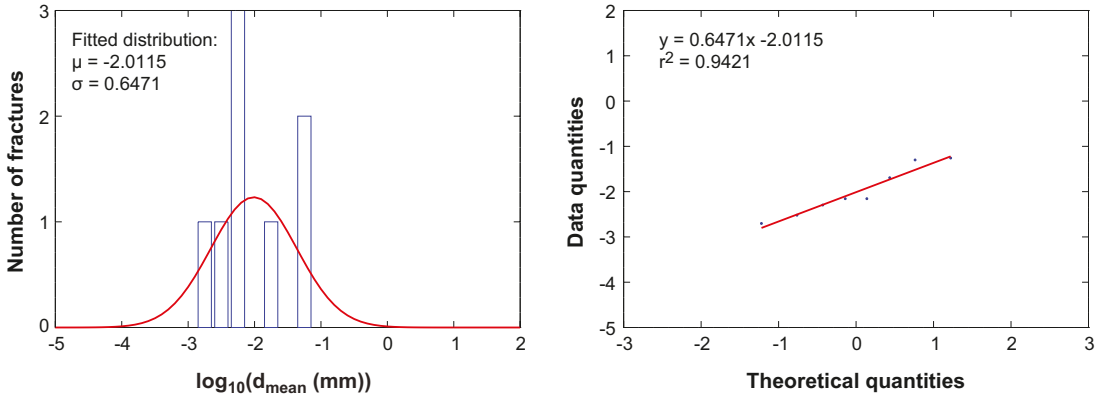


***Figure 3-16.*** *Left: Histogram of $\log_{10}(d_{mean})$ data together with best fit normal distribution. Right: Normal score plot of $\log_{10}(d_{mean})$ data. Data subset used: Hematite from the entire site.*

**Table 3-12. Distribution parameters of populated fractures, hematite.**

| Hematite | | Number of data points | $\log_{10}(d_{mean})$ $\mu$ | $\sigma$ |
|---|---|---|---|---|
| Elevation (mbsl) | GS–1,000[1] | 8 | –2.01 | 0.65 |
| | GS–100 | 5 | –2.37 | 0.31 |
| | 100–300 | 2 | –1.28 | 0.048 |
| | 300–500 | 1 | –1.70 | – |
| | 500–700 | 0 | – | – |
| | 700–1,000 | 0 | – | – |

[1] Data set represents the entire site.

## 3.5 Pyrite

In this section, equivalent tables and figures are presented for pyrite as for calcite in Section 3.1. In Section 3.1 information on how to interpret the tables, figures, and notations is found. An introduction to the rock volumes represented by the data subsets is found in Section 2.2.2.

### 3.5.1 The data subsets

In Table 3-13, information on the number of data points, $f_{quant}$, and $f_{qual}$ is summarised for the different pyrite data subsets. As pyrite can also be mapped as minute spot minerals, where it was found it was mapped quantitatively, making $f_{quant}$ and $f_{qual}$ equal.

The data are illustrated in Figure 3-17, showing the fractions of the fractures where pyrite is found in quantitative amounts or not at all.

As can be seen from Table 3-13 and Figure 3-17, on average 10% of all fractures contain pyrite. In rock volumes where more than 100 fractures were mapped, $f_{quant}$ range from a few to 25%, indicating that there are differences between some of the rock volumes. In particular, it seems that pyrite is more abundant in ENE-NNE deformation zones while pyrite is scarce in rock volume RMF021 (outside the target area). Apart from these two rock volumes $f_{quant}$ range from a 5 to 16% in rock volumes where more than 100 fractures were mapped.

**Table 3-13. Amounts of data in different data subsets, pyrite.**

| Pyrite | | Total number of fractures | Number of data points | $f_{qual}$ (%) | $f_{quant}$ (%) |
|---|---|---|---|---|---|
| Elevation (mbsl) | GS–1,000[1] | 2,071 | 202 | 10 | 10 |
| | GS–100 | 835 | w70 | 8 | 8 |
| | 100–300 | 531 | 86 | 16 | 16 |
| | 300–500 | 543 | 27 | 5 | 5 |
| | 500–700 | 114 | 15 | 13 | 13 |
| | 700–1,000 | 48 | 4 | 8 | 8 |
| Rock domain | RFM012 | 79 | 11 | 14 | 14 |
| | RFM018 | 30 | 2 | 7 | 7 |
| | RFM021 | 226 | 4 | 2 | 2 |
| | RFM029 | 1,596 | 170 | 11 | 11 |
| | RFM044 | 8 | 2 | 25 | 25 |
| | RFM045 | 132 | 13 | 10 | 10 |
| Fracture domain | All FD | 602 | 58 | 10 | 10 |
| | FFM01 | 152 | 12 | 8 | 8 |
| | FFM02 | 321 | 37 | 12 | 12 |
| | FFM03 | 107 | 7 | 7 | 7 |
| | FFM04 | 8 | 0 | 0 | 0 |
| | FFM05 | 3 | 0 | 0 | 0 |
| | FFM06 | 11 | 2 | 18 | 18 |
| Deformation zone | All DZ | 1,333 | 138 | 10 | 10 |
| | GDZ | 640 | 34 | 5 | 5 |
| | WNW-NW | 371 | 30 | 8 | 8 |
| | NNW | 22 | 3 | 14 | 14 |
| | ENE-NNE | 280 | 69 | 25 | 25 |

[1] Data set represents the entire site.

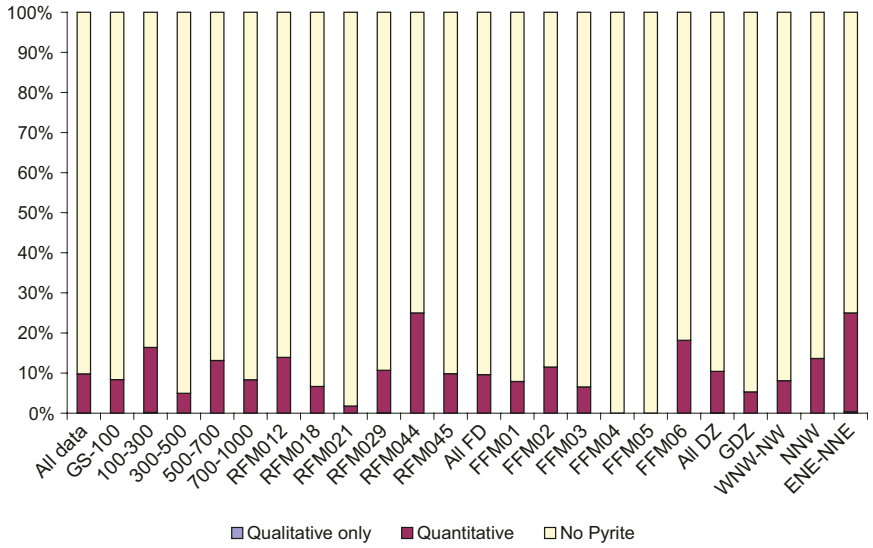


***Figure 3-17.*** *Fractions of fractures populated or unpopulated by pyrite.*

### 3.5.2 Non-parametric analysis

An analysis was made by the Kruskal-Wallis test, indicating with great confidence that the different pyrite data subsets are not all samples of the exact same population. If comparing all separate data subsets, the *p*-value returned is 0.0047.

For all data subsets (including quantitative data only) the arithmetic mean $\bar{x}$ and the standard deviation *STD* of $d_{mean}$ and $\log_{10}(d_{mean})$ were calculated. These data are shown in Table 3-14.

The arithmetic mean $\bar{x}$ of $\log_{10}(d_{mean})$ of each data subset is marked by a ring in Figure 3-18 (left). The uncertainty range of $\mu$ is shown by the black line. In addition, the standard deviation of $\log_{10}(d_{mean})$ for each data subsets is illustrated by the green line. Here one standard deviation on each side of $\bar{x}$ is displayed.

It is seen in Figure 3-18 (left) that although there are significant differences in the arithmetic mean $\bar{x}$ for the data subsets, the uncertainty ranges of the population means $\mu$ generally overlap. In Figure 3-18 (right) one can see that there are similarities in the cumulative distribution functions of the different data subsets. The results shown in Figure 3-18 suggest that in fractures where pyrite occurs, it occurs in similar amounts in the different rock volumes.

The larger ranges in the pyrite analyses as compared to the other minerals in the mapping campaign are partly due to the different methodolody used in the pyrite mapping (see Section 2.4.4).

**Table 3-14. Non-parametric data for pyrite.**

| Pyrite | | Number of data points | $\bar{x}$ of $d_{mean}$ [mm] | *STD* of $d_{mean}$ [mm] | $\bar{x}$ of $\log_{10}(d_{mean}$ [mm]) | *STD* of $\log_{10}(d_{mean}$ [mm]) |
|---|---|---|---|---|---|---|
| Elevation (mbsl) | GS–1,000[1] | 202 | $2.3 \cdot 10^{-3}$ | $1.2 \cdot 10^{-2}$ | –4.01 | 1.25 |
| | GS–100 | 70 | $1.4 \cdot 10^{-3}$ | $2.8 \cdot 10^{-3}$ | –3.99 | 1.24 |
| | 100–300 | 86 | $1.9 \cdot 10^{-3}$ | $6.6 \cdot 10^{-3}$ | –4.14 | 1.27 |
| | 300–500 | 27 | $7.2 \cdot 10^{-3}$ | $2.9 \cdot 10^{-2}$ | –3.69 | 1.26 |
| | 500–700 | 15 | $6.5 \cdot 10^{-4}$ | $1.2 \cdot 10^{-3}$ | –4.22 | 1.19 |
| | 700–1,000 | 4 | $1.8 \cdot 10^{-3}$ | $1.5 \cdot 10^{-3}$ | –2.99 | 0.65 |
| Rock domain | RFM012 | 11 | $2.3 \cdot 10^{-2}$ | $4.6 \cdot 10^{-2}$ | –2.77 | 1.27 |
| | RFM018 | 2 | $3.4 \cdot 10^{-3}$ | $9.2 \cdot 10^{-4}$ | –2.48 | 0.12 |
| | RFM021 | 4 | $7.5 \cdot 10^{-4}$ | $1.5 \cdot 10^{-3}$ | –4.64 | 1.42 |
| | RFM029 | 170 | $1.1 \cdot 10^{-3}$ | $2.6 \cdot 10^{-3}$ | –4.12 | 1.20 |
| | RFM044 | 2 | $3.0 \cdot 10^{-3}$ | 0 | –2.52 | 0 |
| | RFM045 | 13 | $9.9 \cdot 10^{-4}$ | $1.5 \cdot 10^{-3}$ | –3.94 | 1.33 |
| Fracture domain | All FD | 58 | $1.2 \cdot 10^{-3}$ | $3.0 \cdot 10^{-3}$ | –4.23 | 1.28 |
| | FFM01 | 12 | $1.3 \cdot 10^{-3}$ | $2.4 \cdot 10^{-3}$ | –4.32 | 1.49 |
| | FFM02 | 37 | $1.3 \cdot 10^{-3}$ | $3.4 \cdot 10^{-3}$ | –4.22 | 1.25 |
| | FFM03 | 7 | $6.9 \cdot 10^{-4}$ | $1.3 \cdot 10^{-3}$ | –4.22 | 1.23 |
| | FFM04 | 0 | – | – | – | – |
| | FFM05 | 0 | – | – | – | – |
| | FFM06 | 2 | $1.0 \cdot 10^{-3}$ | $1.4 \cdot 10^{-3}$ | –3.90 | 1.70 |
| Deformation zone | All DZ | 138 | $2.9 \cdot 10^{-3}$ | $1.4 \cdot 10^{-2}$ | –3.88 | 1.24 |
| | GDZ | 34 | $1.2 \cdot 10^{-3}$ | $2.8 \cdot 10^{-3}$ | –4.06 | 1.15 |
| | WNW-NW | 30 | $1.9 \cdot 10^{-3}$ | $3.0 \cdot 10^{-3}$ | –3.42 | 0.93 |
| | NNW | 3 | $2.7 \cdot 10^{-3}$ | $5.9 \cdot 10^{-4}$ | –2.58 | 0.10 |
| | ENE-NNE | 69 | $4.3 \cdot 10^{-3}$ | $1.9 \cdot 10^{-2}$ | –3.98 | 1.33 |

[1] Data set represents the entire site.

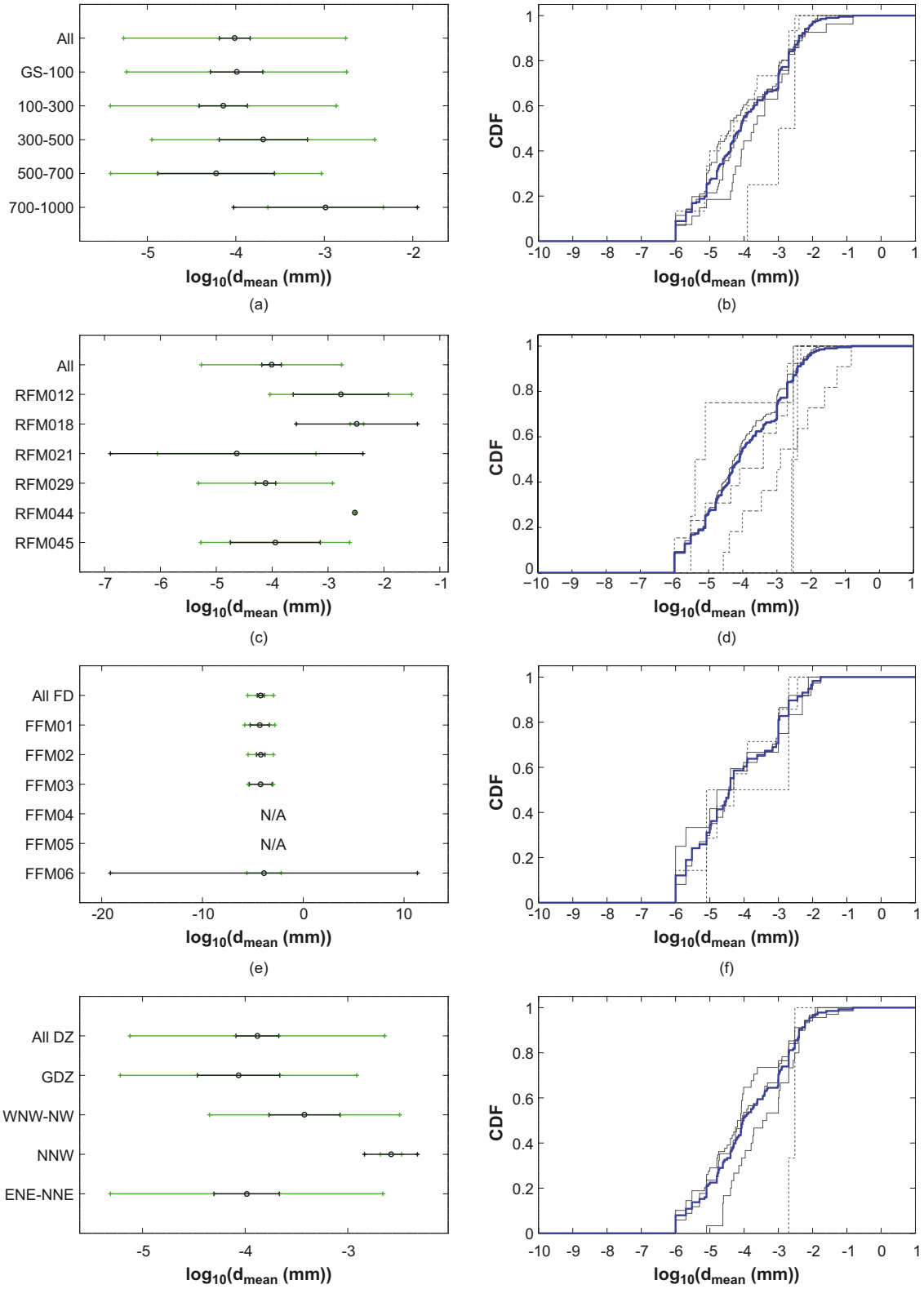


***Figure 3-18.*** *Pyrite: a, c, e, g) Arithmetic mean (black dot) and standard deviation (green range) of data subsets, and uncertainty range (black range) of population mean value. b, d, f, h) Cumulative distribution functions of the separate data subsets (black curves) and of the combined data set (blue curves). CDFs for data subsets with only up to 20 data points are dotted.*

### 3.5.3 Parametric analysis

The normality of the pyrite data subset from the entire site was investigated by means of the Shapiro-Wilk $W$ test. It was shown that the normal distribution is much better fitted to $\log_{10}(d_{mean})$ data than $d_{mean}$ data. The $W$-value retuned for $d_{mean}$ data is 0.17 and for $\log_{10}(d_{mean})$ data the returned $W$-value is 0.96.

Figure 3-19 (left) shows a histogram of $\log_{10}(d_{mean})$ for pyrite data from the entire site, together with the normal distribution that is best fitted to the data. In the right image the associated normal score plot is shown.

It is seen from Figure 3-19 that the normal distribution only fairly well describes the $\log_{10}(d_{mean})$ data, with $r^2 = 0.97$ in the normal score plot. Similar figures are shown for all pyrite data subsets in Appendix A.

By making a normal score plot for each pyrite data subset, taking $\mu$ from the intercept and $\sigma$ from the slope, the data in Table 3-15 are obtained.

Figure 3-20 illustrates the distributions of Table 3-15, where the distribution representing the entire site is shown by the red line. Distributions of data subsets with more than 20 data points are shown by the solid lines, while distributions of data subsets with up to 20 data points are shown by the shaded lines.

Upon examination of Figure 3-20, one can suggest that the best fit distribution for data from the entire site fairly well represents the different rock volumes of the site. There is a notable but not major difference in $\mu$ for WNW-NW deformation zones. The distributions that deviate the most represent data subsets of few data points, such as RFM018 and NNW deformation zones.

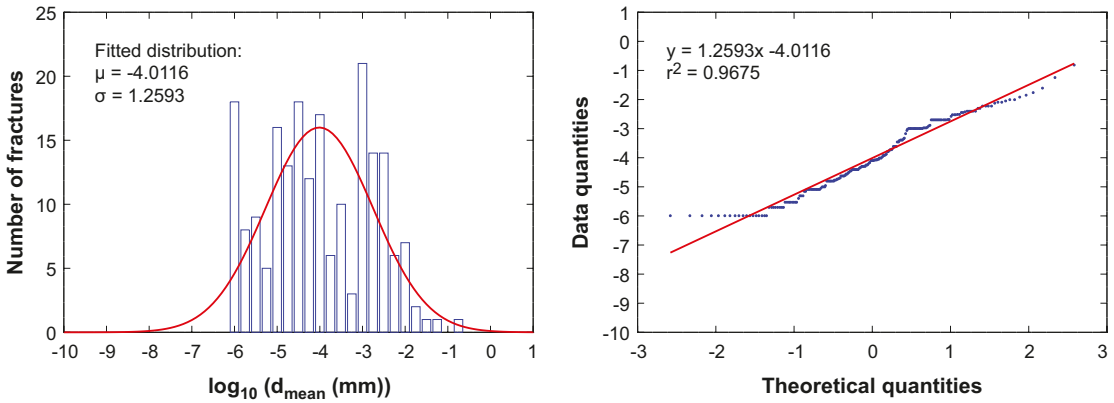


***Figure 3-19.*** *Left: Histogram of $\log_{10}(d_{mean})$ data together with best fit normal distribution. Right: normal score plot of $\log_{10}(d_{mean})$ data. Data subset used: Pyrite from the entire site.*

**Table 3-15. Distribution parameters of populated fractures, pyrite.**

| Pyrite | | Number of data points | $\log_{10}(d_{mean})$ $\mu$ | $\sigma$ |
|---|---|---|---|---|
| Elevation (mbsl) | GS–1,000[1] | 202 | –4.01 | 1.26 |
| | GS–100 | 70 | –3.99 | 1.28 |
| | 100–300 | 86 | –4.14 | 1.29 |
| | 300–500 | 27 | –3.69 | 1.37 |
| | 500–700 | 15 | –4.22 | 1.34 |
| | 700–1,000 | 4 | –2.99 | 0.83 |
| Rock domain | RFM012 | 11 | –2.77 | 1.50 |
| | RFM018 | 2 | –2.48 | 0.20 |
| | RFM021 | 4 | –4.64 | 1.68 |
| | RFM029 | 170 | –4.12 | 1.21 |
| | RFM044 | 2 | –2.52 | 0 |
| | RFM045 | 13 | –3.94 | 1.49 |
| Fracture domain | All FD | 58 | –4.23 | 1.32 |
| | FFM01 | 12 | –4.32 | 1.70 |
| | FFM02 | 37 | –4.22 | 1.32 |
| | FFM03 | 7 | –4.22 | 1.54 |
| | FFM04 | 0 | – | – |
| | FFM05 | 0 | – | – |
| | FFM06 | 2 | –3.90 | 2.78 |
| Deformation zone | All DZ | 138 | –3.88 | 1.26 |
| | GDZ | 34 | –4.06 | 1.23 |
| | WNW-NW | 30 | –3.42 | 0.99 |
| | NNW | 3 | –2.58 | 0.13 |
| | ENE-NNE | 69 | –3.98 | 1.37 |

[1] Data set represents the entire site.

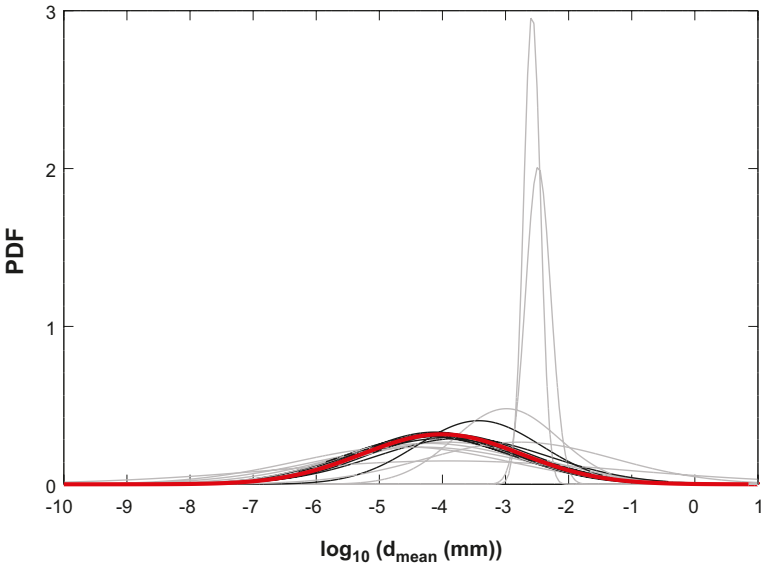


***Figure 3-20.*** *Illustration of normal distributions of Table 3-15. Distributions of data subsets with only up to 20 data points are shaded. Distribution of RFM044 is not shown.*

## 3.6 Fresh fracture surfaces

In the fracture mapping, some fracture surfaces were found to be fresh, meaning that no fracture mineral is detected by the visual mapping method used. It should be emphasised that small amounts of minerals undetectable without a microscope is likely to be present in these fractures. In the site investigation report /Eklund and Mattsson 2009/ this category is named "no detectable minerals". Table 3-16 shows the fraction of the fractures where both the upper and lower fracture surfaces are fresh. The data in Table 3-16 are illustrated in Figure 3-21.

As seen in Figure 3-21, 18% of the investigated fractures display two fresh fracture surfaces. As can be seen there is a slightly higher fraction of unpopulated fractures at, and above, repository depth than below 500 mbsl.

**Table 3-16. Amounts of data in different data subsets, fresh fracture surfaces.**

| Fresh fracture surfaces | | Total number of fractures | Number of fresh fractures | Fraction (%) |
|---|---|---|---|---|
| Elevation (mbsl) | GS–1,000[1] | 2,071 | 383 | 18 |
| | GS–100 | 835 | 133 | 16 |
| | 100–300 | 531 | 102 | 19 |
| | 300–500 | 543 | 137 | 25 |
| | 500–700 | 114 | 8 | 7 |
| | 700–1,000 | 48 | 3 | 6 |
| Rock domain | RFM012 | 79 | 14 | 18 |
| | RFM018 | 30 | 2 | 7 |
| | RFM021 | 226 | 46 | 20 |
| | RFM029 | 1,596 | 312 | 20 |
| | RFM044 | 8 | 1 | 13 |
| | RFM045 | 132 | 8 | 6 |
| Fracture domain | All FD | 602 | 114 | 19 |
| | FFM01 | 152 | 35 | 23 |
| | FFM02 | 321 | 35 | 11 |
| | FFM03 | 107 | 41 | 38 |
| | FFM04 | 8 | 1 | 13 |
| | FFM05 | 3 | 1 | 33 |
| | FFM06 | 11 | 1 | 9 |
| Deformation zone | All DZ | 1,333 | 249 | 19 |
| | GDZ | 640 | 153 | 24 |
| | WNW-NW | 371 | 75 | 20 |
| | NNW | 22 | 0 | 0 |
| | ENE-NNE | 280 | 21 | 8 |

[1] Data set represents the entire site.

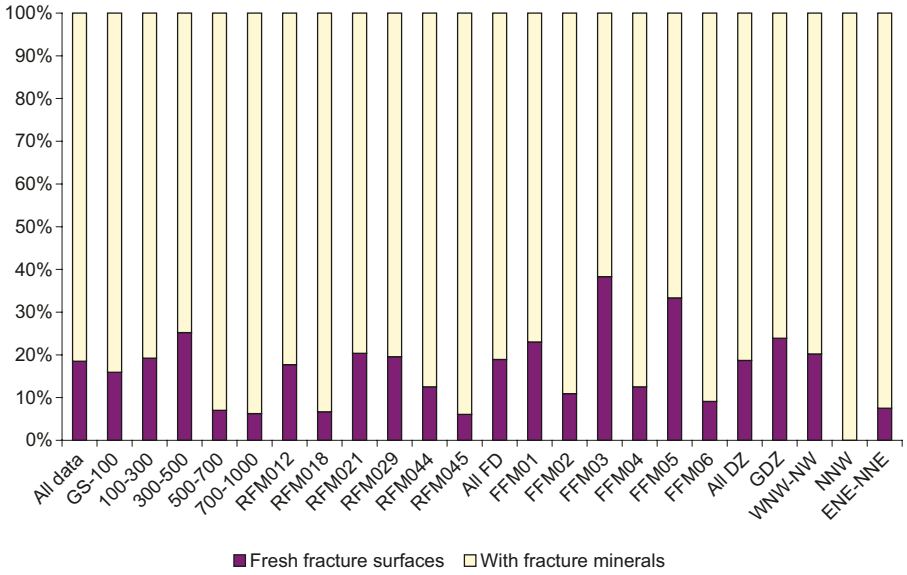


***Figure 3-21.*** *Fractions of fractures with two fresh fracture surfaces for different data subsets.*

## 3.7 Influence of PFL anomaly

If the fracture minerals should have an impact on repository safety, they should be associated with flowing structures. Therefore, the great majority of fractures studied in this campaign are taken from within a meter of the nearest PFL-anomaly. In this section it is investigated if fracture mineral amounts are related to the transmissivity of the PFL-anomaly that the fracture is closest to. The transmissivity is correlated to the groundwater flow rate in the fracture (or fracture zone) at the imposed conditions of the measurements. As the hydraulic gradient is altered during the measurements, it is not certain that the fracture naturally conducts water. Even so, most transmissivities should in one way or another be related to the natural groundwater flow.

In order to do such a study it would be preferable if one had information on exactly which open fractures are conducting water in the PFL-logging. An effort has been initiated by SKB to couple PFL-anomalies with individual fractures, but no result from this effort has been a basis for this analysis. Instead, any open fracture within a distance of one decimetre from the location of a detected PFL-anomaly is coupled to the anomaly and its measured transmissivity. In case of two or more nearby PFL-anomalies, each fracture has been coupled to the nearest anomaly and its transmissivity.

The number of PFL-anomalies included in this comparative study is 397, and the number of fractures at distances up to 1 dm from such an anomaly is 543. Figure 3-22 to Figure 3-25 give plots of $d_{mean}$ versus transmissivity for calcite, chlorite, clay minerals, and pyrite. Also the numbers of data points constituting the plots are shown.

As can be seen in Figure 3-22 to Figure 3-25, the fracture mineral thickness $d_{mean}$ of the studied fracture minerals appears to be unrelated to the transmissivity. For hematite, the data are too scarce to make a comparison. Even if the largest distance to the nearest PFL-anomaly is decreased to 5 cm, no relation can be seen (which is not shown in the figures).

In the quantitative mineral mapping campaign, a small number of fractures (in total 39), which are located at least five metres distant from any detected PFL anomaly, were mapped. In Table 3-17, the number of data points, $f_{qual}$, $f_{quant}$, mean values, and standard deviations for the data subsets are shown.

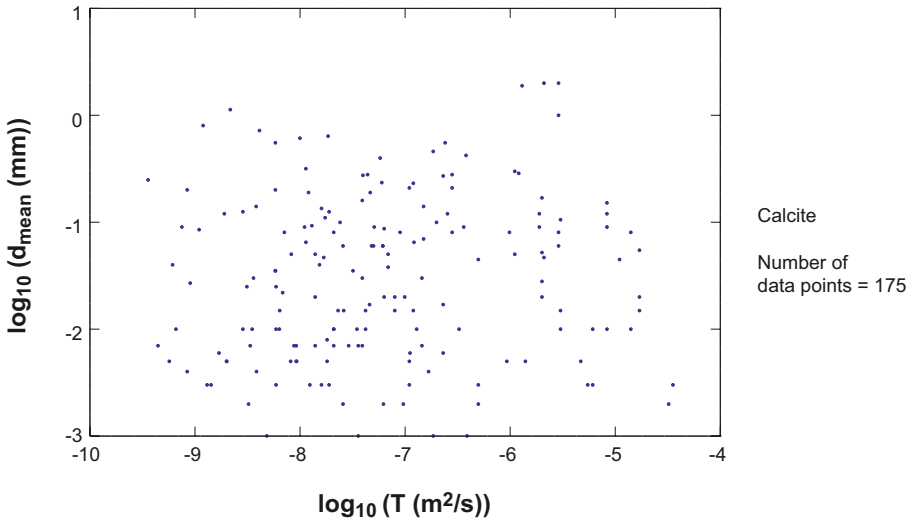


***Figure 3-22.*** *Transmissivity vs. $d_{mean}$ for calcite.*

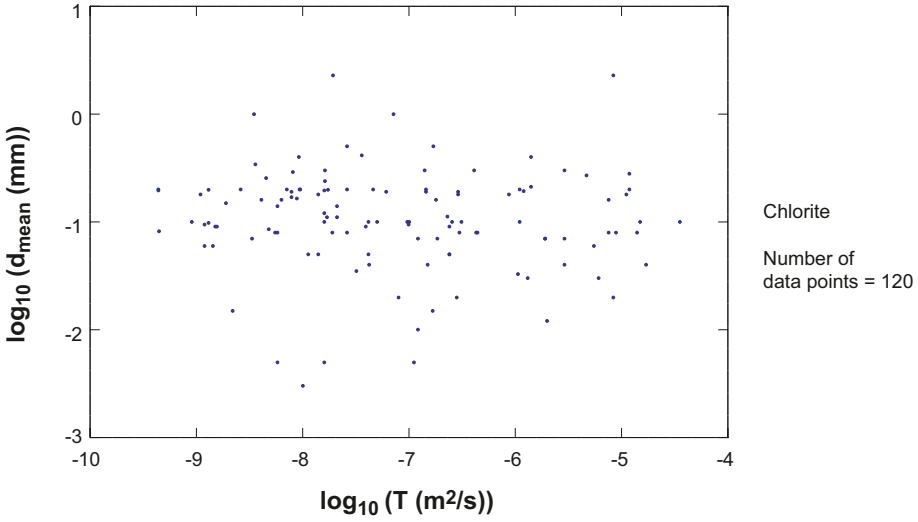


***Figure 3-23.*** *Transmissivity vs. $d_{mean}$ for chlorite.*

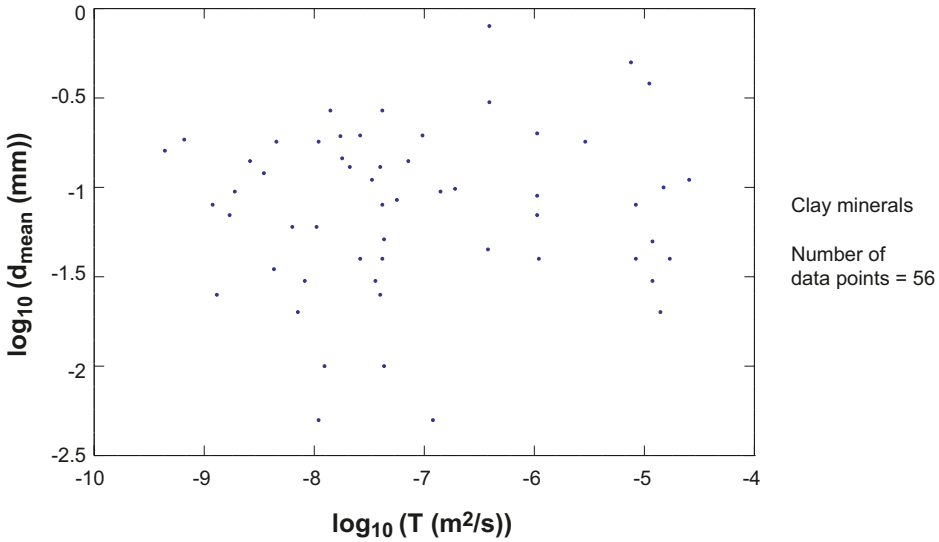


***Figure 3-24.*** *Transmissivity vs. $d_{mean}$ for clay minerals, as a group.*

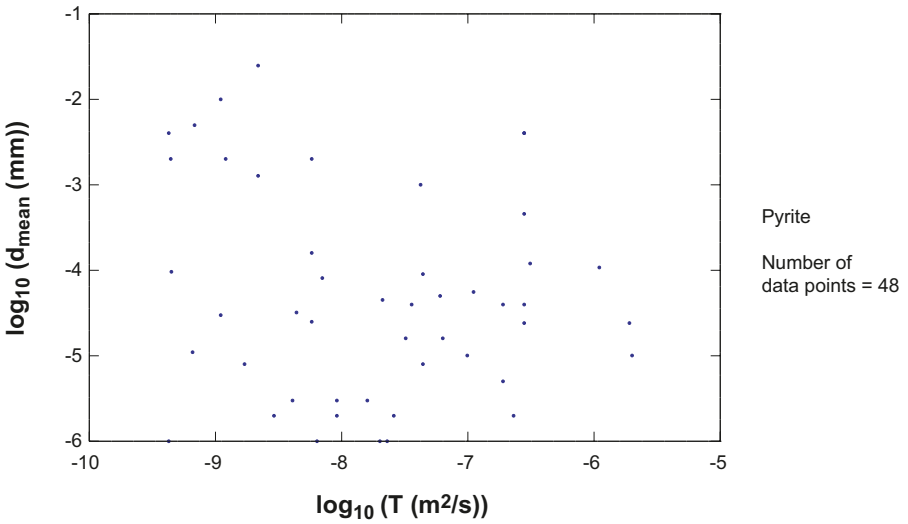


***Figure 3-25.*** *Transmissivity vs. $d_{mean}$ for pyrite.*

**Table 3-17. Data for fractures distant from any PFL-anomaly (in total 39 mapped fractures).**

| Mineral | Number of data points | $f_{qual}$ (%) | $f_{quant}$ (%) | $d_{mean}$ | | $\log_{10}(d_{mean})$ | |
|---|---|---|---|---|---|---|---|
| | | | | $\bar{x}$ | STD | $\bar{x}$ | STD |
| Calcite | 6 | 67 | 15 | 0.12 | 0.048 | –0.95 | 0.16 |
| Chlorite | 18 | 77 | 46 | 0.25 | 0.21 | –0.69 | 0.25 |
| Clay mineral | 1 | 33 | 2.6 | 0.02 | – | –1.70 | – |
| Hematite | 0 | 0 | 0 | – | – | – | – |
| Pyrite | 1 | 2.6 | 2.6 | 0.002 | – | –2.70 | – |

For chlorite there is enough data for a rough comparison with $d_{mean}$ of fractures mainly associated with PFL-anomalies (cf. Table 3-4), even if drawing any conclusion from these few data points is speculative. What can be said is that the results do not contradict the earlier indications that the amount of fracture minerals is generally unrelated to the present groundwater flow in the fracture. For this reason, the decision taken early on to base the statistical analyses on data from all open fractures seems reasonable.

## 3.8 Influence of crush zone

Some drill core segments are so heavily fragmented that they cannot be pieced together into their original positions. Such segments are called crush zones and can be envisioned by gravel. Due to the difficulties in observing discrete fractures in crush zones, the methodology of mapping fracture minerals is somewhat different (see Section 2.1). Crush zones are scarce in the drill core mapped in this site investigation activity, and only 18 crush zones have been studied. In Table 3-18, the number of data points, $f_{qual}$, $f_{quant}$, mean values, and standard deviations for the crush zone data subsets are shown.

**Table 3-18. Data for crush zones (in total 18 mapped crush zones).**

| Mineral | Number of data points | $f_{qual}$ (%) | $f_{quant}$ (%) | $d_{mean}$ | | $Log_{10}(d_{mean})$ | |
|---|---|---|---|---|---|---|---|
| | | | | $\bar{x}$ | *STD* | $\bar{x}$ | *STD* |
| Calcite | 10 | 89 | 56 | 0.014 | $9.4 \cdot 10^{-3}$ | –1.96 | 0.29 |
| Chlorite | 6 | 67 | 33 | 0.078 | 0.023 | –1.13 | 0.14 |
| Clay mineral | 5 | 67 | 28 | 0.058 | 0.033 | –1.34 | 0.39 |
| Hematite | 0 | 0 | 0 | – | – | – | – |
| Pyrite | 1 | 5.6 | 5.6 | $1.3 \cdot 10^{-4}$ | – | –3.90 | – |

For all fracture minerals there are few data points, but for calcite there may be enough data for a rough comparison between crush zone data and discrete fracture data. If comparing the data in Table 3-18 with data in Table 3-2, one can see no major differences. Due to the scarcity of crush zones, and the differences in methodology when mapping crush zones and discrete fractures, it was decided not to include crush zone data in the general analyses in Sections 3.1 to 3.6.

# 4 Visible coverage $C_{vis}$

The visible coverage for the individual mineral layer is one of the parameters reported in the site investigation report /Eklund and Mattsson 2009/. In this section, the visible coverage is reported as averaged over both fracture surfaces of a fracture (see definition of $C_{vis}$ in Section 2.2.1).

## 4.1 The data subsets

In Table 4-1 the number of data points in each data subset is given, together with $f_{quant}^{c}$. The latter is the fraction of the fractures covered by enough fracture minerals to be quantitatively estimated. An introduction to the rock volumes represented by the data subsets is found in Section 2.2.2.

The fractions of fractures where quantitative visible coverages were obtained, $f_{quant}^{c}$, are displayed in Figure 4-1 for the different fracture minerals.

As can be seen, out of the fracture minerals investigated, the one that is most likely found is calcite, followed by chlorite, clay minerals, pyrite, and hematite. Deviations from this order are only found in rock volumes where few fractures have been mapped (e.g. FFM05 where in total only three open fractures where mapped).

**Table 4-1. Number of data points in data subsets.**

| Rock volume | | Calcite | | Chlorite | | Clay minerals | | Hematite | | Pyrite | |
|---|---|---|---|---|---|---|---|---|---|---|---|
| | | No. | $f_{quant}^{c}$ (%) | No. | $f_{quant}^{c}$ (%) | No. | $f_{quant}^{c}$ (%) | No. | $f_{quant}^{c}$ (%) | No. | $f_{quant}^{c}$ (%) |
| Elevation (mbsl) | GS–1,000[1] | 1,177 | 57 | 1,077 | 52 | 573 | 28 | 34 | 1.6 | 203 | 10 |
| | GS–100 | 486 | 58 | 349 | 42 | 282 | 34 | 18 | 2.2 | 70 | 8.0 |
| | 100–300 | 320 | 60 | 310 | 58 | 99 | 19 | 11 | 2.1 | 87 | 16 |
| | 300–500 | 287 | 53 | 291 | 54 | 150 | 28 | 2 | 0.4 | 27 | 5.0 |
| | 500–700 | 62 | 54 | 91 | 80 | 23 | 20 | 2 | 1.8 | 15 | 13 |
| | 700–1,000 | 22 | 46 | 36 | 75 | 19 | 40 | 1 | 2.1 | 4 | 8.0 |
| Rock domain | RFM012 | 33 | 42 | 45 | 57 | 21 | 27 | 4 | 5.1 | 11 | 14 |
| | RFM018 | 17 | 57 | 27 | 90 | 9 | 30 | 0 | 0 | 2 | 7.0 |
| | RFM021 | 146 | 65 | 123 | 54 | 46 | 20 | 8 | 3.5 | 4 | 2.0 |
| | RFM029 | 891 | 56 | 780 | 49 | 450 | 28 | 21 | 1.3 | 171 | 11 |
| | RFM044 | 4 | 50 | 5 | 63 | 3 | 38 | 0 | 0 | 2 | 25 |
| | RFM045 | 86 | 65 | 97 | 73 | 44 | 33 | 1 | 0.8 | 13 | 10 |
| Fracture domain | All FD | 357 | 59 | 333 | 55 | 154 | 26 | 11 | 1.8 | 58 | 10 |
| | FFM01 | 84 | 55 | 87 | 57 | 39 | 26 | 2 | 1.3 | 12 | 8.0 |
| | FFM02 | 221 | 69 | 181 | 56 | 94 | 29 | 9 | 2.8 | 37 | 12 |
| | FFM03 | 41 | 38 | 47 | 44 | 17 | 16 | 0 | 0 | 7 | 7.0 |
| | FFM04 | 5 | 63 | 7 | 88 | 0 | 0 | 0 | 0 | 0 | 0 |
| | FFM05 | 0 | 0 | 2 | 67 | 2 | 67 | 0 | 0 | 0 | 0 |
| | FFM06 | 6 | 55 | 9 | 82 | 2 | 18 | 0 | 0 | 2 | 18 |
| Deformation zone | All DZ | 725 | 54 | 670 | 50 | 399 | 30 | 16 | 1.2 | 139 | 10 |
| | GDZ | 296 | 46 | 289 | 45 | 225 | 35 | 7 | 1.1 | 34 | 5.0 |
| | WNW–NW | 223 | 60 | 162 | 44 | 81 | 22 | 5 | 1.3 | 30 | 8.0 |
| | NNW | 11 | 50 | 19 | 86 | 12 | 55 | 0 | 0 | 3 | 14 |
| | ENE–NNE | 177 | 63 | 184 | 66 | 74 | 26 | 4 | 1.4 | 70 | 25 |

[1] Data set represents the entire site.

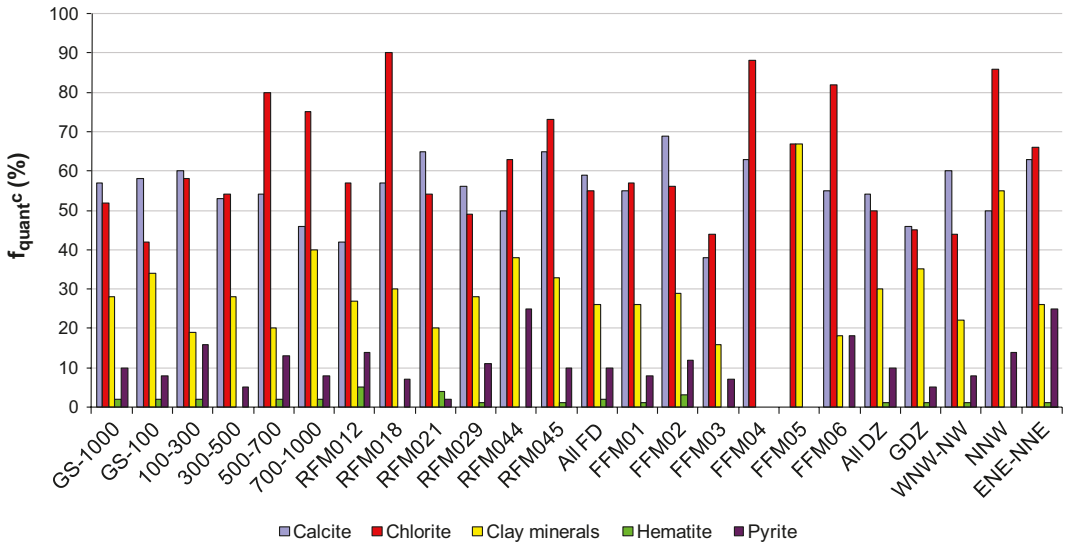


***Figure 4-1.*** *$f_{quant}^{c}$ of the different data subsets in Table 4-1.*

In the quantitative mineral mappingcampaign, whenever a fracture mineral was detected by inspecting the fracture surface from above, it was assigned a quantitative visible coverage. It appears that when very small specks of fracture minerals were found, the visible coverage of the layer was rounded up to 1% or down to non-existing. It should be noted that as the visible coverage of a fracture delivered from this report is averaged over both fracture surfaces, the minimum value possible is 0.5% (one surface with 0% coverage and the opposite surface with 1% coverage). The exception is for pyrite that exists as spot minerals, where the minimum value possible is 0.0005%[2].

## 4.2 Calcite

### 4.2.1 Non-parametric analysis

For all data subsets (including quantitative data only) the arithmetic mean $\bar{x}$ and the standard deviation *STD* of $C_{vis}$ and $\log_{10}(C_{vis})$ were calculated. These data are shown in Table 4-2.

As seen in the table, $C_{vis}$ of calcite is on average 18% in fractures where the mineral is found. For rock volumes where more than 100 data points were obtained, $\bar{x}$ of $C_{vis}$ ranges from 13 to 25%.

By performing a Kruskal-Wallis test on the calcite $C_{vis}$ data for the separate data subsets, it is strongly indicated that they are not all samples of the same population, with $p < 0.0001$.

Figure 4-2 shows the cumulative distribution functions of the data subsets. Combined data sets (All, All FD, and All DZ) are shown in blue lines while separate CDFs are shown in black lines. CDFs representing data sets of more than 20 data points are shown by solid lines while those representing fewer data points are shown by dotted lines.

As can be seen, the CDFs of the data subsets are similar. Based on Table 4-1**,** Table 4-2, and Figure 4-2 one can suggest that fracture surfaces in the different rock volumes at Forsmark are covered by similar fractions of calcite.

[2] 0.0005% = 0.5 × 0.1 mm × 0.1 mm / 10 cm$^{-2}$. See Section 2.1.2 for details.

**Table 4-2. Non-parametric data for calcite.**

| Calcite | | Number of data points | $\bar{x}$ of $C_{vis}$ [%] | *STD* of $C_{vis}$ [%] | $\bar{x}$ of $\log_{10}(C_{vis}$ [%]) | *STD* of $\log_{10}(C_{vis}$ [%]) |
|---|---|---|---|---|---|---|
| Elevation (mbsl) | GS–1,000[1] | 1,177 | 18 | 22 | 0.84 | 0.64 |
| | GS–100 | 486 | 20 | 24 | 0.95 | 0.62 |
| | 100–300 | 320 | 15 | 20 | 0.81 | 0.61 |
| | 300–500 | 287 | 15 | 22 | 0.68 | 0.67 |
| | 500–700 | 62 | 21 | 24 | 0.92 | 0.69 |
| | 700–1,000 | 22 | 11 | 14 | 0.70 | 0.56 |
| Rock domain | RFM012 | 33 | 25 | 29 | 0.93 | 0.76 |
| | RFM018 | 17 | 14 | 17 | 0.77 | 0.63 |
| | RFM021 | 146 | 13 | 18 | 0.78 | 0.56 |
| | RFM029 | 891 | 18 | 22 | 0.85 | 0.65 |
| | RFM044 | 4 | 10 | 14 | 0.68 | 0.61 |
| | RFM045 | 86 | 21 | 26 | 0.87 | 0.71 |
| Fracture domain | All FD | 357 | 16 | 20 | 0.82 | 0.62 |
| | FFM01 | 84 | 11 | 19 | 0.60 | 0.59 |
| | FFM02 | 221 | 17 | 20 | 0.88 | 0.61 |
| | FFM03 | 41 | 17 | 21 | 0.87 | 0.62 |
| | FFM04 | 5 | 18 | 14 | 1.14 | 0.34 |
| | FFM05 | 0 | – | – | – | – |
| | FFM06 | 6 | 28 | 39 | 0.89 | 0.81 |
| Deformation zone | All DZ | 725 | 19 | 24 | 0.86 | 0.66 |
| | GDZ | 296 | 15 | 20 | 0.74 | 0.66 |
| | WNW-NW | 223 | 25 | 28 | 1.03 | 0.63 |
| | NNW | 11 | 5.7 | 8.5 | 0.45 | 0.53 |
| | ENE-NNE | 177 | 19 | 23 | 0.85 | 0.68 |

[1] Data set represents the entire site.

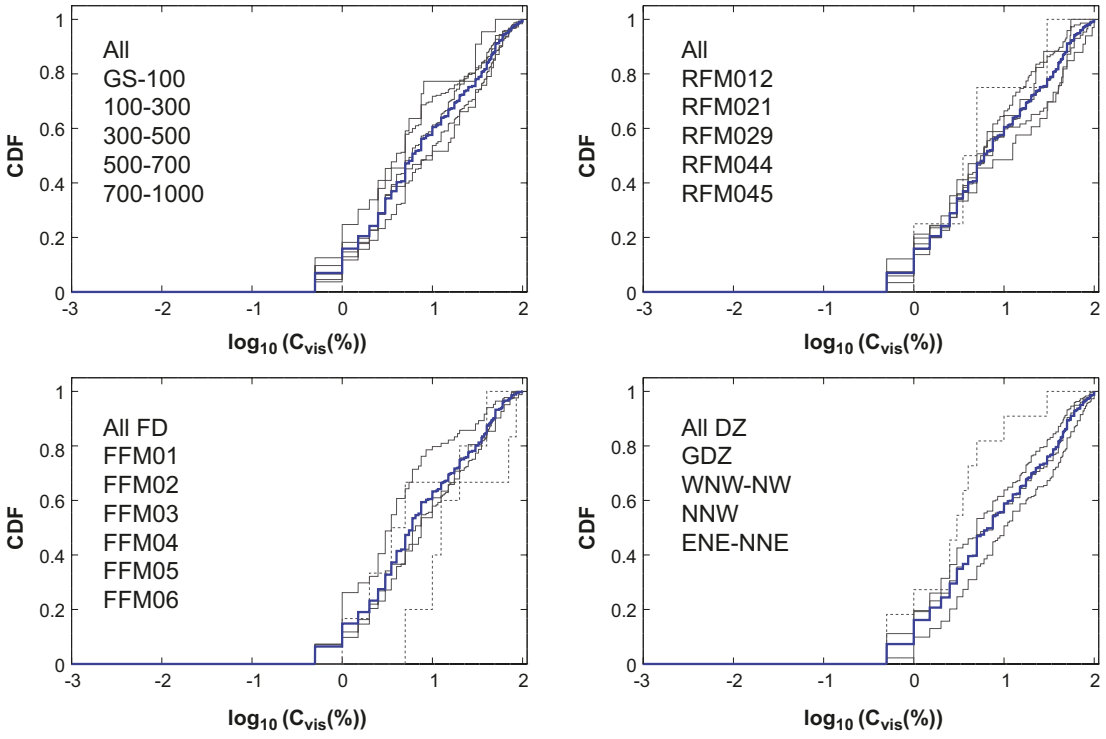


*Figure 4-2. Calcite: Cumulative distribution functions of the separate data subsets (black curves) and of the combined data sets (blue curves). CDFs for data subsets with only up to 20 data points are dotted.*

### 4.2.2 Parametric analysis

As discussed in Section 2.4, the data are not expected to be normally distributed, as the visible coverage ranges from 0 to 100%. Instead the truncated normal distribution may be used. In case of using $C_{vis}$ data, the distribution needs to be truncated at (below) 0% and at (above) 100%. In case of using $\log_{10}(C_{vis})$ data, the distribution needs to be truncated at 2 (100%). For calcite, the data are distributed in such a way that only few $C_{vis}$ data are close to 100%. For example, only 1% of the data has a $C_{vis} > 95\%$. It is more common that the visible coverage for calcite is small, with 40% of the data having a $C_{vis} < 5\%$.

If performing the Shapiro-Wilk $W$ test for $\log_{10}(C_{vis})$ data, the truncation at 2 will not affect the test too much. For calcite data from the entire site, the $W$-value returned is 0.96. For $C_{vis}$ data it is advised against performing the Shapiro-Wilk $W$ test, as the truncation in data at 0% would considerably affect the test.

As the Shapiro-Wilk $W$ test for $\log_{10}(C_{vis})$ data indicates normality, we have chosen to propagate the truncated normal distribution of $\log_{10}(C_{vis})$. Figure 4-3, shows the histogram of $\log_{10}(C_{vis})$ for calcite data from the entire site. Furthermore, the best fit truncated normal distribution (red curve in left figure) and the corresponding normal score plot (right figure) are shown. Similar figures are shown for all fracture mineral data subsets in Appendix B.

To compensate for the truncation in the normal score plot, the linear fit is only based on $C_{vis}$ data $< 100\%$, while $C_{vis}$ data $\geq 100\%$ are censored. As can be seen by the right hand figure, even if there is no theoretical truncation in the lower range, there is a practical truncation stemming from how the methodology was applied.

By making a linear fit in the normal score plot based only on data with $C_{vis} < 100\%$, the $\alpha$ and $\beta$ parameters of Equation 2-2 (corresponding to $\mu$ and $\sigma$ in a normal distribution) could be obtained from the intercept and slope. The data are shown in Table 4-3.

Figure 4-4 illustrates the truncated distributions of Table 4-3, where the distribution representing the entire site is shown by the red line. Distributions of data subsets with more than 20 data points are shown by the solid lines, while distributions of data subsets with up to 20 data points are shown by the shaded lines.

From Figure 4-4 one can see that the best fit distributions for data from the entire site and for the different data subsets very much resemble each other. The deviating distributions are those representing data subsets of only few data points (e.g. FFM04). It should be made clear that the choice of probability distribution is not obvious, and that other choices may be equally valid.

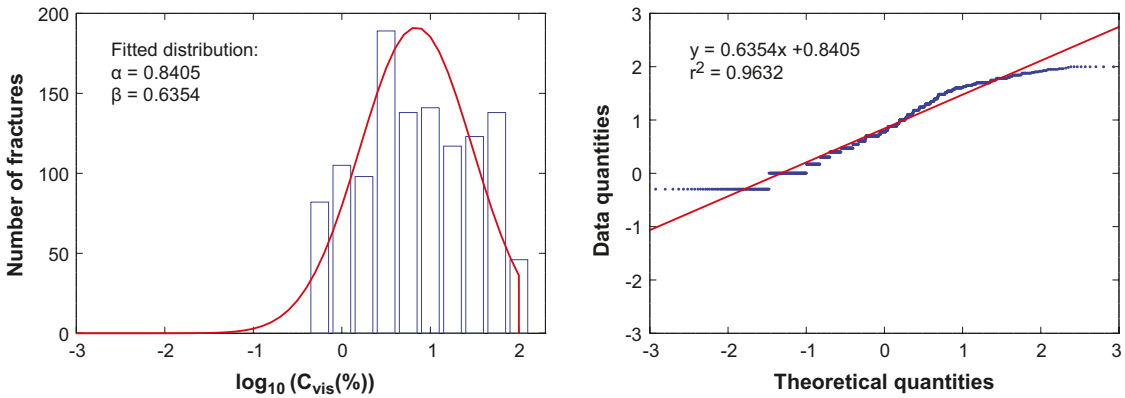


***Figure 4-3.*** *Left: Histogram of $\log_{10}(C_{vis})$ data together with best fit truncated normal distribution. Right: Normal score plot of $\log_{10}(C_{vis})$ data. Data subset used: Calcite from the entire site.*

**Table 4-3. Distribution parameters of populated fractures, calcite.**

| Calcite | | Number of data points | $\log_{10}(C_{vis}$ [%]) $\alpha$ | $\beta$ |
|---|---|---|---|---|
| Elevation (mbsl) | GS–1,000[1] | 1,177 | 0.85 | 0.65 |
| | GS–100 | 486 | 0.96 | 0.63 |
| | 100–300 | 320 | 0.81 | 0.62 |
| | 300–500 | 287 | 0.68 | 0.67 |
| | 500–700 | 62 | 0.93 | 0.73 |
| | 700–1,000 | 22 | 0.70 | 0.61 |
| Rock domain | RFM012 | 33 | 0.94 | 0.84 |
| | RFM018 | 17 | 0.77 | 0.71 |
| | RFM021 | 146 | 0.78 | 0.58 |
| | RFM029 | 891 | 0.85 | 0.65 |
| | RFM044 | 4 | 0.68 | 0.83 |
| | RFM045 | 86 | 0.87 | 0.73 |
| Fracture domain | All FD | 357 | 0.82 | 0.61 |
| | FFM01 | 84 | 0.60 | 0.60 |
| | FFM02 | 221 | 0.88 | 0.61 |
| | FFM03 | 41 | 0.87 | 0.66 |
| | FFM04 | 5 | 1.14 | 0.45 |
| | FFM05 | 0 | – | – |
| | FFM06 | 6 | 0.89 | 0.99 |
| Deformation zone | All DZ | 725 | 0.87 | 0.67 |
| | GDZ | 296 | 0.75 | 0.66 |
| | WNW–NW | 223 | 1.04 | 0.66 |
| | NNW | 11 | 0.45 | 0.61 |
| | ENE-NNE | 177 | 0.86 | 0.69 |

[1] Data set represents the entire site.

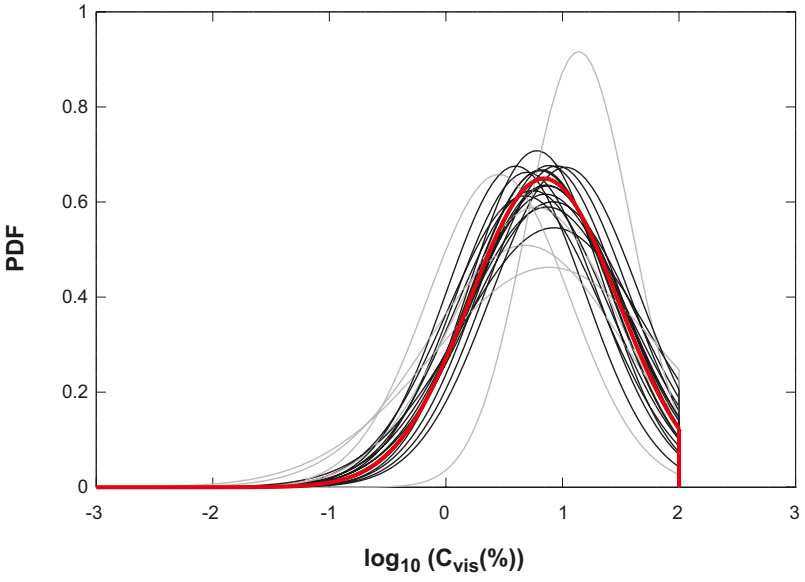


***Figure 4-4.*** *Illustration of truncated normal distributions of Table 4-3. Distributions of data subsets with only up to 20 data points are shaded.*

## 4.3 Chlorite

The analysis of $C_{vis}$ for chlorite corresponds to that for calcite. In Section 4.2 more information on how the analysis is performed is given.

### 4.3.1 Non-parametric analysis

For all data subsets (including quantitative data only) the arithmetic mean $\bar{x}$ and the standard deviation *STD* of $C_{vis}$ and $\log_{10}(C_{vis})$ were calculated. These data are shown in Table 4-4.

As seen in the table, $C_{vis}$ of chlorite is on average 38% in fractures where the mineral is found. For rock volumes where more than 100 data points were obtained, $\bar{x}$ of $C_{vis}$ ranges from 34 to 40%.

By performing a Kruskal-Wallis test on the chlorite $C_{vis}$ data for the separate data subsets, it is strongly indicated that they are not all samples of the same population, with $p = 0.011$.

Figure 4-5 shows the cumulative distribution functions of the data subsets. Combined data sets (All, All FD, and All DZ) are shown in blue lines while separate CDFs are shown in black lines. CDFs representing data subsets of more than 20 data points are shown by solid lines while those representing fewer data are shown by dotted lines.

As can be seen, the CDFs of the data subsets are similar. Based on Table 4-1**,** Table 4-4, and Figure 4-5 one can suggest that the fracture surfaces of the different rock volumes in Forsmark are covered by similar fractions of chlorite.

**Table 4-4. Non-parametric data for chlorite.**

| Chlorite | | Number of data points | $\bar{x}$ of $C_{vis}$ [%] | *STD* of $C_{vis}$ [%] | $\bar{x}$ of $\log_{10}(C_{vis}$ [%]) | *STD* of $\log_{10}(C_{vis}$ [%]) |
|---|---|---|---|---|---|---|
| Elevation (mbsl) | GS–1,000[1] | 1,077 | 38 | 29 | 1.37 | 0.51 |
| | GS–100 | 349 | 37 | 28 | 1.40 | 0.46 |
| | 100–300 | 310 | 38 | 30 | 1.36 | 0.54 |
| | 300–500 | 291 | 36 | 29 | 1.34 | 0.53 |
| | 500–700 | 91 | 41 | 33 | 1.38 | 0.53 |
| | 700–1,000 | 36 | 41 | 32 | 1.43 | 0.47 |
| Rock domain | RFM012 | 45 | 42 | 35 | 1.37 | 0.56 |
| | RFM018 | 27 | 56 | 28 | 1.64 | 0.38 |
| | RFM021 | 123 | 34 | 29 | 1.31 | 0.51 |
| | RFM029 | 780 | 38 | 28 | 1.38 | 0.49 |
| | RFM044 | 5 | 50 | 35 | 1.57 | 0.41 |
| | RFM045 | 97 | 37 | 32 | 1.29 | 0.60 |
| Fracture domain | All FD | 333 | 40 | 29 | 1.40 | 0.52 |
| | FFM01 | 87 | 42 | 30 | 1.42 | 0.54 |
| | FFM02 | 181 | 36 | 28 | 1.35 | 0.50 |
| | FFM03 | 47 | 50 | 31 | 1.52 | 0.52 |
| | FFM04 | 7 | 58 | 33 | 1.69 | 0.30 |
| | FFM05 | 2 | 66 | 23 | 1.81 | 0.15 |
| | FFM06 | 9 | 47 | 36 | 1.36 | 0.71 |
| Deformation zone | All DZ | 670 | 37 | 29 | 1.35 | 0.50 |
| | GDZ | 289 | 34 | 26 | 1.34 | 0.47 |
| | WNW-NW | 162 | 40 | 30 | 1.41 | 0.48 |
| | NNW | 19 | 48 | 32 | 1.50 | 0.52 |
| | ENE-NNE | 184 | 37 | 32 | 1.31 | 0.56 |

[1] Data set represents the entire site.

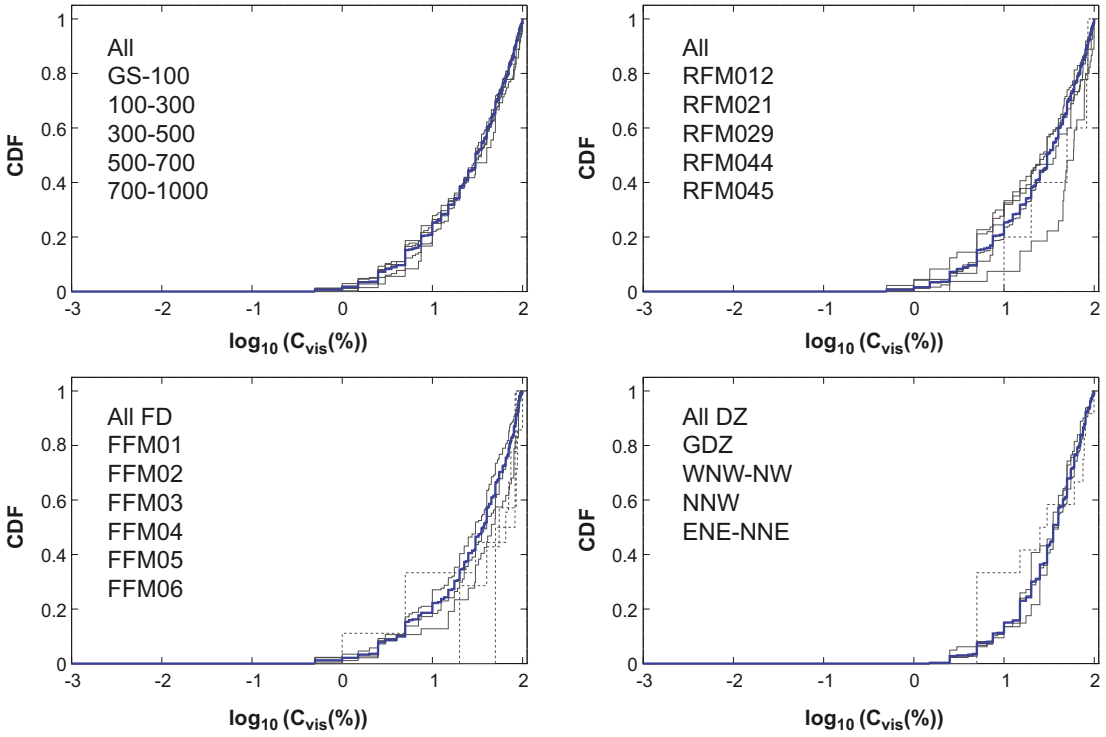


*Figure 4-5. Chlorite: Cumulative distribution functions of the separate data subsets (black curves) and of the combined data sets (blue curves). CDFs for data subsets with up to 20 data points are dotted.*

### 4.3.2 Parametric analysis

As for calcite, the truncation of $C_{vis}$ data at 0% is more pronounced than at 100%. However, in this case there is also a significant truncation of data at 100%. Therefore, if intending to use the truncated normal distribution, the Shapiro-Wilk test may be a poor indication on whether to use $C_{vis}$ or $\log_{10}(C_{vis})$ data. If still using the test the $W$-value returned for $C_{vis}$ data is 0.92, while for $\log_{10}(C_{vis})$ data the $W$-value is 0.91. In the tests, data from the entire site were used. This gives no indication on whether to choose a singly truncated normal distribution for $\log_{10}(C_{vis})$ or a doubly truncated normal distribution for $C_{vis}$. As the $\log_{10}(C_{vis})$ representation was propagated for calcite, we chose to do the same for chlorite.

Figure 4-6 shows a histogram of $\log_{10}(C_{vis})$ for chlorite data from the entire site. Furthermore, the best fit truncated normal distribution (red curve in left figure) and the corresponding normal score plot (right figure) are shown.

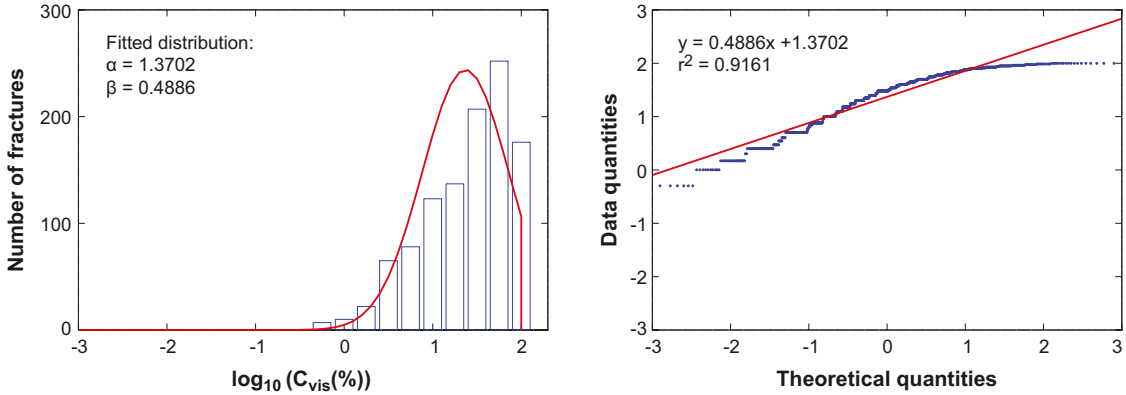


*Figure 4-6. Left: Histogram of $\log_{10}(C_{vis})$ data together with best fit truncated normal distribution. Right: Normal score plot of $\log_{10}(C_{vis})$ data. Data subset used: Chlorite from the entire site.*

By making a linear fit in the normal score plot based on all $C_{vis}$ < 100%, the $\alpha$ and $\beta$ parameters of Equation 2-2 could be obtained from the intercept and slope. The data are shown in Table 4-5.

Figure 4-7 illustrates the truncated distributions of Table 4-5, where the distribution representing the entire site is shown by the red line. Distributions of data subsets with more than 20 data points are shown by the solid lines, while distributions of data subsets with up to 20 data points are shown by the shaded lines.

From Figure 4-7 one can see that the best fit distribution for data from the entire site very much resembles the distributions for the different data subsets. The most deviating distributions are those representing data sets of only few data points (e.g. FFM04). The significantly deviating data subset consisting of more than 20 data points is that of RFM018 (30 data points), where more chlorite is found than on average.

**Table 4-5. Distribution parameters of populated fractures, chlorite.**

| Chlorite | | Number of data points | $\log_{10}(C_{vis}$ [%]) $\alpha$ | $\beta$ |
|---|---|---|---|---|
| Elevation (mbsl) | GS–1,000[1] | 1,077 | 1.38 | 0.51 |
| | GS–100 | 349 | 1.40 | 0.46 |
| | 100–300 | 310 | 1.37 | 0.55 |
| | 300–500 | 291 | 1.34 | 0.53 |
| | 500–700 | 91 | 1.40 | 0.58 |
| | 700–1,000 | 36 | 1.44 | 0.52 |
| Rock domain | RFM012 | 45 | 1.41 | 0.65 |
| | RFM018 | 27 | 1.64 | 0.37 |
| | RFM021 | 123 | 1.31 | 0.53 |
| | RFM029 | 780 | 1.39 | 0.49 |
| | RFM044 | 5 | 1.57 | 0.52 |
| | RFM045 | 97 | 1.30 | 0.61 |
| Fracture domain | All FD | 333 | 1.41 | 0.51 |
| | FFM01 | 87 | 1.43 | 0.54 |
| | FFM02 | 181 | 1.35 | 0.49 |
| | FFM03 | 47 | 1.52 | 0.49 |
| | FFM04 | 7 | 1.72 | 0.42 |
| | FFM05 | 2 | 1.81 | 0.25 |
| | FFM06 | 9 | 1.36 | 0.78 |
| Deformation zone | All DZ | 670 | 1.36 | 0.51 |
| | GDZ | 289 | 1.34 | 0.48 |
| | WNW-NW | 162 | 1.42 | 0.50 |
| | NNW | 19 | 1.53 | 0.59 |
| | ENE-NNE | 184 | 1.32 | 0.58 |

[1] Data set represents the entire site.

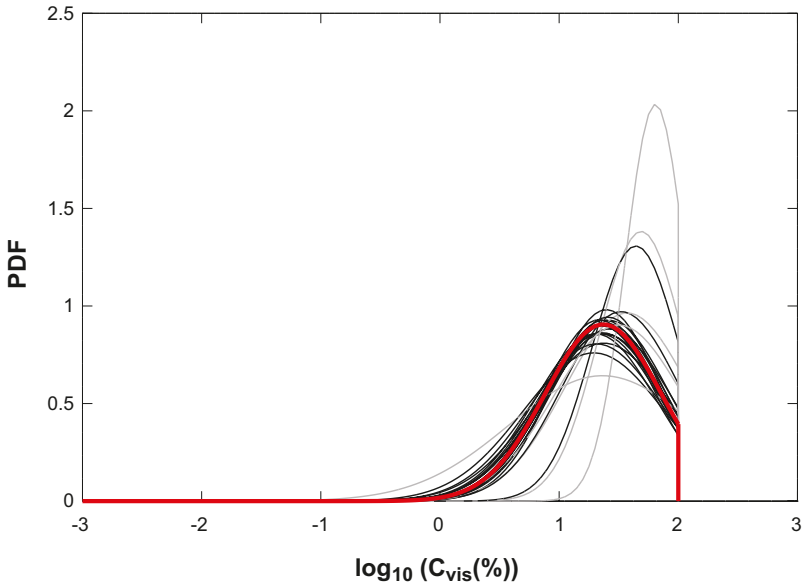


***Figure 4-7.*** *Illustration of truncated normal distributions of Table 4-5. Distributions of data subsets with only up to 20 data points are shaded.*

## 4.4 Clay minerals

The analysis of $C_{vis}$ for clay minerals corresponds to that for calcite. In Section 4.2 more information on how the analysis is performed is given.

### 4.4.1 Non-parametric analysis

For all data subsets (including quantitative data only) the arithmetic mean $\bar{x}$ and the standard deviation *STD* of $C_{vis}$ and $\log_{10}(C_{vis})$ were calculated. These data are shown in Table 4-6.

As seen in the table, $C_{vis}$ of clay minerals is on average 40% in fractures where the mineral is found. For rock volumes where more than 100 data points were obtained, $\bar{x}$ of $C_{vis}$ ranges from 36 to 42%.

By performing a Kruskal-Wallis test on the clay minerals $C_{vis}$ data for the separate data subsets, it is indicated that they may not all be samples of the same population, with $p = 0.15$.

Figure 4-8 shows the cumulative distribution functions of the data subsets. Combined data sets (All, All FD, and All DZ) are shown in blue lines while separate CDFs are shown in black lines. CDFs representing data subsets of more than 20 data points are shown by solid lines while those representing fewer data are shown by dotted lines.

As can be seen, the CDFs of the data subsets are similar. Based on Table 4-1**,** Table 4-6, and Figure 4-8 one can suggest that the fracture surfaces in the different rock volumes in Forsmark are covered by similar fractions of clay minerals.

**Table 4-6. Non-parametric data for clay minerals, as a group.**

| Clay minerals as a group | | Number of data points | $\bar{x}$ of $C_{vis}$ [%] | *STD* of $C_{vis}$ [%] | $\bar{x}$ of $\log_{10}(C_{vis}$ [%]) | *STD* of $\log_{10}(C_{vis}$ [%]) |
|---|---|---|---|---|---|---|
| Elevation (mbsl) | GS–1,000[1] | 573 | 40 | 26 | 1.46 | 0.39 |
| | GS–100 | 282 | 42 | 27 | 1.49 | 0.39 |
| | 100–300 | 99 | 40 | 27 | 1.47 | 0.40 |
| | 300–500 | 150 | 36 | 24 | 1.42 | 0.40 |
| | 500–700 | 23 | 24 | 19 | 1.25 | 0.36 |
| | 700–1,000 | 19 | 48 | 28 | 1.55 | 0.43 |
| Rock domain | RFM012 | 21 | 48 | 22 | 1.63 | 0.21 |
| | RFM018 | 9 | 41 | 30 | 1.46 | 0.41 |
| | RFM021 | 46 | 34 | 21 | 1.43 | 0.34 |
| | RFM029 | 450 | 40 | 27 | 1.46 | 0.40 |
| | RFM044 | 3 | 46 | 33 | 1.55 | 0.41 |
| | RFM045 | 44 | 41 | 27 | 1.48 | 0.40 |
| Fracture domain | All FD | 154 | 36 | 25 | 1.42 | 0.40 |
| | FFM01 | 39 | 33 | 23 | 1.38 | 0.41 |
| | FFM02 | 94 | 38 | 27 | 1.43 | 0.40 |
| | FFM03 | 17 | 39 | 22 | 1.47 | 0.38 |
| | FFM04 | 0 | – | – | – | – |
| | FFM05 | 2 | 30 | 25 | 1.39 | 0.41 |
| | FFM06 | 2 | 15 | 7 | 1.15 | 0.21 |
| Deformation zone | All DZ | 399 | 41 | 27 | 1.48 | 0.39 |
| | GDZ | 225 | 42 | 27 | 1.49 | 0.39 |
| | WNW-NW | 81 | 38 | 26 | 1.44 | 0.40 |
| | NNW | 12 | 40 | 36 | 1.36 | 0.54 |
| | ENE-NNE | 74 | 42 | 26 | 1.51 | 0.37 |

[1] Data set represents the entire site.

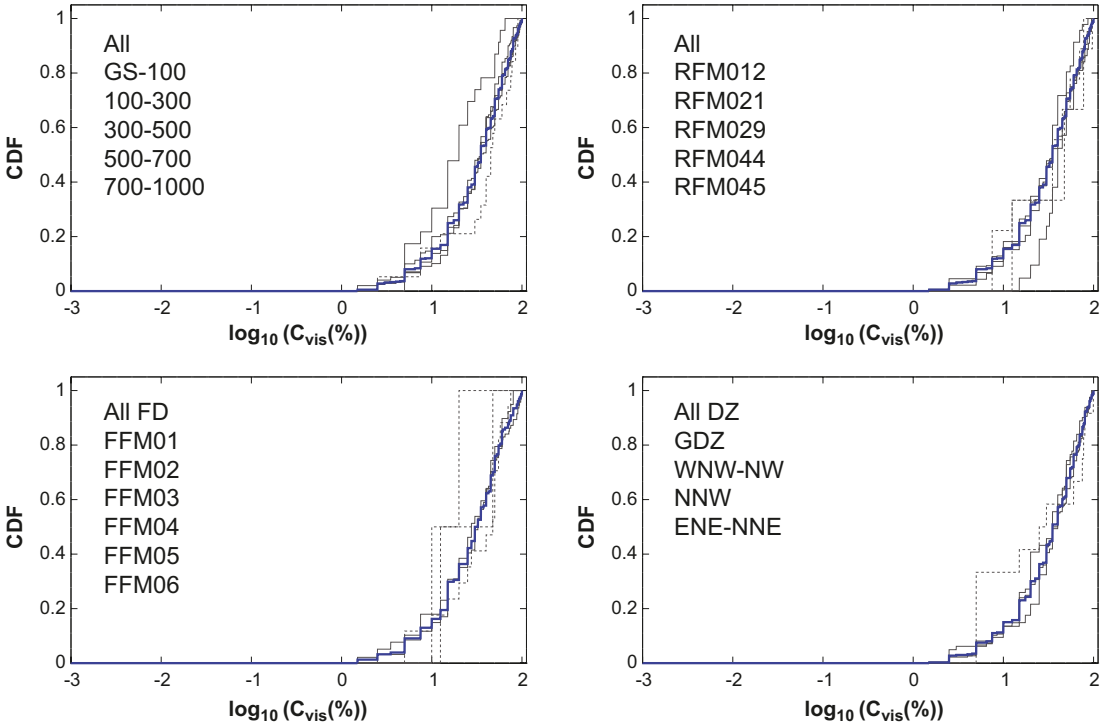


*Figure 4-8. Clay minerals: Cumulative distribution functions of the separate data subsets (black curves) and of the combined data sets (blue curves). CDFs for data subsets with up to 20 data points are dotted.*

### 4.4.2 Parametric analysis

The truncation situation for clay minerals is very much the same as for chlorite. If intending to use the truncated normal distribution, the Shapiro-Wilk test may be a poor indication on whether to use $C_{vis}$ or $\log_{10}(C_{vis})$ data. If anyhow using the test, the $W$-value returned for $C_{vis}$ data is 0.95 while for $\log_{10}(C_{vis})$ data the $W$-value returned is 0.92. In the tests, data from the entire site were used. This gives no indication on whether to choose a singly truncated normal distribution for $\log_{10}(C_{vis})$ or a doubly truncated normal distribution for $C_{vis}$. As the $\log_{10}(C_{vis})$ representation was propagated for calcite, we chose to do the same for clay minerals.

Figure 4-9 shows a histogram of $\log_{10}(C_{vis})$ for clay minerals data from the entire site. Furthermore, the best fit truncated normal distribution (red curve in left figure) and the corresponding normal score plot (right figure) are shown.

By making a linear fit in the normal score plot based on all $C_{vis} < 100\%$, the $\alpha$ and $\beta$ parameters of Equation 2-2 could be obtained from the intercept and slope. The data are shown in Table 4-7.

Figure 4-10 illustrates the truncated distributions of Table 4-7, where the distribution representing the entire site is shown by the red line. Distributions of data subsets with more than 20 data points are shown by the solid lines, while distributions of data subsets with up to 20 data points are shown by the shaded lines.

From Figure 4-10 one can see that the best fit distribution for data from the entire site resembles nearly all of the distributions for the different data subsets. The most deviating distribution is for RFM012, representing only 21 data points.

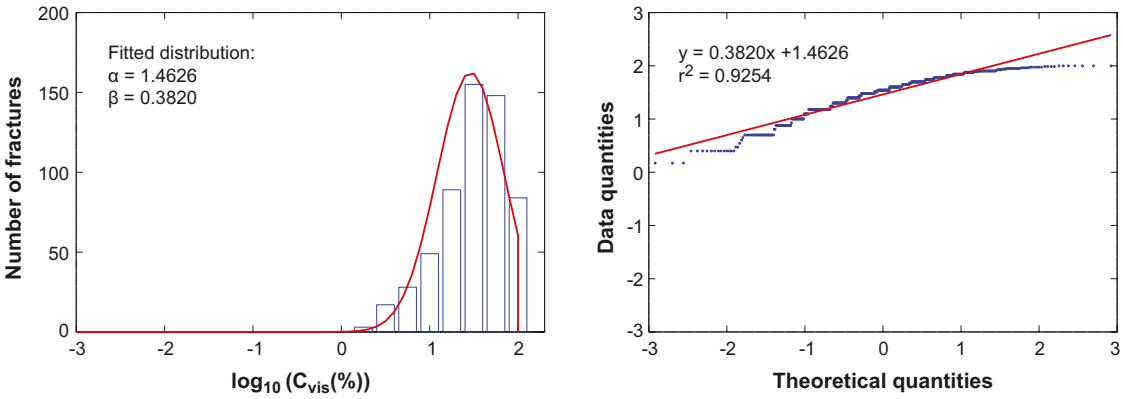


***Figure 4-9.*** *Left: Histogram of $\log_{10}(C_{vis})$ data together with best fit truncated normal distribution. Right: Normal score plot of $\log_{10}(C_{vis})$ data. Data subset used: Clay minerals from the entire site.*

**Table 4-7. Distribution parameters of populated fractures, clay minerals as a group.**

| Clay minerals as a group | | Number of data points | $\log_{10}(C_{vis}$ [%]) $\alpha$ | $\beta$ |
|---|---|---|---|---|
| Elevation (mbsl) | GS–1,000[1] | 573 | 1.47 | 0.40 |
| | GS–100 | 282 | 1.50 | 0.40 |
| | 100–300 | 99 | 1.48 | 0.40 |
| | 300–500 | 150 | 1.42 | 0.39 |
| | 500–700 | 23 | 1.25 | 0.40 |
| | 700–1,000 | 19 | 1.55 | 0.44 |
| Rock domain | RFM012 | 21 | 1.63 | 0.24 |
| | RFM018 | 9 | 1.46 | 0.48 |
| | RFM021 | 46 | 1.43 | 0.35 |
| | RFM029 | 450 | 1.46 | 0.41 |
| | RFM044 | 3 | 1.55 | 0.59 |
| | RFM045 | 44 | 1.48 | 0.41 |
| Fracture domain | All FD | 154 | 1.43 | 0.41 |
| | FFM01 | 39 | 1.38 | 0.43 |
| | FFM02 | 94 | 1.44 | 0.42 |
| | FFM03 | 17 | 1.47 | 0.40 |
| | FFM04 | 0 | – | – |
| | FFM05 | 2 | 1.39 | 0.67 |
| | FFM06 | 2 | 1.15 | 0.35 |
| Deformation zone | All DZ | 399 | 1.49 | 0.39 |
| | GDZ | 225 | 1.50 | 0.40 |
| | WNW-NW | 81 | 1.44 | 0.40 |
| | NNW | 12 | 1.36 | 0.60 |
| | ENE-NNE | 74 | 1.51 | 0.37 |

[1] Data set represents the entire site.

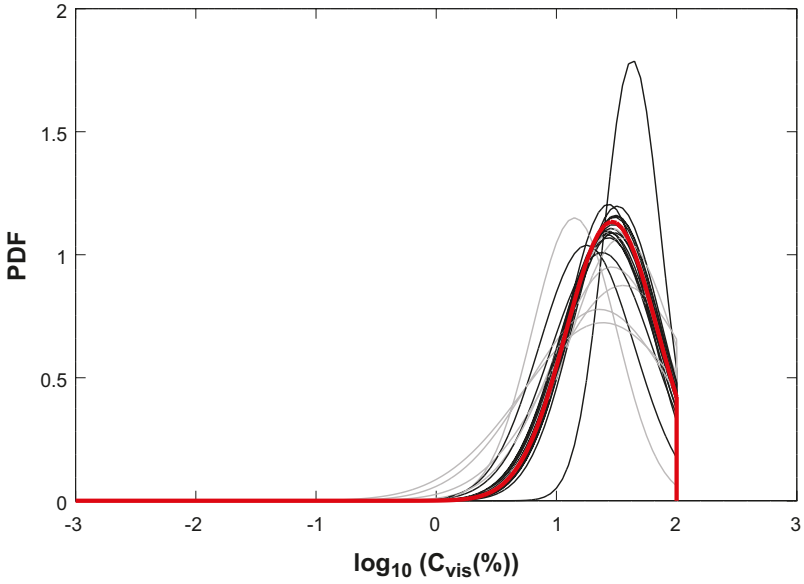


***Figure 4-10.*** *Illustration of truncated normal distributions of Table 4-7. Distributions of data subsets with only up to 20 data points are shaded.*

## 4.5 Hematite

The analysis of $C_{vis}$ for hematite corresponds to that for calcite. In Section 4.2 more information on how the analysis is performed is given. It should be noted that only 34 quantitative $C_{vis}$ data were obtained for hematite. Hence, the results from the analyses are somewhat uncertain.

### 4.5.1 Non-parametric analysis

For all data subsets (including quantitative data only) the arithmetic mean $\bar{x}$ and the standard deviation *STD* of $C_{vis}$ and $\log_{10}(C_{vis})$ were calculated. These data are shown in Table 4-8.

As seen in the table, $\bar{x}$ of $C_{vis}$ of hematite is on average 14% in the few fractures where the mineral is found.

By performing a Kruskal-Wallis test on the few available hematite $C_{vis}$ data for the separate data subsets, it is indicated that they may or may not be samples of the same population, with $p = 0.79$.

Figure 4-11 shows the cumulative distribution functions of the data subsets. Combined data sets (All, All FD, and All DZ) are shown in blue lines while separate CDFs are shown in black lines. CDFs representing data subsets of more than 20 data points are shown by solid lines while those representing fewer data are shown by dotted lines.

Due to the few data available, we refrain from making further non-parametric comparisons between the data subsets.

**Table 4-8. Non-parametric data for hematite.**

| Hematite | | Number of data points | $\bar{x}$ of $C_{vis}$ [%] | *STD* of $C_{vis}$ [%] | $\bar{x}$ of $\log_{10}(C_{vis}$ [%]) | *STD* of $\log_{10}(C_{vis}$ [%]) |
|---|---|---|---|---|---|---|
| Elevation (mbsl) | GS–1,000[1] | 34 | 14 | 22 | 0.79 | 0.55 |
| | GS–100 | 18 | 12 | 19 | 0.69 | 0.57 |
| | 100–300 | 11 | 22 | 28 | 1.04 | 0.56 |
| | 300–500 | 2 | 4.3 | 1.1 | 0.62 | 0.11 |
| | 500–700 | 2 | 5.0 | 3.5 | 0.64 | 0.34 |
| | 700–1,000 | 1 | 3.0 | – | 0.48 | – |
| Rock domain | RFM012 | 4 | 16 | 7.8 | 1.18 | 0.19 |
| | RFM018 | 0 | – | – | – | – |
| | RFM021 | 8 | 13 | 25 | 0.72 | 0.55 |
| | RFM029 | 21 | 15 | 23 | 0.76 | 0.59 |
| | RFM044 | 0 | – | – | – | – |
| | RFM045 | 1 | 3.0 | – | 0.48 | – |
| Fracture domain | All FD | 11 | 12 | 14 | 0.86 | 0.46 |
| | FFM01 | 2 | 10 | 7 | 0.94 | 0.34 |
| | FFM02 | 9 | 13 | 15 | 0.84 | 0.50 |
| | FFM03 | 0 | – | – | – | – |
| | FFM04 | 0 | – | – | – | – |
| | FFM05 | 0 | – | – | – | – |
| | FFM06 | 0 | – | – | – | – |
| Deformation zone | All DZ | 16 | 15 | 25 | 0.78 | 0.61 |
| | GDZ | 7 | 10 | 10 | 0.73 | 0.62 |
| | WNW-NW | 5 | 22 | 40 | 0.77 | 0.73 |
| | NNW | 0 | – | – | – | – |
| | ENE-NNE | 4 | 17 | 25 | 0.87 | 0.62 |

[1] Data set represents the entire site.

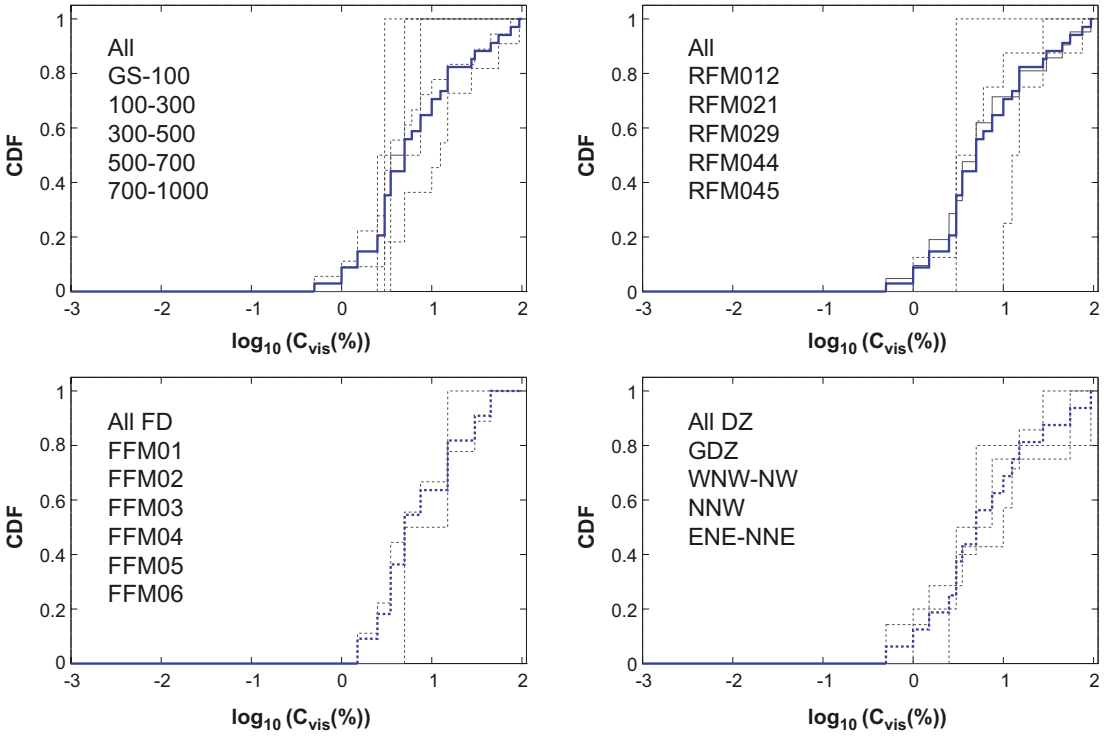


***Figure 4-11.*** *Hematite: Cumulative distribution functions of the separate data subsets (black curves) and of the combined data sets (blue curves). CDFs for data subsets with up to 20 data points are dotted.*

### 4.5.2 Parametric analysis

For hematite the truncation situation is similar as for calcite, with the truncation affecting the normality of $C_{vis}$ data but not so much the normality of $\log_{10}(C_{vis})$ data. For $\log_{10}(C_{vis})$ data from the entire site, the $W$-value returned from a Shapiro-Wilk test is 0.97. This indicates that the $\log_{10}(C_{vis})$ representation can be propagated for hematite.

Figure 4-12 shows a histogram of $\log_{10}(C_{vis})$ for hematite data from the entire site. Furthermore, the best fit truncated normal distribution (red curve in left figure) and the corresponding normal score plot (right figure) are shown.

By making a linear fit in the normal score plot based on all $C_{vis} < 100\%$, the $\alpha$ and $\beta$ parameters of Equation 2-2 can be obtained from the intercept and slope. The data are shown in Table 4-9.

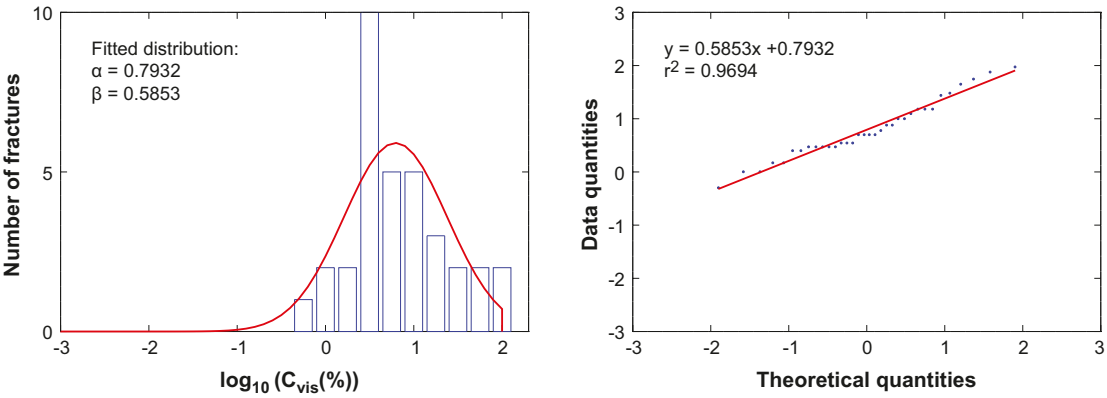


***Figure 4-12.*** *Left: Histogram of $\log_{10}(C_{vis})$ data together with best fit truncated normal distribution. Right: Normal score plot of $\log_{10}(C_{vis})$ data. Data subset used: Hematite from the entire site.*

**Table 4-9. Distribution parameters of populated fractures, hematite.**

| Hematite | | Number of data points | $\log_{10}(C_{vis})$ $\alpha$ | $\beta$ |
|---|---|---|---|---|
| Elevation (mbsl) | GS–1,000[1] | 34 | 0.79 | 0.59 |
| | GS–100 | 18 | 0.69 | 0.63 |
| | 100–300 | 11 | 1.04 | 0.66 |
| | 300–500 | 2 | 0.62 | 0.18 |
| | 500–700 | 2 | 0.64 | 0.55 |
| | 700–1,000 | 1 | 0.48 | – |
| Rock domain | RFM012 | 4 | 1.18 | 0.25 |
| | RFM018 | 0 | – | – |
| | RFM021 | 8 | 0.72 | 0.62 |
| | RFM029 | 21 | 0.76 | 0.65 |
| | RFM044 | 0 | – | – |
| | RFM045 | 1 | 0.48 | – |
| Fracture domain | All FD | 11 | 0.86 | 0.54 |
| | FFM01 | 2 | 0.94 | 0.55 |
| | FFM02 | 9 | 0.84 | 0.60 |
| | FFM03 | 0 | – | – |
| | FFM04 | 0 | – | – |
| | FFM05 | 0 | – | – |
| | FFM06 | 0 | – | – |
| Deformation zone | All DZ | 16 | 0.78 | 0.69 |
| | GDZ | 7 | 0.73 | 0.76 |
| | WNW-NW | 5 | 0.77 | 0.89 |
| | NNW | 0 | – | – |
| | ENE-NNE | 4 | 0.87 | 0.80 |

[1] Data set represents the entire site.

Figure 4-13 illustrates the truncated distributions of Table 4-9, where the distribution representing the entire site is shown by the red line. Distributions of data subsets with more than 20 data points are shown by the solid lines, while distributions of data subsets with up to 20 data points are shown by the shaded lines.

Due to the scarcity of data, we refrain from making further comparisons for hematite.

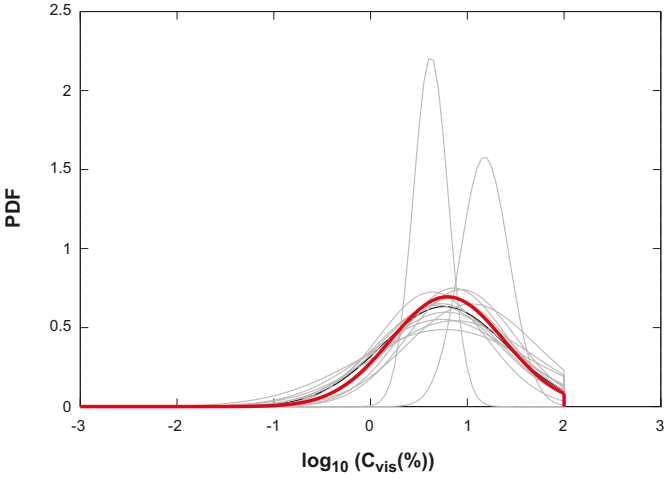


***Figure 4-13.*** *Illustration of truncated normal distributions of Table 4-9. Distributions of data sets with only up to 20 data points are shaded.*

## 4.6 Pyrite

The analysis of $C_{vis}$ for pyrite corresponds to that for calcite. In Section 4.2 more information on how the analysis is performed is given.

### 4.6.1 Non-parametric analysis

For all data subsets (including quantitative data only) the arithmetic mean $\bar{x}$ and the standard deviation *STD* of $C_{vis}$ and $\log_{10}(C_{vis})$ were calculated. These data are shown in Table 4-10.

As seen in the table, $C_{vis}$ of pyrite is on average only 0.45% in fractures where the mineral is found.

By performing a Kruskal-Wallis test on the pyrite $C_{vis}$ data for the separate data subsets, it is indicated that they may not all be samples of the same population, with $p = 0.11$.

Figure 4-5 shows the cumulative distribution functions of the data subsets. Combined data sets (All, All FD, and All DZ) are shown in blue lines while separate CDFs are shown in black lines. CDFs representing data subsets of more than 20 data points are shown by solid lines while those representing fewer data are shown by dotted lines.

As can be seen, the CDFs of the data subsets of more than 20 data points are very similar. Based on Table 4-1, Table 4-10, and Figure 4-14 one can suggest that the fracture surfaces of the different rock volumes in Forsmark are covered by similar fractions of pyrite.

**Table 4-10. Non-parametric data for pyrite.**

| Pyrite | | Number of data points | $\bar{x}$ of $C_{vis}$ [%] | *STD* of $C_{vis}$ [%] | $\bar{x}$ of $\log_{10}(C_{vis}$ [%]) | *STD* of $\log_{10}(C_{vis}$ [%]) |
|---|---|---|---|---|---|---|
| Elevation (mbsl) | GS–1,000[1] | 203 | 0.45 | 1.06 | –1.52 | 1.19 |
| | GS–100 | 70 | 0.55 | 1.17 | –1.48 | 1.23 |
| | 100–300 | 87 | 0.45 | 1.17 | –1.61 | 1.22 |
| | 300–500 | 27 | 0.34 | 0.62 | –1.35 | 1.07 |
| | 500–700 | 15 | 0.23 | 0.41 | –1.69 | 1.15 |
| | 700–1,000 | 4 | 0.38 | 0.25 | –0.70 | 0.80 |
| Rock domain | RFM012 | 11 | 0.74 | 0.92 | –0.76 | 0.98 |
| | RFM018 | 2 | 0.73 | 0.39 | –0.17 | 0.25 |
| | RFM021 | 4 | 0.38 | 0.75 | –1.94 | 1.42 |
| | RFM029 | 171 | 0.44 | 1.12 | –1.59 | 1.18 |
| | RFM044 | 2 | 0.50 | 0.00 | –0.30 | 0.00 |
| | RFM045 | 13 | 0.34 | 0.46 | –1.38 | 1.31 |
| Fracture domain | All FD | 58 | 0.49 | 1.36 | –1.66 | 1.25 |
| | FFM01 | 12 | 0.36 | 0.72 | –1.77 | 1.38 |
| | FFM02 | 37 | 0.58 | 1.64 | –1.62 | 1.24 |
| | FFM03 | 7 | 0.20 | 0.36 | –1.78 | 1.21 |
| | FFM04 | 0 | – | – | – | – |
| | FFM05 | 0 | – | – | – | – |
| | FFM06 | 2 | 0.50 | 0.71 | –1.35 | 1.91 |
| Deformation zone | All DZ | 139 | 0.45 | 0.93 | –1.42 | 1.17 |
| | GDZ | 34 | 0.55 | 1.35 | –1.58 | 1.18 |
| | WNW-NW | 30 | 0.61 | 1.00 | –0.96 | 0.96 |
| | NNW | 3 | 0.50 | 0.00 | –0.30 | 0.00 |
| | ENE-NNE | 70 | 0.35 | 0.64 | –1.53 | 1.19 |

[1] Data set represents the entire site.

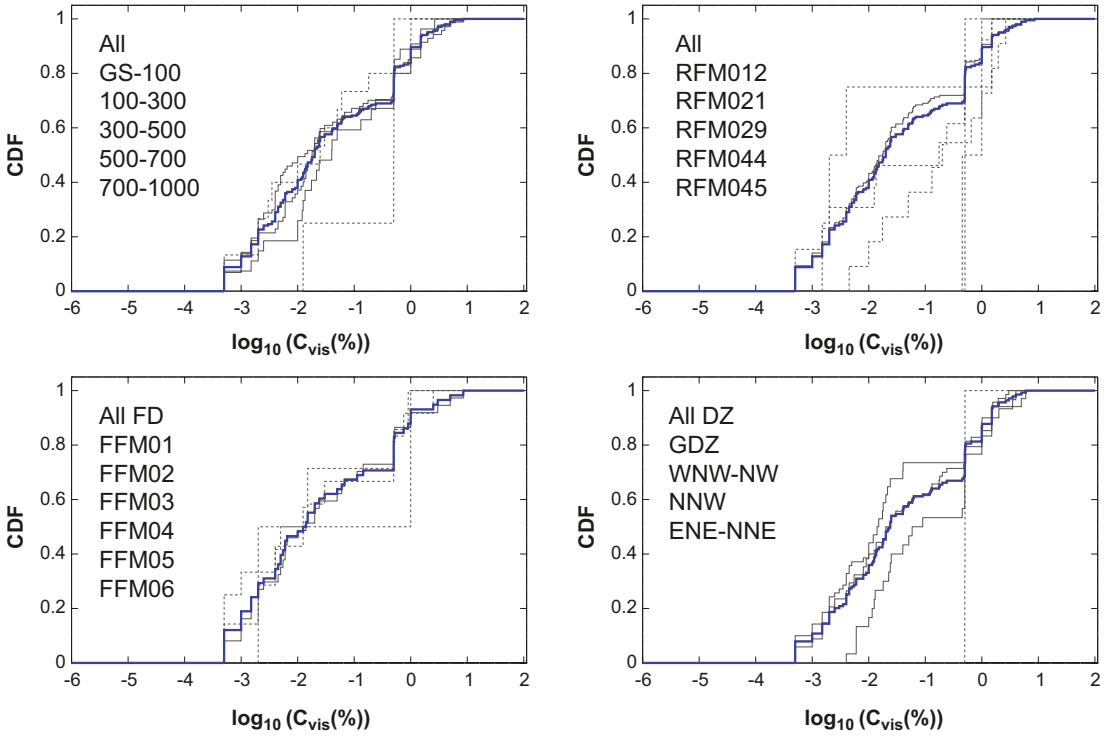


***Figure 4-14.*** *Pyrite: Cumulative distribution functions of the separate data subsets (black curves) and of the combined data sets (blue curves). CDFs for data subsets with up to 20 data points are dotted.*

### 4.6.2 Parametric analysis

For pyrite, no $C_{vis}$ is close to 100% and most $C_{vis}$ data are below 1%. For pyrite, the Shapiro-Wilk test is a good test for normality for $\log_{10}(C_{vis})$ data. For $C_{vis}$ data, however, the truncation issue at 0% affects the test too much. The returned $W$-value for $\log_{10}(C_{vis})$ data is 0.94, wherefore we have chosen to propagate this representation of the data.

Figure 4-15 shows a histogram of $\log_{10}(C_{vis})$ for pyrite data from the entire site. Furthermore, the best fit (truncated) normal distribution (red curve in left figure) and the corresponding normal score plot (right figure) are shown.

The resolution/rounding issue that applies for $d_{mean}$ for pyrite (see Section 2.4.4) applies in a similar fashion for $C_{vis}$. Here, the minimum value of $C_{vis}$ for layer minerals is 0.5% ($\log_{10}(C_{vis}) = -0.3$), a bar that is much overrepresented in Figure 4-15. The minimum value of $\log_{10}(C_{vis})$ for spot minerals is –3.3.

By making a linear fit in the normal score plot based on all $C_{vis} < 100\%$, which in this case is all data, the $\alpha$ and $\beta$ parameters of Equation 2-2 could be obtained from the intercept and slope. The data are shown in Table 4-11.

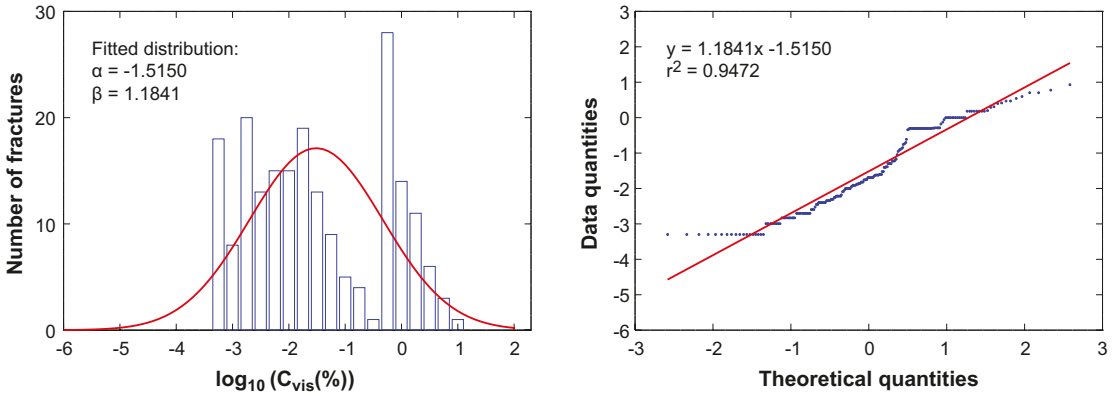


***Figure 4-15.*** *Left: Histogram of $log_{10}(C_{vis})$ data together with best fit truncated normal distribution. Right: Normal score plot of $log_{10}(C_{vis})$ data. Data subset used: pyrite from the entire site.*

**Table 4-11. Distribution parameters of populated fractures, pyrite.**

| Pyrite | | Number of data points | $log_{10}(C_{vis}$ [%]) $\alpha$ | $\beta$ |
|---|---|---|---|---|
| Elevation (mbsl) | GS–1,000[1] | 203 | –1.52 | 1.18 |
| | GS–100 | 70 | –1.48 | 1.26 |
| | 100–300 | 87 | –1.61 | 1.22 |
| | 300–500 | 27 | –1.35 | 1.16 |
| | 500–700 | 15 | –1.69 | 1.29 |
| | 700–1,000 | 4 | –0.70 | 0.88 |
| Rock domain | RFM012 | 11 | –0.76 | 1.14 |
| | RFM018 | 2 | –0.17 | 0.40 |
| | RFM021 | 4 | –1.94 | 1.68 |
| | RFM029 | 171 | –1.59 | 1.17 |
| | RFM044 | 2 | –0.30 | 0 |
| | RFM045 | 13 | –1.38 | 1.45 |
| Fracture domain | All FD | 58 | –1.66 | 1.28 |
| | FFM01 | 12 | –1.77 | 1.56 |
| | FFM02 | 37 | –1.62 | 1.30 |
| | FFM03 | 7 | –1.78 | 1.47 |
| | FFM04 | 0 | – | – |
| | FFM05 | 0 | – | – |
| | FFM06 | 2 | –1.35 | 3.13 |
| Deformation zone | All DZ | 139 | –1.42 | 1.18 |
| | GDZ | 34 | –1.58 | 1.23 |
| | WNW-NW | 30 | –0.96 | 1.01 |
| | NNW | 3 | –0.30 | 0 |
| | ENE-NNE | 70 | –1.53 | 1.22 |

[1] Data set represents the entire site.

Figure 4-16 illustrates the truncated distributions of Table 4-11, where the distribution representing the entire site is shown by the red line. Distributions of data subsets with more than 20 data points are shown by the solid lines, while distributions of data subsets with up to 20 data points are shown by the shaded lines.

From Figure 4-16 one can see that the best fit distribution for data from the entire site very much resembles the distributions for the different data subsets. The deviating distributions are the one representing deformation zone WNW-NW, shifted towards higher visble coverage, and those representing data sets of only few data points (e.g. RFM018).

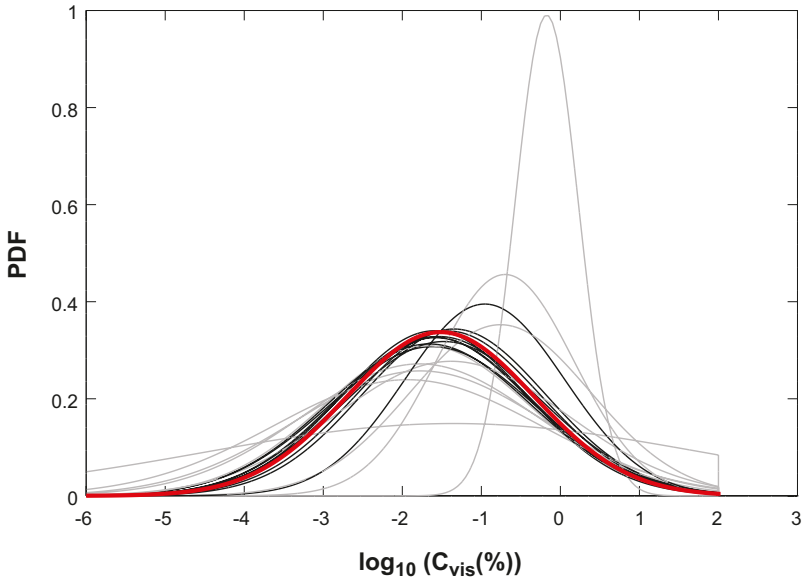


***Figure 4-16.*** *Illustration of truncated normal distributions of Table 4-11. Distributions of data subsets with only up to 20 data points are shaded. Distributions for RFM044 and NNW are not shown.*

# 5 Distribution parameters suggested for use in subsequent modelling

## 5.1 Tabulated distribution parameters

In Chapters 3 and 4 it has been shown that the different rock volumes of the Forsmark site generally hold fracture minerals of similar amounts and visible coverages. This is best seen from the cumulative distribution functions of $\log_{10}(d_{mean})$ and $\log_{10}(C_{vis})$ for the different data subsets. It is also shown that the normal distribution fairly well describes $\log_{10}(d_{mean})$ data while the truncated normal distribution fairly well describes $\log_{10}(C_{vis})$ data.

In this chapter we suggest a set of data for each fracture minerals in form of probability distribution function parameters for $\log_{10}(d_{mean})$ and $\log_{10}(C_{vis})$. The parameters of the distributions are given in Table 5-1 and Table 5-2. These data may be used as input in subsequent hydrogeochemical and radionuclide transport modelling. The background to the suggested data is summarised in Section 5.2.

**Table 5-1. Normal distributions of $\log_{10}(d_{mean})$, suggested for use in SR-Site.**

| Fracture mineral | $\mu$ of $\log_{10}(d_{mean})$ | $\sigma$ of $\log_{10}(d_{mean})$ | $f_{quant}$ (%) |
|---|---|---|---|
| Calcite | –1.47 | 0.70 | 32 |
| Chlorite | –0.93 | 0.46 | 24 |
| Clay minerals, as a group | –1.09 | 0.44 | 11 |
| Hematite | –2.01 | 0.65 | 0.4 |
| Pyrite | –4.01 | 1.26 | 10 |
| Equation of PDF associated with the parameters | $\varphi(\log_{10}(d_{mean})) = \frac{1}{\sigma\sqrt{2\pi}}\exp\left(-\frac{(\log_{10}(d_{mean})-\mu)^2}{2\sigma^2}\right)$ | | |

**Table 5-2. Truncated normal distributions of $\log_{10}(C_{vis})$, suggested for use in SR-Site.**

| Fracture mineral | $\alpha$ of $\log_{10}(C_{vis})$ | $\beta$ of $\log_{10}(C_{vis})$ | $f_{quant}^c$ (%) |
|---|---|---|---|
| Calcite | 0.85 | 0.65 | 57 |
| Chlorite | 1.38 | 0.51 | 52 |
| Clay minerals, as a group | 1.47 | 0.40 | 28 |
| Hematite | 0.79 | 0.59 | 2 |
| Pyrite | –1.52 | 1.18 | 10 |
| Equation of PDF associated with the parameters | For $C_{vis} \le 100\%$: $\varphi(\log_{10}(C_{vis})) = \frac{\frac{1}{\beta\sqrt{2\pi}}\exp\left(-\frac{(\log_{10}(C_{vis})-\alpha)^2}{2\beta^2}\right)}{\int_{-\infty}^{2}\frac{1}{\beta\sqrt{2\pi}}\exp\left(-\frac{(\log_{10}(C_{vis})-\alpha)^2}{2\beta^2}\right)}$ For $C_{vis} > 100\%$: $\varphi(\log_{10}(C_{vis})) = 0$ | | |

## 5.2 Summarised background to suggested data

This section summarises the reasons for suggesting the probability distribution and distribution parameters in Table 5-1 and Table 5-2. In Chapters 3 and 4, the cumulative distribution functions and best fit probability distributions for the data subsets are given for the studied fracture minerals. In Figure 5-1 to Figure 5-10, all the CDFs for each mineral are shown, and also the CDF for the suggested best fit distribution of Table 5-1 or Table 5-2.

### 5.2.1 Calcite

In Figure 5-1 the CDFs for $\log_{10}(d_{mean})$ data for calcite are displayed. As in Chapter 3 and 4, CDFs representing data subsets of more than 20 data points are shown by solid lines. CDFs representing data subsets of up to 20 data points are shown by dotted lines. The CDF for data from the entire site is shown by a blue curve. The CDF for the best fit distribution for calcite, given in Table 5-1, is shown by the red curve.

The corresponding plot for the calcite $\log_{10}(C_{vis})$ is shown in Figure 5-2. The red curve shows the CDF of the best fit truncated normal distribution given in Table 5-2.

As can be seen in Figure 5-1 and Figure 5-2, the best fit distributions fairly well describe the CDFs of the different data subsets. Generally, the larger the data subset is, the less the CDF deviates from the best fit distribution CDF. This is especially true for $\log_{10}(d_{mean})$ data from the entire site. Based on the appearance of the figures, we suggest that the distributions for calcite in Table 5-1 and Table 5-2 reasonably well represent all rock volumes at the site. If a reduced data set is required as input data in subsequent modelling, these distributions may be used.

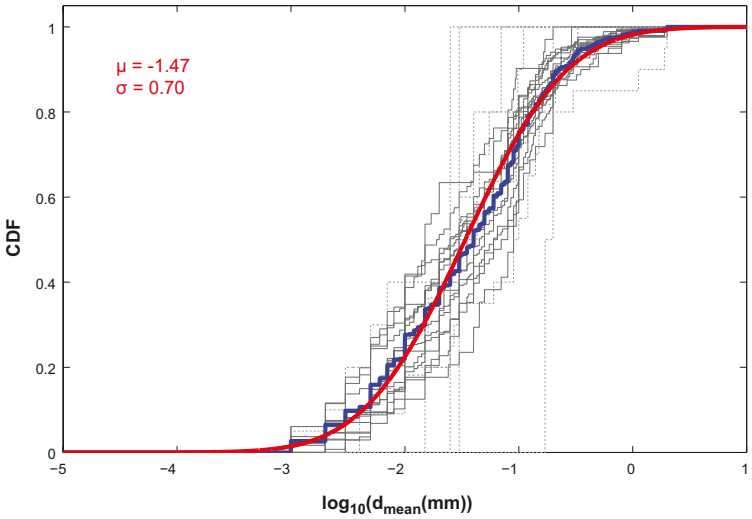


***Figure 5-1.*** *Calcite – $d_{mean}$: Cumulative distribution functions of the separate data subsets (black curves) and of the data from the entire site (blue curve). CDFs for data subsets with up to 20 data points are dotted. The red curve represents the CDF of the best fitted normal distribution for data from the entire site.*

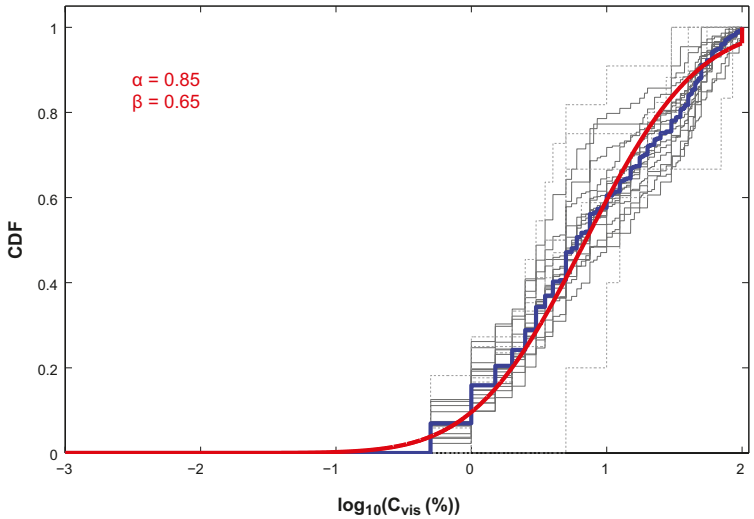


***Figure 5-2.*** *Calcite – $C_{vis}$: Cumulative distribution functions of the separate data subsets (black curves) and of the data from the entire site (blue curve). CDFs for data subsets with up to 20 data points are dotted. The red curve represents the CDF of the best fitted truncated normal distribution for data from the entire site.*

### 5.2.2 Chlorite

The corresponding figures to Figure 5-1 and Figure 5-2 are displayed below for chlorite.

Based on the appearance of the figures, the same conclusions are drawn for chlorite as for calcite. We suggest that the distributions for chlorite in Table 5-1 and Table 5-2 reasonably well represent all rock volumes at the site.

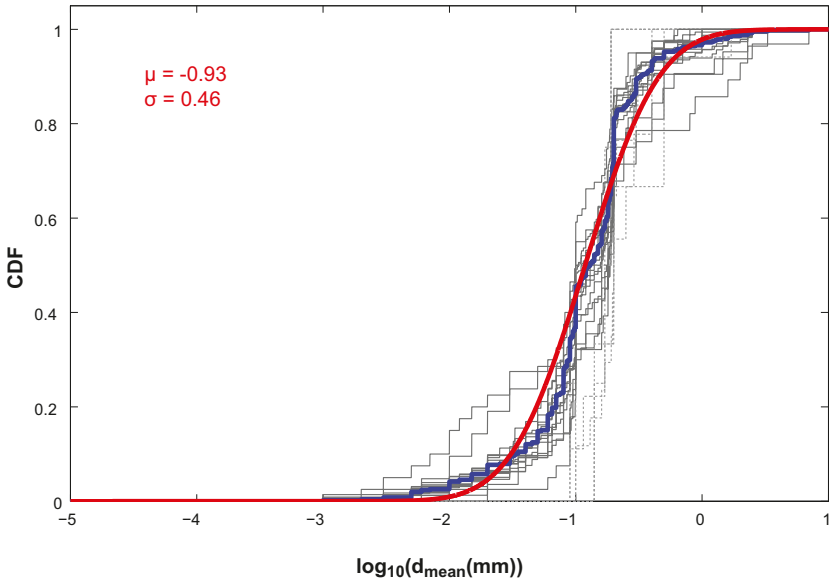


***Figure 5-3.*** *Chlorite – $d_{mean}$: Cumulative distribution functions of the separate data subsets (black curves) and of the data from the entire site (blue curve). CDFs for data subsets with up to 20 data points are dotted. The red curve represents the CDF of the best fitted normal distribution for data from the entire site.*

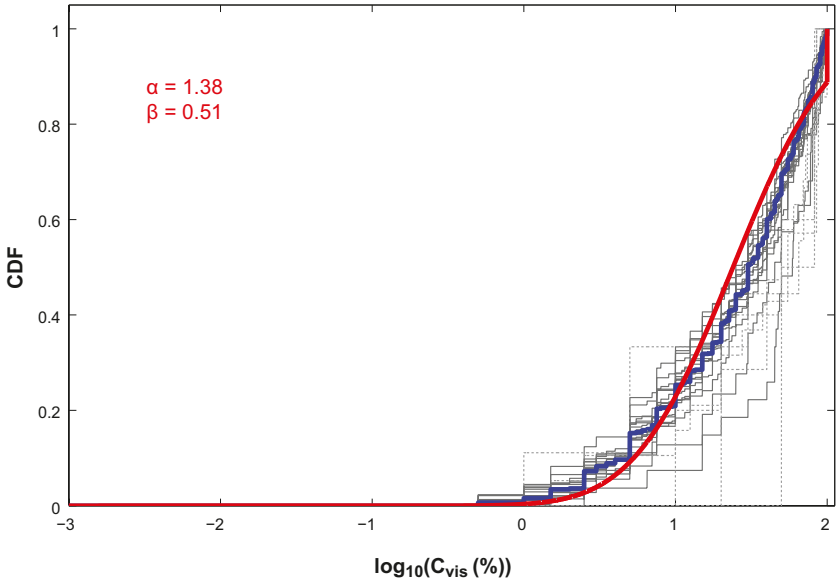


***Figure 5-4.*** *Chlorite – $C_{vis}$: Cumulative distribution functions of the separate data subsets (black curves) and of the data from the entire site (blue curve). CDFs for data subsets with up to 20 data points are dotted. The red curve represents the CDF of the best fitted truncated normal distribution for data from the entire site.*

### 5.2.3 Clay minerals, as a group

The corresponding figures to Figure 5-1 and Figure 5-2 are displayed below for clay minerals, as a group.

Based on the appearance of the figures, the same conclusions are drawn for clay minerals as for calcite. We suggest that the distributions for clay minerals in Table 5-1 and Table 5-2 reasonably well represent all rock volumes at the site.

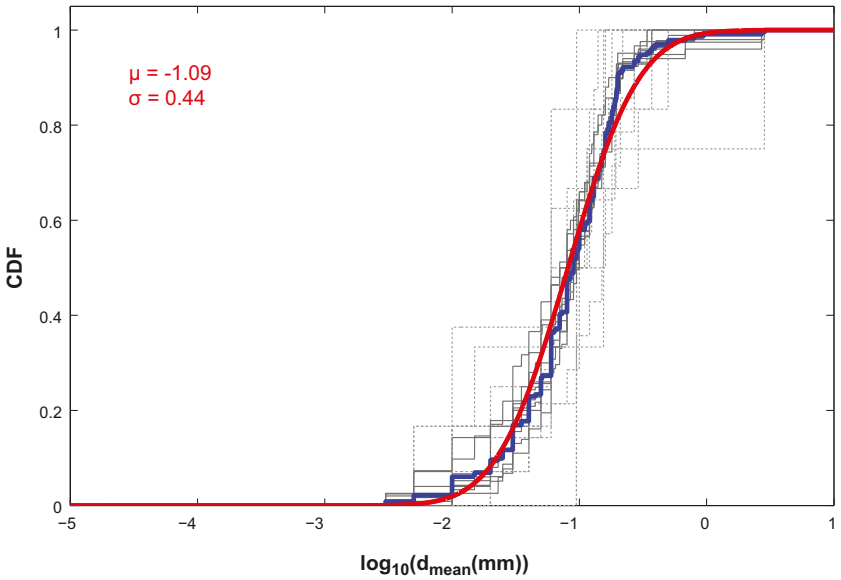


***Figure 5-5.*** *Clay minerals – $d_{mean}$: Cumulative distribution functions of the separate data subsets (black curves) and of the data from the entire site (blue curve). CDFs for data subsets with up to 20 data points are dotted. The red curve represents the CDF of the best fitted normal distribution for data from the entire site.*

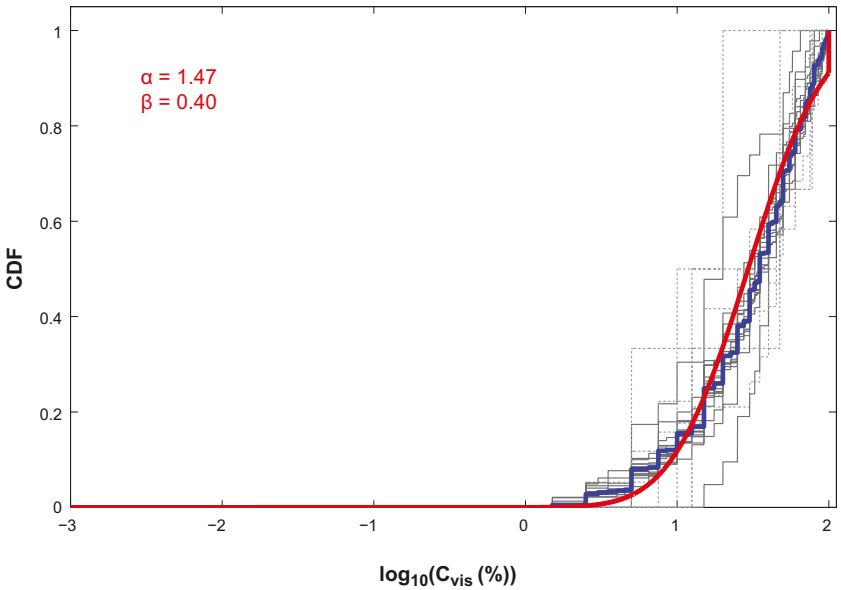


***Figure 5-6.*** *Clay minerals – $C_{vis}$: Cumulative distribution functions of the separate data subsets (black curves) and of the data from the entire site (blue curve). CDFs for data subsets with up to 20 data points are dotted. The red curve represents the CDF of the best fitted truncated normal distribution for data from the entire site.*

### 5.2.4 Hematite

The corresponding figures to Figure 5-1 and Figure 5-2 are displayed below for hematite.

For hematite there are so few data points that it is uncertain to what degree the distributions in Table 5-1 and Table 5-2 describe the occurrence of hematite. Out of necessity we suggest that these distributions are used in subsequent modelling, but with a caution that they are uncertain. It should be carefully noted that hematite was found in less than two percent of the mapped fractures.

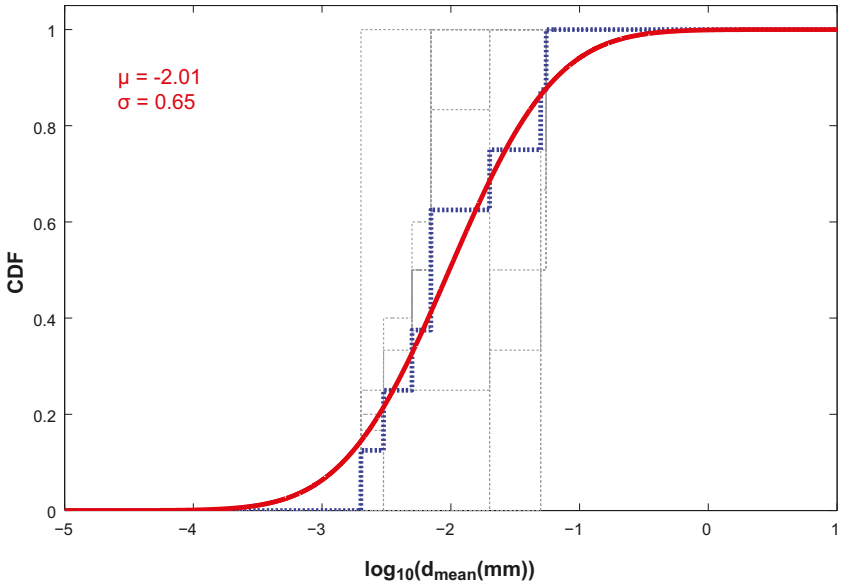


*Figure 5-7. Hematite – $d_{mean}$: Cumulative distribution functions of the separate data subsets (black curves) and of the data from the entire site (blue curve). CDFs for data subsets with up to 20 data points are dotted. The red curve represents the CDF of the best fitted normal distribution for data from the entire site.*

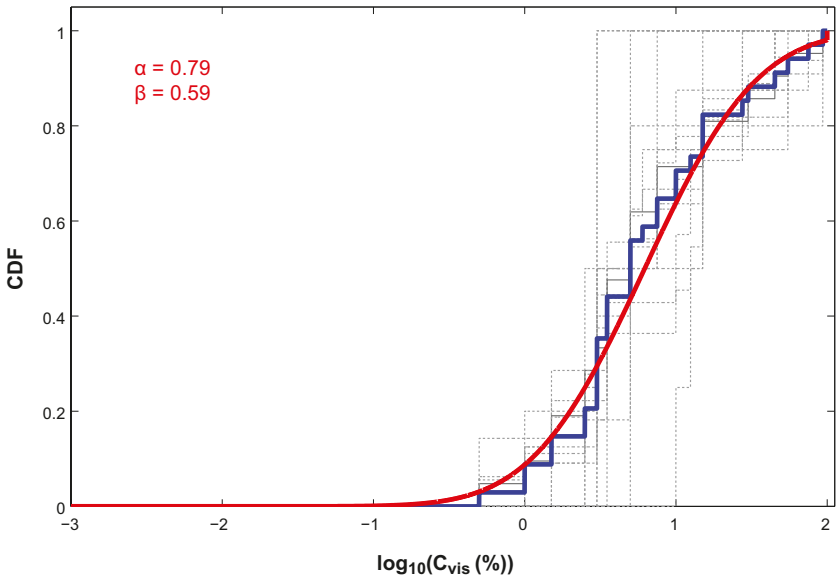


*Figure 5-8. Hematite – $C_{vis}$: Cumulative distribution functions of the separate data subsets (black curves) and of the data from the entire site (blue curve). CDFs for data subsets with up to 20 data points are dotted. The red curve represents the CDF of the best fitted truncated normal distribution for data from the entire site.*

### 5.2.5 Pyrite

The corresponding figures to Figure 5-1 and Figure 5-2 are displayed below for pyrite.

As pyrite occurs as both spot mineral and layer mineral, the obtained CDFs range over more orders of magnitudes than those of the other studied minerals. Even so, based on the appearance of the figures, the same conclusions are drawn for pyrite as for calcite. We suggest that the distributions for pyrite in Table 5-1 and Table 5-2 reasonably well represent all rock volumes at the site.

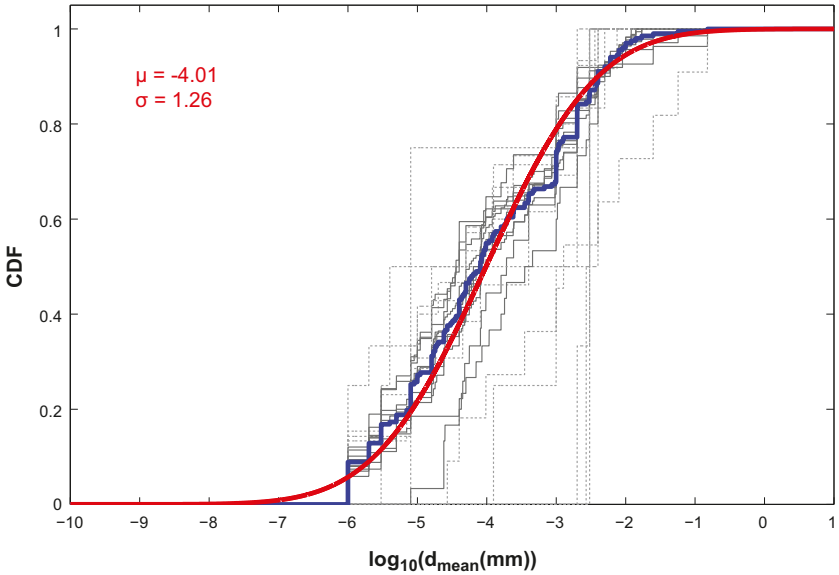


***Figure 5-9.*** *Pyrite – $d_{mean}$: Cumulative distribution functions of the separate data subsets (black curves) and of the data from the entire site (blue curve). CDFs for data subsets with up to 20 data points are dotted. The red curve represents the CDF of the best fitted normal distribution for data from the entire site.*

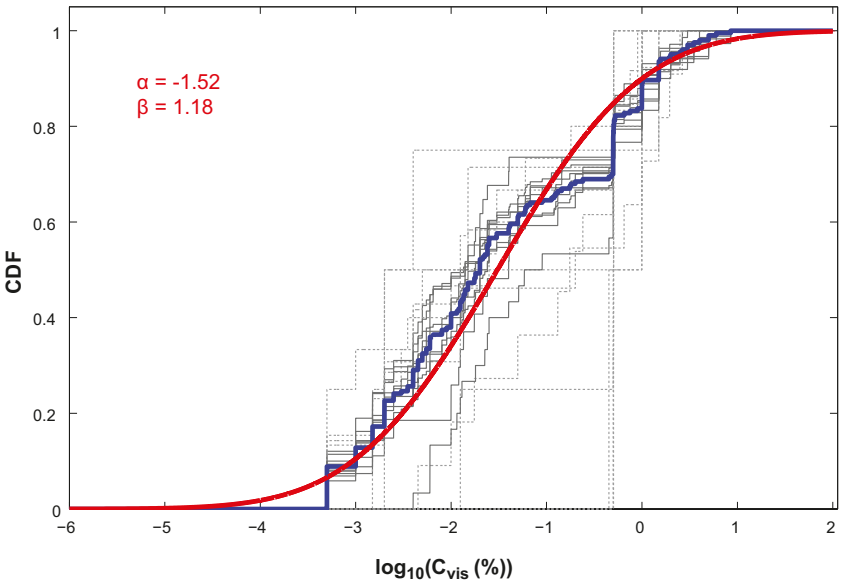


***Figure 5-10.*** *Pyrite – $C_{vis}$: Cumulative distribution functions of the separate data subsets (black curves) and of the data from the entire site (blue curve). CDFs for data subsets with up to 20 data points are dotted. The red curve represents the CDF of the best fitted truncated normal distribution for data from the entire site.*

# 6 Conclusions

This document reports a statistical analysis of occurrences, amounts, and coverages of fracture minerals at the Forsmark site. In the quantitative mineral mapping campaign, over two thousand open fractures have been quantitatively mapped. In total, hundreds of meters of drill core has been revisited /Eklund and Mattsson 2009/. The analysis in the present report concerns the data from this quantitative mapping. In about half of the cases where a fracture mineral could be found, the averaged fracture mineral thickness $d_{mean}$ could be estimated. In all the cases where a fracture mineral could be observed as the outer layer on the fracture surface, the visible coverage $C_{vis}$ could be estimated. As so many fractures were quantitatively mapped, and as so much data was delivered from the quantitative mineral mapping campaign, the statistical analysis made can in general be considered as reliable and the results can be considered as representative for the site.

A main conclusion from this work is that the occurrences, amounts, and coverages of the studied fracture minerals in general are similar for the different rock volumes at the site. One may have expected differences between, for example, fractures in deformation zones and fracture domains, but no such difference is easily detected. However, within the studied rock volumes there is a substantial spatial variability.

In the analysis, fractures were associated with closely located flow anomalies. For the studied fracture minerals, no relation between $d_{mean}$ and the transmissivity of the flow anomalies could be seen. This indicates that there is no clear relation between the amounts of fracture minerals and the present groundwater flow situation in a fracture. This is not surprising, as many of the fractures and fracture minerals are considered to be old, even on a geologic time scale.

Both parametric and non–parametric methods have been used in the statistical analyses. From the parametric analyses, one can conclude that the normal distribution can be used to represent $\log_{10}(d_{mean})$ data, while the truncated normal distribution can be used to represent $\log_{10}(C_{vis})$ data. These distributions can be used as input to subsequent hydrogeochemical and radionuclide transport modelling. If the model can handle the parameterisation of the different rock volumes, the modeller can choose to import data for the individual volumes, given in Chapters 3 and 4. Such data may be based on few fractures and in such a case, the representativity and reliability can be questioned. If distribution parameters are required for the model, we suggest those given in Chapter 5, which can be used for the entire site. For calcite, chlorite, clay minerals, and pyrite, these distribution parameters are based upon many data points, making the results reliable. Hematite, however, was only found in few fractures making the results from the $d_{mean}$ and $C_{vis}$ analyses uncertain.

All in all, both the quantitative mineral mapping campaign and the subsequent analysis of data can be considered as successful, delivering unprecedented data.

# 7 References

SKB's (Svensk Kärnbränslehantering AB) publications can be found at www.skb.se/publications.


**Barr D R, Sherrill E T, 1999.** Mean and variance of truncated normal distributions. The American Statistician, 53, pp 357–361.

**Brantberger M, Zetterqvist A, Arnbjerg-Nielsen T, Olsson T, Outters N, Syrjänen P, 2006.** Final repository for spent nuclear fuel. Underground design Forsmark, Layout D1. SKB R-06-34, Svensk Kärnbränslehantering AB.

**Cohen A C, 1950.** Estimating the mean and variance of normal populations from singly truncated and doubly truncated samples. The Annals of Mathematical Statistics, 21, pp 557–569.

**Drake H, Sandström B, Tullborg E-L, 2006.** Mineralogy and geochemistry of rocks and fracture fillings from Forsmark and Oskarshamn: compilation of data for SR-Can. SKB R-06-109, Svensk Kärnbränslehantering AB.

**Eklund S, Mattsson K-J, 2008.** Oskarshamn site investigation. Quantitative mapping of fracture minerals in Laxemar. SKB P-08-38, Svensk Kärnbränslehantering AB.

**Eklund S, Mattsson K-J, 2009.** Forsmark site investigation. Quantitative mapping of fracture minerals in Forsmark. SKB P-08-47, Svensk Kärnbränslehantering AB.

**Johnson R A, 1994.** Miller and Freund's probability & statistics for engineers. 5th ed. Englewood Cliffs, NJ: Prentice Hall.

**Lindquist A, Hjerne C, Nordqvist R, Byegård J, Walger E, Ludvigson J-E, Wass E, 2008.** Forsmark site investigation. Confirmatory hydraulic interference test and tracer test at drill site 2. SKB P-08-13, Svensk Kärnbränslehantering AB.

**NIST, 2009.** NIST/SEMATECH e-Handbook of Statistical Methods. [Online]. Available at: http://www.itl.nist.gov/div898/handbook/. National Institute of Standards and Technology. [03 June 2009].

**Pöllänen J, Sokolnicki M, 2004.** Forsmark site investigation. Difference flow logging in borehole KFM03A. SKB P-04-189, Svensk Kärnbränslehantering AB.

**Pöllänen J, Sokolnicki M, Rouhiainen P, 2004.** Difference flow logging in borehole KFM05A. Forsmark site investigation. SKB P-04-191, Svensk Kärnbränslehantering AB.

**Rouhiainen P, Pöllänen J, 2003.** Forsmark site investigation. Difference flow logging of borehole KFM01A. SKB P-03-28, Svensk Kärnbränslehantering AB.

**Rouhiainen P, Pöllänen J, 2004a.** Forsmark site investigation. Difference flow logging in borehole KFM02A. SKB P-04-188, Svensk Kärnbränslehantering AB.

**Rouhiainen P, Pöllänen J, 2004b.** Forsmark site investigation. Difference flow logging in borehole KFM04A. SKB P-04-190, Svensk Kärnbränslehantering AB.

**Rouhiainen P, Sokolnicki M, 2005.** Forsmark site investigation. Difference flow logging in borehole KFM06A. SKB P-05-15, Svensk Kärnbränslehantering AB.

**Sandström B, Tullborg E-L, Smellie J, MacKenzie A B, Suksi J, 2008.** Fracture mineralogy of the Forsmark site. SDM-Site Forsmark. SKB R-08-102, Svensk Kärnbränslehantering AB.

**Shapiro S S, Wilk M B, 1965.** An analysis of variance test for normality (complete samples). Biometrika, 52, pp 591–611.

**SKB, 2008.** Site description of Forsmark at completion of the site investigation phase. SDM-Site Forsmark. SKB TR-08-05, Svensk Kärnbränslehantering AB.

**SKB, 2010.** Data report for the safety assessment SR-Site. SKB TR-10-52, Svensk Kärnbränslehantering AB.

**Sokolnicki M, Pöllänen J, Pekkanen J, 2006.** Forsmark site investigation. Difference flow logging in borehole KFM10A. SKB P-06-190, Svensk Kärnbränslehantering AB.

**Sokolnicki M, Rouhiainen P, 2005a.** Forsmark site investigation. Difference flow logging in borehole KFM08A. SKB P-05-43, Svensk Kärnbränslehantering AB.

**Sokolnicki M, Rouhiainen P, 2005b.** Forsmark site investigation. Difference flow logging in borehole KFM07A. SKB P-05-63, Svensk Kärnbränslehantering AB.

**Stephens M B, Fox A, La Pointe P R, Simeonov A, Isaksson H, Hermanson J, Öhman J, 2007.** Geology Forsmark. Site descriptive modelling Forsmark stage 2.2. SKB R-07-45, Svensk Kärnbränslehantering AB.

**Stephens M, Simeonov A, Isaksson H, 2008.** Bedrock geology Forsmark. Modelling stage 2.3. Implications for and verification of the deterministic geological models based on complementary data. SKB R-08-64, Svensk Kärnbränslehantering AB.

**Teurneau B, Forsmark T, Forssman I, Rhén I, Zinn E, 2008.** Correlation of Posiva Flow Log anomalies to core mapped features in KFM01D, KFM07C, KFM08A, KFM08C and KFM10A. Forsmark site investigation. SKB P-07-127, Svensk Kärnbränslehantering AB.

**Väisäsvaara J, Pekkanen J, 2007.** Forsmark site investigation. Difference flow logging in borehole KFM11A. SKB P-07-85, Svensk Kärnbränslehantering AB.

**Väisäsvaara J, Pöllänen J, 2007.** Difference flow logging in borehole KFM02B. SKB P-07-83, Svensk Kärnbränslehantering AB.

**Väisäsvaara J, Leppänen H, Pekkanen J, 2006a.** Forsmark site investigation. Difference flow logging in borehole KFM01D. SKB P-06-161, Svensk Kärnbränslehantering AB.

**Väisäsvaara J, Pekkanen J, Pöllänen J, 2006b.** Forsmark site investigation. Difference flow logging in borehole KFM07C. SKB P-06-247, Svensk Kärnbränslehantering AB.

# Appendix A

## Fracture mineral thickness, $d_{mean}$, in Forsmark

### A1 All fractures in Forsmark (2,071 fractures)

#### A1.1 Calcite (All)

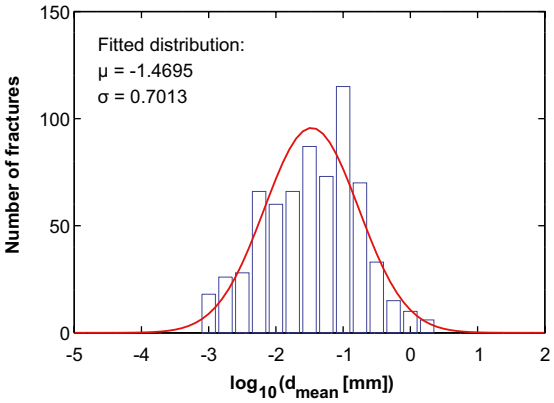


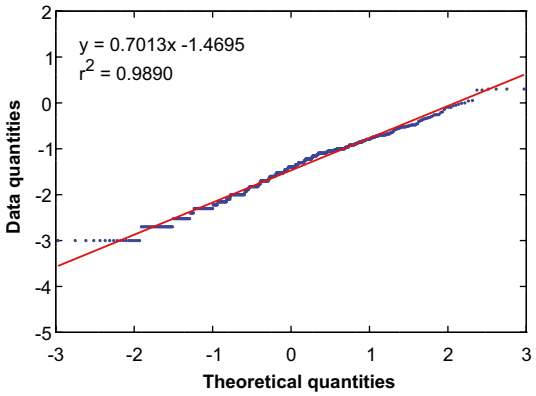


#### A1.2 Chlorite (All)

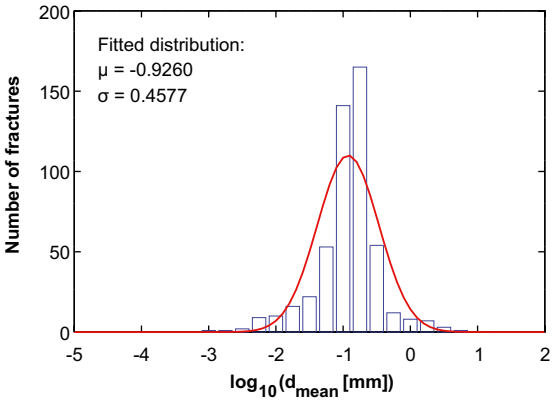


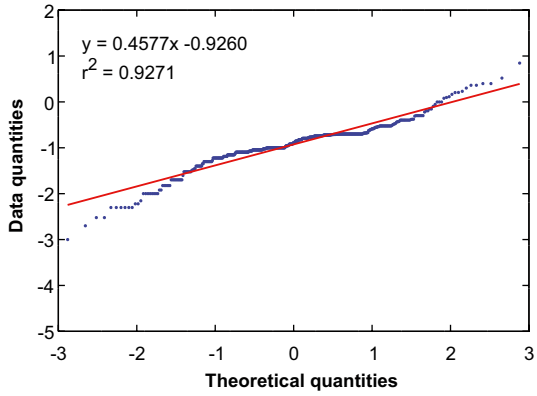


#### A1.3 Clay minerals (All)

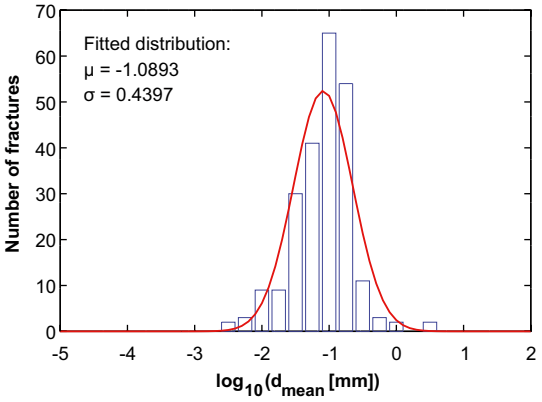


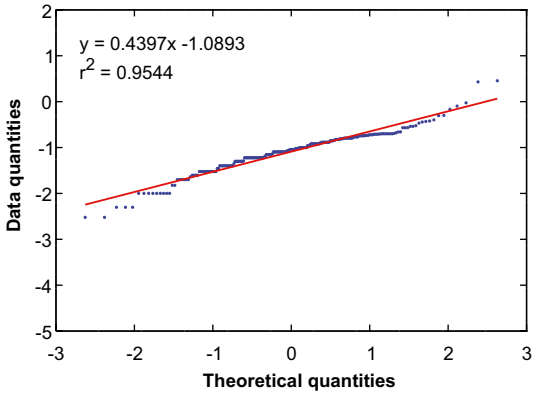

### A1.4 Hematite (All)

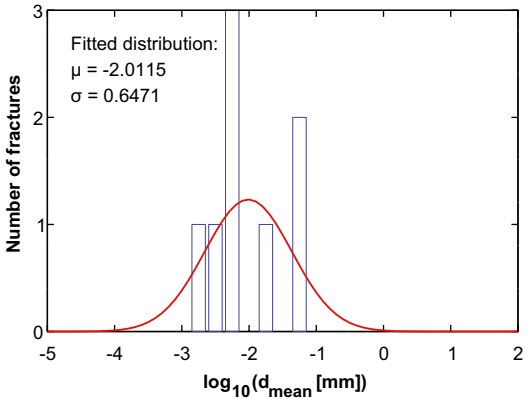


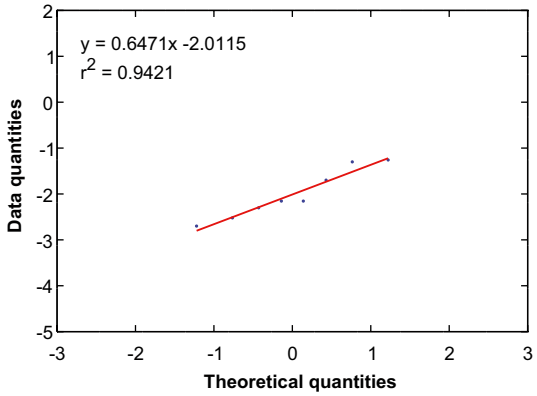


### A1.5 Pyrite (All)

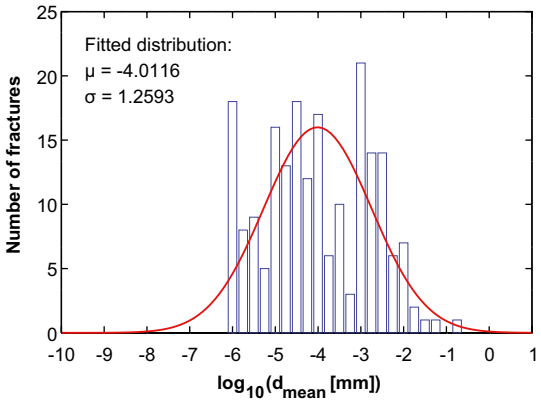


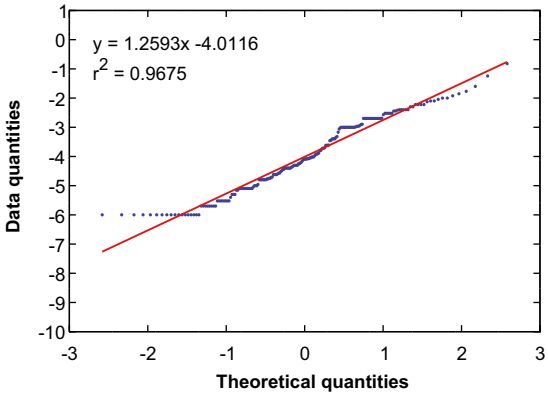


## A2 Different elevations

### A2.1 0 – 100 m (835 fractures)

***Calcite (0 – 100 m)***

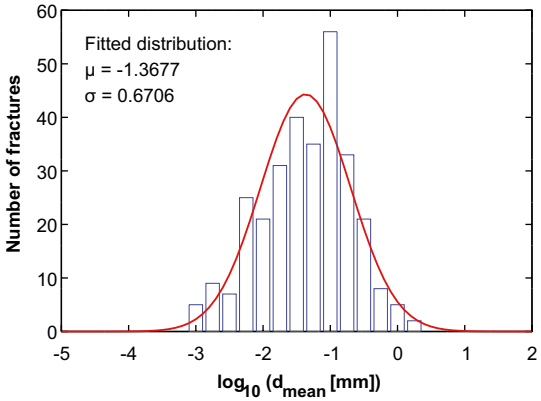


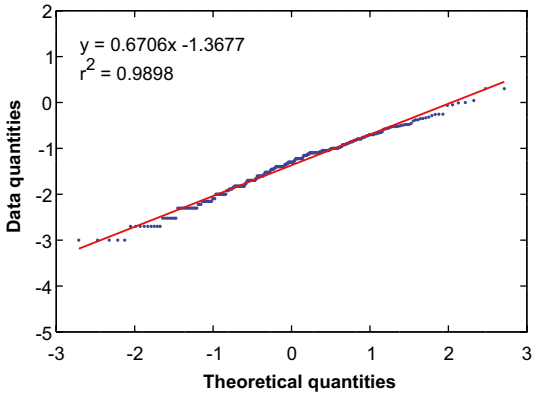

### *Chlorite (0 – 100 m)*

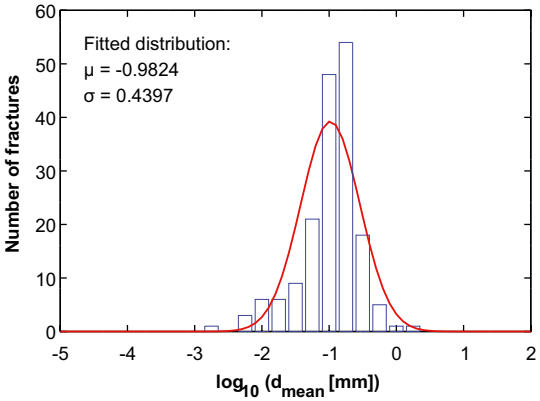


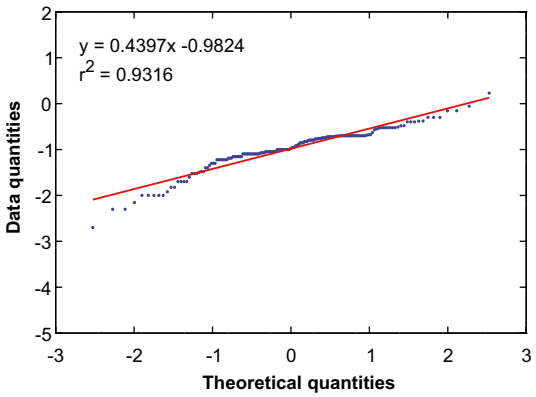


### *Clay minerals (0 – 100 m)*

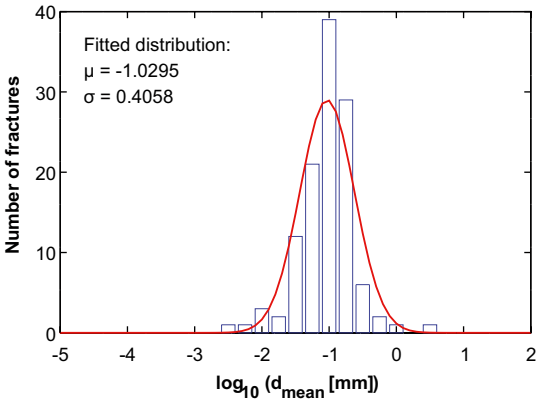


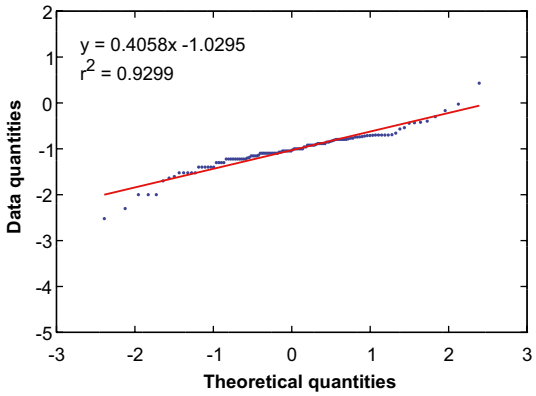


### *Hematite (0 – 100 m)*

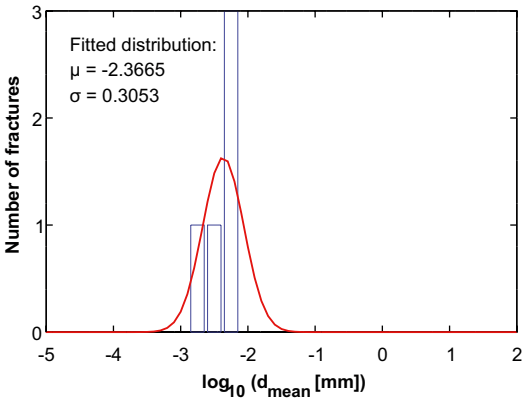


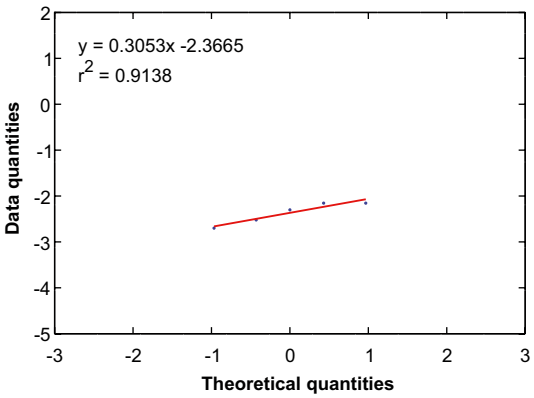

### *Pyrite (0 – 100 m)*

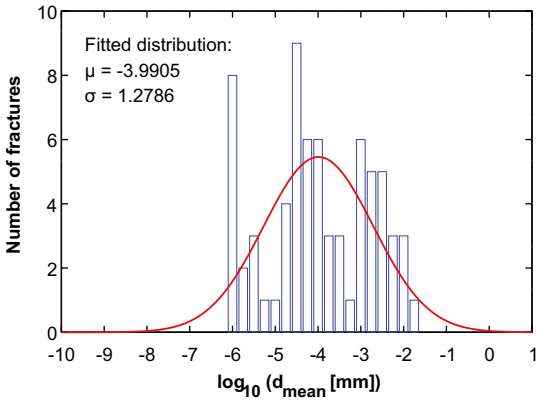


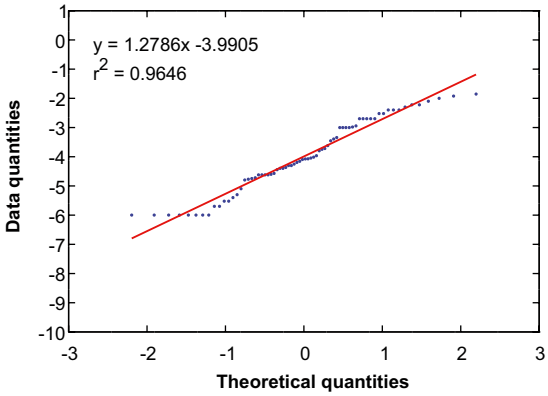


## A2.2 100 – 300 m (531 fractures)

### *Calcite (100 – 300 m)*

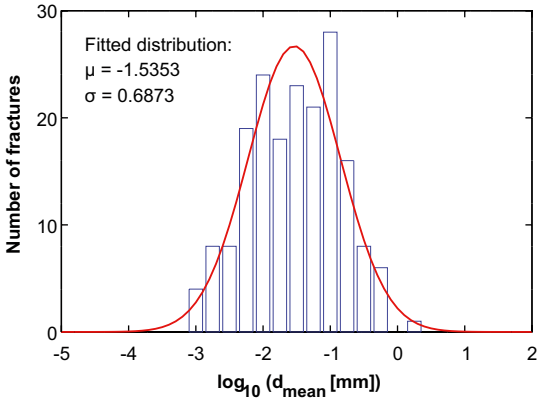


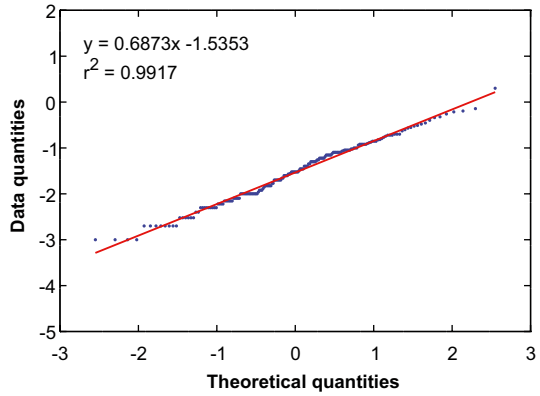


### *Chlorite (100 – 300 m)*

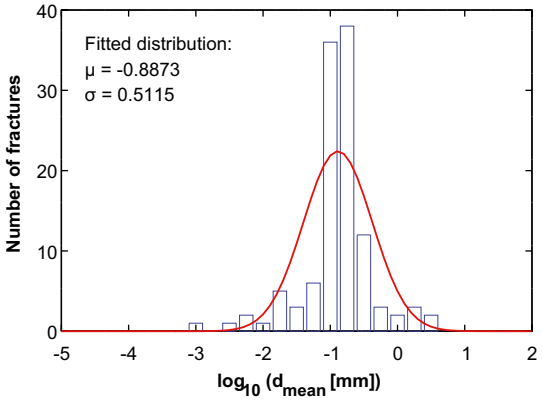


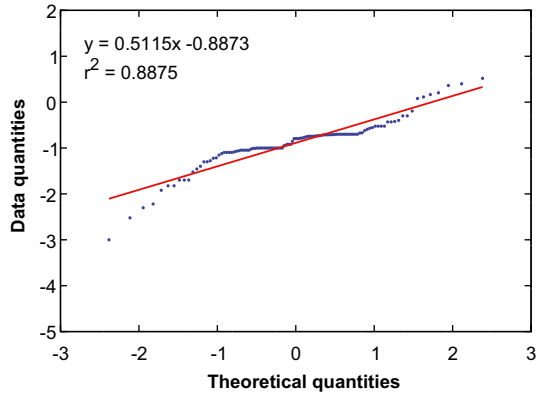

### *Clay minerals (100 – 300 m)*

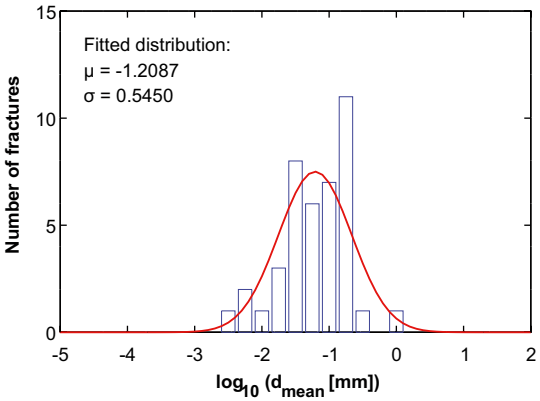


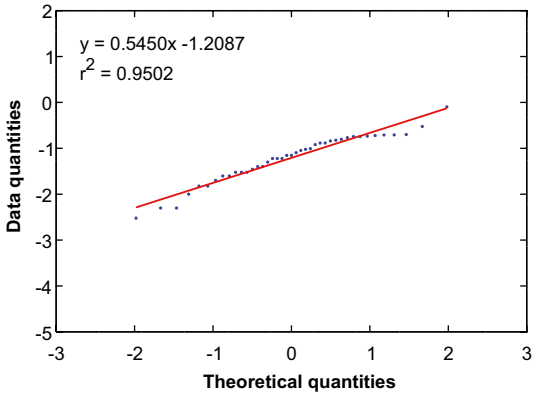


### *Hematite (100 – 300 m)*

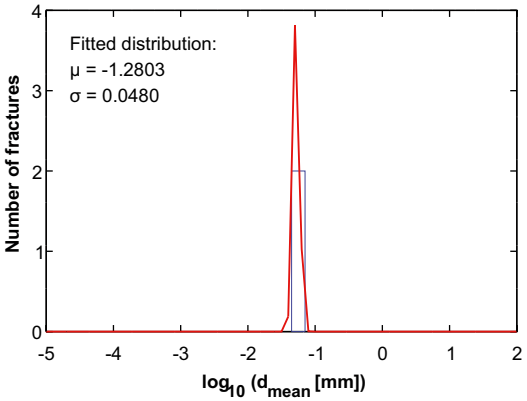


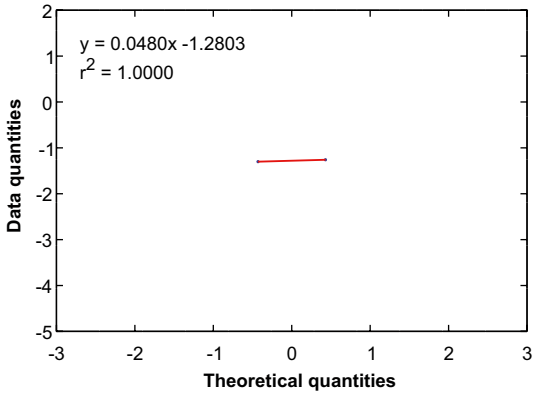


### *Pyrite (100 – 300 m)*

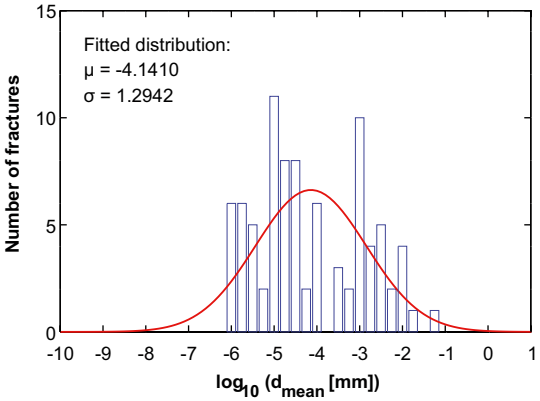


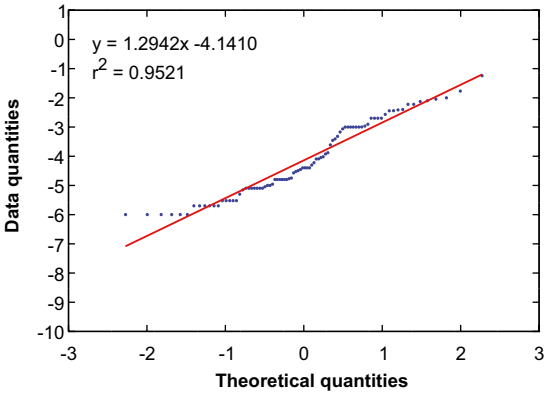

## A2.3 300 – 500 m (543 fractures)

### *Calcite (300 – 500 m)*

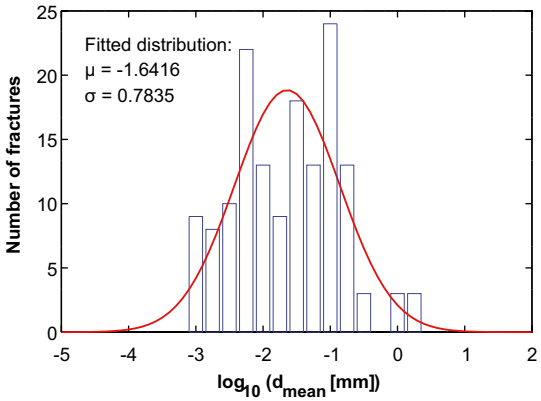


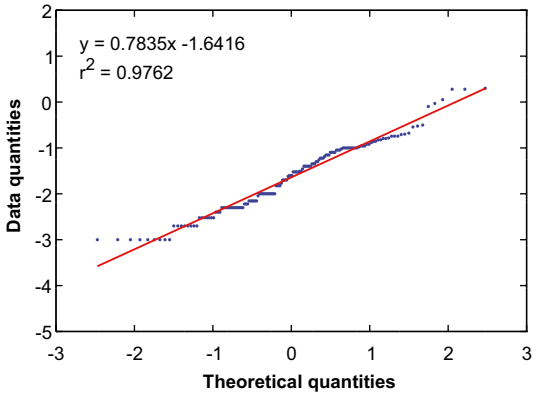


### *Chlorite (300 – 500 m)*

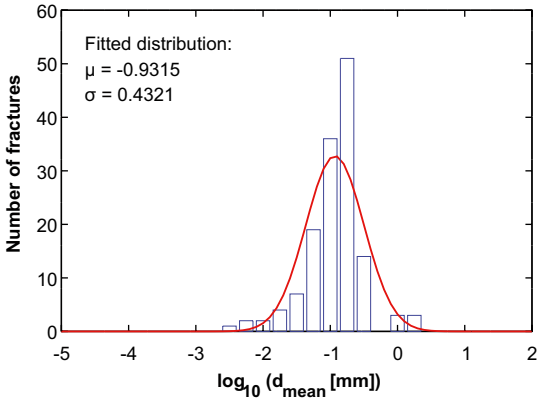


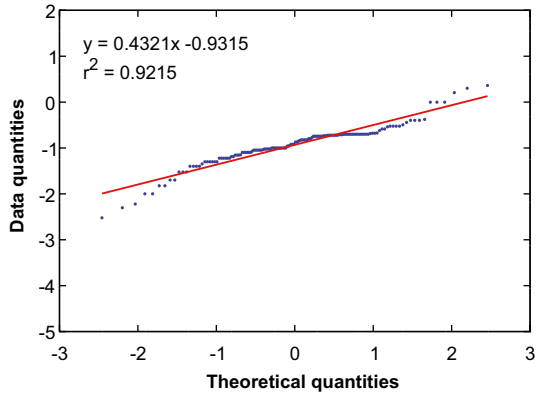


### *Clay minerals (300 – 500 m)*

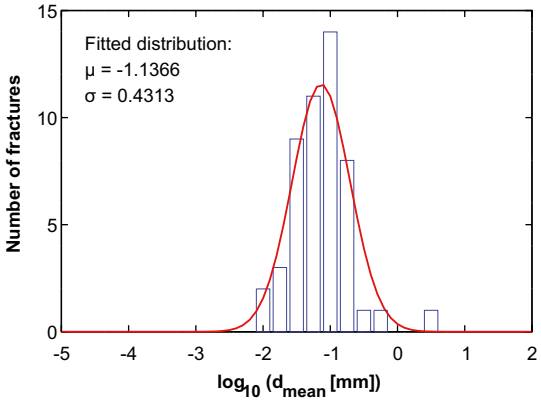


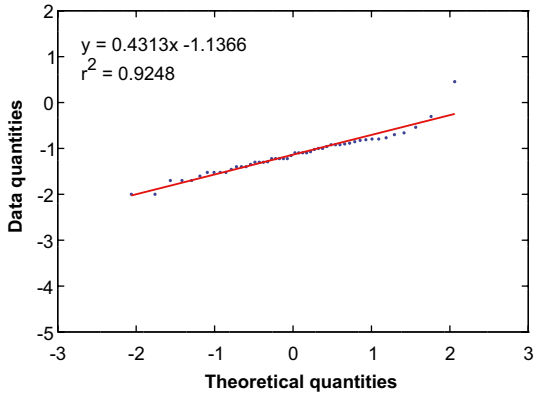

### *Hematite (300 – 500 m)*

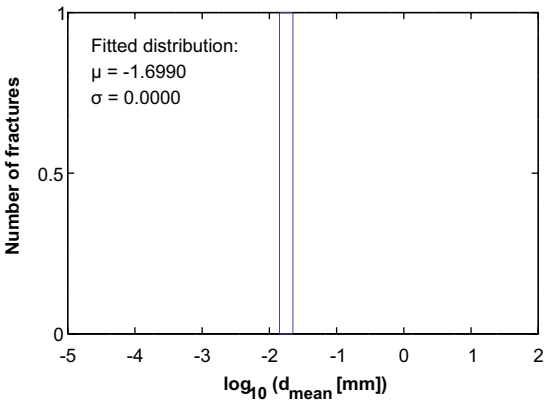


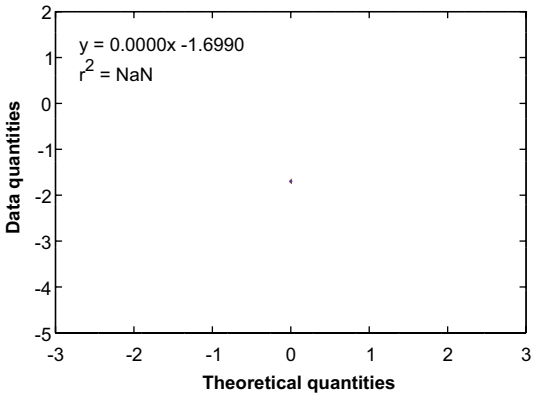


### *Pyrite (300 – 500 m)*

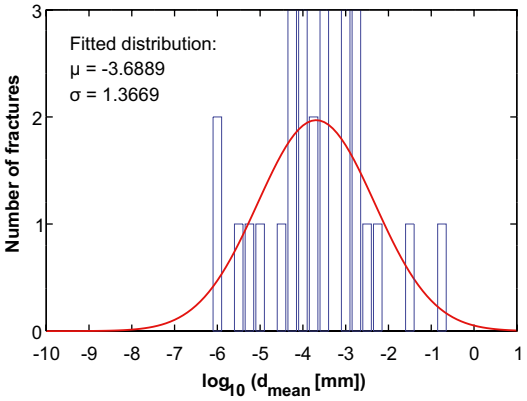


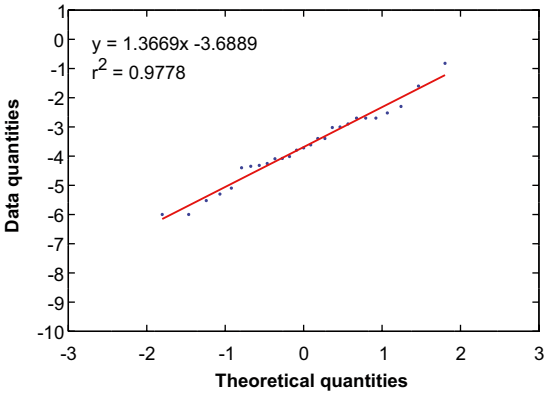


## A2.4 500 – 700 m (114 fractures)

### *Calcite (500 – 700 m)*

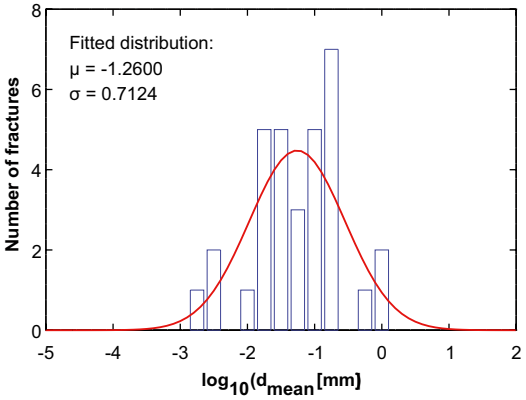


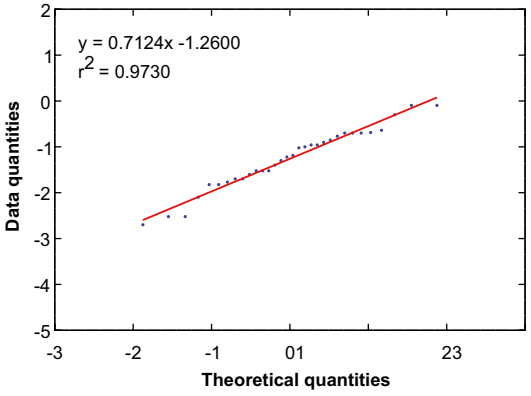

### *Chlorite (500 – 700 m)*

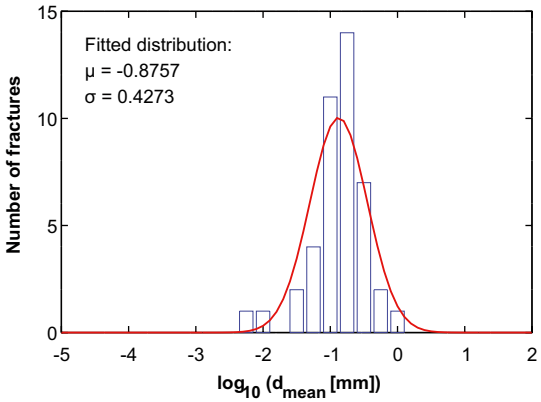


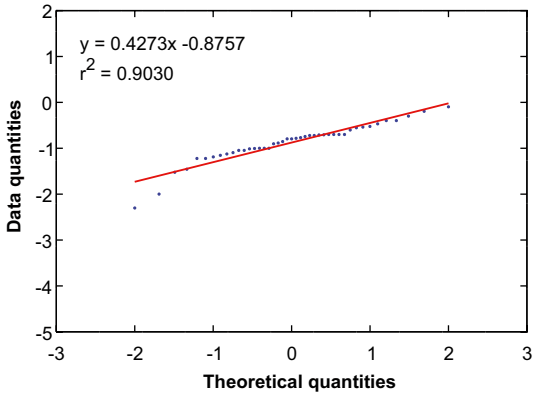


### *Clay minerals (500 – 700 m)*

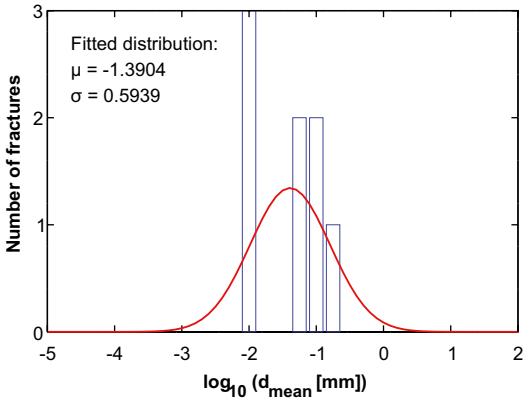


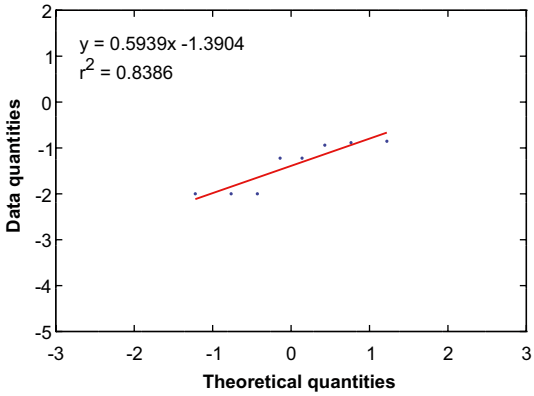


### *Hematite (500 – 700 m)*

***N/A***

### *Pyrite (500 – 700 m)*

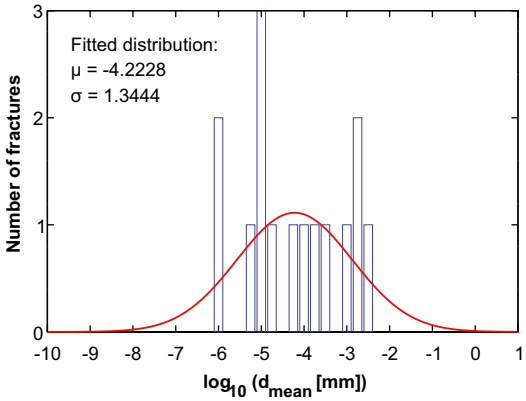


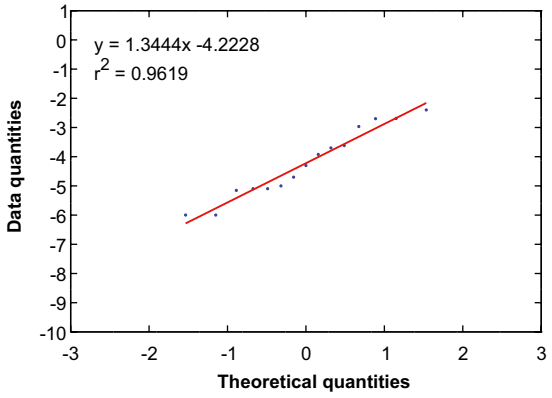

## A2.5 700 – 1,000 m (48 fractures)

### *Calcite (700 – 1,000 m)*

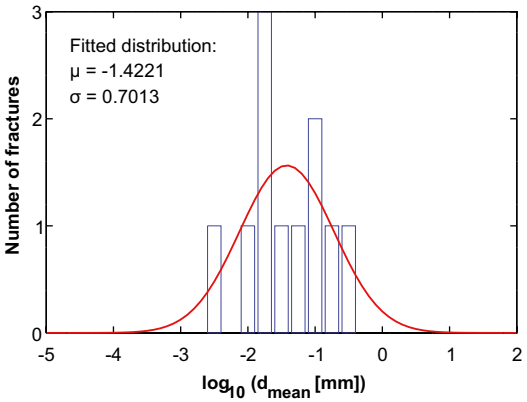


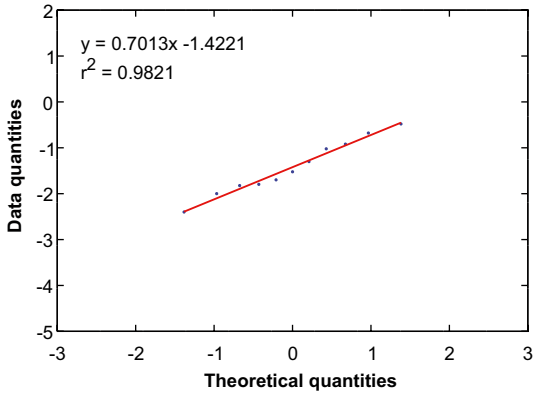


### *Chlorite (700 – 1,000 m)*

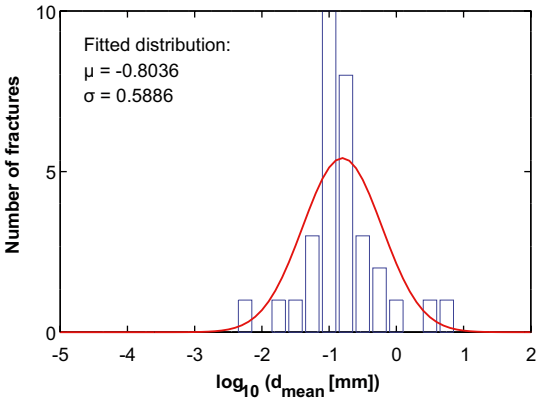


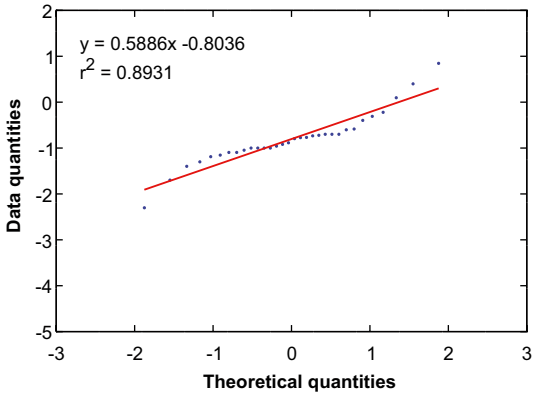


### *Clay minerals (700 – 1,000 m)*

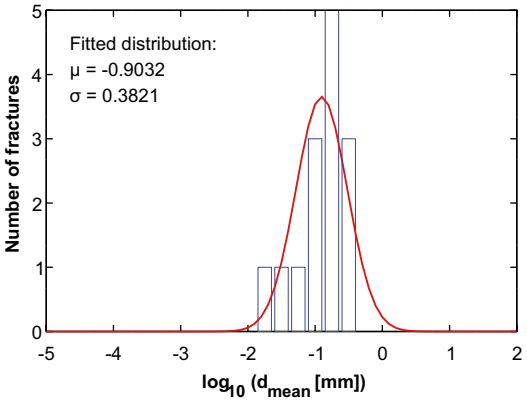


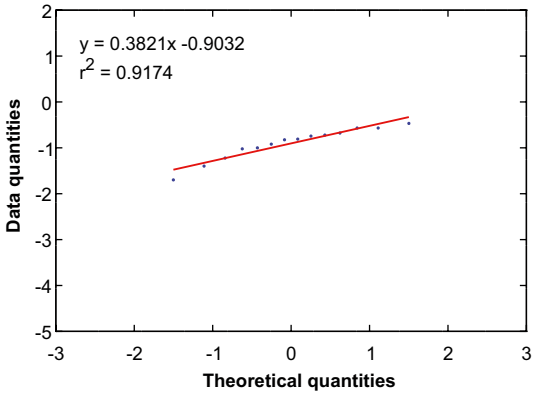


### *Hematite (700 – 1,000 m)*

***N/A***

### *Pyrite (700 – 1,000 m)*

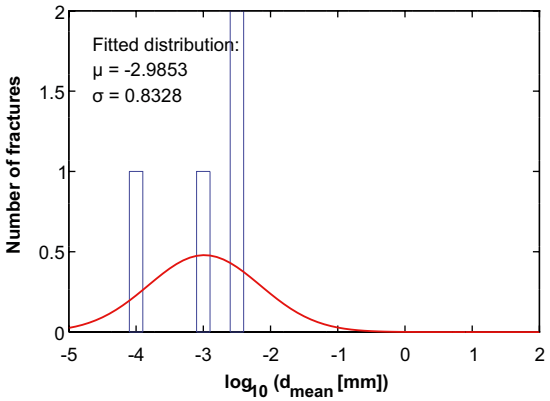


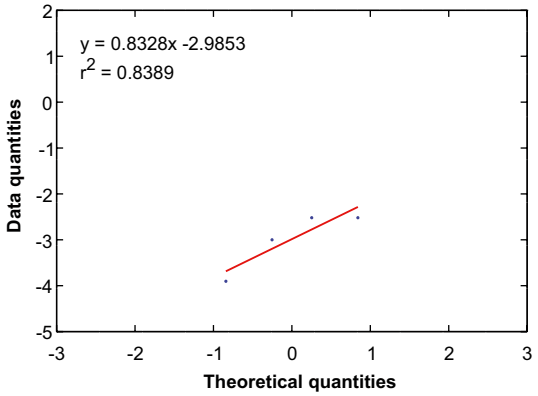


## A3 Rock domains

### A3.1 RFM012 (79 fractures)

### *Calcite (RFM012)*

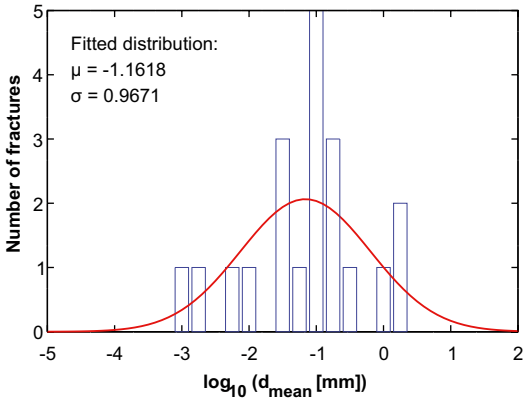


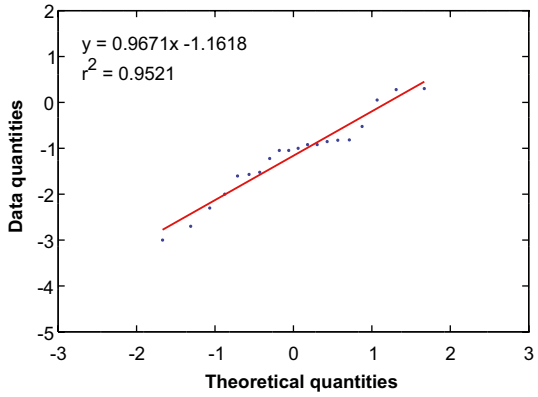


### *Chlorite (RFM012)*

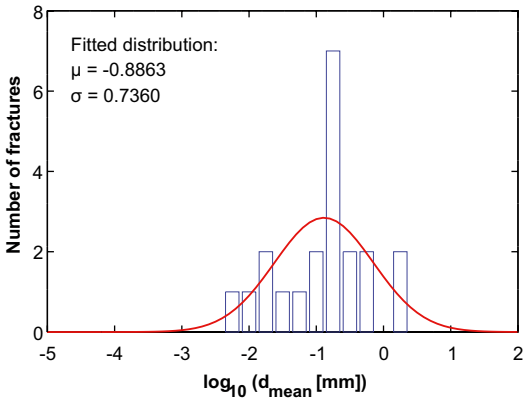


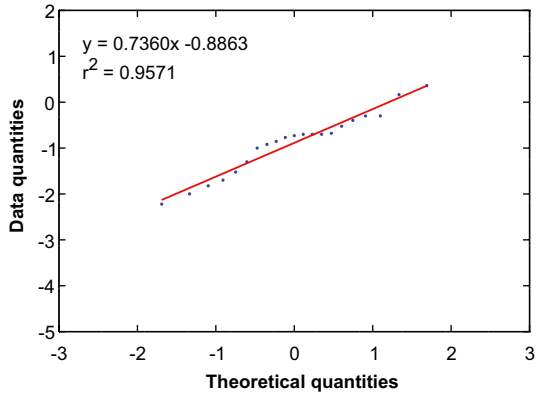

### *Clay minerals (RFM012)*

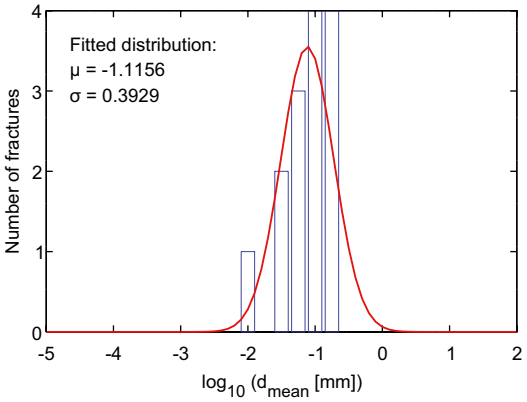


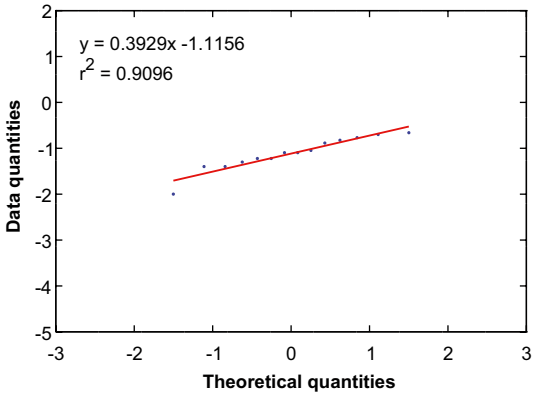


### *Hematite (RFM012)*

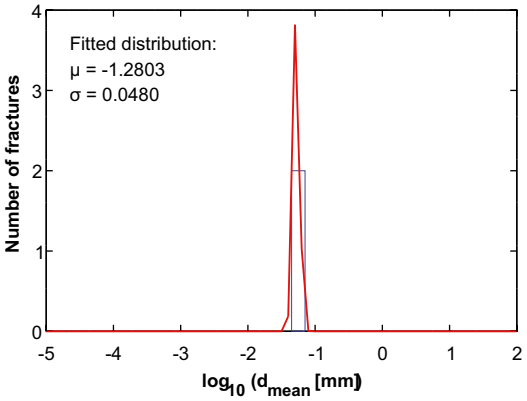


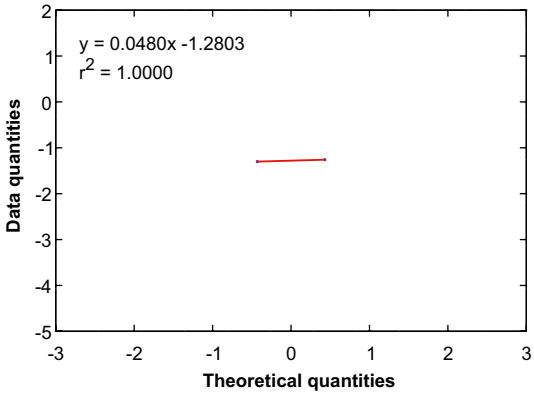


### *Pyrite (RFM012)*

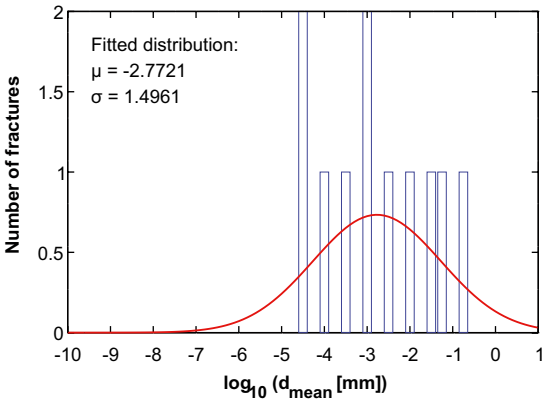


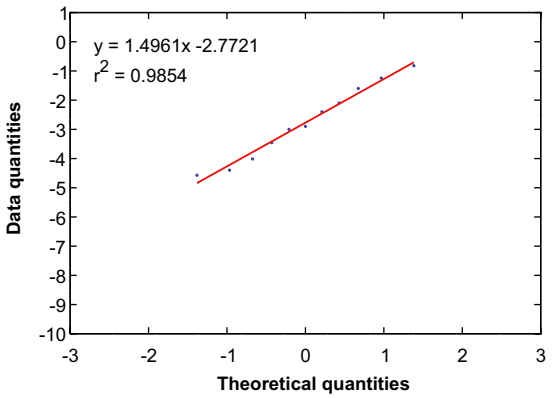

## A3.2 RFM018 (30 fractures)

### *Calcite (RFM018)*

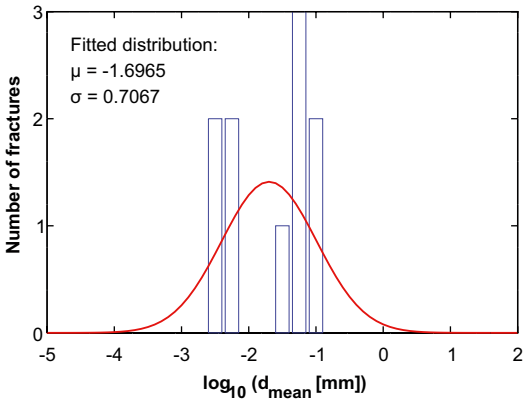


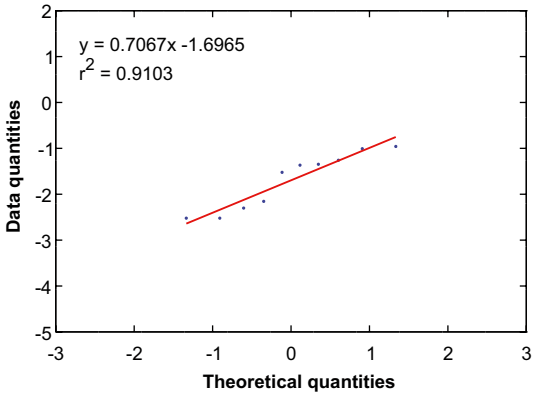


### *Chlorite (RFM018)*

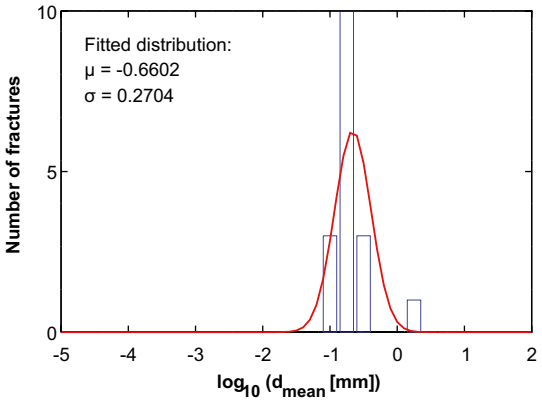


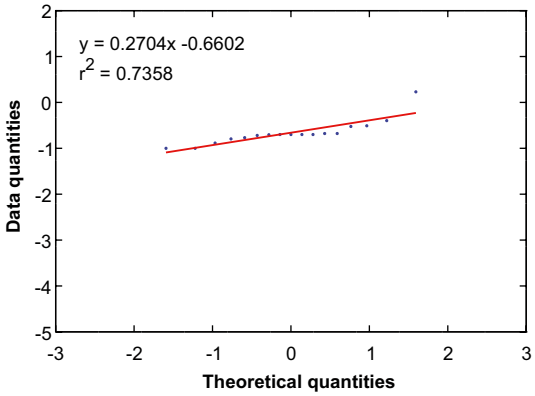


### *Clay minerals (RFM018)*

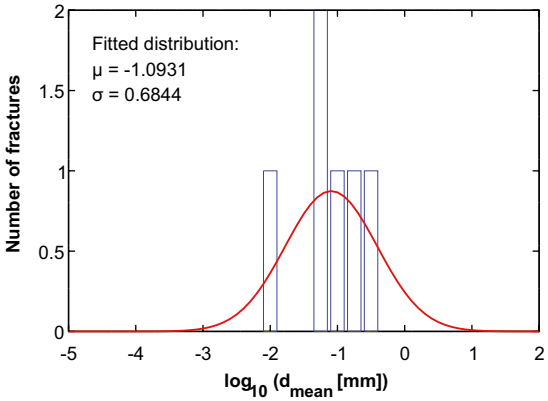


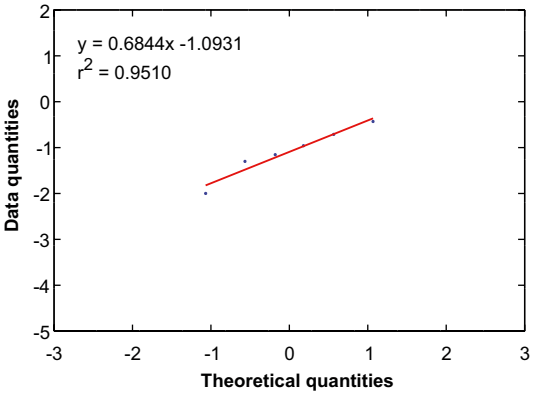


### *Hematite (RFM018)*

***N/A***

### *Pyrite (RFM018)*

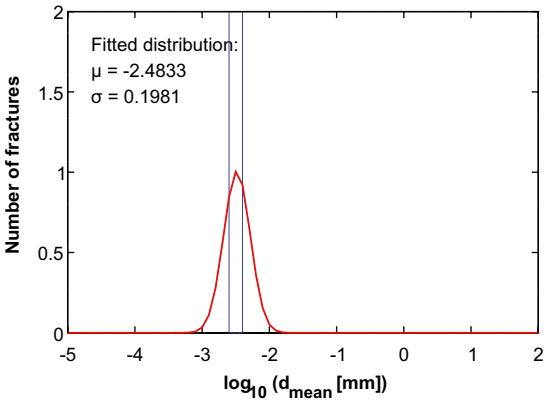


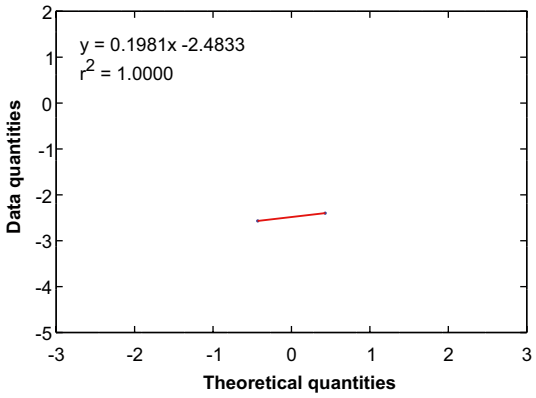


## A3.3 RFM021 (226 fractures)

### *Calcite (RFM021)*

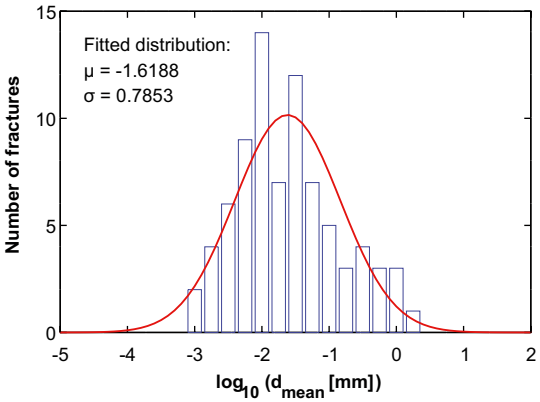


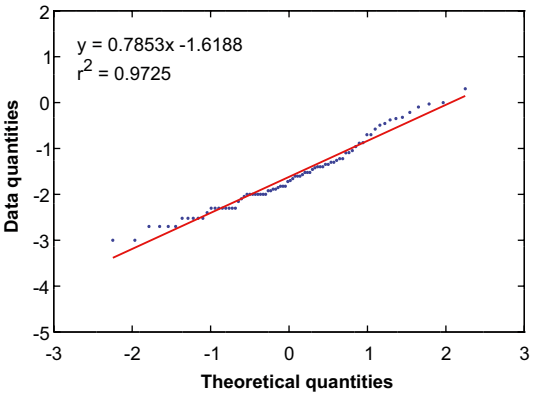


### *Chlorite (RFM021)*

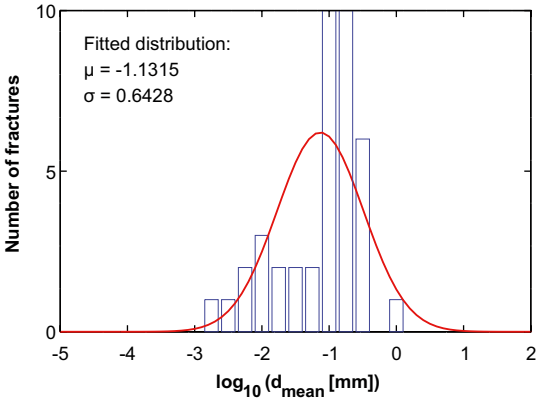


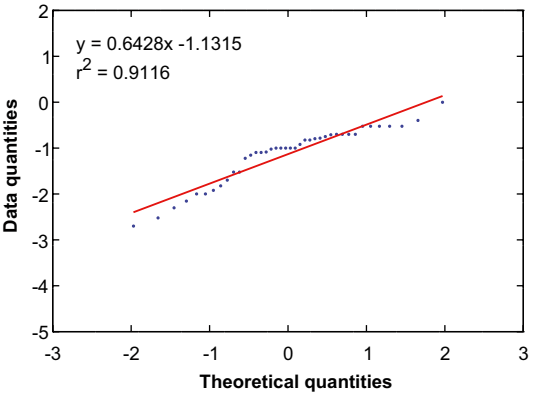

### *Clay minerals (RFM021)*

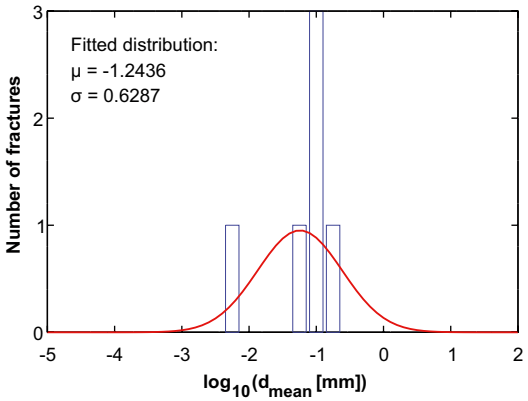


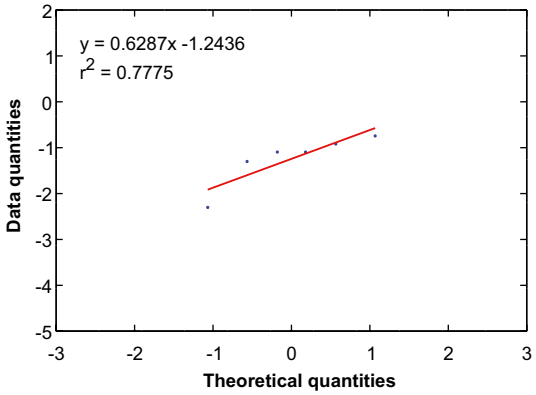


### *Hematite (RFM021)*

***N/A***

### *Pyrite (RFM021)*

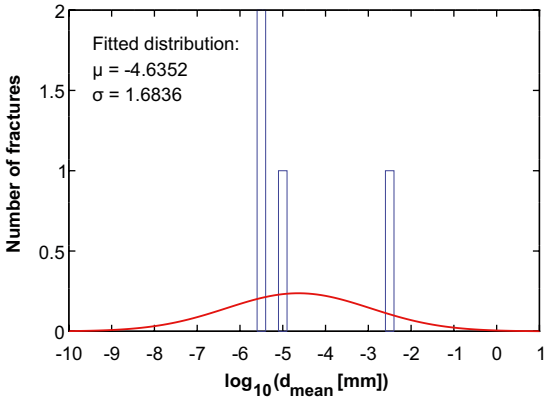


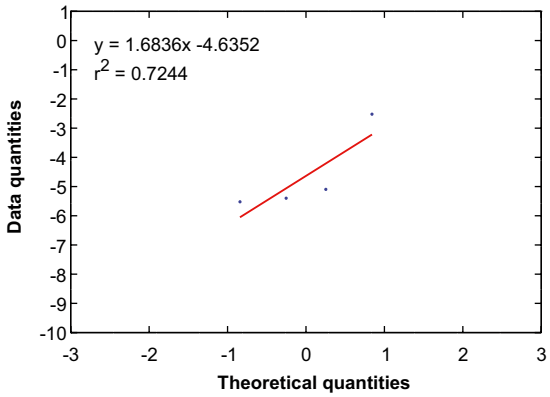


## A3.4 RFM029 (1,596 fractures)

### *Calcite (RFM029)*

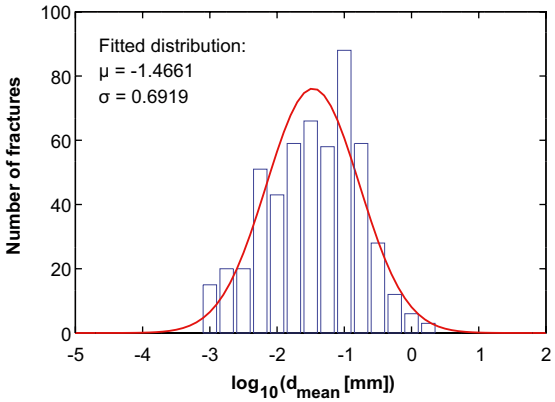


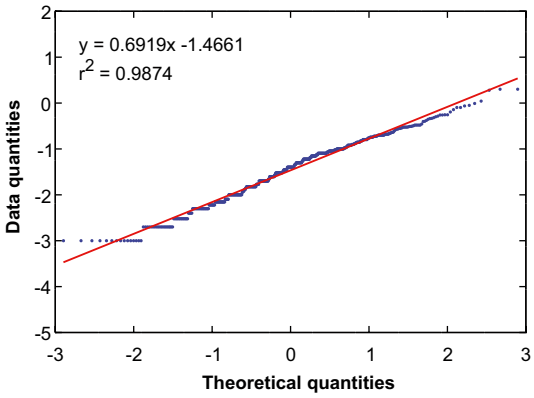

### *Chlorite (RFM029)*

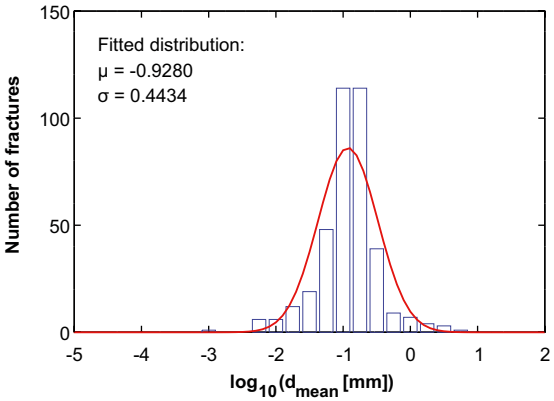


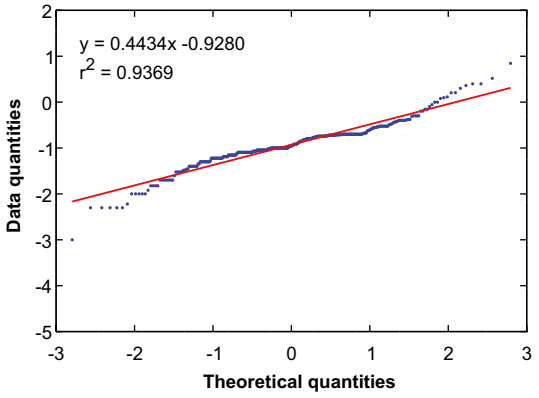


### *Clay minerals (RFM029)*

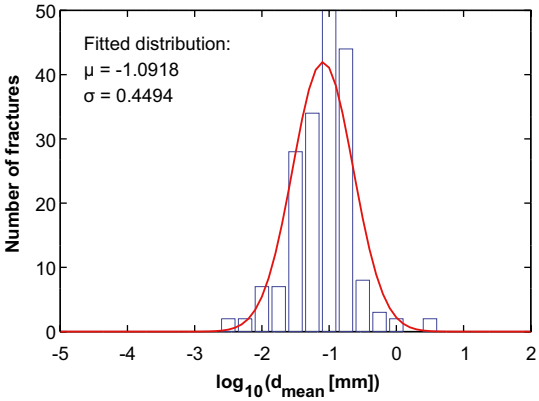


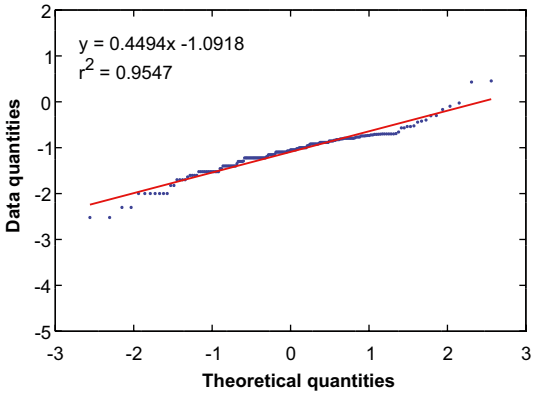


### *Hematite (RFM029)*

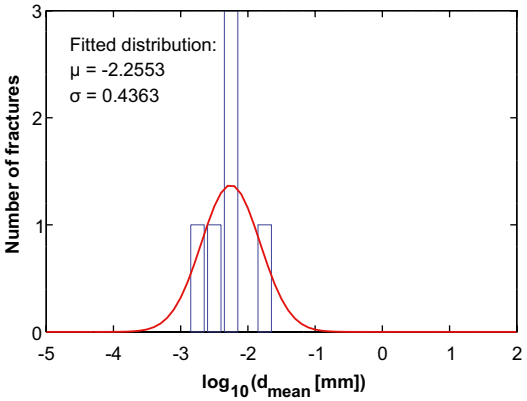


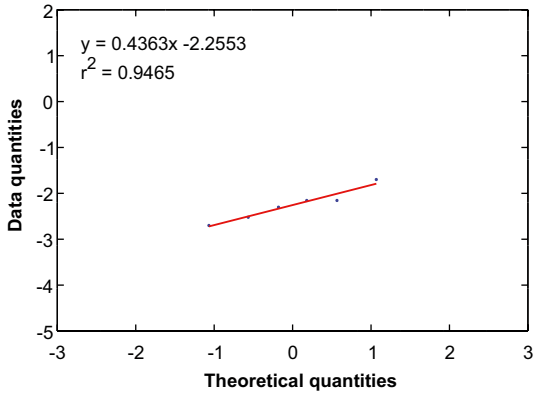

### *Pyrite (RFM029)*

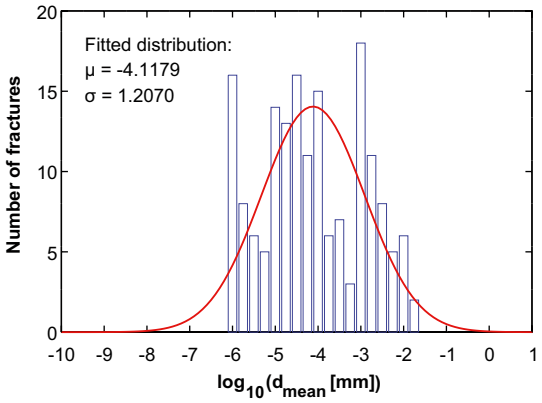


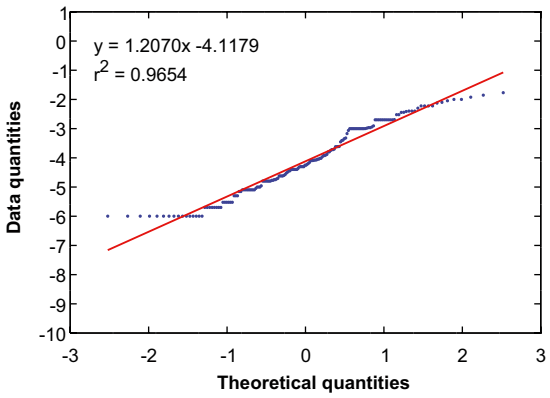


## A3.5 RFM044 (8 fractures)

### *Calcite (RFM044)*

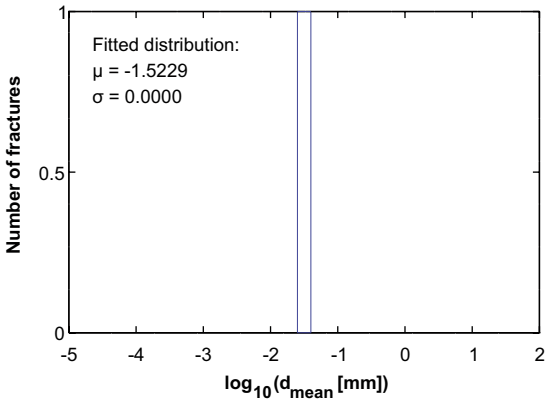


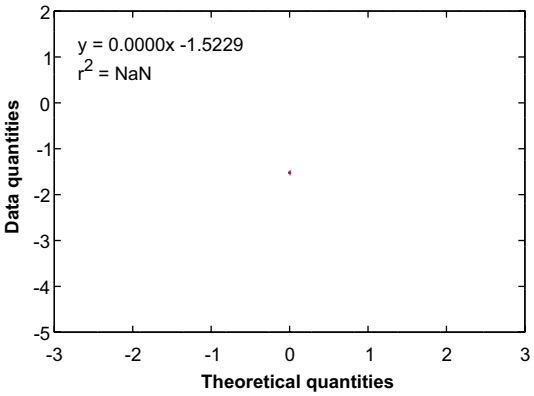


### *Chlorite (RFM044)*

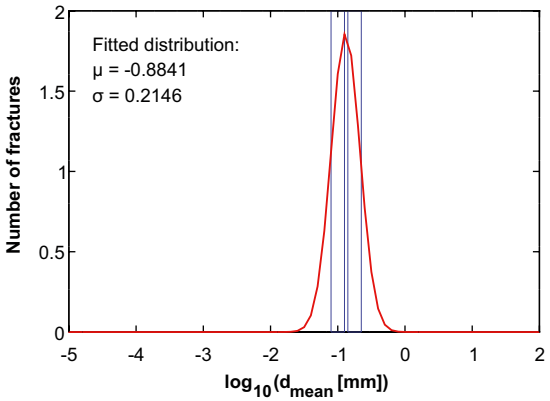


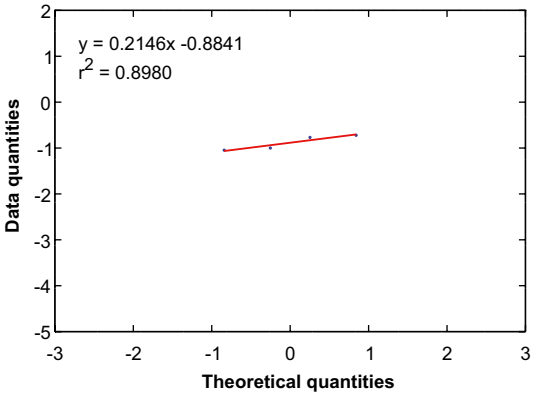

### *Clay minerals (RFM044)*

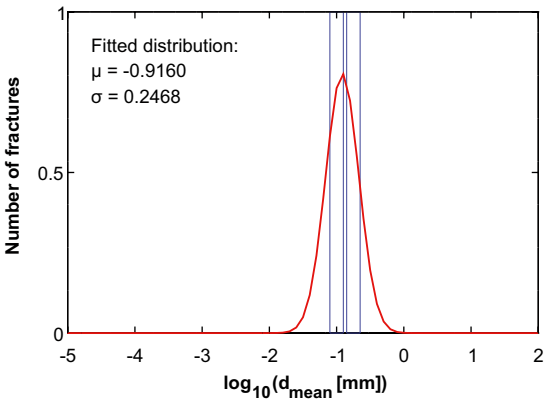


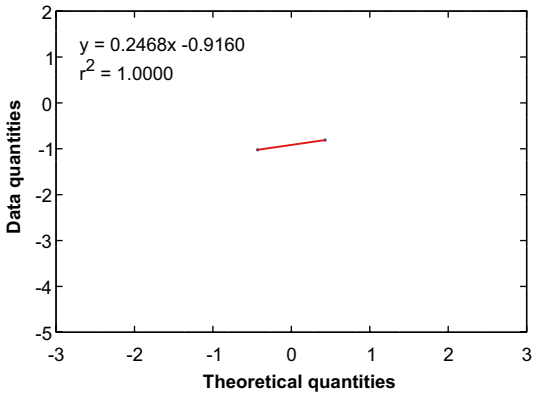


### *Hematite (RFM044)*

***N/A***

### *Pyrite (RFM044)*

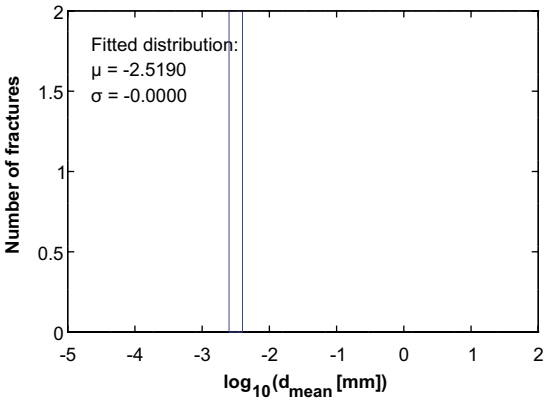


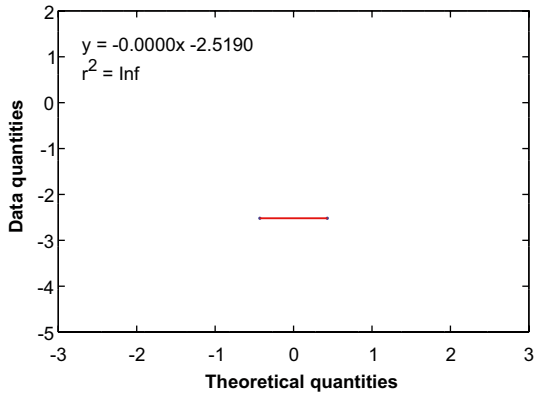


## A3.6 RFM045 (132 fractures)

### *Calcite (RFM045)*

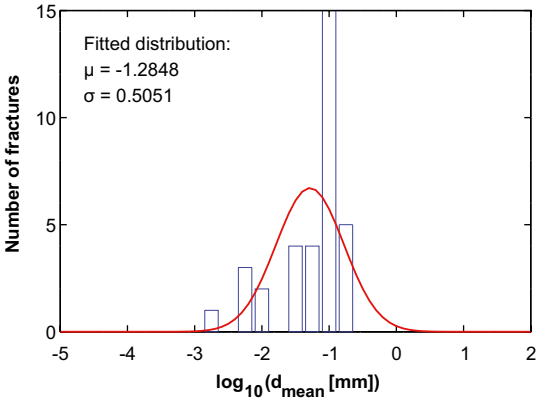


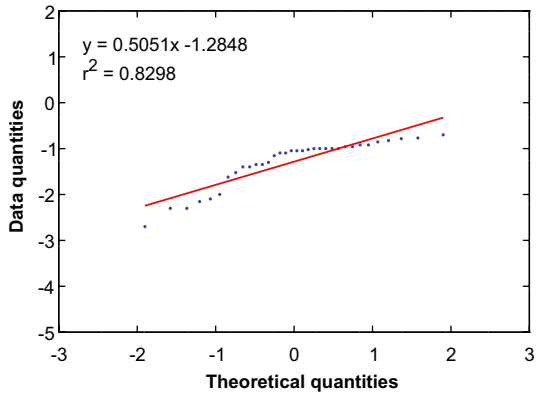

### *Chlorite (RFM045)*

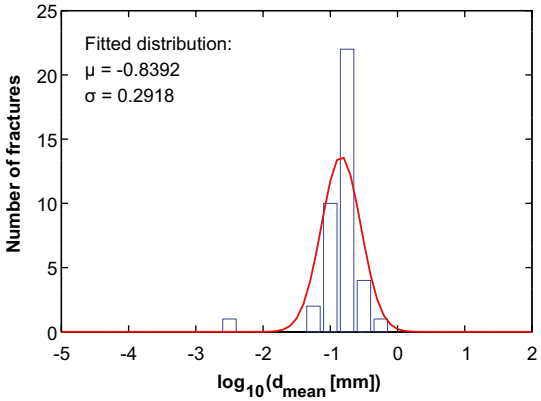


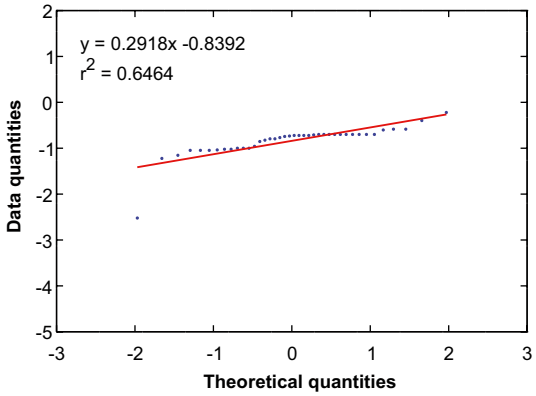


### *Clay minerals (RFM045)*

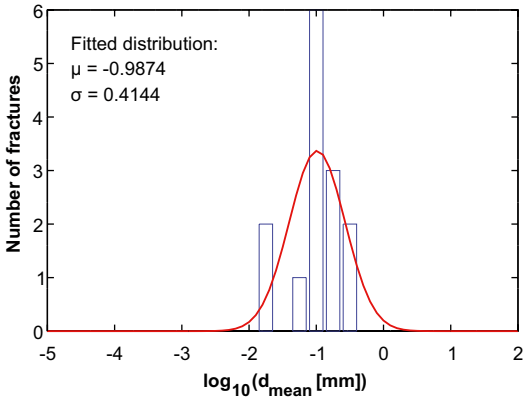


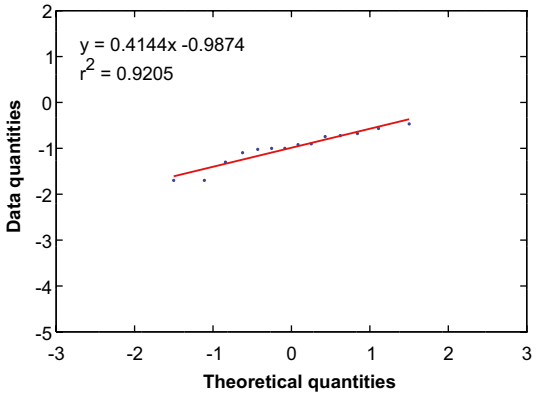


### *Hematite (RFM045)*

***N/A***

### *Pyrite (RFM045)*

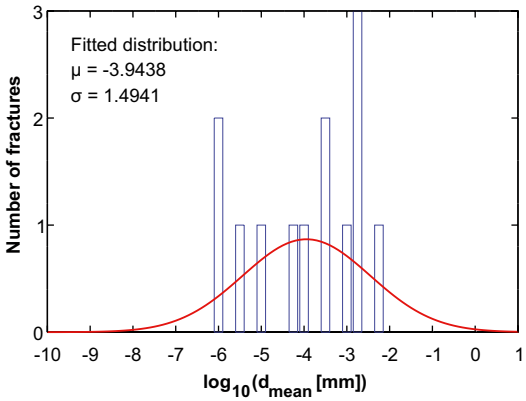


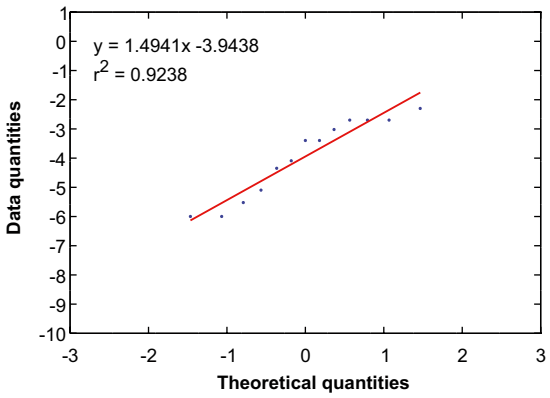

# A4 Fracture domains

## A4.1 All fracture domains (602 fractures)

### *Calcite (All FD)*

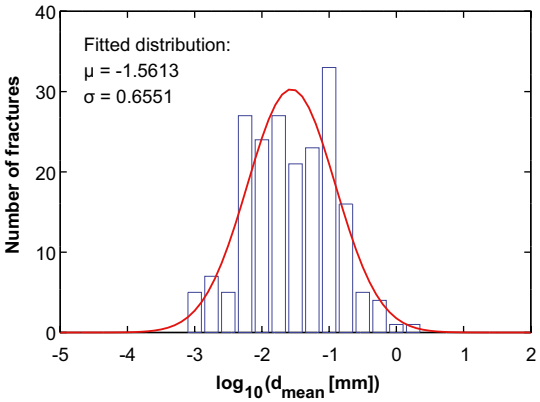


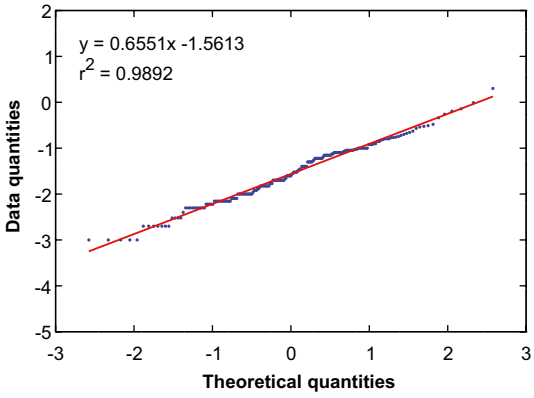


### *Chlorite (All FD)*

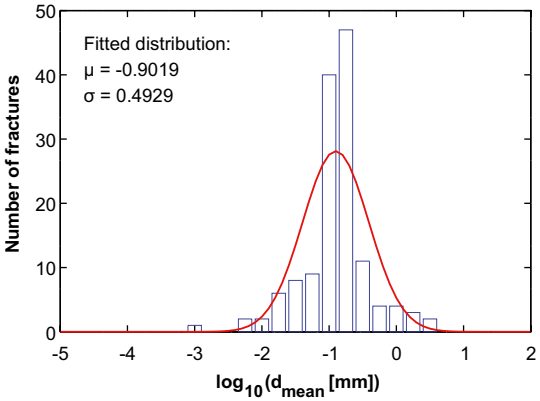


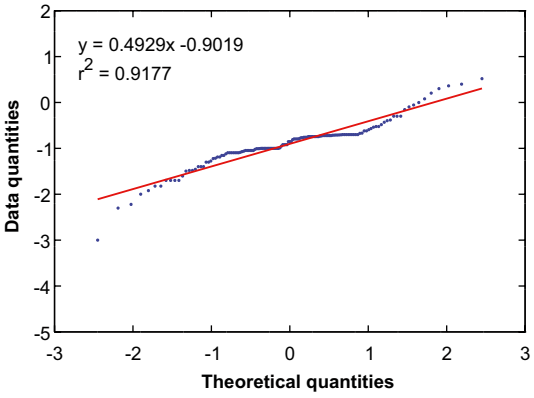


### *Clay minerals (All FD)*

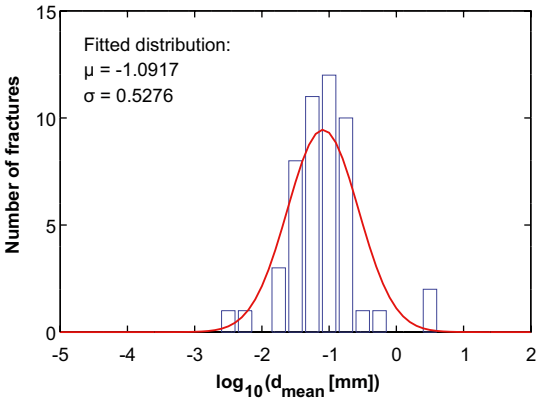


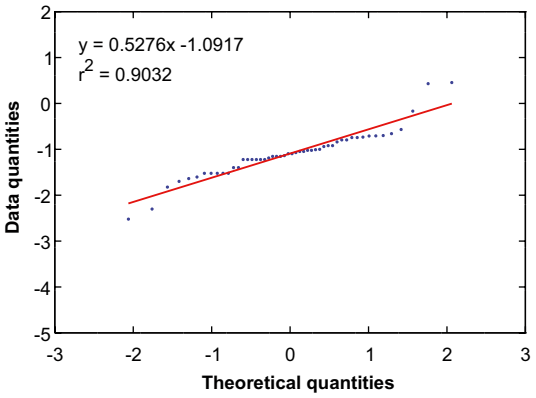

### *Hematite (All FD)*

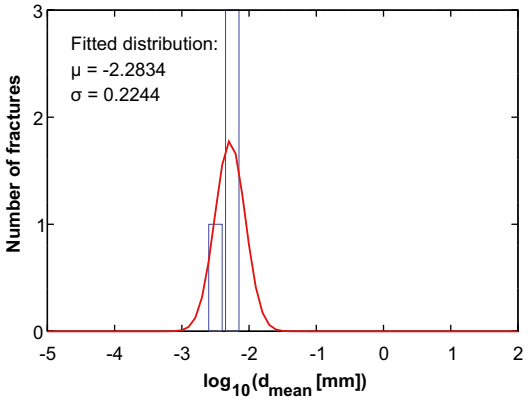


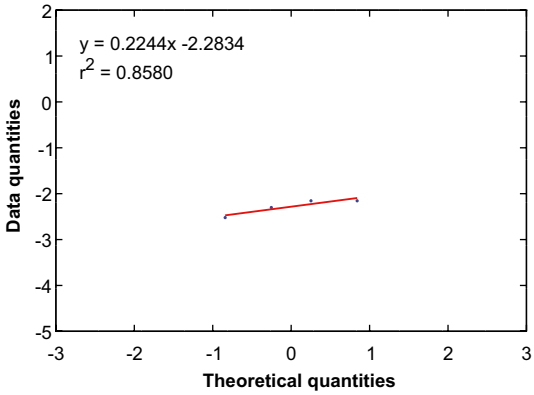


### *Pyrite (All FD)*

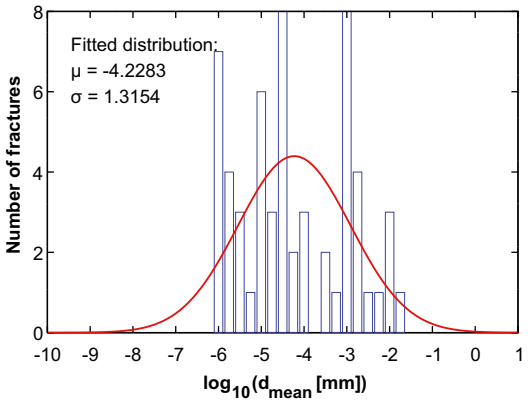


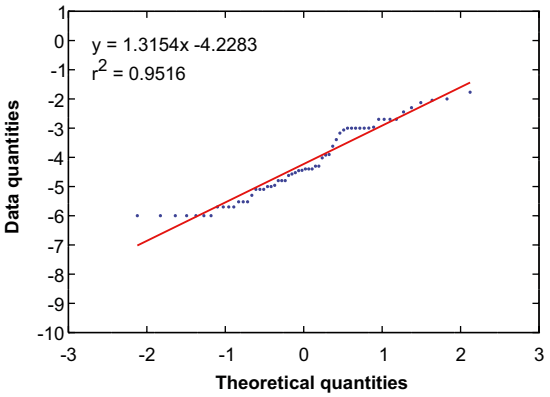


## A4.2 FFM01 (152 fractures)

### *Calcite (FFM01)*

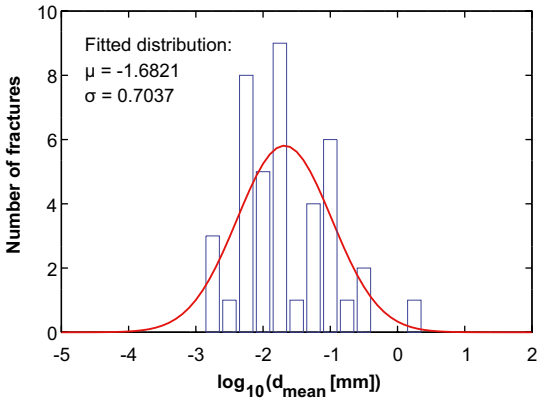


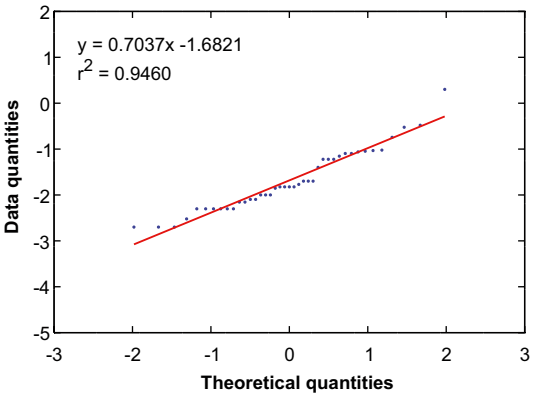

### *Chlorite (FFM01)*

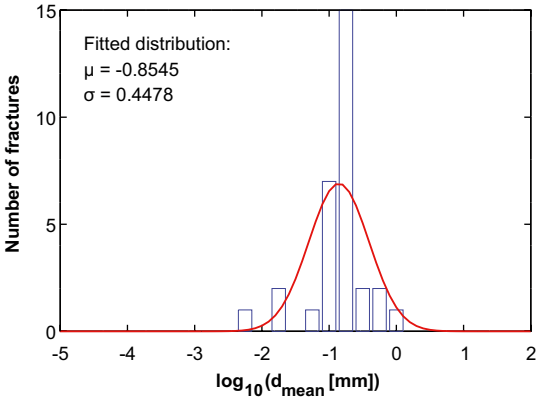


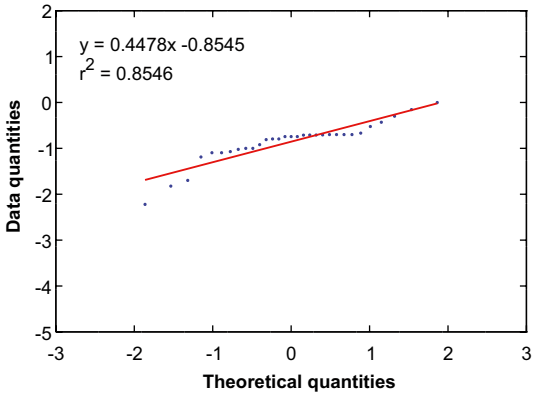


### *Clay minerals (FFM01)*

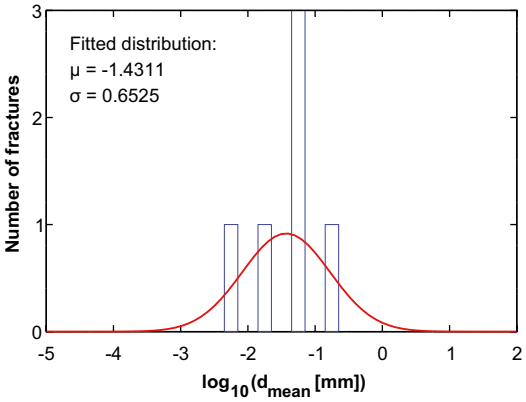


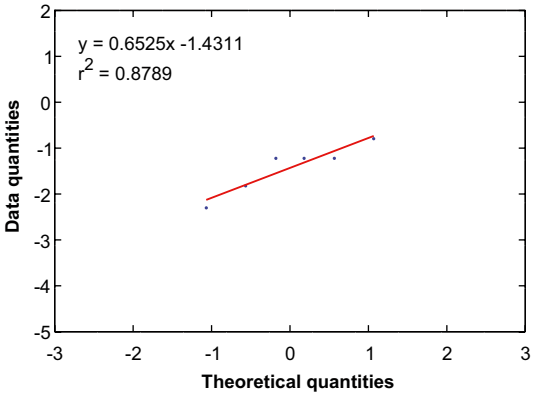


### *Hematite (FFM01)*

***N/A***

### *Pyrite (FFM01)*

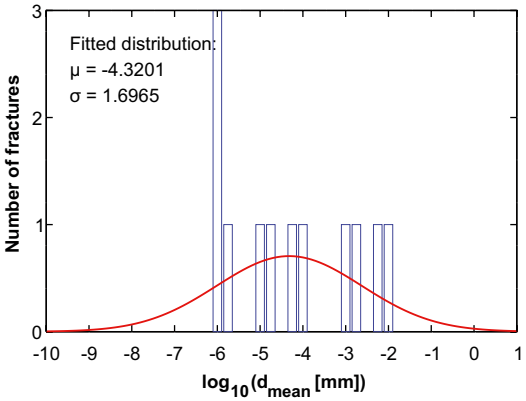


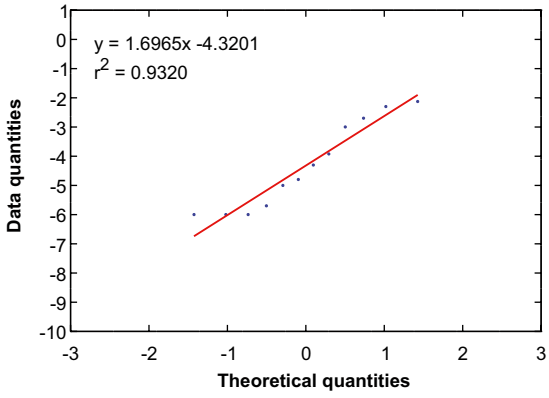

## A4.3 FFM02 (321 fractures)

### *Calcite (FFM02)*

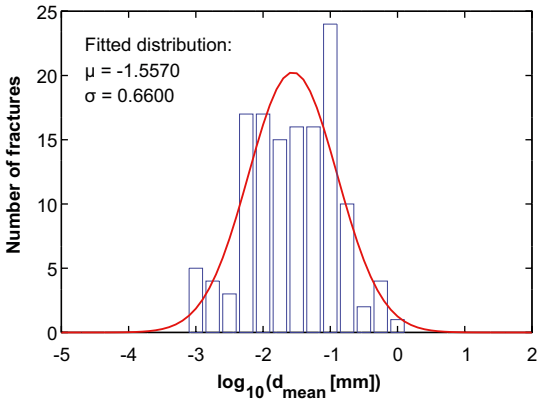


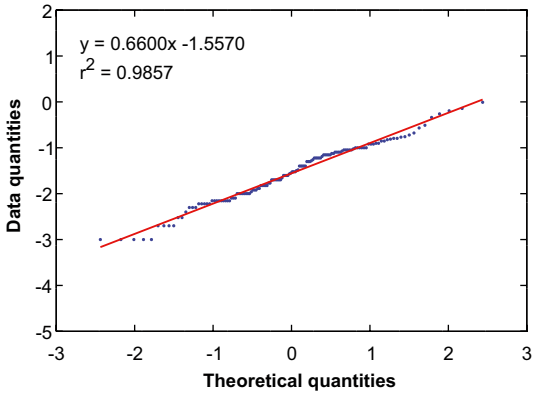


### *Chlorite (FFM02)*

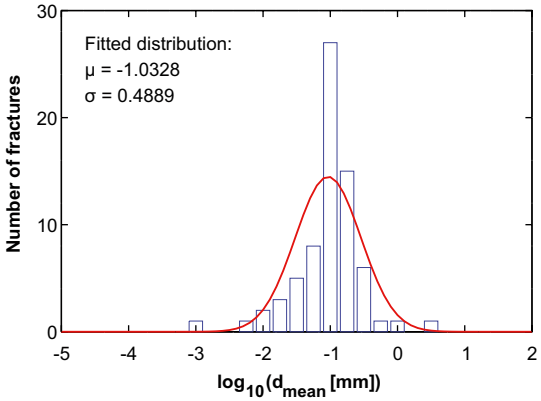


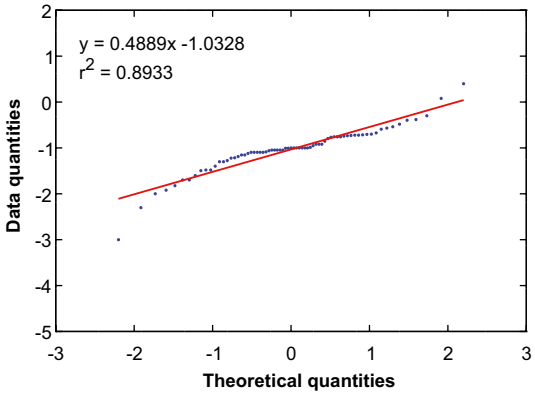


### *Clay minerals (FFM02)*

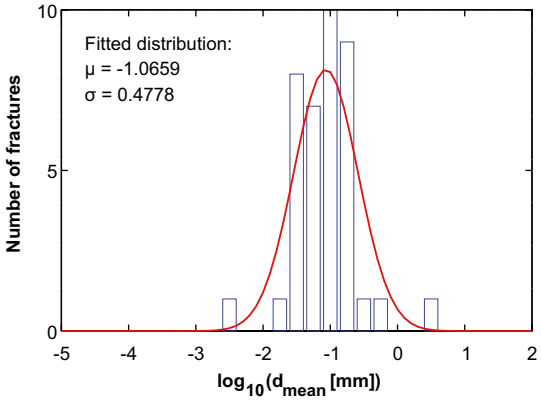


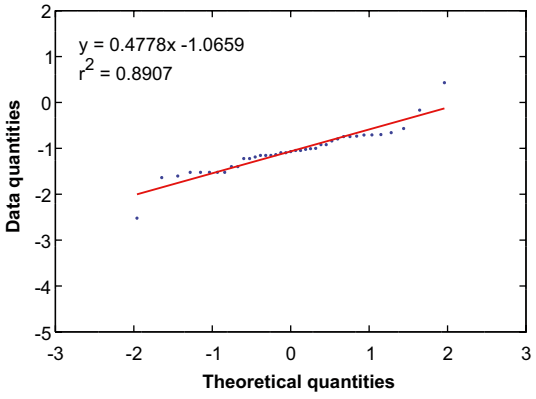

### *Hematite (FFM02)*

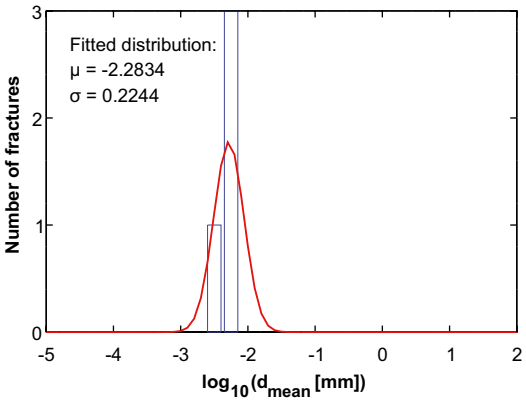


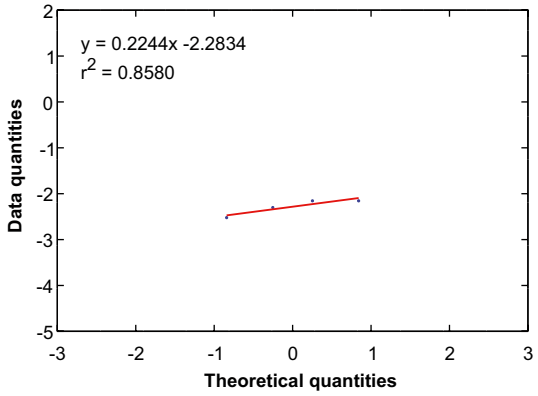


### *Pyrite (FFM02)*

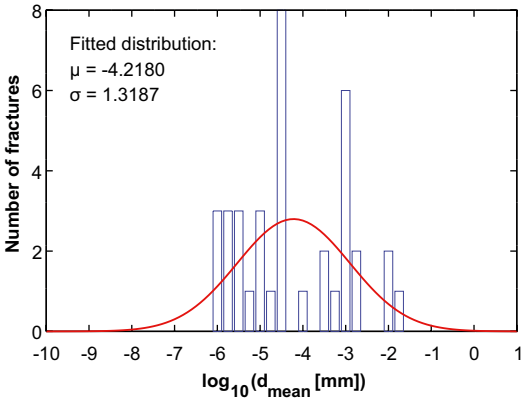


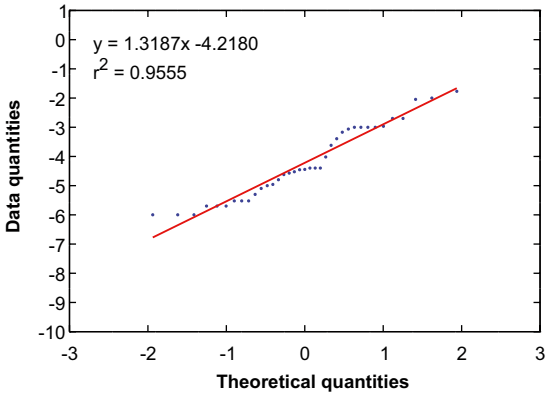


## A4.4 FFM03 (107 fractures)

### *Calcite (FFM03)*

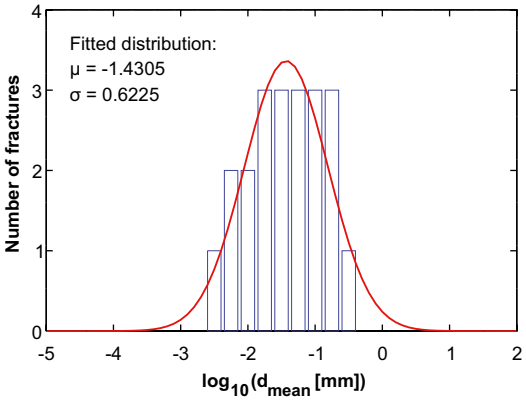


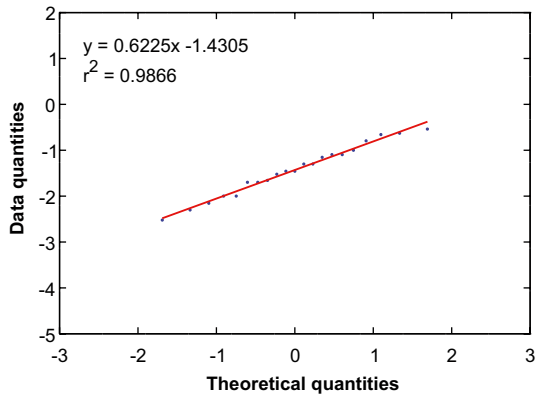

### *Chlorite (FFM03)*

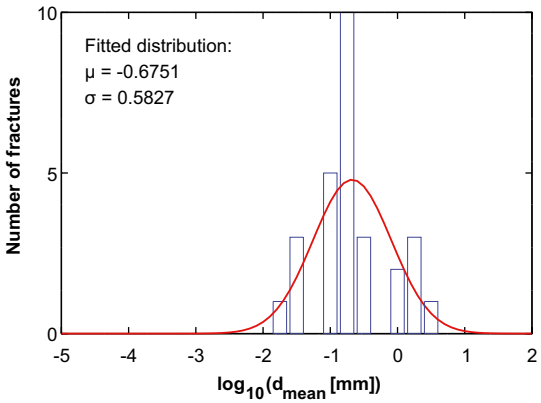


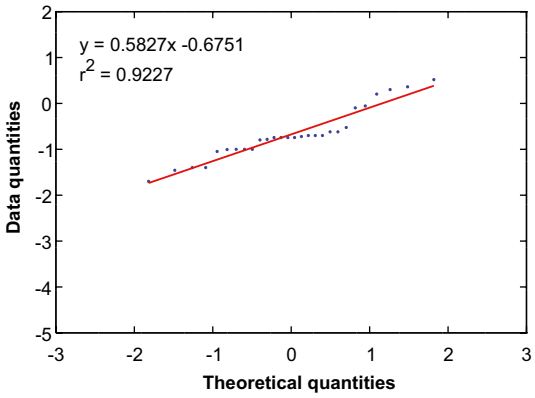


### *Clay minerals (FFM03)*

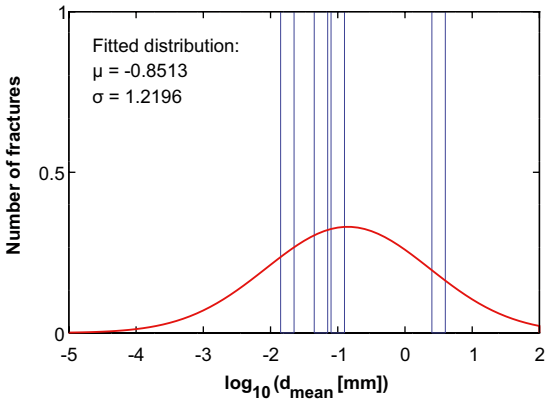


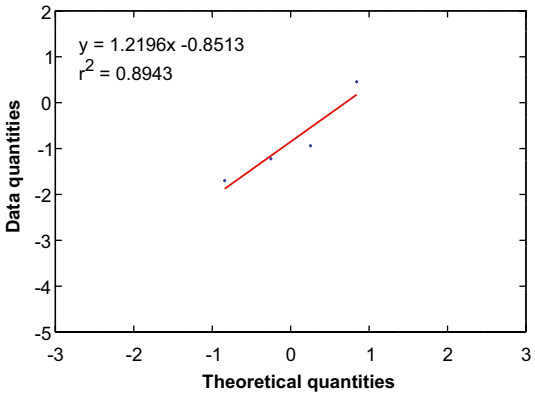


### *Hematite (FFM03)*

***N/A***

### *Pyrite (FFM03)*

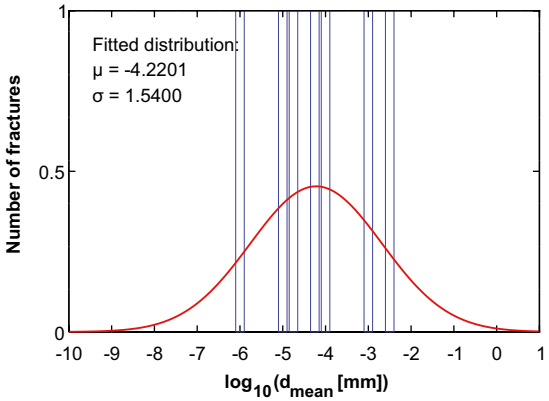


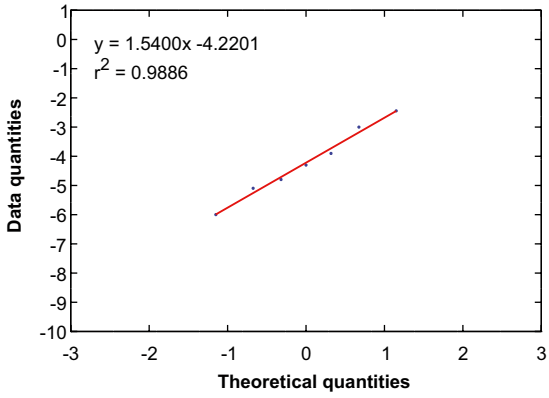

## A4.5 FFM04 (8 fractures)

### *Calcite (FFM04)*

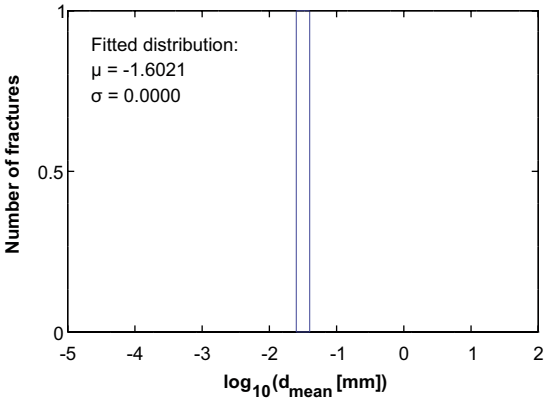


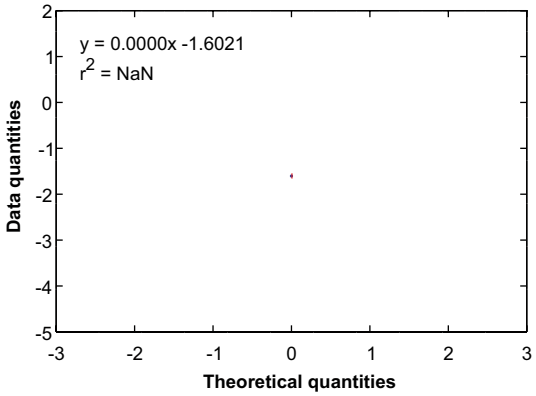


### *Chlorite (FFM04)*

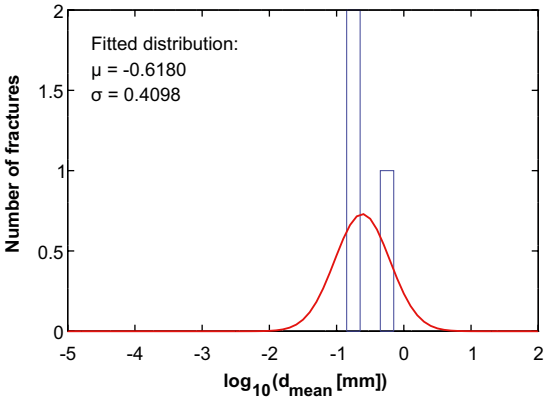


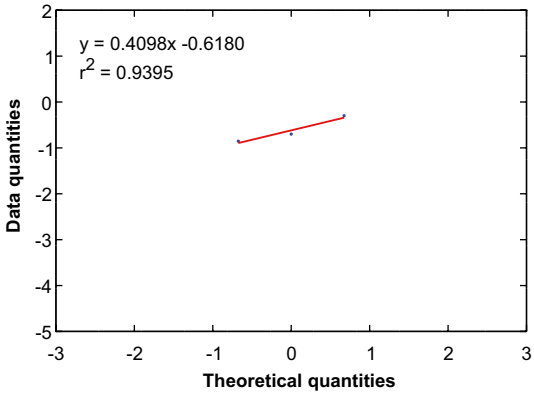


### *Clay minerals (FFM04)*

***N/A***

### *Hematite (FFM04)*

***N/A***

### *Pyrite (FFM04)*

***N/A***

## A4.6 FFM05 (3 fractures)

### *Calcite (FFM05)*

***N/A***

### *Chlorite (FFM05)*

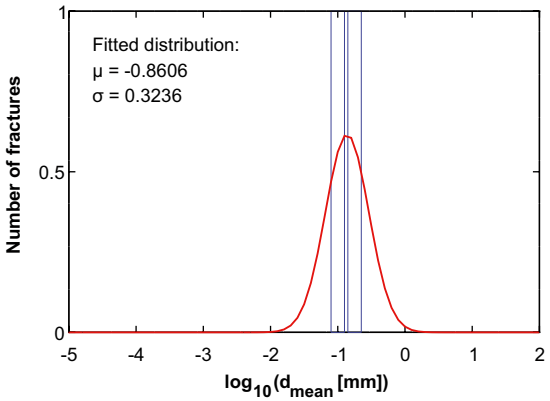


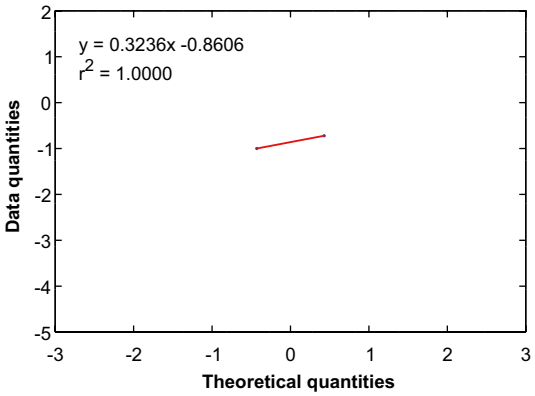


### *Clay minerals (FFM05)*

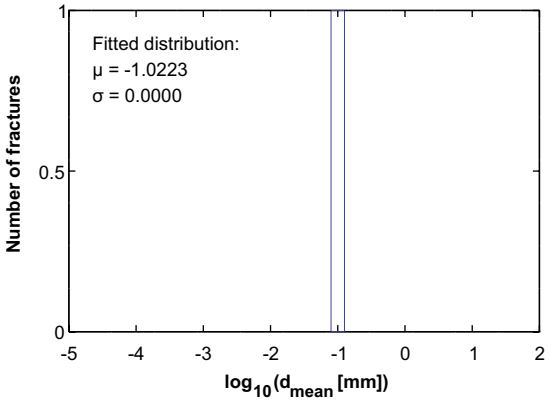


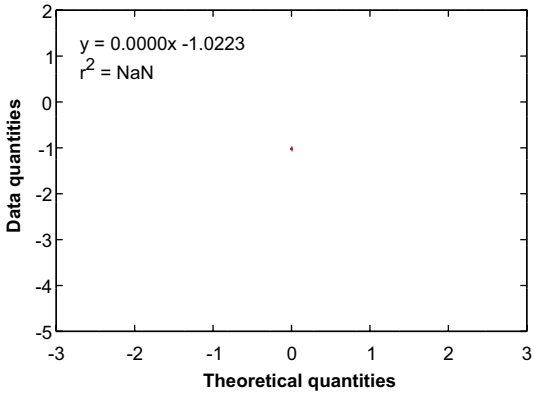


### *Hematite (FFM05)*

***N/A***

### *Pyrite (FFM05)*

***N/A***

## A4.7 FFM06 (11 fractures)

### *Calcite (FFM06)*

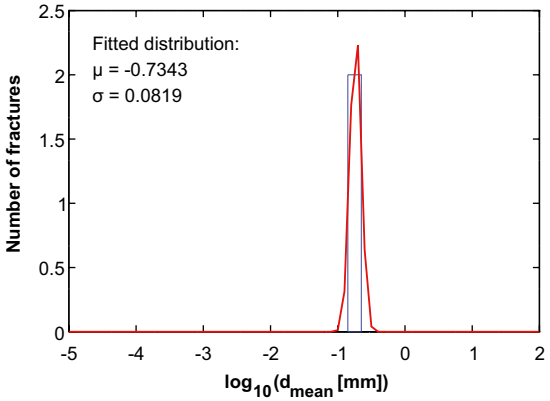


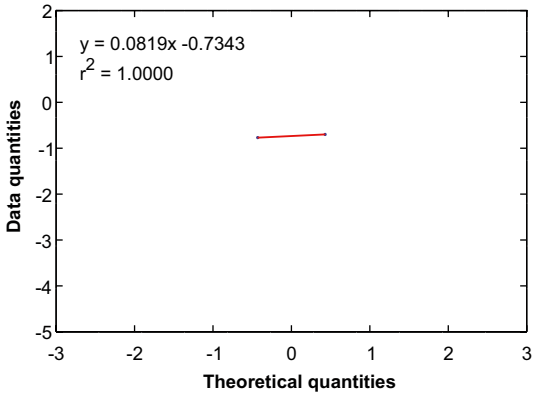

### *Chlorite (FFM06)*

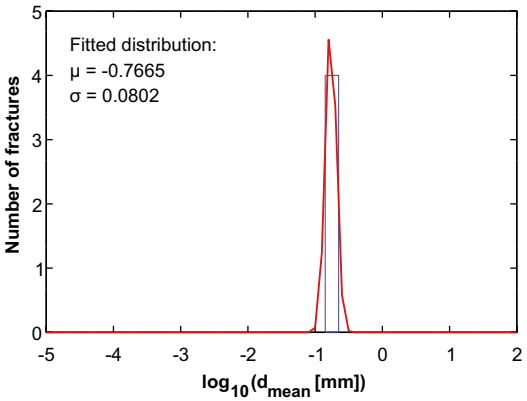


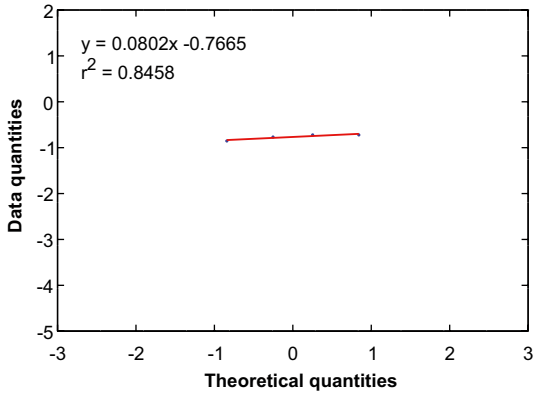


### *Clay minerals (FFM06)*

***N/A***

### *Hematite (FFM06)*

***N/A***

### *Pyrite (FFM06)*

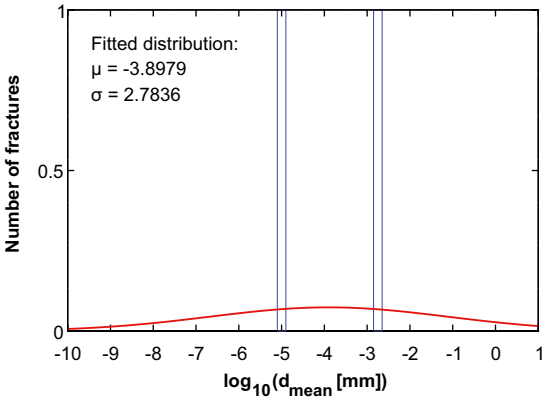


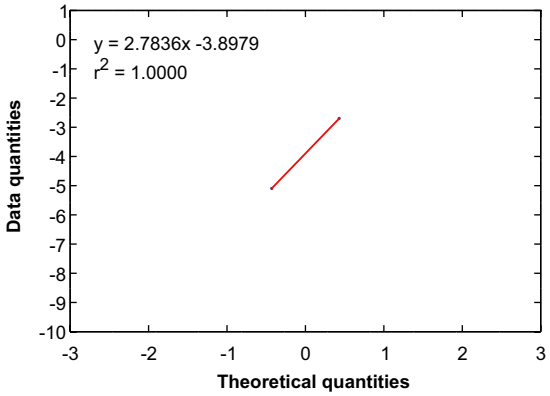


## A5 Deformation zones

### A5.1 All deformation zones (1,333 fractures)

### *Calcite (All DZ)*

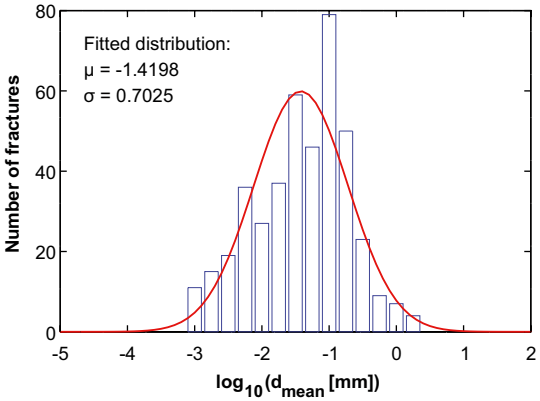


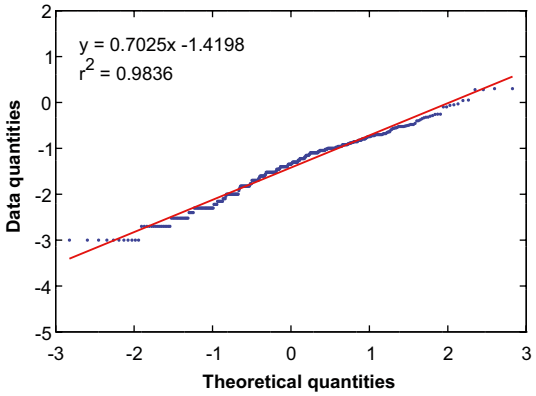

### *Chlorite (All DZ)*

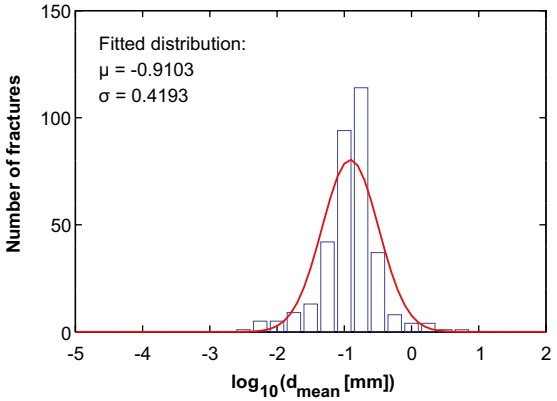


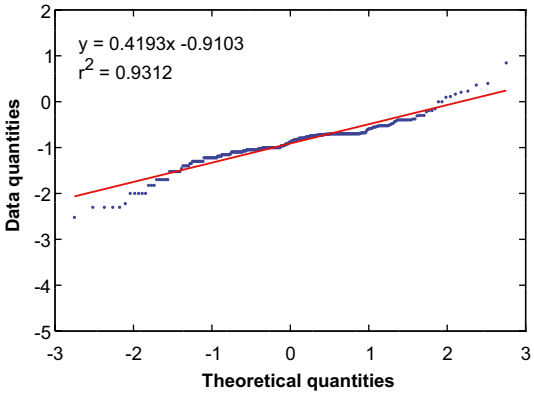


### *Clay minerals (All DZ)*

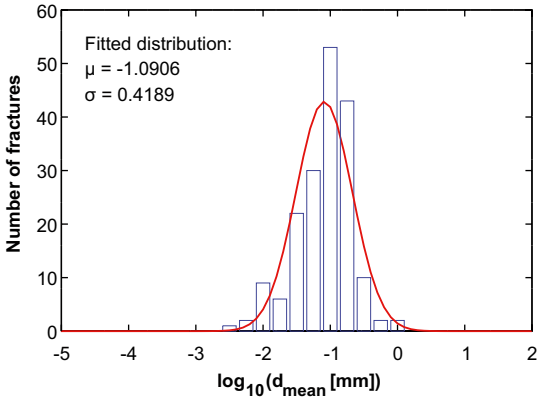


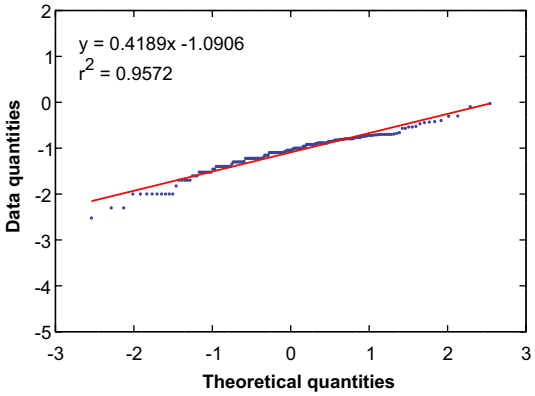


### *Hematite (All DZ)*

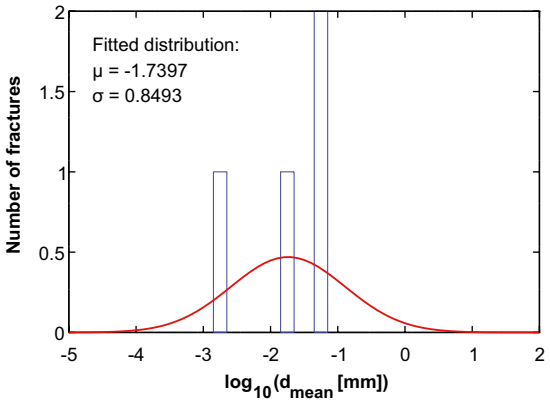


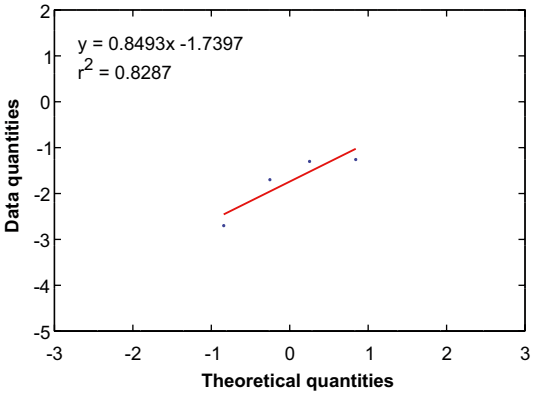

### *Pyrite (All DZ)*

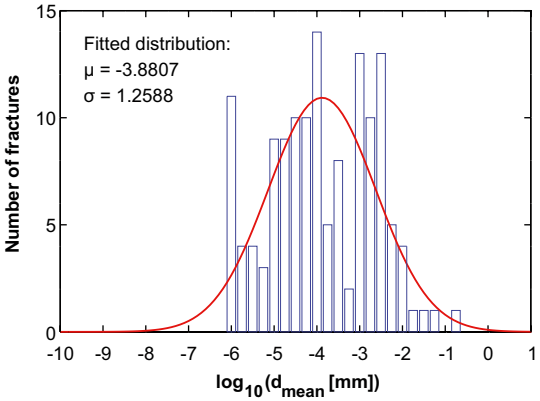


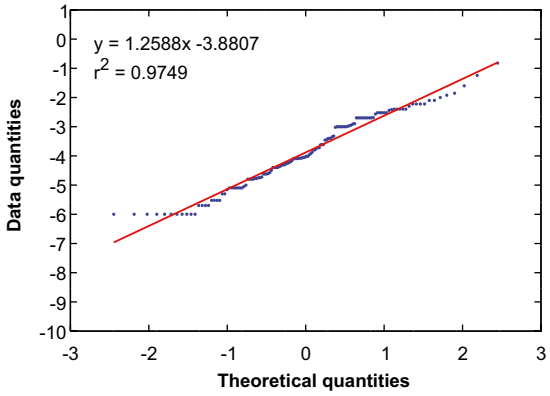


## A5.2 GDZ (640 fractures)

### *Calcite (GDZ)*

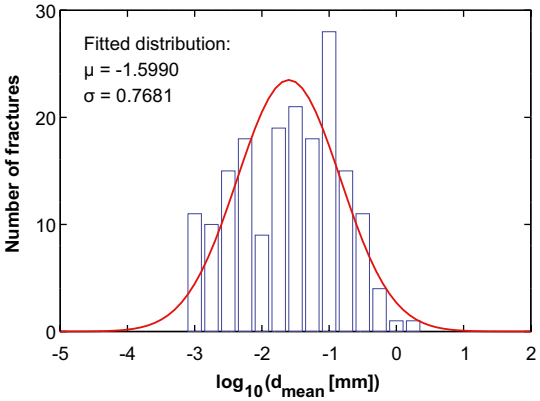


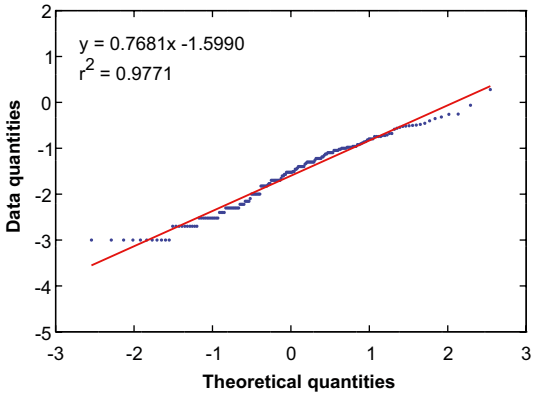


### *Chlorite (GDZ)*

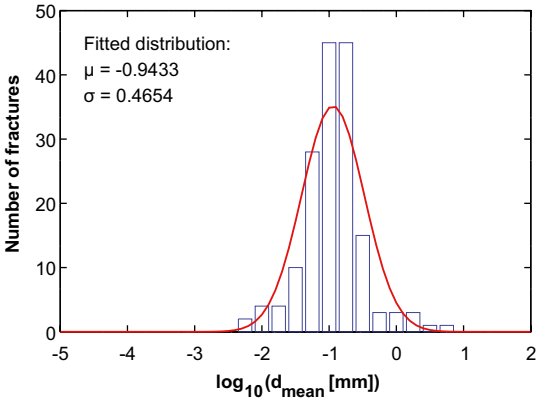


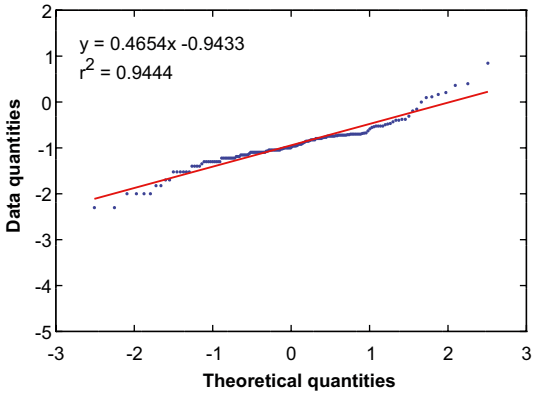

### *Clay minerals (GDZ)*

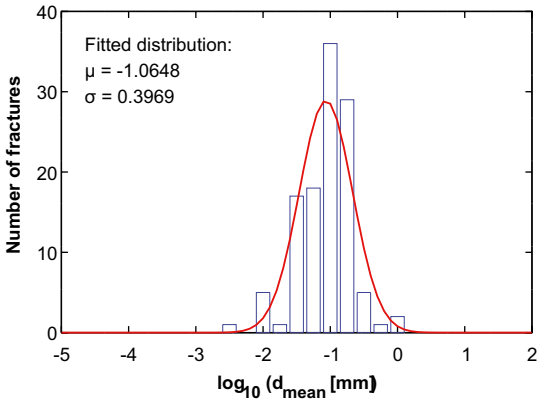


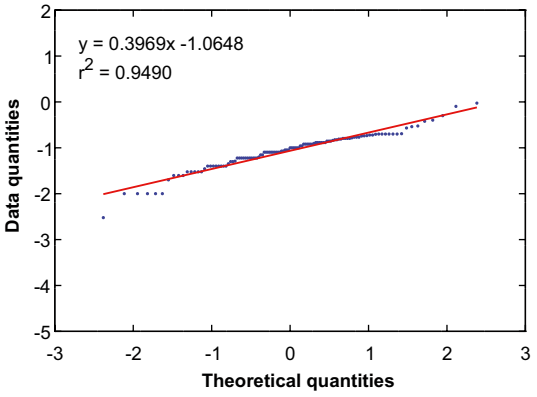


### *Hematite (GDZ)*

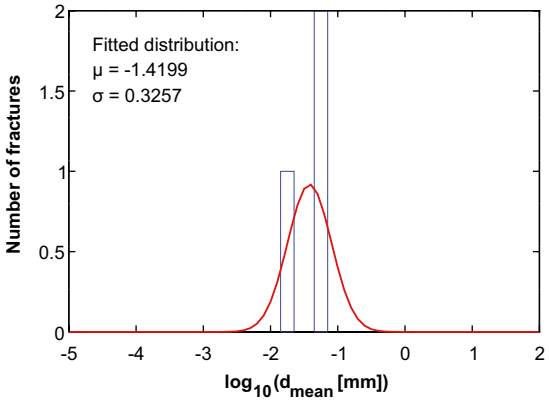


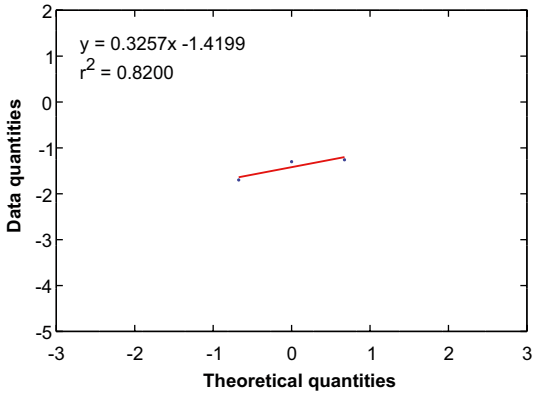


### *Pyrite (GDZ)*

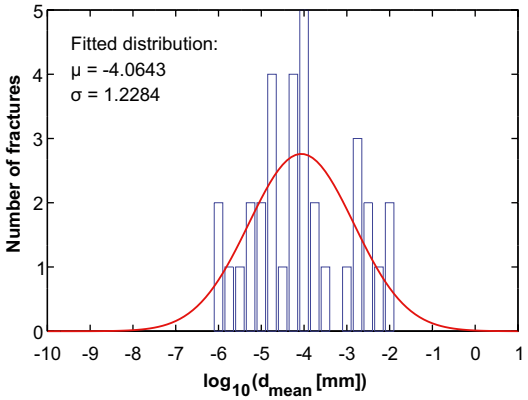


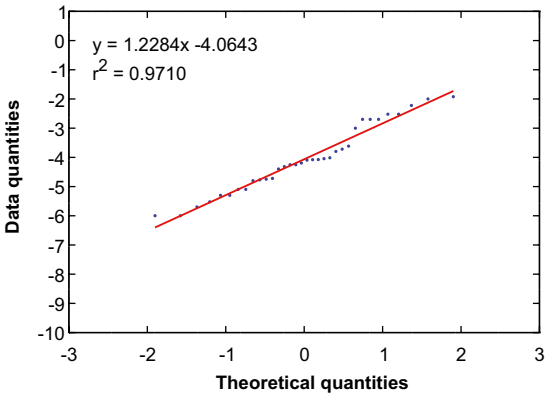

## A5.3 SDZ (WNW to NW) (371 fractures)

### *Calcite (WNW to NW)*

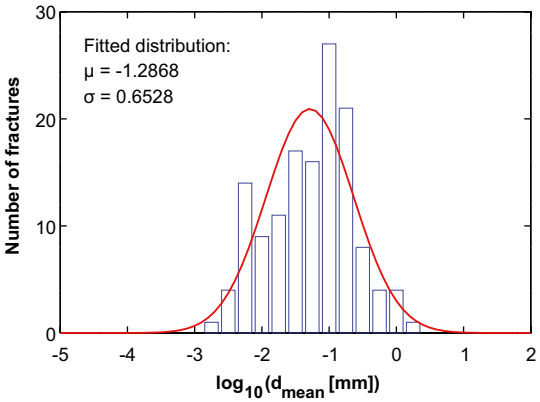


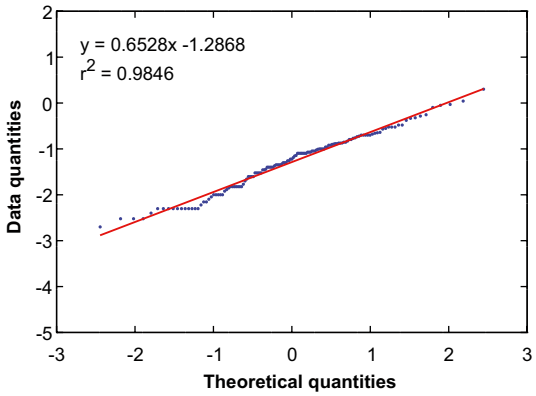


### *Chlorite (WNW to NW)*

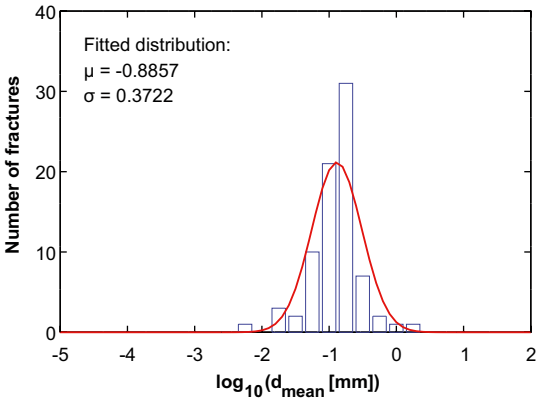


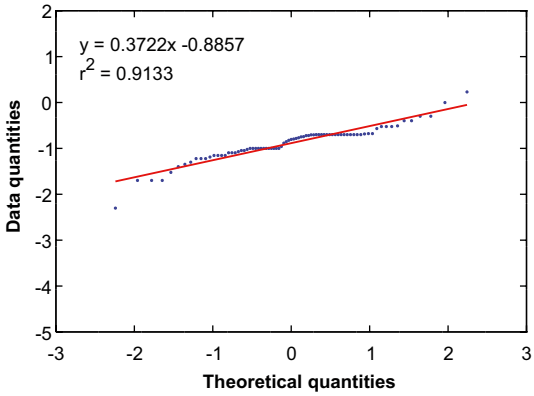


### *Clay minerals (WNW to NW)*

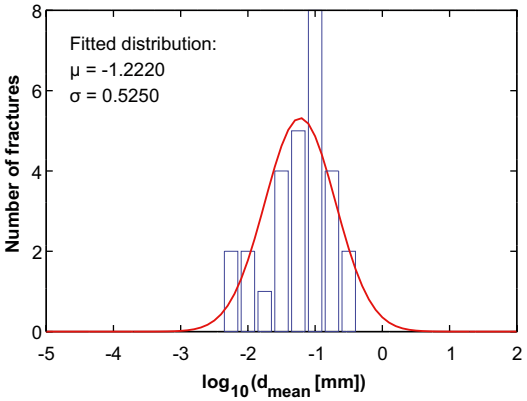


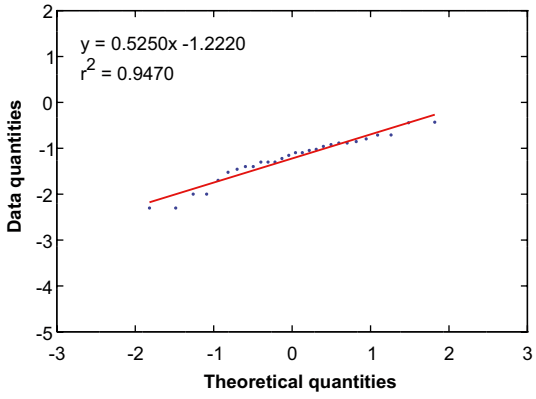

### *Hematite (WNW - NW)*

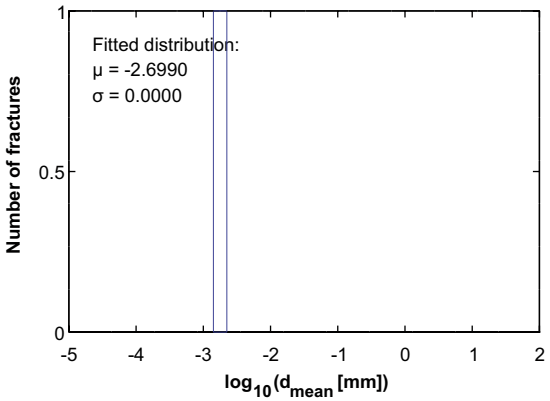


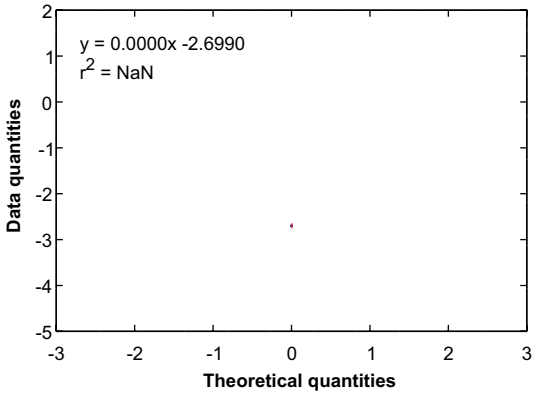


### *Pyrite (WNW to NW)*

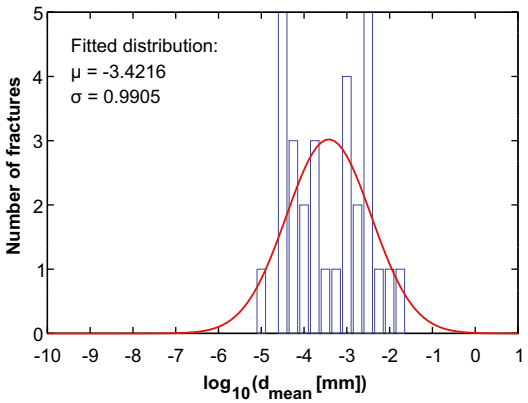


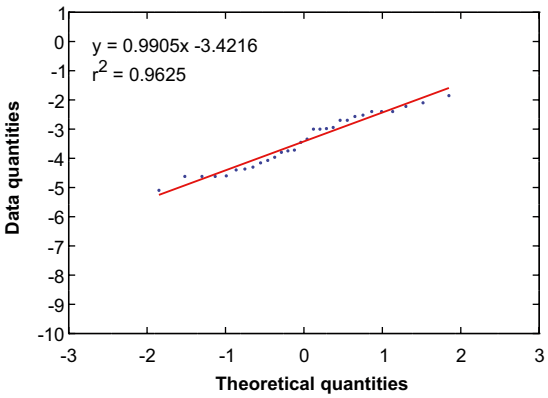


## A5.4 SDZ (NNW) (22 fractures)

### *Calcite (NNW)*

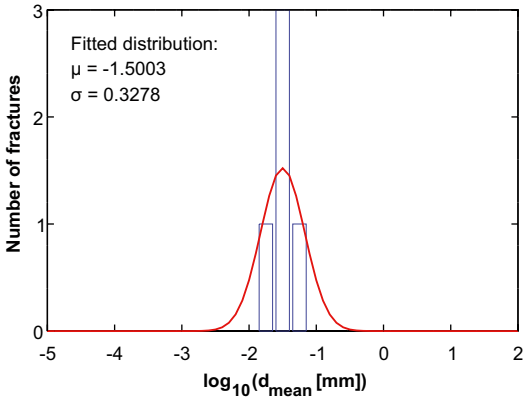


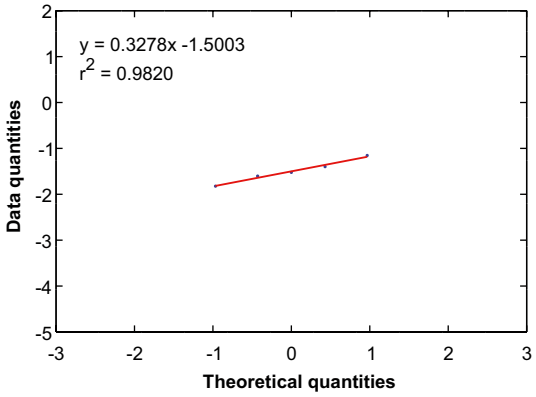

### *Chlorite (NNW)*

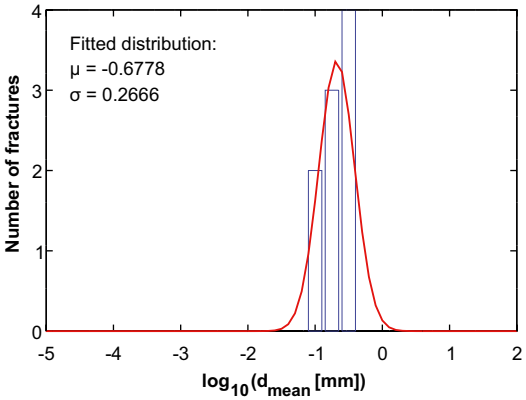


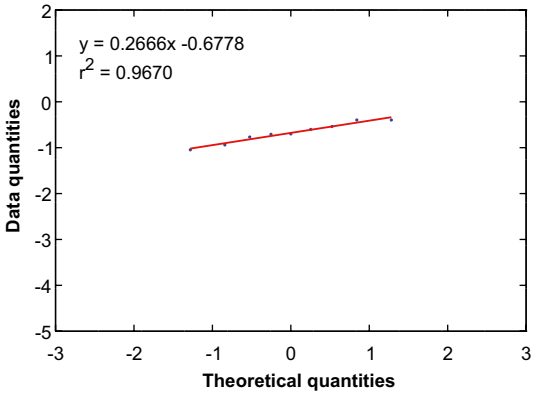


### *Clay minerals (NNW)*

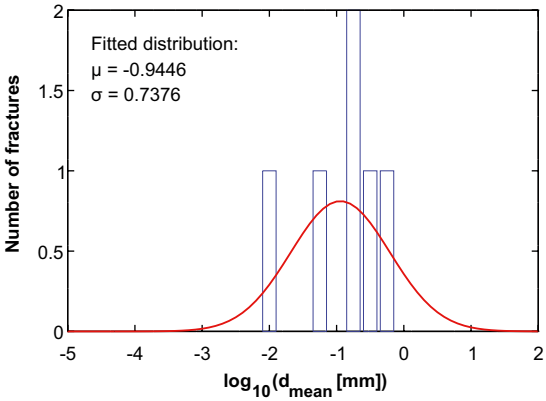


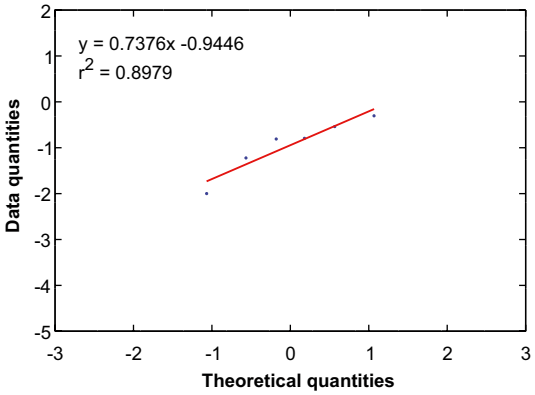


### *Hematite (NNW)*

***N/A***

### *Pyrite (NNW)*

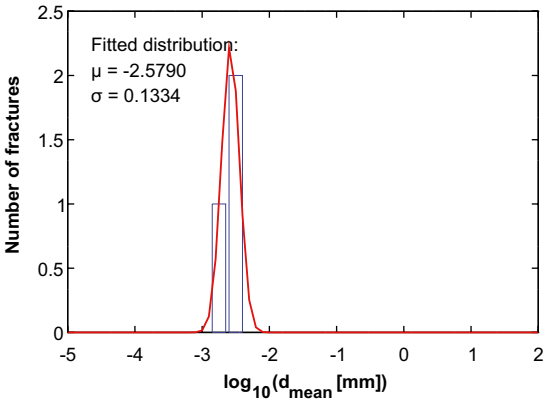


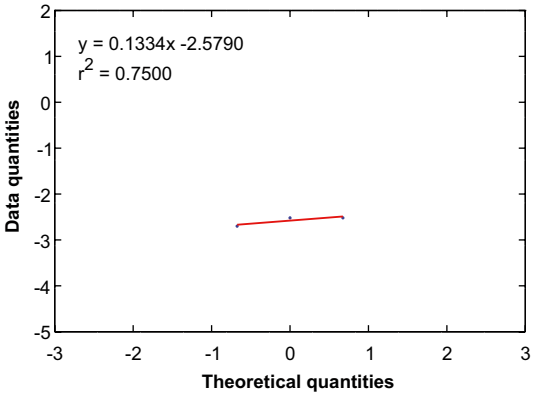

## A5.5 SDZ (ENE to NNE) (280 fractures)

### *Calcite (ENE to NNE)*

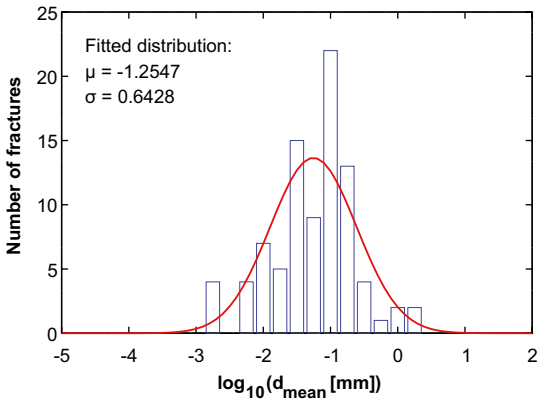


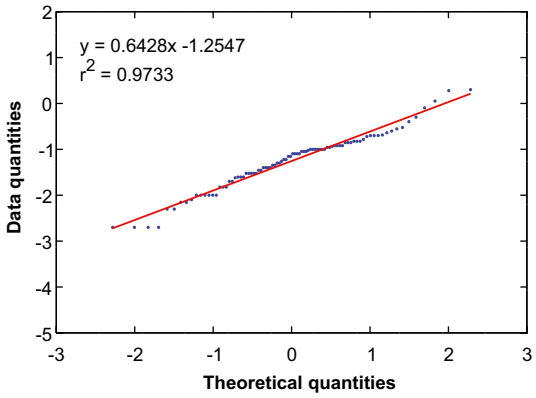


### *Chlorite (ENE to NNE)*

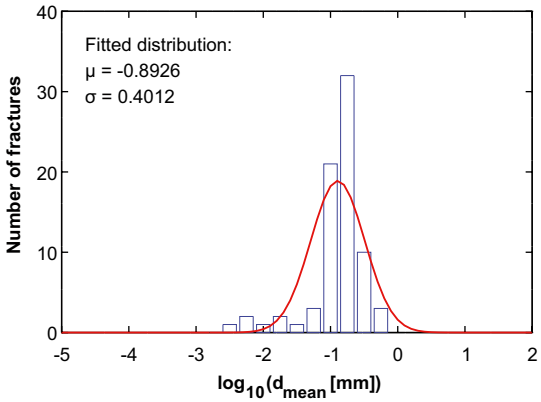


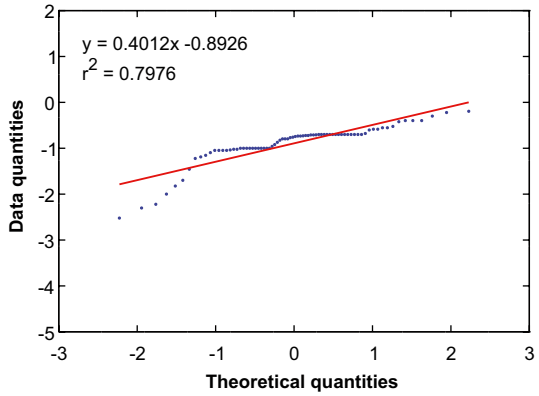


### *Clay minerals (ENE to NNE)*

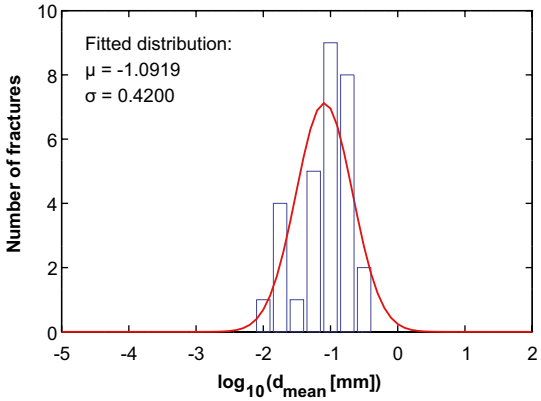


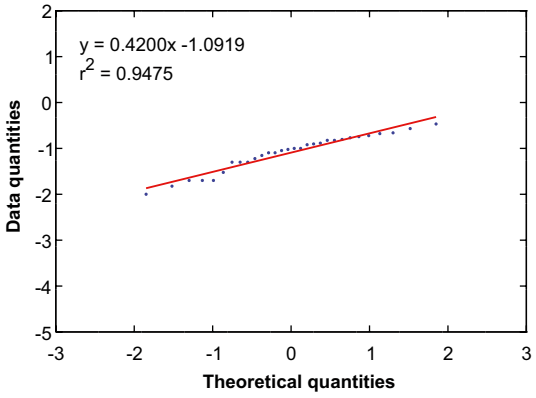


### *Hematite (ENE to NNE)*

***N/A***

### *Pyrite (ENE to NNE)*

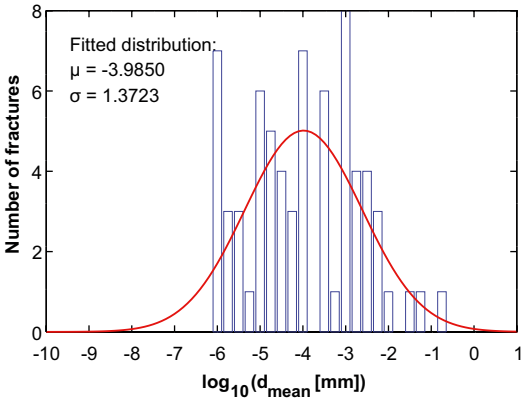


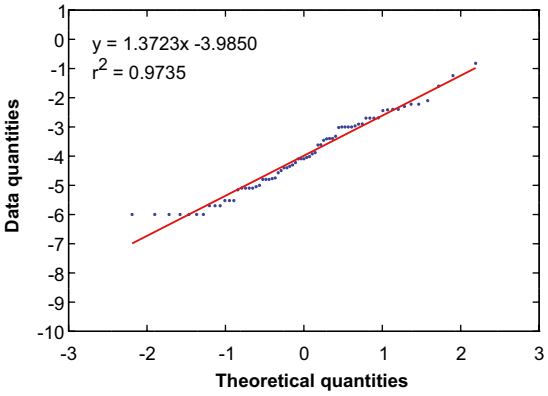

# Appendix B

## Mineral visible coverage, $C_{vis}$, in Forsmark

### B1 All fractures in Forsmark (2,071 fractures)

#### B1.1 Calcite (All)

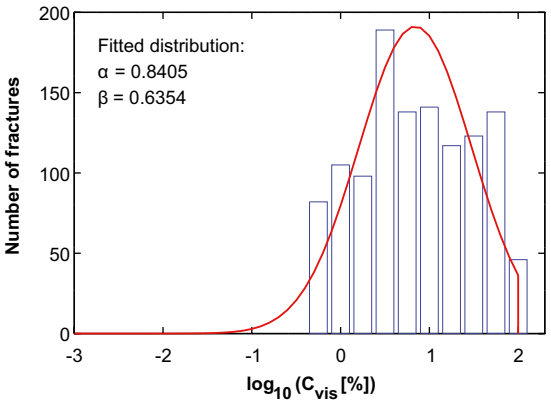


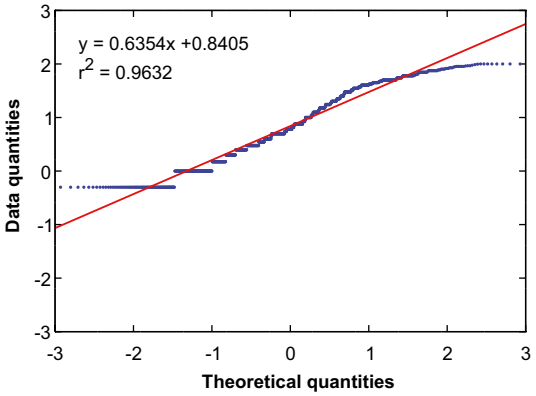


#### B1.2 Chlorite (All)

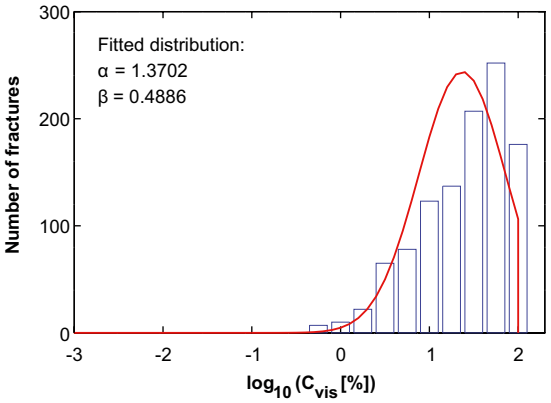


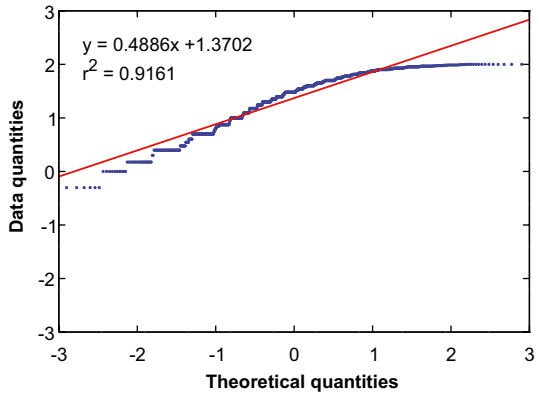


#### B1.3 Clay minerals (All)

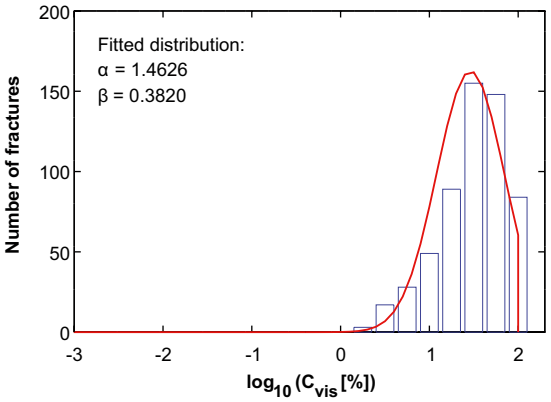


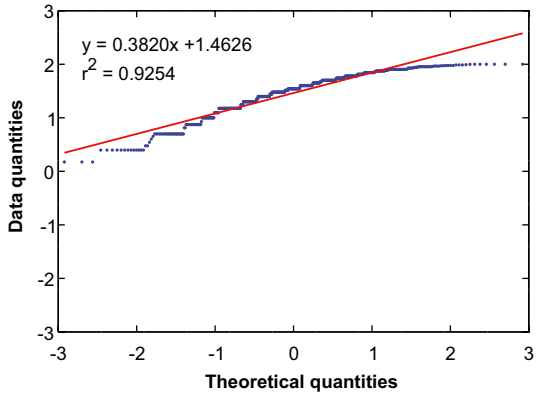

### B1.4 Hematite (All)

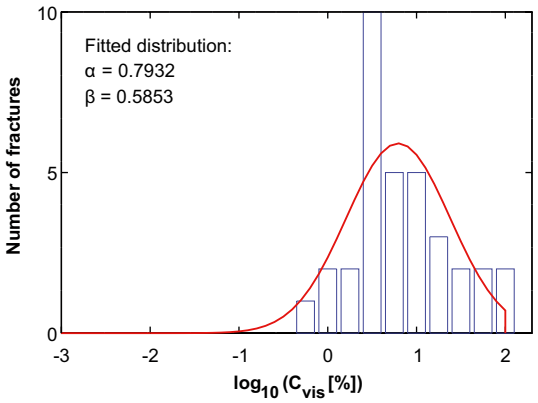


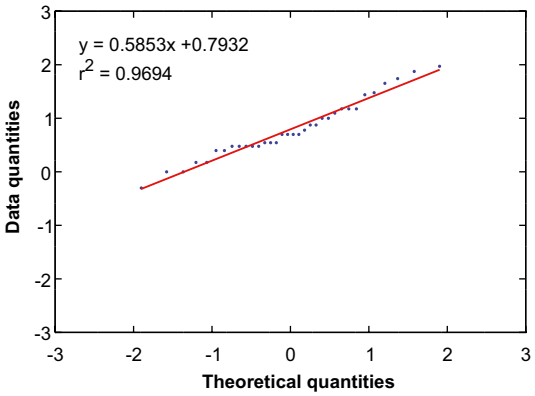


### B1.5 Pyrite (All)

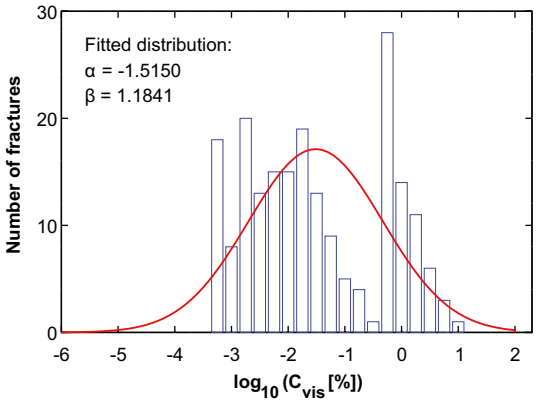


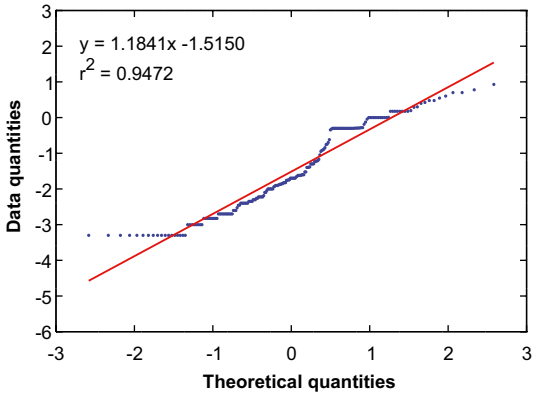


## B2 Rock domain RFM029 (1,596 fractures)

### B2.1 Calcite (RFM029)

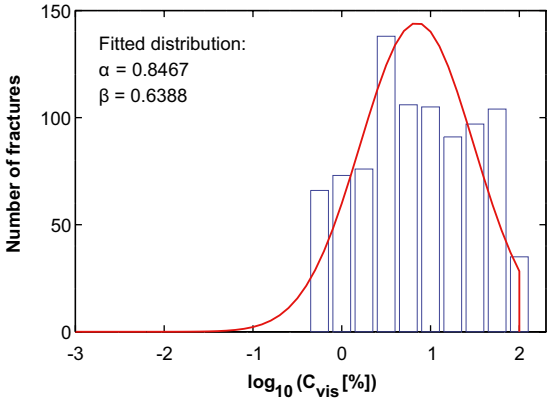


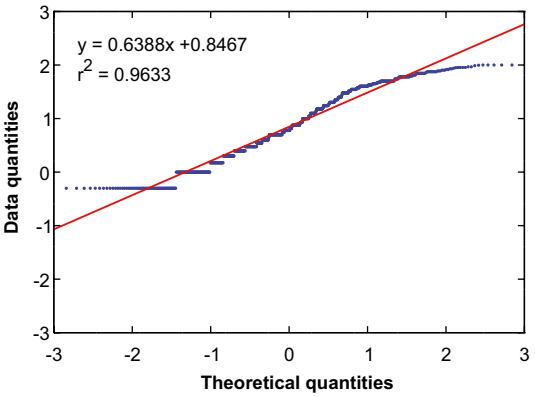

## B2.2 Chlorite (RFM029)

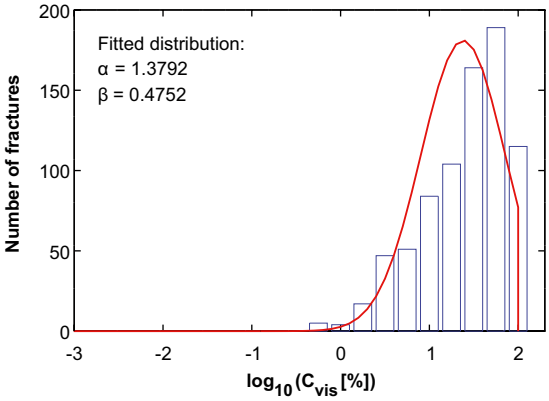


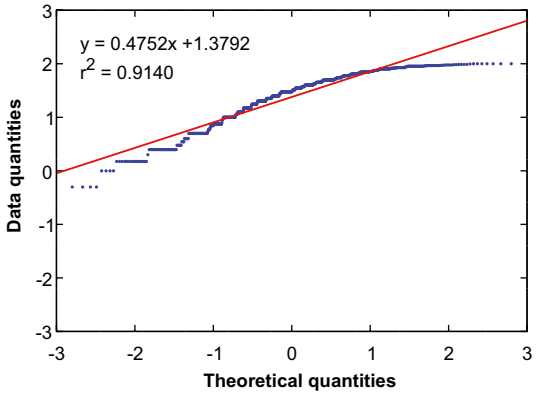


## B2.3 Clay minerals (RFM029)

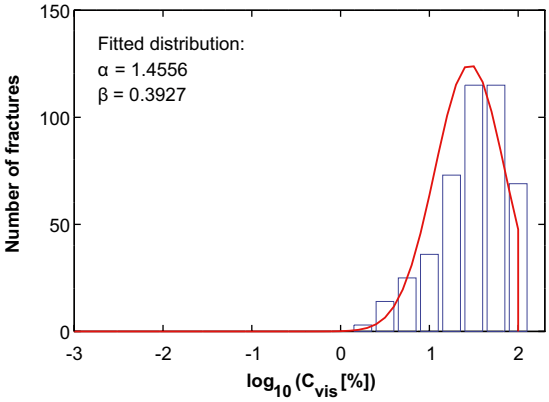


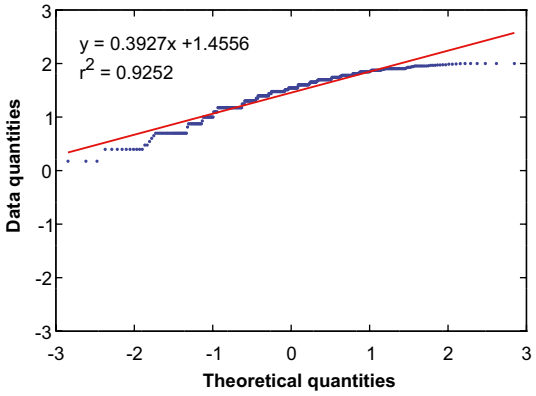


## B2.4 Hematite (RFM029)

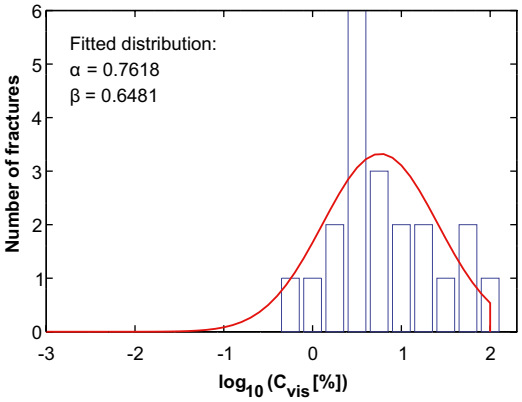


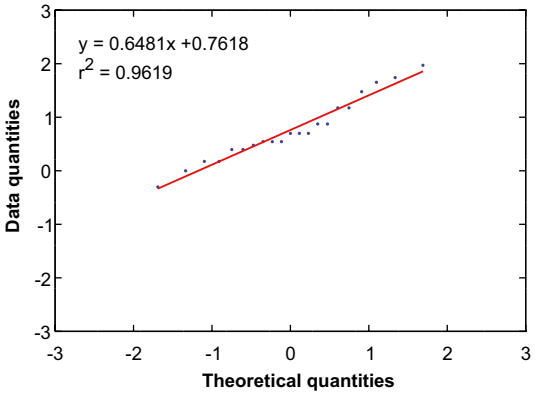

### B2.5 Pyrite (RFM029)

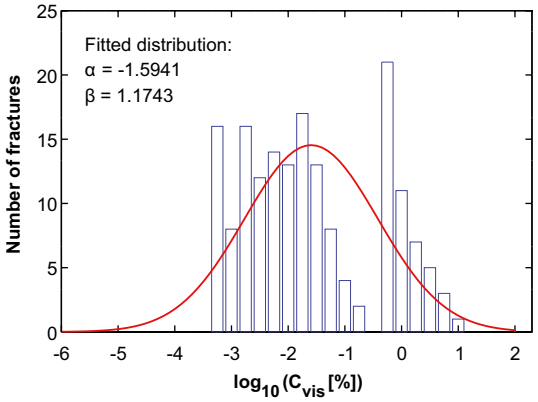


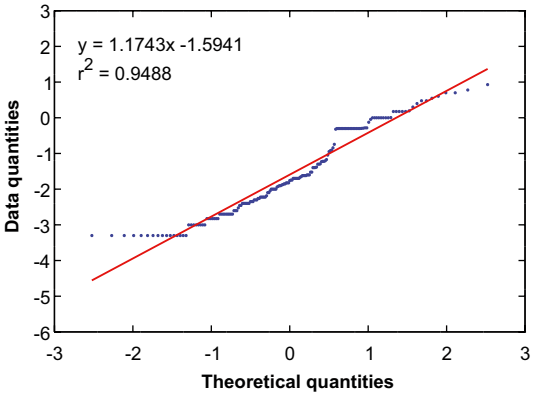


## B3 All fracture domains (602 fractures)

### B3.1 Calcite (All FD)

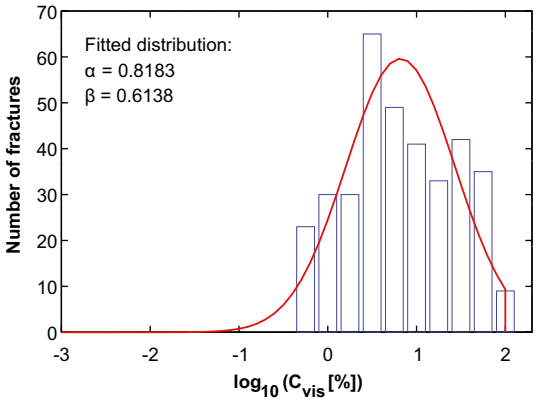


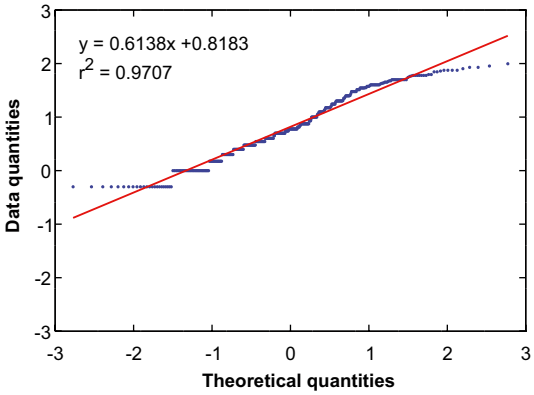


### B3.2 Chlorite (All FD)

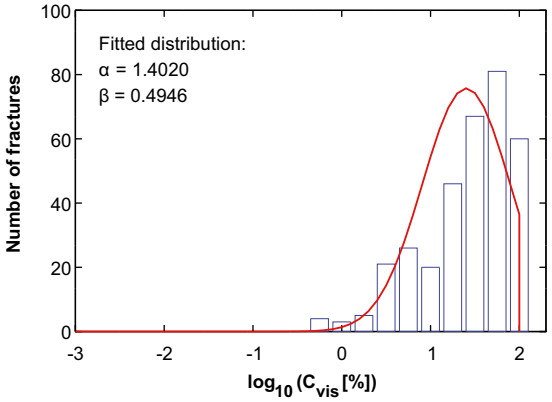


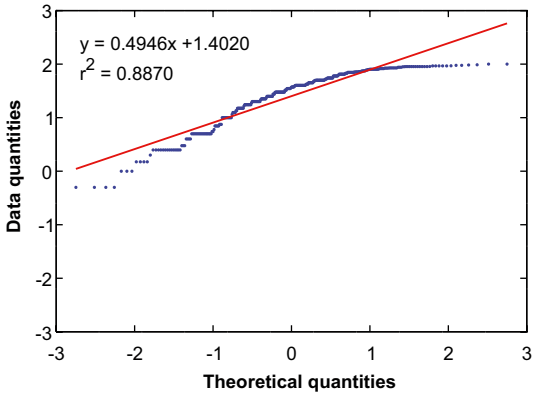

## B3.3 Clay minerals (All FD)

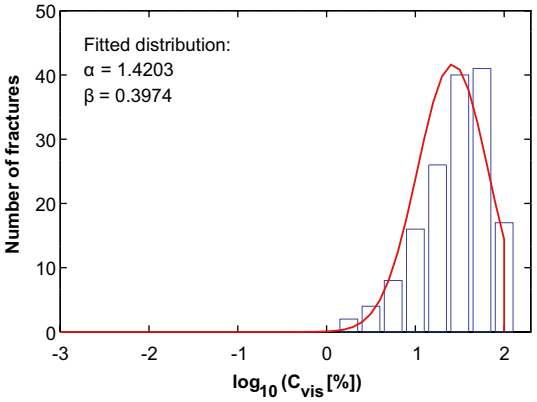


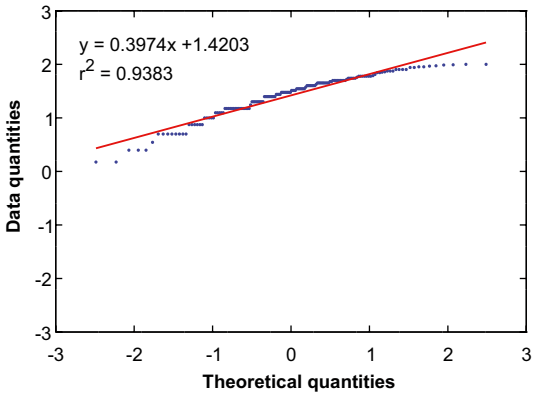


## B3.4 Hematite (All FD)

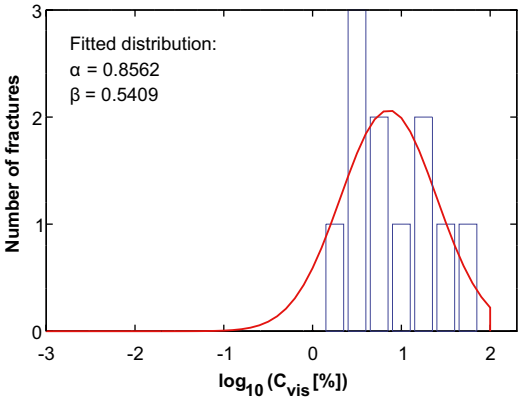


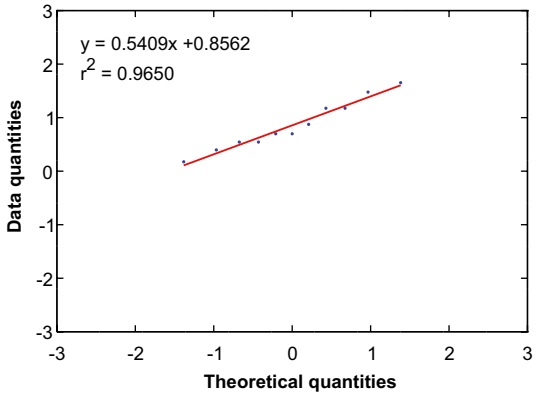


## B3.5 Pyrite (All FD)

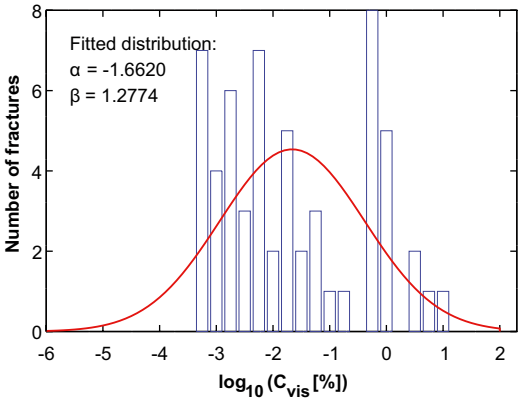


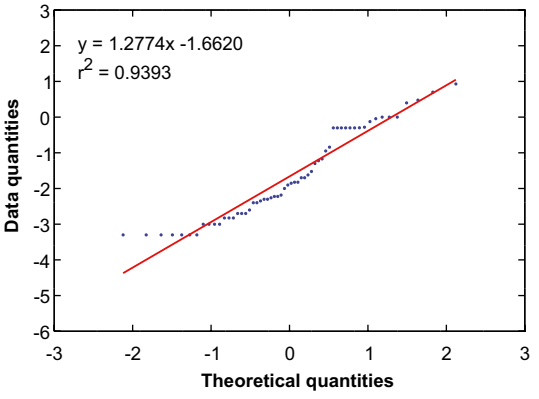

## B4 All deformation zones (1,333 fractures)

### B4.1 Calcite (All DZ)

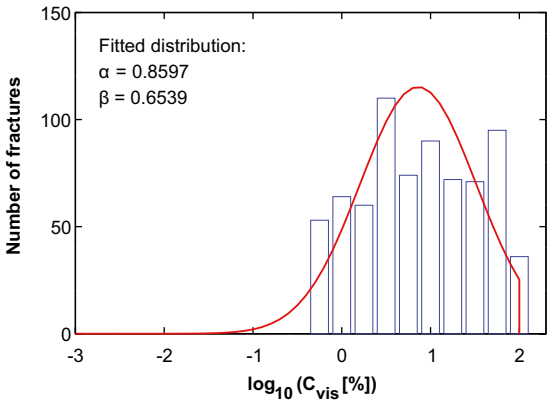


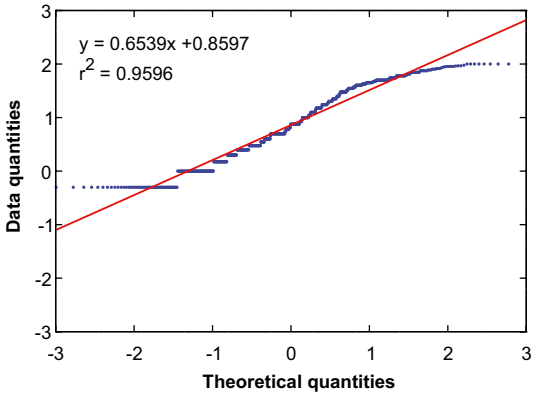


### B4.2 Chlorite (All DZ)

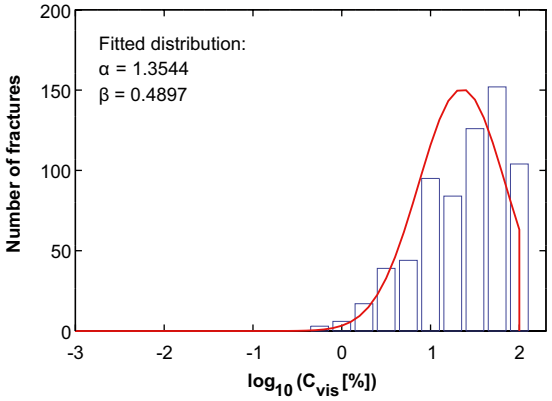


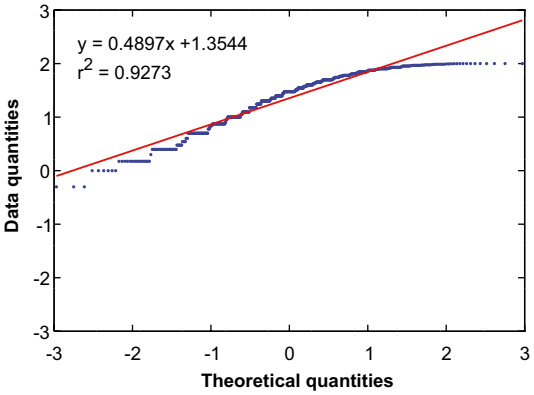


### B4.3 Clay minerals (All DZ)

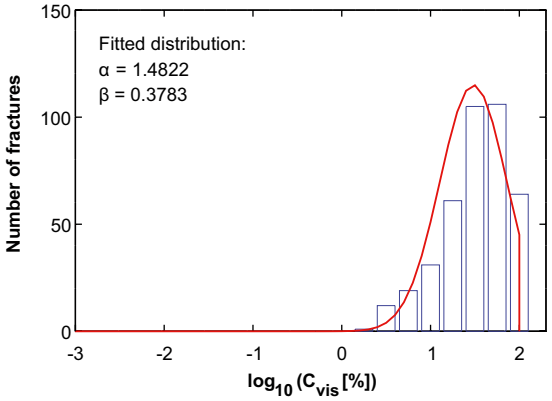


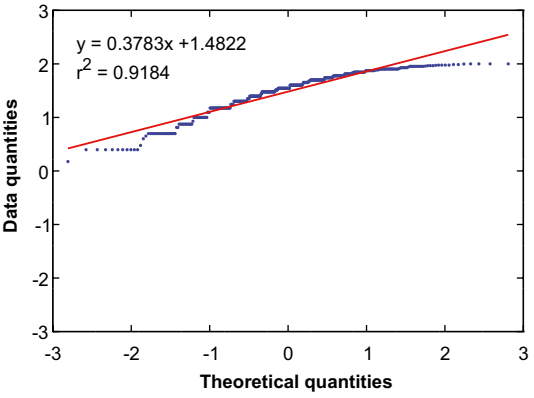

## B4.4 Hematite (All DZ)

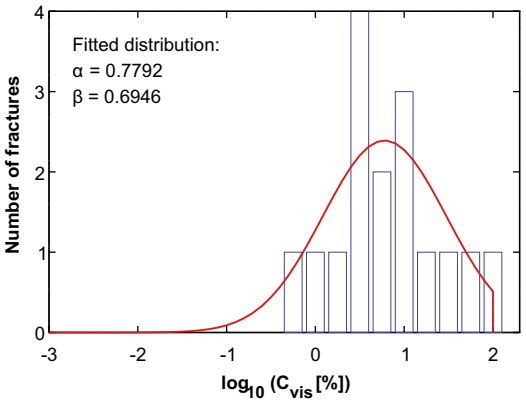


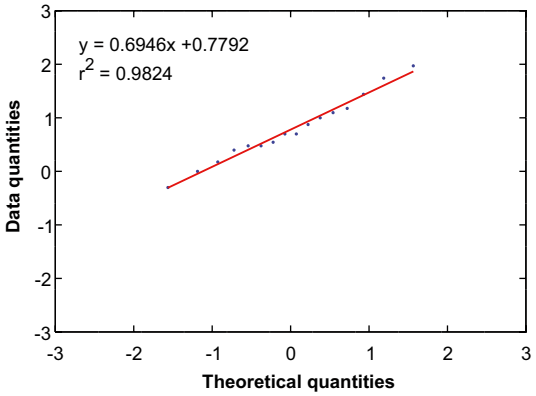


## B4.5 Pyrite (All DZ)

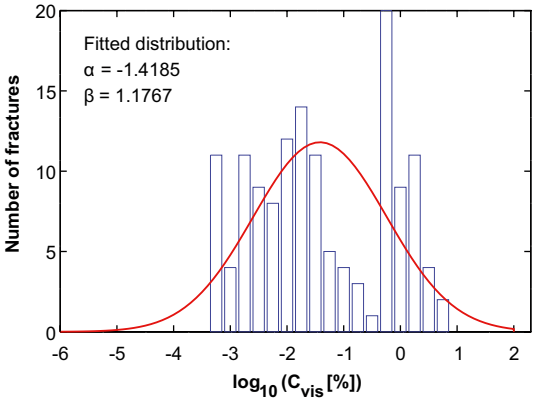


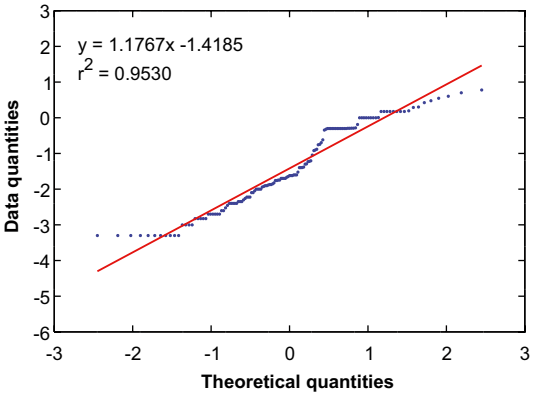

# Appendix C

## Information on data qualification

All data supplied as input to the SR-Site safety assessment modelling should be qualified, that is they should be both scientifically justifiable and quality assured. The data delivered in this report may be used as input to SR-Site and therefore, we have appended information in line with what is requested in an instruction of how data quantification should be performed, and what issues one should reflect upon in the process. This instruction is given in a SKB internal document associated with the SR-Site Data report /SKB 2010/. The structure of this section is according to the supplier part of this instruction.

### C1 Modelling in SR-Site

This Section is reserved for the customer of the data (i.e. the SR-Site safety assessment modelling team).

### C2 Experience from SR-Can

This Section is reserved for the customer of the data (i.e. the SR-Site safety assessment modelling team). What can be said is that in SR-Can, only some semi-quantitative information existed on amounts and coverages of fracture minerals /Drake et al. 2006/.

### C3 Supplier input on handling of data in SR-Site and SR-Can

We are not aware of the strategy for implementing these data in SR-Site modelling. Furthermore, we have no suggestions on how, or if, this should be done.

### C4 Sources of information and documentation of data qualification

All input data analysed in this report are produced within the Forsmark site investigation programme, and have been obtained in accordance with the SKB quality assurance system. The input data are presented in the site investigation report /Eklund and Mattsson 2009/.

The fracture mineral mapping has been performed according to the method description MD 143.009 and activity plan AP PF 400-07-056. The site investigation report, method description, and activity plan have been examined as part of the data qualification, and are found adequate.

Numerical data from the quantitative mineral mapping campaign have been taken from the database Sicada (Data Delivery ID: Sicada_09_062, Delivery Date: 2009-05-06). The delivery is a combination of the databases “GE054 mineral volume mapping” and “P_fract_core_eshi”.

Information on the geological structures (rock domain, fracture domain, and deformation zone) is included in the Sicada delivery. The exception is for boreholes KFM02B, KFM08D, and KFM011A. The rock volumes assumed to intersect these boreholes are listed in Appendix E. The main documents containing information on geological structures are /Stephens et al. 2007, 2008/.

The programs used for sorting data into different data subsets, making illustrations, and performing statistical analyses are:

- GNU Octave version 3.0.0. John W. Eaton. Department of Chemical Engineering. University of Wisconsin, USA.
- Analyse-it version 2.12. Analyse-it Software LTD.

All data obtained in the site investigations are judged to be qualified. According to the data qualification instruction, a number of issues should be reflected and commented upon. This is done in Table C-1.

**Table C-1 Issues to be reflected upon in data qualification.**

| | Question in data qualification instruction | Answer |
|---|---|---|
| Issues concerning input data | Is the acquirement of observed data, for example in the site investigation, performed in agreement with a widespread quality management system (e.g. the ISO 9000 series or equivalent)? | Yes |
| | Is it possible to trace relevant quality management documents (for example method descriptions, field notes, etc.) for the measurements? | Yes. Activity plan and method description have been examined. Questions have been dealt with through personal communication with the authors of the site investigation report. |
| | Is it possible to extract relevant information on the data quality, variability, and representativity from documents reporting the acquirement of data? | Yes. Available information in the site investigation report, activity plan, and method description has been examined. Information from calibrations given in the site investigation report has been examined. |
| | Are concerns associated with the observed data and nonconformities of the measurements transparently described? | Yes, This is done in the site investigation report. The nonconformities reported concern in many cases parts of the drill core where mapping could not be performed, as samples from the drill core had been taken to the laboratory, as part of other campaigns. However, the combined length of drill core sections that could not be mapped is small in comparison to that which could be mapped. Nonconformities arising from missing core pieces and sections are listed in Appendix 2 in /Eklund and Mattson 2009/.<br>In addition, calibration of the fracture mineral thickness was excluded from the Forsmark campaign (but included in a similar campaign in Laxemar). |
| | Is the performed data acquirement programme sufficient to catch data uncertainty and natural variability and do the acquired data represent that which was intended (site, rock domain, copper canister, population, etc.)? | Yes. These issues are discussed in this present report. |
| Issues concerning data refinement | Are concerns and nonconformities described in the supporting documents (for example site investigation reports) propagated to, and handled in, the data refinement? | Yes. Such concerns and nonconformities have been examined and are part of the input to this analysis. Questions have been dealt with through personal communication with the authors of the site investigation report. |
| | In refining observed data by use of more or less complex modelling, is this done in accordance with documented methods? | Refinement of data has been performed by elementary arithmetic operations. The statistical methods used in the analysis are well-defined standard methods. |
| | In case of more complex modelling, which may have implication for data qualification, is the details of the modelling described in a task description or in the document reporting the modelling results? | No complex modelling is used in the data refinement. |
| | Has comparative/alternative modelling been performed to evaluate artefacts induced in the modelling, and to evaluate whether the refined data are reasonable? | No alternative modelling has been performed, as no complex modelling is used in data refinement. |

## C5 Conditions for which data are supplied

No external conditions, such as temperature, should affect the observed data. However, there is a risk that some of the fracture minerals have been mechanically removed from the facture surface in the drilling and sample preparation. Furthermore, fracture minerals may have been affected by wear in previous drill core mapping, where they may also have been exposed to diluted HCl solution. Also de-stressing, general weathering and oxidation are conceivable sources of alteration.

## C6 Conceptual uncertainty

When selecting drill core sections that should be mapped, the locations of flow anomalies have been used. As a flow anomaly has not been associated with a specific fracture, it has been assumed that all fractures in a section surrounding the flow anomaly should represent the flow path. This assumption is conceptually uncertain.

Even if a fracture may allow water flow, channelling is postulated to occur and there is no way of knowing if the fracture surface mapped has been exposed to flowing water. This is valid even if one, by some means, has the ability to conclude that the fracture plane conducts water, and also has been conducting water prior to the drilling of the borehole. This evokes conceptual uncertainty.

The quantitative mapping of the amount of fracture minerals is carried out on a surface with a diameter of approximately 5 cm. This surface is then set to represent the entire fracture plane which surface area is unknown. This introduces a major uncertainty.

In the fracture mapping, it is assumed that the coverage and thickness of a fracture mineral that is over layered by another fracture mineral can be estimated, without removing the covering layer. It is uncertain to what extent this is true.

The distributions presented in this report, and their associated shapes, are not based on process understanding of the occurrence of fracture minerals, but should be seen as empirical.

Only a fraction of all fractures in the potential repository host rock has been investigated. Some uncertainty still remains concerning to what extent the obtained results can be extrapolated to other parts of the repository host rock.

## C7 Data uncertainty due to precision, bias, and representativity

In this Section the precision, bias, and representativity of the data are discussed. In the data qualification instruction it is requested to put numerical values on the data uncertainty, to the extent possible.

The data uncertainty introduced by the analysis made in this report is judged to be small in comparison to data uncertainty introduced when selecting the fractures and estimating the parameters during the mapping.

In the quantitative mineral mapping campaign, the data uncertainty of the estimated visible coverage and layer mineral thickness was investigated by performing calibrations. Concerning the visible coverage, the calibration was made on 16 samples prior to the campaign. Firstly the visible coverage was estimated by standard mapping methods, and thereafter the fracture surface was photographed and subsequent image analysis was performed. Figure C-1 displays the result from the calibration, indicating precision and bias errors of a few percents only.

No calibration was made for the total coverage. It is subjectively estimated that the error may be a factor of few larger for the total coverage than for the visible coverage.

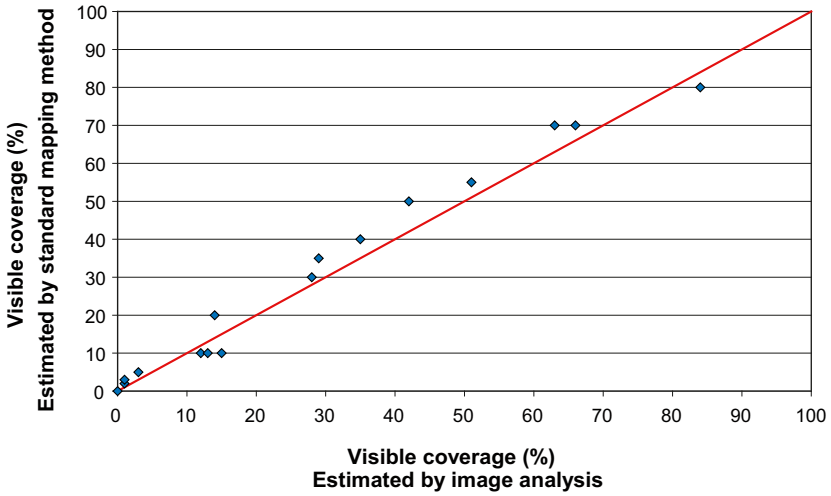


***Figure C-1.*** *Results from calibration of visible coverage. Data from Appendix 3 in /Eklund and Mattsson 2009/.*

For the layer mineral thickness, no calibration was performed in the Forsmark campaign. However, such a calibration was performed in a similar campaign in Laxemar using the same methodology /Eklund and Mattsson 2008/. As the same team of operators performed the fracture mineral mapping in Laxemar and Forsmark, and as the geological settings of the two sites are similar, it is assumed that the calibration results can be used to estimate the data uncertainty in the Forsmark campaign. In Laxemar, reasonably successful calibrations were made on eight samples. First the layer mineral thickness was estimated by standard mapping methods. Thereafter, the sample was sawed into two pieces, along the axis of the cylindrical drill core. The cuts were photographed and image analysis was performed. Figure C-2 shows the results from the calibration.

From the calibration, one can suggest precision errors of around 0.1 mm or less. However, the layer mineral thickness of both the drill core edge and the saw cut may be biased as fracture minerals may have been mechanically removed by the drilling and sawing. Concerning $d_{mean}$ and $C_{vis}$ the precision should not significantly affect the mean value of the distribution but only the data spread. By examining the results in Chapters 3 and 4, generally the natural variability is the key contributor to the spread, why the achieved precision is judged as sufficient.

As discussed in Section 2.4.4 of this present report, the rounding in the mapping makes the results biased towards certain favoured data values. According to the method description (MD 143.009), the layer thickness is estimated in 0.1 mm steps, while coverages should be estimated as 1, 2, 3, 5, 7, 10, 15, 20, 25, 30, 40, 50, 60, 70, 80, 90, or 100%. Concerning $\log_{10}(d_{mean})$, as seen in the normal score plot in for example Figure 2-8, this does affect the slope and intercept of linear fitting, from where $\mu$ and $\sigma$ of the normal distribution are acquired. The same holds true for $\log_{10}(C_{vis})$ and the $\alpha$ and $\beta$ parameters of Equation 2-2. However, the effect is not major. It is subjectively estimated that the mean value should not be shifted by more than a factor (in many cases much less). Also there may be a bias towards lower fracture mineral amounts and coverages, due to mechanical wear and alteration in the drilling and in subsequent handling and storage of the drill core. This bias is difficult to estimate but is probably not more than a factor or so.

The representativity discussion is divided in two issues. Firstly, the mapped fractures may or may not have conducted water prior to the excavation. This complicates the matter of assigning data for subsequent use in modelling where flow paths are of concern. It is difficult to estimate the error this evokes but it appears that the presence of fracture minerals is unrelated to the present groundwater flow rate (see Section 3.7). It is recognised that the above reasoning is somewhat circular. Secondly, the limited set of open fractures mapped may not represent the entire rock volume of interest for a potential repository. However, the results of this report indicate that open fractures located in one part of the rock are populated by fracture minerals in a similar fashion as open fractures of another part of the rock.

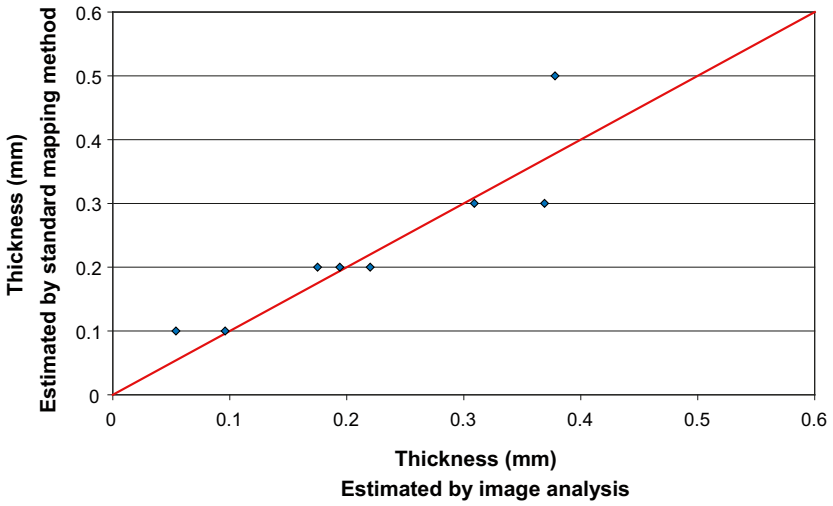


***Figure C-2.*** *Results from calibration of layer mineral thickness. Data from Appendix 4 in /Eklund and Mattsson 2008/.*

All in all it is judged that the delivered $d_{mean}$ and $C_{vis}$ results are off by less than an order of magnitude but perhaps by as much as a factor of few. It is acknowledged that these estimates are subjective. More precise estimates of the uncertainty would be difficult to defend.

## C8 Spatial and temporal variability

In Chapters 3 and 4, the spatial variability of $d_{mean}$ and $C_{vis}$ is investigated for different rock volumes. The averaged fracture mineral thickness and coverages do have a temporal variability over geological time periods, but it is assumed that during the time frame of consequence for repository safety, this variability is insignificant.

## C9 Correlations

In this work, parameters from the site investigation report have been combined by elementary arithmetic operation (see Section 2.2). Otherwise, no correlation has been used.

## C10 Results of supplier's data qualification

Results and recommended data for the Forsmark site concerning the averaged fracture mineral thickness and visible coverage are supplied in Chapter 5 of this report (Table 5-1 and Table 5-2), as suggested for use in subsequent modelling.

# Appendix D

## Quantitative mapping of fracture minerals in Forsmark.

### Basis for selecting drill core sections

### Abstract

It has previously been proposed in a justification document[3] to investigate the quantitative abundance of fracture minerals in open fractures by way of drill core mapping. Drill core sections associated with hydrogeological flow anomalies, detected by the Posiva Flow Log (PFL), as well as drill core sections distant from such anomalies are suggested to be mapped.

The main part of the campaign is devoted to mapping drill core sections associated with in total 401 PFL-anomalies. Such a drill core section is in this document called a PFL-section and comprises the rock surrounding the anomaly 1 m at each side.

Out of the 401 PFL-sections that should be mapped, 323 anomalies are found within the area of interest for repository layout studies, the so-called Forsmark target area. 78 anomalies that should be investigated for comparison are found in the peripheral area. In Table D-1, the numbers of PFL-sections to be mapped in different elevation ranges are shown. Also the numbers for PFL-anomalies in different transmissivity ranges are shown.

In the justification document, it is proposed to also map some drill core distant to the nearest PFL-anomaly. Here it is suggested to map in total 60 m of such drill core from the boreholes KFM01D, KFM03A, KFM06A, and KFM08D.

Furthermore, which is not suggested in the justification document, an extra effort must be made to map shallow drill cores. In Forsmark there is no shallow borehole where both the drill core exists and PFL-logging in the borehole has been performed. Therefore, even if there is no way of knowing whether the borehole has a PFL-section or not, shallow drill cores must be mapped. Here it is suggested to map in total 104 m of such shallow drill core from the boreholes KFM01C, KFM03B, KFM06B, and KFM08B.

**Table D-1. Summary of PFL-anomalies of interest for the campaign.**

| Borehole | $E >$ –100 masl | –100 ≥ $E \geq$ –400 masl | –400 > $E \geq$ –600 masl | $E <$ –600 masl | $T <$ $10^{-8}$ m²/s | $10^{-8} \leq T \leq 10^{-6}$ m²/s | $T >$ $10^{-6}$ m²/s |
|---|---|---|---|---|---|---|---|
| KFM01A | – | – | – | – | – | – | – |
| KFM01D | 7 | 26 | 1 | – | 13 | 19 | 2 |
| KFM02A | – | – | 49 | 1 | 23 | 26 | 1 |
| KFM02B | 5 | 14 | 22 | – | 2 | 25 | 14 |
| KFM03A | – | 12 | 10 | 11 | 11 | 19 | 3 |
| KFM04A | 10 | 11 | 1 | 1 | 7 | 10 | 6 |
| KFM05A | 12 | 13 | – | 2 | 10 | 13 | 4 |
| KFM06A | – | 21 | 1 | 5 | 16 | 10 | 1 |
| KFM07A[1] | – | – | – | 3 | – | – | – |
| KFM07C | 1 | 14 | – | – | 6 | 7 | 2 |
| KFM08A | – | – | 3 | – | 1 | 1 | 1 |
| KFM08C | – | – | 9 | – | 7 | 2 | – |
| KFM08D[2] | 11 | 17 | 5 | 2 | 15 | 17 | 2 |
| KFM10A | 32 | 24 | – | – | 14 | 27 | 15 |
| KFM11A | 21 | 21 | 3 | – | 16 | 24 | 5 |
| **Total** | **99** | **173** | **104** | **25** | **141** | **200** | **56** |

[1] No transmissivity obtained for the three selected anomalies.

[2] No transmissivity obtained for one selected anomalies.

[3] Internal document “Forsmark kompletterande undersökningar. Statistisk och kvantitativ kartering av sprickmineral”.

The suggested campaign in Forsmark has as an objective to be comparable to a similar campaign in Oskarshamn, in terms of total length of mapped drill core. The suggested length of drill core to be mapped is 767 m.

In the planning of this campaign, the above mentioned justification document has been used as a general guideline, rather than as a controlling document.

## D1 Introduction

### The Forsmark site, drill sites and core drilled boreholes

Figure D-1 shows the Forsmark candidate area as marked by the red border, drill sites, and the core-drilled boreholes. Detailed maps of each drill site are shown in Figure D-2.

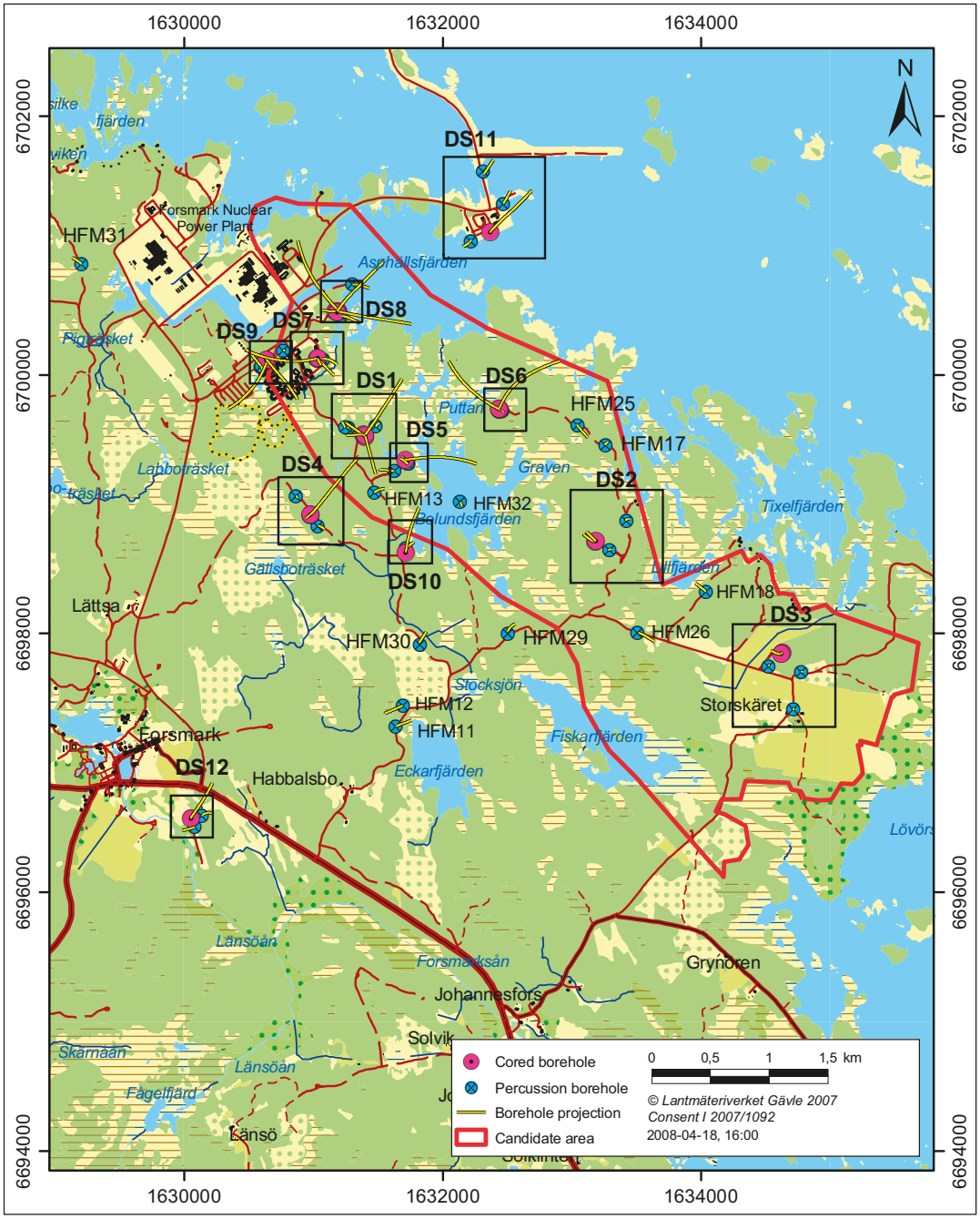


***Figure D-1.*** *Map of the Forsmark site indicating the candidate area and the drill sites. Detailed maps of each drill site is given in Figure D-2. The Figure is adopted from /SKB 2008/.*

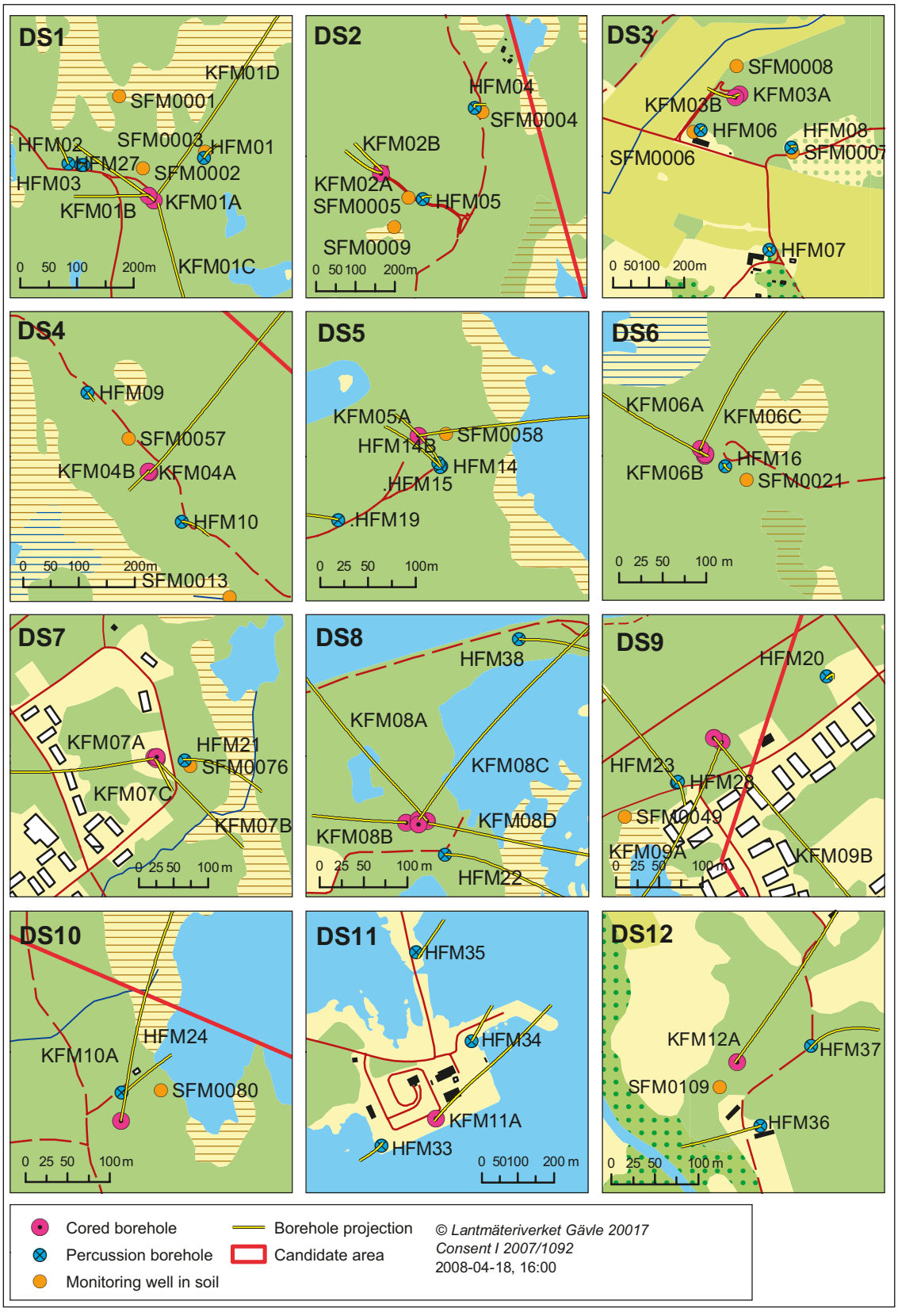


***Figure D-2.*** *Detailed maps of each drill site that show the location and projection of core- and percussion-drilled boreholes. An overview map is shown in Figure D-1. The Figure is adopted from /SKB 2008/.*

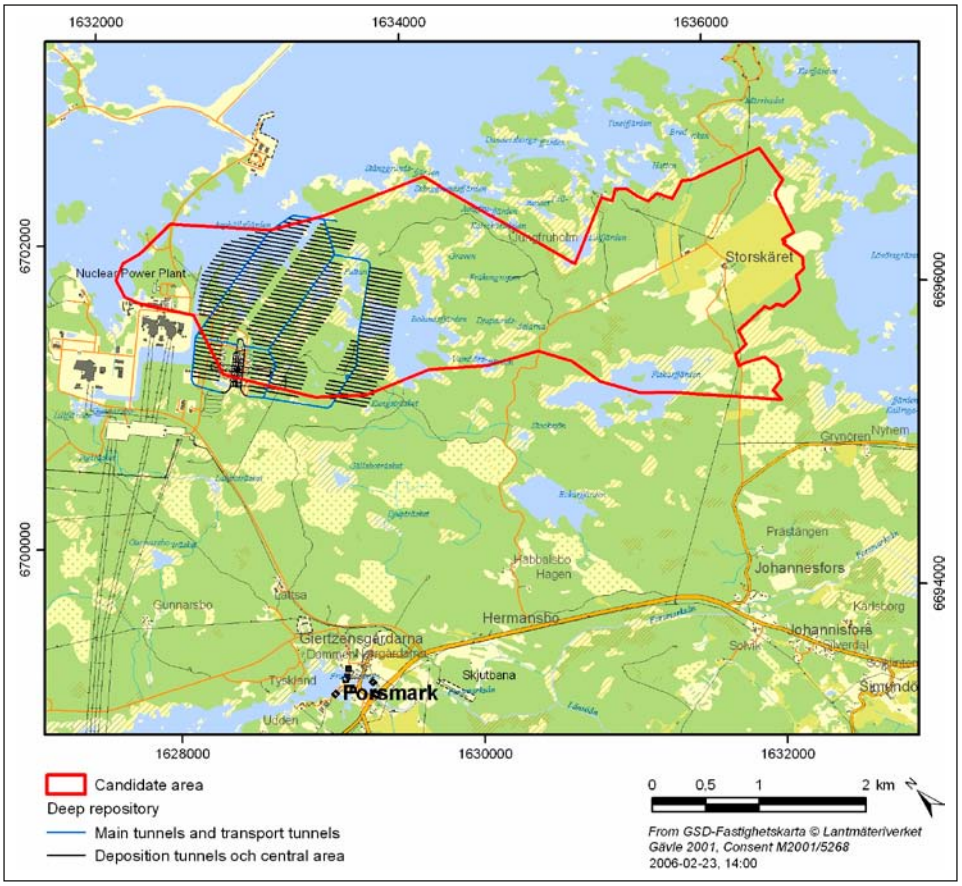


***Figure D-3.*** *Base case of the D1 repository design study. Figure adopted from /Brantberger et al. 2006/.*

Figure D-3 shows the base case of the D1 repository design study /Brantberger et al. 2006/.

As can be seen from Figures D-1 and D-3, most boreholes are of direct importance for characterizing the target area. The boreholes are named based on from which drill site (DS) they are drilled. In total there are 12 drill sites at Forsmark. The following drill sites are located within or in the direct vicinity of the target area: DS1, DS2, DS4, DS5, DS6, DS7, DS8, DS9, and DS10. The following drill sites can be seen as peripheral: DS3, DS11 and DS12.

## D2 Some definitions and clarifications

### Approximate elevation

In this document, the approximate elevation is approximated from the borehole length, elevation at the surface, and inclination at the surface. In reality the boreholes may be curved, making the approximated elevation somewhat overestimated or underestimated. This error is deemed acceptable for the purpose of this document. In reports handling the result of the campaign, exact coordinates should be used. In this document masl and mbsl are used as units of elevation, which are abbreviations for "metres above sea level" and "metres below sea level", respectively.

### PFL-anomalies and PFL-sections

The choice of boreholes and drill core sections to be investigated in this campaign is largely based on hydrogeologic measurements with the Posiva Flow Log (PFL). This tool can detect flow anomalies with a vertical resolution of 0.1 m. In this document, a 2 m long drill core section that is comprised of the rock surrounding a PFL-anomaly, one metre at each side, is called a PFL-section. Of course, if the spacing between two investigated PFL-anomalies is less than 2 m, the overlapping drill core is not logged twice and therefore the total length of drill core is less than the product of the number of investigated PFL-sections and 2 m.

Concerning PFL-anomalies, many of them are in the background reports marked as uncertain. As stated in the reports, e.g. /Pöllänen and Sokolnicki 2004/:

*"Some fracture-specific results were rated to be "uncertain"... The criterion of "uncertain" was in most cases a minor flow rate (< 30 mL/h). In some cases fracture anomalies were unclear, since the distance between them was less than one metre."*

However, for this present campaign, fractures of low hydraulic conductivity are of great importance and should therefore not be excluded. Furthermore, closely spaced anomalies are being handled by mapping the drill core including the closely spaced anomalies. Therefore, in this campaign no distinctions are made on beforehand between PFL-anomalies marked as uncertain or not in the background documents. In future work, however, it is recommended to investigate whether this decision affects the obtained data.

## D3 Detected PFL-anomalies at the site

PFL-loggings has presently been performed and reported in 15 boreholes within the Forsmark site investigation. These boreholes are located at 10 out of the 12 drill sites. Table D-1 shows the boreholes wherein PFL-logging has been performed.

As is seen in Table D-2, no loggings has presently been performed and reported at DS9 and DS12. In Table D-2 the references to the PFL-logging background reports (SKB Site Investigation Reports) are also shown.

Figure D-4 shows the approximate elevation of the 769 PFL-anomalies detected at the Forsmark site. It should be noted that different boreholes penetrated down to different depths, and that the PFL-loggings may not have been performed over the entire length of the borehole. Especially the upper 100 m or so of the boreholes are generally not logged. Accounts for the exact ranges of the PFL-loggings can be found in the references shown in Table D-2.

As can be seen in Figure D-4 there is a wealth of PFL anomalies between the elevations 100 to 400 mbsl. However, below 400 mbsl the frequency of PFL anomalies decreases and below 500 mbsl, only 39 anomalies have been detected within Forsmark site investigation. Figure D-5 shows a histogram of number of PFL-anomalies detected per 100 m section (elevation) within the site investigation.

**Table D-2. Drill sites, boreholes and references to PFL-loggings.**

| Drill site | Borehole | PFL reference |
|---|---|---|
| DS1 | KFM01A | P-03-28 |
| | KFM01D | P-06-161 |
| DS2 | KFM02A | P-04-188 |
| | KFM02B | P-07-83 |
| DS3 | KFM03A | P-04-189 |
| DS4 | KFM04A | P-04-190 |
| DS5 | KFM05A | P-04-191 |
| DS6 | KFM06A | P-05-15 |
| DS7 | KFM07A | P-05-63 |
| | KFM07C | P-06-247 |
| DS8 | KFM08A | P-05-43 |
| | KFM08C | P-06-189 |
| | KFM08D | P-07-84 |
| DS9 | – | |
| DS10 | KFM10A | P-06-190 |
| DS11 | KFM11A | P-07-85 |
| DS12 | – | |

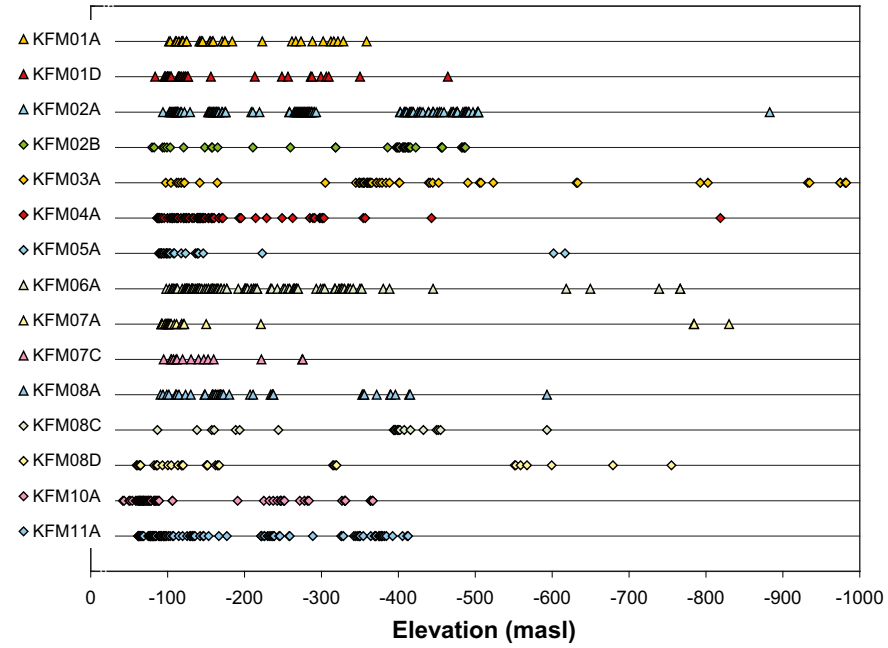


***Figure D-4.*** *Approximate elevation of all PFL-anomalies detected at the Forsmark site.*

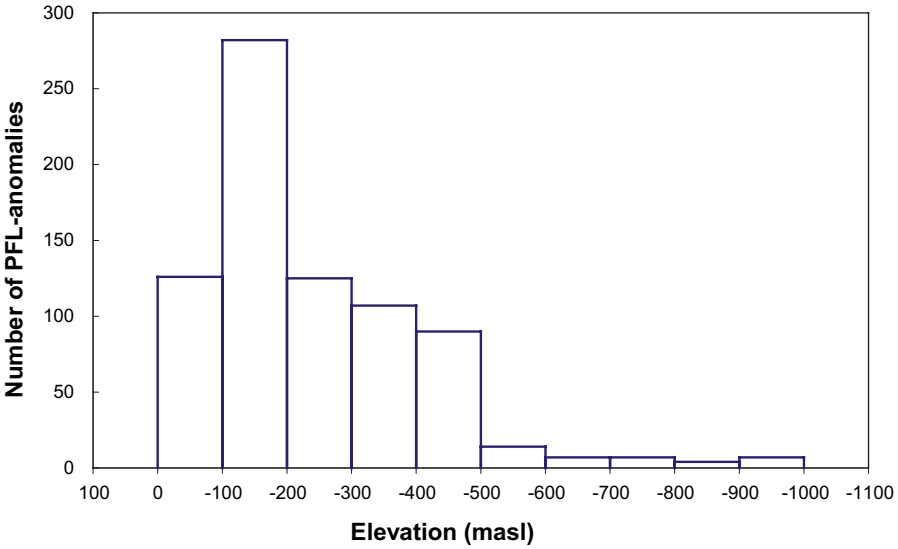


***Figure D-5.*** *Histogram of number of PFL-anomalies detected per 100 m section in Forsmark*

In the next few sections, the reasons for choosing PFL-sections for drill core mapping are accounted for. The selection can be seen as a means of reducing the length of the drill core to be mapped. The aim is to reduce the 769-anomalies detected in PLU to the around 400 PFL-anomalies that are to be investigated according to the justification document.

## D4 Expected nonconformities

It this work, it has not been checked whether the PFL-sections suggested suffer from drill core loss or loss of BIPS image. It is likely that some do and in that case the PFL-section may have to be excluded from the list given in this document. However, it is judged that the loss of mapped PFL-section will be small in the context of the entire campaign.

## D5 Horizontal spatial representativity in data selection

As around 400 PFL-anomalies should be targeted out of the 769 detected in the site investigation, data reduction is needed. Drill cores from all drill sites can be mapped, with the exception of DS9 and DS12 where no PFL-logging has been performed.

Concerning DS12, this is a peripheral drill site and need not to be investigated. Concerning DS9, it is quite closely situated to DS1, DS7, and DS8 and the exclusion of this drill site leaves no major gap in the coverage of the target area. It is considered sufficient in this campaign, concerning the spatial representativity, to obtain data from DS1, DS2, DS4, DS5, DS6, DS7, DS8, DS10, and DS11, but not necessarily from all boreholes of the drill sites.

As is accounted for in section D.7, the drill core from the following boreholes should be mapped regarding PFL-sections: KFM01D, KFM02A, KFM02B, KFM03A, KFM04A, KFM05A, KFM06A, KFM07A, KFM07C, KFM08A, KFM08C, KFM08D, KFM10A, and KFM11A. These boreholes are shown in Figure D-2.

Concerning drill site 2, there is a special request from the SKB RetNet group to investigate drill cores from both boreholes KFM02A and KFM02B, as a tracer tests have been performed between the boreholes.

Concerning drill core sections distant from the nearest PFL-anomaly and shallow drill core sections, boreholes from drill site DS1, DS3, DS6, and DS8 were chosen.

## D6 Vertical spatial representativity in data selection

According to the justification document, out of the 400 PFL anomalies that should be investigated, about 180 should be distributed between the elevations 300 and 600 mbsl, 200 should be distributed at elevations above 300 mbsl, and about 30 should be located below 600 mbsl.

In the following section the choice of PFL-sections to be mapped for each concerned borehole in Figure D-2 is accounted for. The degree of fracturing decreases below 400 mbsl, and therefore as a general approach, all anomalies below 400 mbsl were selected for the campaign. Furthermore, as there are few shallow anomalies detected, all anomalies above the elevation 85 mbsl were included in the campaign. Between 85 and 400 mbsl, there was significant data reduction that is accounted for in the section D.4. Figure D-6 shows the approximate elevation of the 401 anomalies that were finally chosen for the campaign.

In total 99 PFL-anomalies were chosen for the rock above 100 mbsl. Between 100 and 400 mbls, 173 anomalies were chosen and between 400 and 600 mbsl, 104 anomalies were chosen. Below 600 mbsl, 25 PFL-anomalies were chosen.

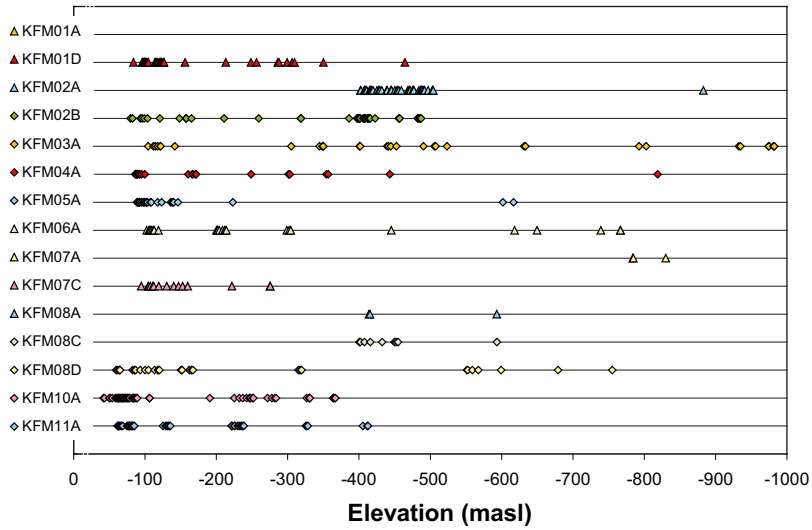


***Figure D-6.*** *PFL-anomalies chosen to be investigated in the campaign.*

## D7 Basis for selecting PFL anomalies in different boreholes

### Basis for reduction of data points

This campaign should investigate around 400 PFL anomalies and therefore, data reduction is required. To not reduce the possibility of studying the local variability between adjacent flow paths within a hydraulic conductor domain, it was decided that when necessary the borehole should be divided into sections, at least 20 m long, and that whole sections should be included or discarded. The choice of which sections should be included could either be made randomly of periodically. For this campaign the latter approach was used. For example, if dividing the borehole into 25 m long sections, included sections could be 100 – 125, 200 – 225, 300 – 325 mbsl, and so forth.

It has been suggested as a possibility to choose PFL anomalies based on their transmissivity. Therefore, three transmissivity subdivisions were assigned: low transmissivity ($T < 10^{-8}$ m$^2$/s), medium transmissivity ($10^{-8} \leq T \leq 10^{-6}$ m$^2$/s), and high transmissivity ($T > 10^{-6}$ m$^2$/s). However, it was argued that choosing PFL anomalies in order to equally divide them on the three subdivisions would likely induce a bias in the data selection. Therefore, it was finally decided against including the transmissivity as a basis for selecting PFL anomalies.

Based on a similar reasoning as for transmissivity, it was decided against basing the choice of PFL anomalies on the fracture orientation, rock type and fracture frequency of the host rock, etc.

If there are more than one borehole in a specific drill-site, and they have a similar distribution of PFL-anomalies, one of the boreholes were randomly chosen to represent that drill-site. However, no PFL anomalies below 400 metres are discarded.

#### KFM01A

In KFM01A, in total 34 PFL-anomalies were detected in the flow loggings /Rouhiainen and Pöllänen 2003/. It was decided not to include any PFL-sections from KFM01A. Instead KFM01D should represent the drill site.

#### KFM01D

In KFM01D, in total 34 PFL-anomalies were detected in the flow loggings /Väisäsvaara et al. 2006a/. All of these anomalies were selected as basis for assigning PFL-sections. The transmissivity and elevation of the anomalies are shown in Figure D-7.

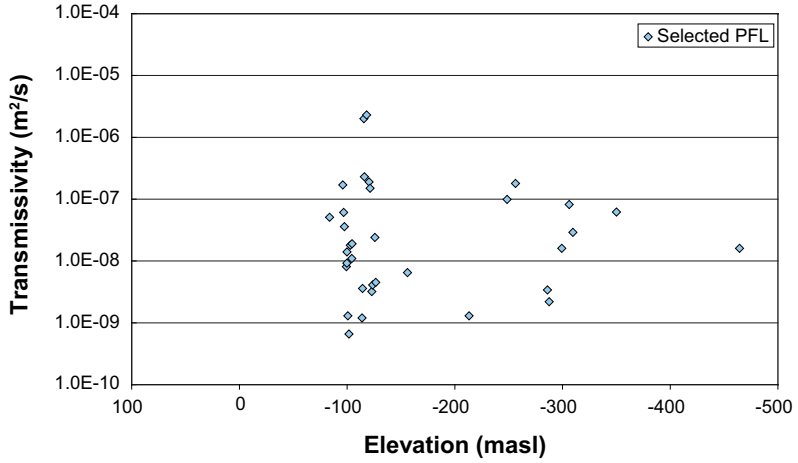


***Figure D-7.*** *Transmissivity of selected PFL-anomalies in KFM01D.*

### KFM02A

In borehole KFM02A, there is a special interest to map fractures between the borehole lengths 411–441 m, as this section was used for tracer injection in a tracer test between KFM02A and KFM02B /Lindquist et al. 2008/.

In accordance with the general approach of the campaign to include all PFL-anomalies detected below 400 mbsl at the site, this was done in KFM02A. PFL-anomalies above 400 mbsl were excluded from the campaign, as it was decided that KFM02B should represent drill site 2.

Out of the 125 PFL-anomalies detected in KFM02A /Rouhiainen and Pöllänen 2004a/, 50 were chosen as basis for assigning PFL-sections. The transmissivity and elevation of selected and discarded anomalies are shown in Figure D-8.

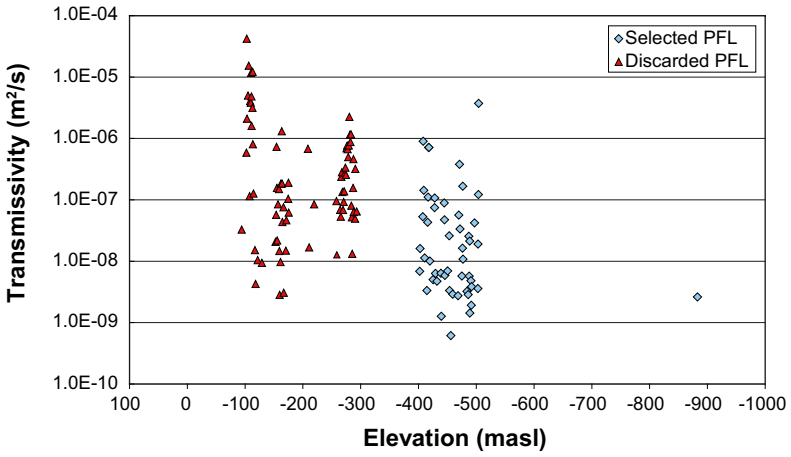


***Figure D-8.*** *Transmissivity of selected and discarded PFL-anomalies in KFM02A.*

### KFM02B

In borehole KFM02B, there is a special interest to map fractures between the borehole lengths 408.5–434 m, as this section was used for tracer withdrawal in a tracer test between KFM02A and KFM02B /Lindquist et al. 2008/.

All 41 PFL-anomalies detected in KFM02B /Väisäsvaara and Pöllänen 2007/ were selected as basis for assigning PFL-sections. Their transmissivity and elevation are shown in Figure D-9.

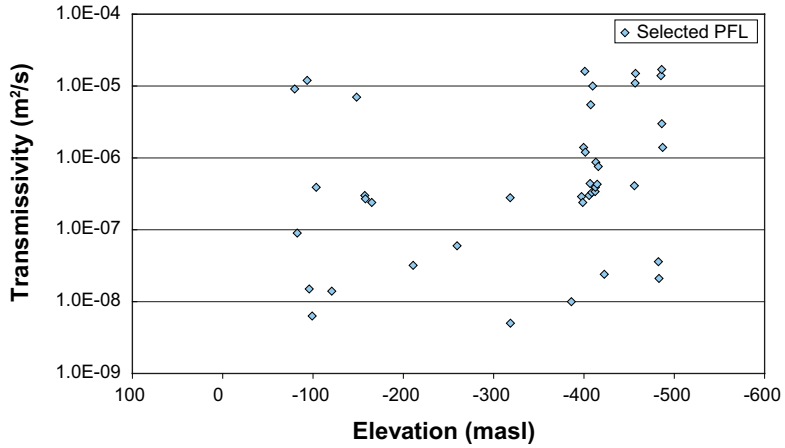


***Figure D-9.*** *Transmissivity of selected PFL-anomalies in KFM02B.*

### KFM03A

KFM03A is a peripheral borehole. In accordance with the general approach of the campaign to include all PFL-anomalies detected below 400 mbsl at the site, this was done in KFM03A.

Above 400 mbsl, the borehole was divided into 50 m sections based on elevation. The PFL-anomalies in every other section were selected as basis for assigning PFL-sections. Borehole sections between the elevations 100–150, 200–250, and 300–350 mbsl were included in the campaign.

33 out of the 52 PFL-anomalies detected in the flow logging /Pöllänen and Sokolnicki 2004/ were selected for the campaign. The transmissivity and elevation of selected and discarded anomalies are shown in Figure D-10.

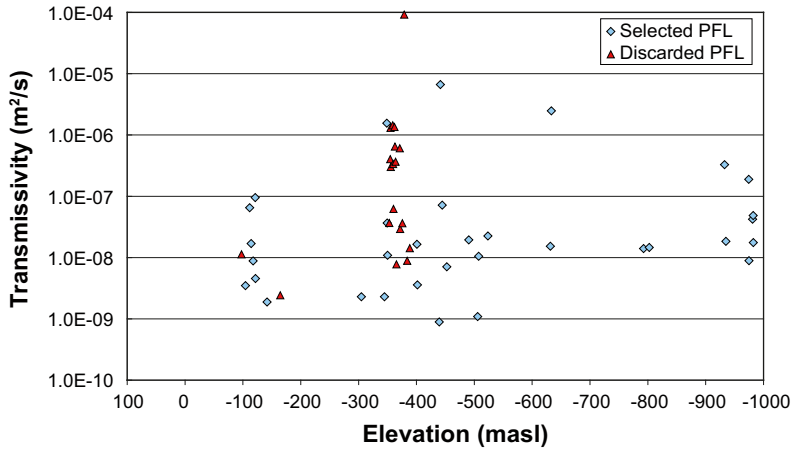


***Figure D-10.*** *Transmissivity of selected and discarded PFL-anomalies in KFM03A.*

### KFM04A

For KFM04A, it was decided to include all PFL anomalies below 300 mbsl. Between 80–300 mbsl, the borehole was divided into 20 m sections. PFL-anomalies in every fourth section were selected as basis for assigning PFL-sections. Borehole sections between the elevations 80–100, 160–180, and 240–260 mbsl were included in the campaign.

23 out of the 71 PFL-anomalies detected in the flow logging /Rouhiainen and Pöllänen 2004b/ were selected for the campaign. The transmissivity and elevation of selected and discarded anomalies are shown in Figure D-11.

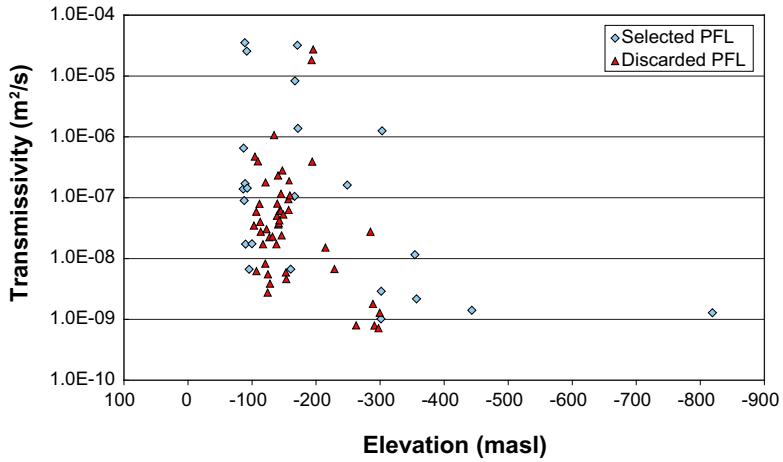


***Figure D-11.*** *Transmissivity of selected and discarded PFL-anomalies in KFM04A.*

### KFM05A

In KFM05A, in total 27 PFL-anomalies were detected in the flow loggings /Pöllänen et al. 2004/. All of these anomalies were selected as basis for assigning PFL-sections. The transmissivity and elevation of the anomalies are shown in Figure D-12.

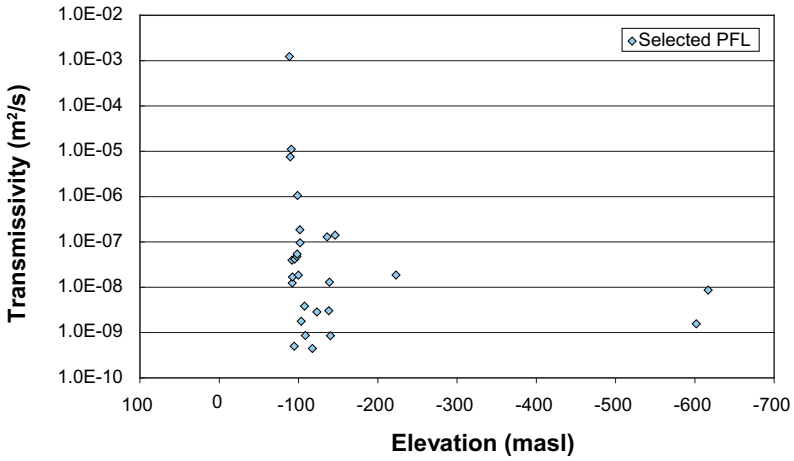


***Figure D-12.*** *Transmissivity of selected PFL-anomalies in KFM05A.*

### KFM06A

In accordance with the general approach of the campaign to include all PFL-anomalies detected below 400 mbsl at the site, this was done in KFM06A. Above 400 mbsl, the borehole was divided into 20 m sections. PFL-anomalies in every fifth section were selected as basis for assigning PFL-sections. Borehole sections between the elevations 100–120, 200–220, and 300–320 mbsl were included in the campaign.

27 out of the 99 PFL-anomalies detected in the flow logging /Rouhiainen and Sokolnicki 2005/ were selected for the campaign. The transmissivity and elevation of selected and discarded anomalies are shown in Figure D-13.

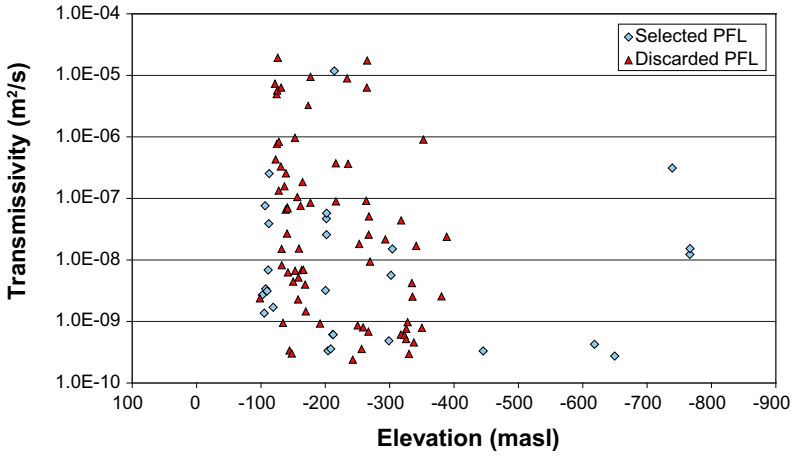


***Figure D-13.*** *Transmissivity of selected and discarded PFL-anomalies in KFM06A.*

### KFM07A

In accordance with the general approach of the campaign to include all PFL-anomalies detected below 400 mbsl at the site, this was done in KFM07A. Above 400 mbsl all PFL-anomalies were discarded as it was decided that KFM07C should represent the drill site.

3 out of the 26 PFL-anomalies detected in the flow logging /Sokolnicki and Rouhiainen 2005b/ were selected for the campaign. The transmissivity and elevation of the discarded anomalies are shown in Figure D-14. The elevation of the selected anomalies is shown in Figure D-14 by blue lines as no transmissivities were obtained for these anomalies in /Sokolnicki and Rouhiainen 2005b/.

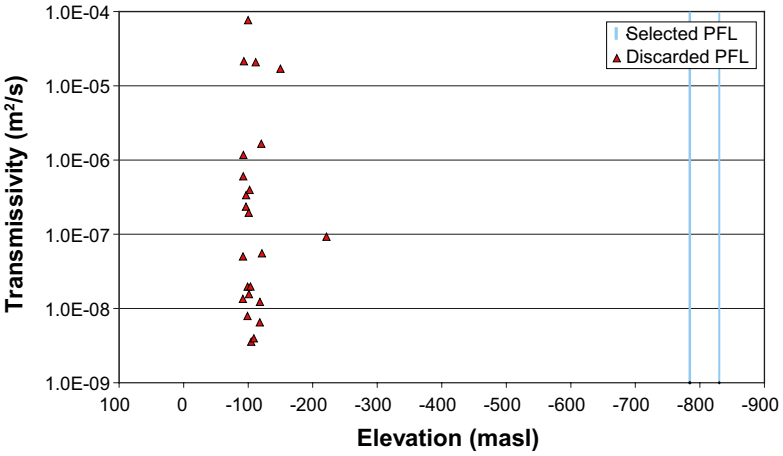


***Figure D-14.*** *Transmissivity and/or elevation of selected and discarded PFL-anomalies in KFM07A.*

### KFM07C

In KFM07C, in total 15 PFL-anomalies were detected in the flow loggings /Väisäsvaara et al. 2006b/. All of these anomalies were selected as basis for assigning PFL-sections. The transmissivity and elevation of the anomalies are shown in Figure D-15.

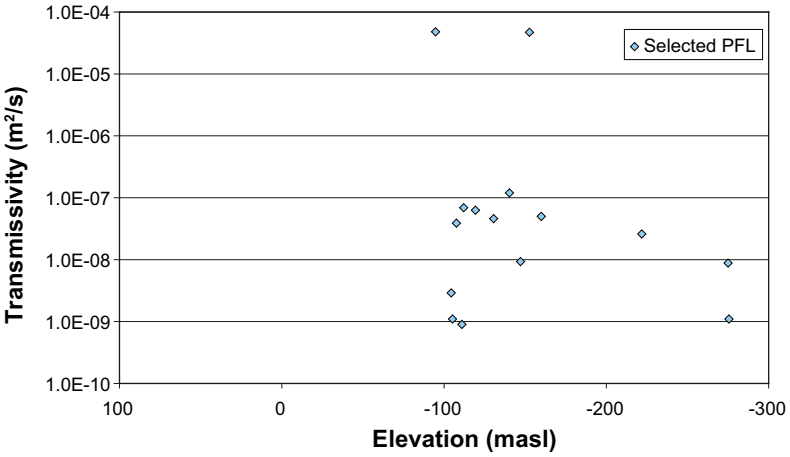


***Figure D-15.*** *Transmissivity of selected PFL-anomalies in KFM07C.*

### KFM08A

In accordance with the general approach of the campaign to include all PFL-anomalies detected below 400 mbsl at the site, this was done in KFM08A. Above 400 mbsl all PFL-anomalies were discarded as it was decided that KFM08D should represent the drill site.

3 out of the 41 PFL-anomalies detected in the flow logging /Sokolnicki and Rouhiainen 2005a/ were selected for the campaign. The transmissivity and elevation of the selected and discarded anomalies are shown in Figure D-16.

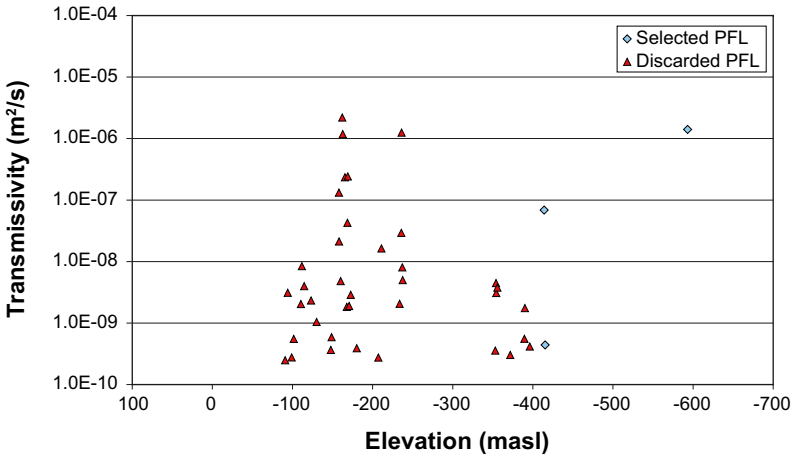


***Figure D-16.*** *Transmissivity of selected and discarded PFL-anomalies in KFM08A.*

### KFM08C

In accordance with the general approach of the campaign to include all PFL-anomalies detected below 400 mbsl at the site, this was done in KFM08C. Above 400 mbsl all PFL-anomalies were discarded as it was decided that KFM08D should represent the drill site.

9 out of the 21 PFL-anomalies detected in the flow logging /Sokolnicki and Rouhiainen 2005a/ were selected for the campaign. The transmissivity and elevation of the selected and discarded anomalies are shown in Figure D-17.

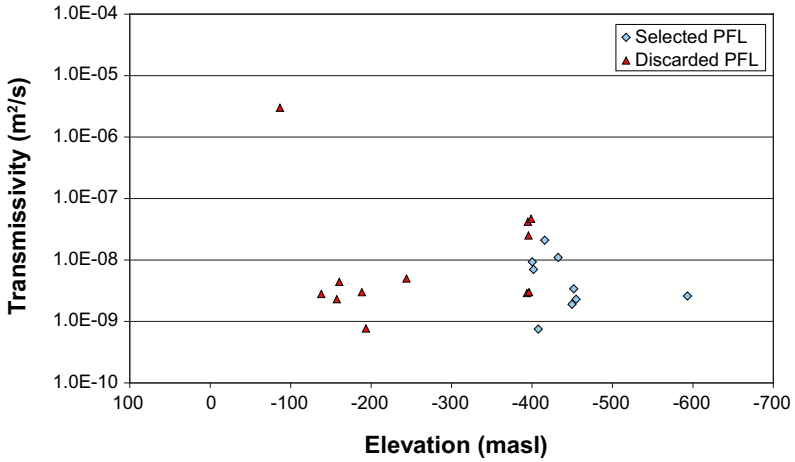


***Figure D-17.*** *Transmissivity of selected and discarded PFL-anomalies in KFM08C.*

### KFM08D

In KFM08D, in total 15 PFL-anomalies were detected in the flow loggings /Väisäsvaara et al. 2006b/. All of these anomalies were selected as basis for assigning PFL-sections. The transmissivity and elevation of the anomalies are shown in Figure D-18. For the PFL-anomaly at 755 mbsl, no transmissivity was obtained in /Väisäsvaara et al. 2006b/ and thus the anomaly is marked by a blue line in Figure D-18.

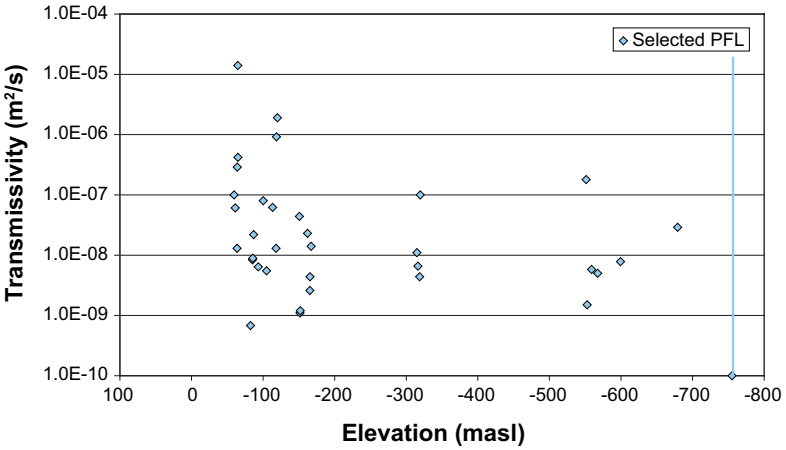


***Figure D-18.*** *Transmissivity and/or elevation of selected PFL-anomalies in KFM08D.*

### KFM10A

In KFM10A, in total 56 PFL-anomalies were detected in the flow loggings /Sokolnicki et al. 2006/. All of these anomalies were selected as basis for assigning PFL-sections. A reason for selecting so many anomalies from this borehole is that the shallowest PFL-anomalies at the site were obtained here. The transmissivity and elevation of the anomalies are shown in Figure D-19.

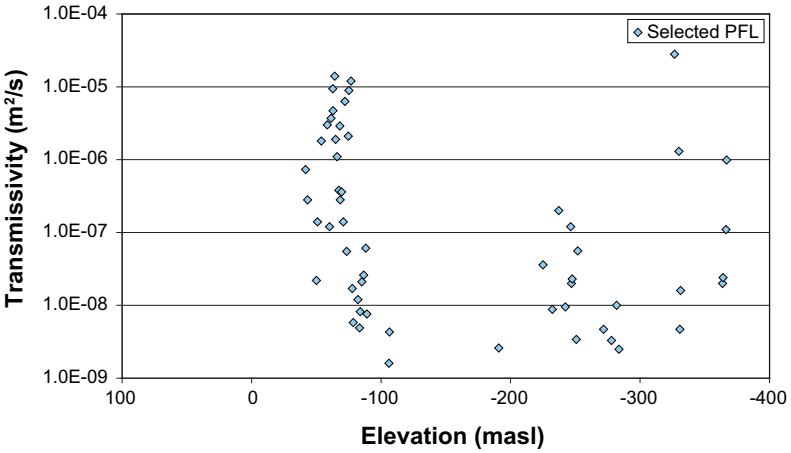


***Figure D-19.*** *Transmissivity of selected and discarded PFL-anomalies in KFM10A.*

### KFM11A

KFM11A is a peripheral borehole. In accordance with the general approach of the campaign to include all PFL-anomalies detected above 85 mbsl and below 400 mbsl at the site, this was done in KFM11A.

Below 100 m, the borehole was divided into 20 m sections. The PFL-anomalies in every fifth section were selected as basis for assigning PFL-sections. Borehole sections between the elevations 120–140, 220–240, and 320–340 mbsl were included in the campaign.

45 out of the 92 PFL-anomalies detected in the flow logging /Väisäsvaara and Pekkanen 2007/ were selected for the campaign. The transmissivity and elevation of selected and discarded anomalies are shown in Figure D-20.

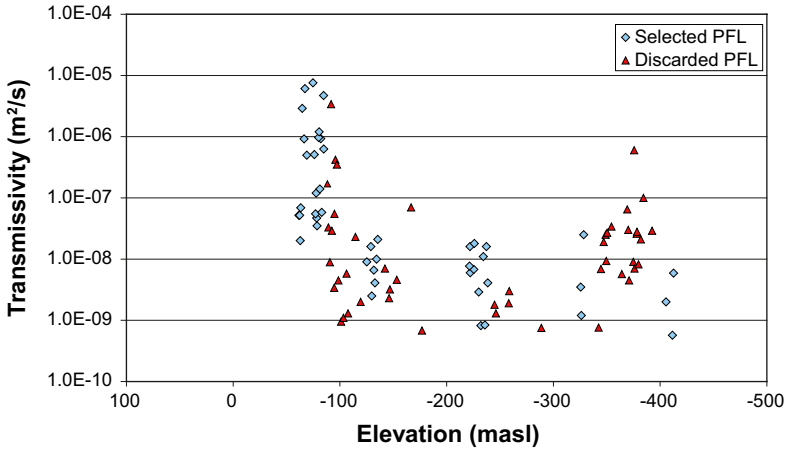


***Figure D-20.*** *Transmissivity of selected and discarded PFL-anomalies in KFM11A.*

## D8 Basis for selecting shallow sections and sections with no PFL-anomaly

According to the justification document, fracture minerals in drill core sections where no flow anomaly has been detected should also be mapped. Such drill core sections should have the distance to the nearest PFL-anomaly of at least 5 m. In the justification document it was suggested that 50 m of such drill core sections should be mapped. Here it is suggested to extend this drill core length to 60 m below the elevation 100 m.

As no PFL logging has been performed in the upper 50 or 60 m at the Forsmark site, an extra effort, not suggested in the justification document, is needed in this campaign. It is suggested to map 104 m of drill core from above 60 mbsl. In this shallow part of the rock, no PFL-measurements have been performed and reported and therefore, it is unknown to what extent fractures to be mapped are associated with flowing structures.

Based on the suggested location of the repository (see Figure D-3), it was decided to focus on boreholes from drill sites DS1, DS6, and DS8. In addition the peripheral drill site DS3 was chosen.

### Selection of shallow drill core sections

For the mapping of shallow drill core, the boreholes KFM01C, KFM03B, KFM06B, and KFM08B were chosen. The reason for this choice was simply that these boreholes are core drilled also at shallow depths, as opposed to many other boreholes from which no shallow drill core exists.

At first, it was decided that each drill core section should have the borehole length 5 m. The scheme shown in Table D-3 was used for the selection of drill core sections, where the elevation of the upper location for each section (secup) is shown.

**Table D-3. Scheme used in selecting shallow drill core sections (Secup is given).**

| Borehole | KFM03B | KFM06B | KFM08B | KFM01C |
|---|---|---|---|---|
| Elevation (mbsl) | 0 | 5 | 10 | 15 |
| | 20 | 25 | 30 | 35 |
| | 40 | 45 | 50 | 55 |

However, requests were made to map one shallow borehole continuously down to the elevation of about 60 mbsl. Therefore, it is suggested to make such an effort even if not described in the justification document. Borehole KFM06B was chosen for this extra investigation.

The secup and seclow elevation for each section was approximated as described in Section D.2 of this document. The borehole lengths that should be mapped are accounted for in Table D-4.

**Table D-4. Shallow borehole sections to be mapped.**

| Borehole | KFM03B | KFM06B | KFM08B | KFM01C |
|---|---|---|---|---|
| Borehole length (m) secup – seclow | 8.5–13.5 | 6–65 | 14.5–19.5 | 23.5–28.5 |
| | 28.5–33.5 | | 37.5–42.5 | 49.5–54.5 |
| | 48.5–53.5 | | 61–66 | 75.5–80.5 |

### Selection of sections distant to PFL-anomaly

For the mapping of drill core sections distant to the nearest PFL-anomaly, the boreholes KFM01D, KFM03A, KFM06A, and KFM08D were chosen.

It was decided that each section should have the borehole length 5 m. The scheme shown in Table D-5 was used for planning the selection of drill core sections, where the elevation of the upper location for each section (secup) is shown.

**Table D-5. Scheme used in selecting drill core sections with no PFL-anomaly.**

| Borehole | KFM08D | KFM06A | KFM03A | KFM01D |
|---|---|---|---|---|
| Elevation (mbsl) | 50 | 100 | 150 | 200 |
| Secup | 250 | 300 | 350 | 400 |
| | 450 | 500 | 550 | 600 |

The secup shown in Table D-5 needed to be modified in case there was a detected PFL-anomaly in the vicinity of the suggested location. Especially finding a suitable section in KFM06A at around 100 mbsl was unsuccessful. The suggested secup in elevation, as well as secup and seclow in borehole length, are shown for the 12 suggested sections in Table D-6. The elevation for each section was approximated as described in Section D.2 of this document.

**Table D-6. Borehole sections with no PFL-anomaly to be mapped.**

| Borehole | KFM08D | KFM06A | KFM03A | KFM01D |
|---|---|---|---|---|
| Approximate elevation (mbsl) | 69 | 222 | 147 | 200 |
| | 250 | 283 | 295 | 400 |
| | 450 | 500 | 550 | 600 |
| Borehole length (m) | 92.5–97.5 | 226–231 | 156–161 | 248–253 |
| | 308.5–313.5 | 287–292 | 304–309 | 492.5–497.5 |
| | 552.5–557.5 | 504–509 | 560.5–565.5 | 737–742 |

## D9 Lists of drill core sections to be mapped

All values are borehole length. Adjusted borehole length of the drill cores should be used.

**Table D-7: KFM01C – total drill core length 15 m.**

| Borehole | Adjusted Secup (m) | Adjusted Seclow (m) | Location of PFL-anomaly |
|---|---|---|---|
| KFM01C | 23.5 | 28.5 | No PFL-logging in section |
| KFM01C | 49.5 | 54.5 | No PFL-logging in section |
| KFM01C | 75.5 | 80.5 | No PFL-logging in section |

**Table D-8: KFM01D – total drill core length 67 m.**

| Borehole | Adjusted Secup (m) | Adjusted Seclow (m) | Location of PFL-anomaly |
|---|---|---|---|
| KFM01D | 105 | 107 | 106 |
| KFM01D | 119.9 | 123.7 | 120.9 |
| KFM01D | | | 121.9 |
| KFM01D | | | 122.7 |
| KFM01D | 124 | 132.4 | 125 |
| KFM01D | | | 125.5 |
| KFM01D | | | 125.7 |
| KFM01D | | | 126.7 |
| KFM01D | | | 128 |
| KFM01D | | | 129.5 |
| KFM01D | | | 131.2 |
| KFM01D | | | 131.4 |
| KFM01D | 141.8 | 146.5 | 142.8 |
| KFM01D | | | 143.4 |
| KFM01D | | | 144.9 |
| KFM01D | | | 145.5 |
| KFM01D | 147 | 149 | 148 |
| KFM01D | 149.8 | 155.9 | 150.8 |
| KFM01D | | | 151.9 |
| KFM01D | | | 153.9 |
| KFM01D | | | 154.9 |
| KFM01D | 156.4 | 159.4 | 157.4 |
| KFM01D | | | 158.4 |
| KFM01D | 193.4 | 195.4 | 194.4 |
| KFM01D | 248 | 253 | No PFL-anomaly |
| KFM01D | 263.3 | 265.3 | 264.3 |
| KFM01D | 306.4 | 308.4 | 307.4 |
| KFM01D | 315.9 | 317.9 | 316.9 |
| KFM01D | 352.2 | 356.2 | 353.2 |
| KFM01D | | | 355.2 |
| KFM01D | 368.5 | 370.5 | 369.5 |
| KFM01D | 376.9 | 378.9 | 377.9 |
| KFM01D | 381 | 383 | 382 |
| KFM01D | 430.5 | 432.5 | 431.5 |
| KFM01D | 492.5 | 497.5 | No PFL-anomaly |
| KFM01D | 570.2 | 572.2 | 571.2 |
| KFM01D | 732 | 737 | No PFL-anomaly |

**Table D-9: KFM02A – total drill core length 63.4 m.**

| Borehole | Adjusted Secup (m) | Adjusted Seclow (m) | Location of PFL-anomaly |
|---|---|---|---|
| KFM02A | 410.2 | 412.8 | 411.2 |
| KFM02A | | | 411.8 |
| KFM02A | 415.5 | 420.9 | 416.5 |
| KFM02A | | | 417.3 |
| KFM02A | | | 418.4 |
| KFM02A | | | 419.9 |
| KFM02A | 422.7 | 429.9 | 423.7 |
| KFM02A | | | 425.1 |
| KFM02A | | | 425.9 |
| KFM02A | | | 426.8 |
| KFM02A | | | 427.2 |
| KFM02A | | | 428.9 |
| KFM02A | 433.4 | 435.4 | 434.4 |
| KFM02A | 436 | 439.5 | 437 |
| KFM02A | | | 437.3 |
| KFM02A | | | 438.5 |
| KFM02A | 440.2 | 442.2 | 441.2 |
| KFM02A | 447.1 | 449.8 | 448.1 |
| KFM02A | | | 448.8 |
| KFM02A | 453 | 455.9 | 454 |
| KFM02A | | | 454.4 |
| KFM02A | | | 454.9 |
| KFM02A | 458.7 | 460.7 | 459.7 |
| KFM02A | 461.5 | 464.2 | 462.5 |
| KFM02A | | | 463.2 |
| KFM02A | 464.3 | 466.3 | 465.3 |
| KFM02A | 467.6 | 469.6 | 468.6 |
| KFM02A | 476.8 | 482.2 | 477.8 |
| KFM02A | | | 479.2 |
| KFM02A | | | 480.4 |
| KFM02A | | | 481.2 |
| KFM02A | 483.6 | 487.4 | 484.6 |
| KFM02A | | | 485.6 |
| KFM02A | | | 486.1 |
| KFM02A | | | 486.4 |
| KFM02A | 492.4 | 494.4 | 493.4 |
| KFM02A | 494.5 | 502.4 | 495.5 |
| KFM02A | | | 496.5 |
| KFM02A | | | 497.3 |
| KFM02A | | | 498.1 |
| KFM02A | | | 498.3 |
| KFM02A | | | 500.3 |
| KFM02A | | | 500.9 |
| KFM02A | | | 501.4 |
| KFM02A | 505.5 | 507.5 | 506.5 |
| KFM02A | 511.3 | 514.6 | 512.3 |
| KFM02A | | | 512.6 |
| KFM02A | | | 513.1 |
| KFM02A | | | 513.6 |
| KFM02A | 893 | 895 | 894 |

**Table D-10: KFM02B – total drill core length 58.7 m.**

| Borehole | Adjusted Secup (m) | Adjusted Seclow (m) | Location of PFL-anomaly |
|---|---|---|---|
| KFM02B | 87.6 | 89.6 | 88.6 |
| KFM02B | 90.4 | 92.4 | 91.4 |
| KFM02B | 101.6 | 103.6 | 102.6 |
| KFM02B | 103.9 | 105.9 | 104.9 |
| KFM02B | 107.2 | 109.2 | 108.2 |
| KFM02B | 111.7 | 113.7 | 112.7 |
| KFM02B | 129.2 | 131.2 | 130.2 |
| KFM02B | 157.1 | 159.1 | 158.1 |
| KFM02B | 166.3 | 169 | 167.3 |
| KFM02B | | | 168 |
| KFM02B | 174.2 | 176.2 | 175.2 |
| KFM02B | 220.7 | 222.7 | 221.7 |
| KFM02B | 270 | 272 | 271 |
| KFM02B | 329.7 | 332 | 330.7 |
| KFM02B | | | 331 |
| KFM02B | 398.4 | 400.4 | 399.4 |
| KFM02B | 409.8 | 416.1 | 410.8 |
| KFM02B | | | 412.2 |
| KFM02B | | | 413.1 |
| KFM02B | | | 414.5 |
| KFM02B | | | 415.1 |
| KFM02B | 418.4 | 424.3 | 419.4 |
| KFM02B | | | 420.5 |
| KFM02B | | | 421.1 |
| KFM02B | | | 422.3 |
| KFM02B | | | 423.3 |
| KFM02B | 425.1 | 430.6 | 426.1 |
| KFM02B | | | 426.3 |
| KFM02B | | | 426.9 |
| KFM02B | | | 428.4 |
| KFM02B | | | 429.6 |
| KFM02B | 435.4 | 437.4 | 436.4 |
| KFM02B | 469.2 | 472.5 | 470.2 |
| KFM02B | | | 471 |
| KFM02B | | | 471.5 |
| KFM02B | 496.1 | 498.8 | 497.1 |
| KFM02B | | | 497.8 |
| KFM02B | 499 | 503 | 500 |
| KFM02B | | | 500.8 |
| KFM02B | | | 501 |
| KFM02B | | | 502 |

**Table D-11: KFM03A – total drill core length 70.2 m.**

| Borehole | Adjusted Secup (m) | Adjusted Seclow (m) | Location of PFL-anomaly |
|---|---|---|---|
| KFM03A | 112.2 | 114.2 | 113.2 |
| KFM03A | 119.6 | 121.6 | 120.6 |
| KFM03A | 122.1 | 124.1 | 123.1 |
| KFM03A | 125.5 | 127.5 | 126.5 |
| KFM03A | 129.2 | 131.7 | 130.2 |
| KFM03A | | | 130.7 |
| KFM03A | 149.8 | 151.8 | 150.8 |
| KFM03A | 156 | 161 | No PFL-anomaly |
| KFM03A | 313.4 | 315.4 | 314.4 |
| KFM03A | 304 | 309 | No PFL-anomaly |
| KFM03A | 353.4 | 355.4 | 354.4 |
| KFM03A | 357.5 | 360.6 | 358.5 |
| KFM03A | | | 359.1 |
| KFM03A | | | 359.6 |
| KFM03A | 409.7 | 412.5 | 410.7 |
| KFM03A | | | 411.5 |
| KFM03A | 448.4 | 452.3 | 449.4 |
| KFM03A | | | 451.3 |
| KFM03A | 453.6 | 455.6 | 454.6 |
| KFM03A | 461.4 | 463.4 | 462.4 |
| KFM03A | 499.5 | 501.5 | 500.5 |
| KFM03A | 514.9 | 518.7 | 515.9 |
| KFM03A | | | 517.7 |
| KFM03A | 532.7 | 534.7 | 533.7 |
| KFM03A | 560.5 | 565.5 | No PFL-anomaly |
| KFM03A | 641.2 | 644.9 | 642.2 |
| KFM03A | | | 643.9 |
| KFM03A | 802.8 | 804.8 | 803.8 |
| KFM03A | 812.7 | 814.7 | 813.7 |
| KFM03A | 943.2 | 945.2 | 944.2 |
| KFM03A | 945.5 | 947.5 | 946.5 |
| KFM03A | 985.2 | 987.5 | 986.2 |
| KFM03A | | | 986.5 |
| KFM03A | 991.9 | 995 | 992.9 |
| KFM03A | | | 993.8 |
| KFM03A | | | 994 |

**Table D-12: KFM03B – total drill core length 15 m.**

| Borehole | Adjusted Secup (m) | Adjusted Seclow (m) | Location of PFL-anomaly |
|---|---|---|---|
| KFM03B | 8.5 | 13.5 | No PFL-logging in section |
| KFM03B | 28.5 | 33.5 | No PFL-logging in section |
| KFM03B | 48.5 | 53.5 | No PFL-logging in section |

**Table D-13: KFM04A – total drill core length 35.0 m.**

| Borehole | Adjusted Secup (m) | Adjusted Seclow (m) | Location of PFL-anomaly |
|---|---|---|---|
| KFM04A | 108.6 | 114.9 | 109.6 |
| KFM04A | | | 110.3 |
| KFM04A | | | 111.4 |
| KFM04A | | | 112.4 |
| KFM04A | | | 112.8 |
| KFM04A | | | 113.9 |
| KFM04A | 115.1 | 118 | 116.1 |
| KFM04A | | | 117 |
| KFM04A | 119.2 | 121.2 | 120.2 |
| KFM04A | 124.3 | 126.3 | 125.3 |
| KFM04A | 194.3 | 196.3 | 195.3 |
| KFM04A | 201.1 | 203.8 | 202.1 |
| KFM04A | | | 202.8 |
| KFM04A | 206.1 | 209.2 | 207.1 |
| KFM04A | | | 208.2 |
| KFM04A | 296.1 | 298.1 | 297.1 |
| KFM04A | 356.8 | 360.8 | 357.8 |
| KFM04A | | | 358.2 |
| KFM04A | | | 359.8 |
| KFM04A | 418 | 420 | 419 |
| KFM04A | 420.9 | 422.9 | 421.9 |
| KFM04A | 520.5 | 522.5 | 521.5 |
| KFM04A | 953.8 | 955.8 | 954.8 |

**Table D-14: KFM05A – total drill core length 38.9 m.**

| Borehole | Adjusted Secup (m) | Adjusted Seclow (m) | Location of PFL-anomaly |
|---|---|---|---|
| KFM05A | 107.9 | 114.3 | 108.9 |
| KFM05A | | | 110.1 |
| KFM05A | | | 111.6 |
| KFM05A | | | 112.6 |
| KFM05A | | | 112.9 |
| KFM05A | | | 113.3 |
| KFM05A | 114.8 | 117.5 | 115.8 |
| KFM05A | | | 116.5 |
| KFM05A | 118.7 | 122.9 | 119.7 |
| KFM05A | | | 120.2 |
| KFM05A | | | 120.6 |
| KFM05A | | | 121.9 |
| KFM05A | 123.1 | 127.1 | 124.1 |
| KFM05A | | | 124.4 |
| KFM05A | | | 126.1 |
| KFM05A | 129.9 | 133.2 | 130.9 |
| KFM05A | | | 132.2 |
| KFM05A | 141.4 | 143.4 | 142.4 |
| KFM05A | 148 | 150 | 149 |
| KFM05A | 162.9 | 164.9 | 163.9 |
| KFM05A | 165.4 | 169.7 | 166.4 |
| KFM05A | | | 167.2 |
| KFM05A | | | 168.7 |
| KFM05A | 174.6 | 176.6 | 175.6 |
| KFM05A | 263.4 | 265.4 | 264.4 |
| KFM05A | 701.7 | 703.7 | 702.7 |
| KFM05A | 719 | 721 | 720.0 |

**Table D-15: KFM06B – total drill core length 59 m.**

| Borehole | Adjusted Secup (m) | Adjusted Seclow (m) | Location of PFL-anomaly |
|---|---|---|---|
| KFM06B | 6 | 65 | No PFL-logging in section |

**Table D-16: KFM06A – total drill core length 57.1 m.**

| Borehole | Adjusted Secup (m) | Adjusted Seclow (m) | Location of PFL-anomaly |
|---|---|---|---|
| KFM06A | 105.4 | 107.4 | 106.4 |
| KFM06A | 108.3 | 112.5 | 109.3 |
| KFM06A | | | 110.6 |
| KFM06A | | | 111.5 |
| KFM06A | 112.6 | 117.9 | 113.6 |
| KFM06A | | | 115.4 |
| KFM06A | | | 116.4 |
| KFM06A | | | 116.9 |
| KFM06A | 122.1 | 124.1 | 123.1 |
| KFM06A | 203.4 | 207.2 | 204.4 |
| KFM06A | | | 205.7 |
| KFM06A | | | 205.9 |
| KFM06A | | | 206.2 |
| KFM06A | 207.3 | 209.3 | 208.3 |
| KFM06A | 211.6 | 213.6 | 212.6 |
| KFM06A | 214.6 | 219.2 | 215.6 |
| KFM06A | | | 216.3 |
| KFM06A | | | 218.2 |
| KFM06A | 226 | 231 | No PFL-anomaly |
| KFM06A | 287 | 292 | No PFL-anomaly |
| KFM06A | 302.0 | 304.0 | 303.0 |
| KFM06A | 305.2 | 307.2 | 306.2 |
| KFM06A | 307.4 | 309.4 | 308.4 |
| KFM06A | 448.4 | 450.4 | 449.4 |
| KFM06A | 504 | 509 | No PFL-anomaly |
| KFM06A | 621.4 | 623.4 | 622.4 |
| KFM06A | 652.9 | 654.9 | 653.9 |
| KFM06A | 742.3 | 744.3 | 743.3 |
| KFM06A | 769.6 | 771.8 | 770.6 |
| KFM06A | | | 770.8 |

**Table D-17: KFM07A – total drill core length 4.9 m.**

| Borehole | Adjusted Secup (m) | Adjusted Seclow (m) | Location of PFL-anomaly |
|---|---|---|---|
| KFM07A | 915.3 | 918.2 | 916.3 |
| KFM07A | | | 917.2 |
| KFM07A | 969.0 | 971.0 | 970 |

**Table D-18: KFM07C – total drill core length 26.4 m.**

| Borehole | Adjusted Secup (m) | Adjusted Seclow (m) | Location of PFL-anomaly |
|---|---|---|---|
| KFM07C | 97.4 | 99.4 | 98.4 |
| KFM07C | 107.1 | 109.9 | 108.1 |
| KFM07C | | | 108.9 |
| KFM07C | 110.3 | 112.3 | 111.3 |
| KFM07C | 113.7 | 116.8 | 114.7 |
| KFM07C | | | 115.8 |
| KFM07C | 122.1 | 124.1 | 123.1 |
| KFM07C | 133.3 | 135.3 | 134.3 |
| KFM07C | 143.1 | 145.1 | 144.1 |
| KFM07C | 149.9 | 151.9 | 150.9 |
| KFM07C | 155.5 | 157.5 | 156.5 |
| KFM07C | 162.8 | 164.8 | 163.8 |
| KFM07C | 224.9 | 226.9 | 225.9 |
| KFM07C | 278.3 | 280.8 | 279.3 |
| KFM07C | | | 279.8 |

**Table D-19: KFM08A – total drill core length 5.5 m.**

| Borehole | Adjusted Secup (m) | Adjusted Seclow (m) | Location of PFL-anomaly |
|---|---|---|---|
| KFM08A | 479.5 | 483.0 | 480.5 |
| KFM08A | | | 482 |
| KFM08A | 686.0 | 688.0 | 687 |

**Table D-20: KFM08B – total drill core length 15 m.**

| Borehole | Adjusted Secup (m) | Adjusted Seclow (m) | Location of PFL-anomaly |
|---|---|---|---|
| KFM08B | 14.5 | 19.5 | No PFL-logging in section |
| KFM08B | 35.7 | 42.5 | No PFL-logging in section |
| KFM08B | 61 | 66 | No PFL-logging in section |

**Table D-21: KFM08C – total drill core length 17.7 m.**

| Borehole | Adjusted Secup (m) | Adjusted Seclow (m) | Location of PFL-anomaly |
|---|---|---|---|
| KFM08C | 461.3 | 465.0 | 462.3 |
| KFM08C | | | 464 |
| KFM08C | 469.7 | 471.7 | 470.7 |
| KFM08C | 479.0 | 481.0 | 480 |
| KFM08C | 498.0 | 500.0 | 499 |
| KFM08C | 517.8 | 519.8 | 518.8 |
| KFM08C | 520.4 | 522.4 | 521.4 |
| KFM08C | 523.6 | 525.6 | 524.6 |
| KFM08C | 682.6 | 684.6 | 683.6 |

**Table D-22: KFM08D – total drill core length 70.8 m.**

| Borehole | Adjusted Secup (m) | Adjusted Seclow (m) | Location of PFL-anomaly |
|---|---|---|---|
| KFM08D | 74.8 | 78.8 | 75.8 |
| KFM08D | | | 77.8 |
| KFM08D | 79.9 | 83.4 | 80.9 |
| KFM08D | | | 81.4 |
| KFM08D | | | 82.1 |
| KFM08D | | | 82.4 |
| KFM08D | 92.5 | 97.5 | No PFL-anomaly |
| KFM08D | 102.9 | 104.9 | 103.9 |
| KFM08D | 106.3 | 110.2 | 107.3 |
| KFM08D | | | 107.6 |
| KFM08D | | | 109.2 |
| KFM08D | 116 | 118 | 117 |
| KFM08D | 124.6 | 126.6 | 125.6 |
| KFM08D | 130.1 | 132.1 | 131.1 |
| KFM08D | 140.6 | 142.6 | 141.6 |
| KFM08D | 146.4 | 150.8 | 147.4 |
| KFM08D | | | 148 |
| KFM08D | | | 149.8 |
| KFM08D | 186.1 | 189.6 | 187.1 |
| KFM08D | | | 188.3 |
| KFM08D | | | 188.6 |
| KFM08D | 200.2 | 202.2 | 201.2 |
| KFM08D | 204 | 208.2 | 205 |
| KFM08D | | | 205.3 |
| KFM08D | | | 207.2 |
| KFM08D | 308.5 | 313.5 | No PFL-anomaly |
| KFM08D | 386.7 | 390.2 | 387.7 |
| KFM08D | | | 389.2 |
| KFM08D | 391.2 | 394.3 | 392.2 |
| KFM08D | | | 393.3 |
| KFM08D | 552.2 | 557.2 | No PFL-anomaly |
| KFM08D | 675.2 | 678.9 | 676.2 |
| KFM08D | | | 677.9 |
| KFM08D | 684.5 | 686.5 | 685.5 |
| KFM08D | 694.8 | 696.8 | 695.8 |
| KFM08D | 733.8 | 735.8 | 734.8 |
| KFM08D | 831.2 | 833.2 | 832.2 |
| KFM08D | 924.1 | 926.1 | 925.1 |

**Table D-23: KFM10A – total drill core length 86.1 m.**

| Borehole | Adjusted Secup (m) | Adjusted Seclow (m) | Location of PFL-anomaly |
|---|---|---|---|
| KFM10A | 59.3 | 63.3 | 60.3 |
| KFM10A | | | 62.3 |
| KFM10A | 70.1 | 73.3 | 71.1 |
| KFM10A | | | 72.3 |
| KFM10A | 75.2 | 77.2 | 76.2 |
| KFM10A | 81.1 | 83.1 | 82.1 |
| KFM10A | 83.4 | 104.9 | 84.4 |
| KFM10A | | | 85.9 |
| KFM10A | | | 87.7 |
| KFM10A | | | 87.9 |
| KFM10A | | | 89.6 |
| KFM10A | | | 90.5 |
| KFM10A | | | 92 |
| KFM10A | | | 93.8 |
| KFM10A | | | 94.8 |
| KFM10A | | | 95.1 |
| KFM10A | | | 96.5 |
| KFM10A | | | 98.3 |
| KFM10A | | | 99.9 |
| KFM10A | | | 101.6 |
| KFM10A | | | 103.3 |
| KFM10A | | | 103.9 |
| KFM10A | 105 | 109.3 | 106 |
| KFM10A | | | 107.3 |
| KFM10A | | | 108.3 |
| KFM10A | 112 | 119.7 | 113 |
| KFM10A | | | 114.6 |
| KFM10A | | | 115.2 |
| KFM10A | | | 116.9 |
| KFM10A | | | 118.7 |
| KFM10A | 119.9 | 123 | 120.9 |
| KFM10A | | | 122 |
| KFM10A | 143.3 | 145.7 | 144.3 |
| KFM10A | | | 144.7 |
| KFM10A | 253.9 | 255.9 | 254.9 |
| KFM10A | 298.5 | 300.5 | 299.5 |
| KFM10A | 307.8 | 309.8 | 308.8 |
| KFM10A | 314.3 | 316.3 | 315.3 |
| KFM10A | 321 | 323 | 322 |
| KFM10A | 326.3 | 329.8 | 327.3 |
| KFM10A | | | 328.1 |
| KFM10A | | | 328.8 |
| KFM10A | 331.9 | 335.5 | 332.9 |
| KFM10A | | | 334.5 |
| KFM10A | 359.5 | 361.5 | 360.5 |
| KFM10A | 367.4 | 369.4 | 368.4 |
| KFM10A | 372.6 | 374.6 | 373.6 |
| KFM10A | 375 | 377 | 376 |
| KFM10A | 430.9 | 432.9 | 431.9 |
| KFM10A | 435.3 | 439 | 436.3 |
| KFM10A | | | 437.3 |
| KFM10A | | | 438 |
| KFM10A | 479.3 | 481.8 | 480.3 |
| KFM10A | | | 480.8 |
| KFM10A | 482.8 | 485.4 | 483.8 |
| KFM10A | | | 484.4 |

**Table D-24: KFM11A – total drill core length 61.1 m.**

| Borehole | Adjusted Secup (m) | Adjusted Seclow (m) | Location of PFL-anomaly |
|---|---|---|---|
| KFM11A | 72.8 | 83.3 | 73.8 |
| KFM11A | | | 74.6 |
| KFM11A | | | 75.3 |
| KFM11A | | | 75.9 |
| KFM11A | | | 77.4 |
| KFM11A | | | 79.4 |
| KFM11A | | | 80.3 |
| KFM11A | | | 82.3 |
| KFM11A | 87.9 | 101.5 | 88.9 |
| KFM11A | | | 90.4 |
| KFM11A | | | 91.7 |
| KFM11A | | | 92.4 |
| KFM11A | | | 92.9 |
| KFM11A | | | 93.3 |
| KFM11A | | | 95.1 |
| KFM11A | | | 95.6 |
| KFM11A | | | 96.4 |
| KFM11A | | | 97.3 |
| KFM11A | | | 98.4 |
| KFM11A | | | 100.3 |
| KFM11A | | | 100.5 |
| KFM11A | 145.7 | 147.7 | 146.7 |
| KFM11A | 150 | 153 | 151 |
| KFM11A | | | 152 |
| KFM11A | 153.2 | 159.5 | 154.2 |
| KFM11A | | | 155.4 |
| KFM11A | | | 157.1 |
| KFM11A | | | 158.5 |
| KFM11A | 255.9 | 258.6 | 256.9 |
| KFM11A | | | 257.4 |
| KFM11A | | | 257.6 |
| KFM11A | 260.5 | 263 | 261.5 |
| KFM11A | | | 262 |
| KFM11A | 265.8 | 267.8 | 266.8 |
| KFM11A | 268 | 270 | 269 |
| KFM11A | 270.7 | 277.5 | 271.7 |
| KFM11A | | | 273.4 |
| KFM11A | | | 275 |
| KFM11A | | | 276.5 |
| KFM11A | 375.2 | 377.8 | 376.2 |
| KFM11A | | | 376.8 |
| KFM11A | 378.3 | 380.3 | 379.3 |
| KFM11A | 466.6 | 468.6 | 467.6 |
| KFM11A | 473.6 | 476.7 | 474.6 |
| KFM11A | | | 475.7 |

# Appendix E

## Assumed rock volumes in KFM02B, KFM08D, and KFM11A

Based on the bedrock geology model of Forsmark site descriptive modelling – stage 2.2, predictions of fracture domains and deformation zones were made for boreholes KFM02B, KFM08D and KFM11A /Stephens et al. 2008/. These predictions were made before the boreholes were drilled and studied. Upon drilling and studying the boreholes, single hole interpretations were made. Results from the single hole interpretations were compared with the predictions and as a result, the predictions were adjusted. In this present work it is assumed that the adjusted predictions are valid. The rock volumes assumed to intersect the boreholes are given in Table E-1. The table is based on the following tables in /Stephens et al. 2008/:

- For borehole KFM02B: Tables 3-5 to 3-7.
- For borehole KFM08D: Tables 4-5 to 4-7 .
- For borehole KFM11A: Tables 5-5 and 5-6.

It should be carefully noted that in /Stephens et al. 2008/ only predictions exist for these boreholes, which should not be interpreted as bedrock geology models. If proper modelling is performed in the future, the outcome may be different.

**Table E-1. Rock volumes assumed to intersect boreholes KFM02B, KFM08D and KFM11A.**

| Borehole | Secup | Seclow | Rock domain | Fracture domain | Deformation zone |
|---|---|---|---|---|---|
| KFM02B | 88.56 | 98 | RFM029 | FFM03 | |
| KFM02B | 98 | 115 | RFM029 | | ZFM866 |
| KFM02B | 115 | 145 | RFM029 | FFM03 | |
| KFM02B | 145 | 204 | RFM029 | | ZFMA3 |
| KFM02B | 204 | 411 | RFM029 | FFM03 | |
| KFM02B | 411 | 431 | RFM029 | | ZFMA2 |
| KFM02B | 431 | 462 | RFM029 | FFM01 | |
| KFM02B | 462 | 473 | RFM029 | | ZFMF1 |
| KFM02B | 473 | 485 | RFM029 | FFM01 | |
| KFM02B | 485 | 512 | RFM029 | | ZFMF1 |
| KFM02B | 512 | 573.54 | RFM029 | FFM01 | |
| KFM08D | 59.45 | 184 | RFM029 | FFM01 | |
| KFM08D | 184 | 210 | RFM029 | | ZFMENE2120 |
| KFM08D | 210 | 318 | RFM029 | FFM01 | |
| KFM08D | 318 | 324 | RFM029 | | ZFMENE0159A |
| KFM08D | 324 | 371 | RFM029 | FFM01 | |
| KFM08D | 371 | 395.65 | RFM029 | | ZFMENE0159B |
| KFM08D | 395.65 | 546 | RFM045 | FFM06 | |
| KFM08D | 546 | 571 | RFM045 | | ZFMNNE2309 |
| KFM08D | 571 | 621 | RFM045 | FFM06 | |
| KFM08D | 621 | 634 | RFM045 | | ZFMENE2320 |
| KFM08D | 634 | 644 | RFM045 | FFM06 | |
| KFM08D | 644 | 689 | RFM045 | | ZFMNNE2308 |
| KFM08D | 689 | 737 | RFM045 | FFM06 | |
| KFM08D | 737 | 749 | RFM045 | | ZFMNNE2293 |
| KFM08D | 479 | 819 | RFM045 | FFM06 | |
| KFM08D | 819 | 842 | RFM045 | | ZFMENE0168 |
| KFM08D | 842 | 903 | RFM045 | FFM06 | |
| KFM08D | 903 | 941.75 | RFM045 | | ZFMNNE2300 |
| KFM11A | 71.6 | 245 | RFM021 | Not predicted as outside target volume | |
| KFM11A | 245 | 824 | RFM021 | | ZFMWNW0813<br>ZFMWNW0001<br>ZFMWNW1127 |
| KFM11A | 824 | 851.21 | RFM021 | Not predicted as outside target volume | |